

AD-A044 241

ROCKWELL INTERNATIONAL THOUSAND OAKS CALIF SCIENCE --ETC F/G 11/6
NONDESTRUCTIVE INSPECTION OF PHOSPHORIC ACID ANODIZED ALUMINUM --ETC(U)
APR 77 T SMITH

UNCLASSIFIED

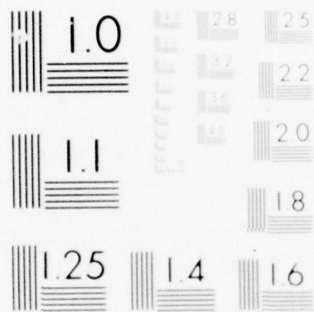
SC5026.22TR

AFML-TR-77-42

NL

1 OF 3
AD
A044241





MICROCOPY RESOLUTION TEST CHART
NATIONAL BUREAU OF STANDARDS-1963-A

AD A 044 241

AFML-TR-77-42

V

12

NONDESTRUCTIVE INSPECTION OF PHOSPHORIC ACID ANODIZED ALUMINUM PANELS FOR CONTAMINATION

ROCKWELL INTERNATIONAL SCIENCE CENTER
THOUSAND OAKS, CALIFORNIA 91360

APRIL 1977

TECHNICAL REPORT AFML-TR-77-42
Final Report for Period March 1975 - December 1976

Approved for public release; distribution unlimited.

AD No. _____
DDC FILE COPY

AIR FORCE MATERIALS LABORATORY
AIR FORCE WRIGHT AERONAUTICAL LABORATORIES
AIR FORCE SYSTEMS COMMAND
WRIGHT-PATTERSON AIR FORCE BASE, OHIO 45433

DDC
RECEIVED
SEP 19 1977
B

NOTICE

When Government drawings, specifications, or other data are used for any purpose other than in connection with a definitely related Government procurement operation, the United States Government thereby incurs no responsibility nor any obligation whatsoever; and the fact that the government may have formulated, furnished, or in any way supplied the said drawings, specifications, or other data, is not to be regarded by implication or otherwise as in any manner licensing the holder or any other person or corporation, or conveying any rights or permission to manufacture, use, or sell any patented invention that may in any way be related thereto.

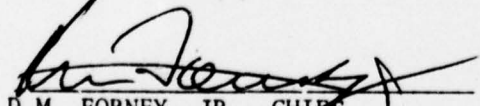
This report has been reviewed by the Information Office (IO) and is releasable to the National Technical Information Service (NTIS). At NTIS, it will be available to the general public, including foreign nations.

This technical report has been reviewed and is approved for publication.

R.L. Crane

R. L. Crane
Project Monitor

FOR THE DIRECTOR


D.M. FORNEY, JR., CHIEF
NONDESTRUCTIVE EVALUATION BRANCH
Metals and Ceramics Division
Air Force Materials Laboratory

Copies of this report should not be returned unless return is required by security considerations, contractual obligations, or notice on a specific document.

UNCLASSIFIED

SECURITY CLASSIFICATION OF THIS PAGE (When Data Entered)

19 REPORT DOCUMENTATION PAGE		READ INSTRUCTIONS BEFORE COMPLETING FORM	
1. REPORT NUMBER AFML-TR-77-42	2. GOVT ACCESSION NO.	3. RECIPIENT'S CATALOG NUMBER	
4. TITLE (and Subtitle) NONDESTRUCTIVE INSPECTION OF PHOSPHORIC ACID ANODIZED ALUMINUM PANELS FOR CONTAMINATION.		5. TYPE OF REPORT & PERIOD COVERED 03-15-75 through 12-15-76	
7. AUTHOR(s) Tennyson/Smith		6. PERFORMING ORG. REPORT NUMBER SC5026.22TR	
9. PERFORMING ORGANIZATION NAME AND ADDRESS Science Center, Rockwell International 1049 Camino Dos Rios Thousand Oaks, Calif. 91360		8. CONTRACT OR GRANT NUMBER(s) F33615-75-C-5235	
11. CONTROLLING OFFICE NAME AND ADDRESS Air Force Materials Laboratory (LLP) Air Force Systems Command Wright-Patterson Air Force Base, Ohio 45433		10. PROGRAM ELEMENT, PROJECT, TASK AREA & WORK UNIT NUMBERS 7351	
14. MONITORING AGENCY NAME & ADDRESS (if different from Controlling Office) 264p.		12. REPORT DATE 11 Apr 1977	
		13. NUMBER OF PAGES 252	
		15. SECURITY CLASS. (of this report) Unclassified	
		15a. DECLASSIFICATION/DOWNGRADING SCHEDULE	
16. DISTRIBUTION STATEMENT (of this Report) Approved for public release; distribution unlimited			
17. DISTRIBUTION STATEMENT (of the abstract entered in Block 20, if different from Report) B			
18. SUPPLEMENTARY NOTES			
19. KEY WORDS (Continue on reverse side if necessary and identify by block number) NONDESTRUCTIVE INSPECTION, ADHESIVE BONDING OF ALUMINUM, ELLIPSOMETRY, SURFACE POTENTIAL DIFFERENCE, PHOTOELECTRON EMISSION, WETTABILITY, COMPUTER MAPPING			
20. ABSTRACT (Continue on reverse side if necessary and identify by block number) This report describes a study of nondestructive inspection (NDI) for contami- nants on phosphoric acid anodized aluminum alloys (Al 7075-T6 and Al 2024-T3). Contamination is used in the broad sense to include surface preparation process errors (such as incorrect anodize time or voltage) and handling damage as well as organic contamination from humans and smog. Panels were deliberately contaminated to various levels and then inspected by automated scanning with three surface tools. The tools were, ellipsometry, surface			

DD FORM 1 JAN 73 1473 EDITION OF 1 NOV 65 IS OBSOLETE

UNCLASSIFIED

SECURITY CLASSIFICATION OF THIS PAGE (When Data Entered)

389949

JP

UNCLASSIFIED

SC5026.22TR

SECURITY CLASSIFICATION OF THIS PAGE(When Data Entered)

potential difference (SPD), and water contact angle. Ellipsometry proved to be the most useful, detecting all types of contamination. SPD was partially successful for processing errors and organic contamination but was not successful for handling damage. Contact angle measurements were successful for nonpolar organic contamination only. The anodic films are too thick for useful photoelectron emission (PEE) but this technique is very useful for other surface treatment such as FPL etch. The best NDI instrument should include ellipsometry and SPD but ellipsometry alone will probably be adequate. SPD alone would not be adequate.

ACCESSION for	
NTIS	White Section <input checked="" type="checkbox"/>
DDC	Buff Section <input type="checkbox"/>
UNANNOUNCED	<input type="checkbox"/>
JUSTIFICATION	
BY	
DISTRIBUTION/AVAILABILITY CODES	
Dist.	AVAIL. and/or SPECIAL
A	

UNCLASSIFIED

SECURITY CLASSIFICATION OF THIS PAGE(When Data Entered)

FOREWORD

This report covers work conducted as Task II "Characterization of Surfaces Prior to Adhesive Bonding" from March 1975 to December 1976 under the direction of Dr. Tennyson Smith, Manager and Principal Investigator, with Gary W. Lindberg assisting. We acknowledge the assistance of R. K. Elsley with respect to computer programming and operation.

This work was conducted under United States Air Force Contract F33615-75-C-5235, Project No. 7351 and was administered under the direction of the Metals Behavior Branch, Metals and Ceramics Division, Air Force Materials Laboratory, Wright Patterson Air Force Base, Ohio. The project monitors were R. L. Crane and J. C. Tanzola.

SUMMARY

This report describes a study of nondestructive inspection (NDI) for contaminants on phosphoric acid anodized aluminum alloys. Contamination is used in the broad sense to include surface preparation process errors, handling damage as well as organic contamination from human sources and smog. Anodized panels were deliberately contaminated to various levels and then inspected by automated scanning with three surface tools. The tools were ellipsometry, surface potential difference and water contact angle measurements. The results for these tools are summarized as follows.

The ellipsometric parameter Δ is considered successful for 25 of the 32 contaminants. Four of the contaminants not detected by Δ were not detected by SPD or contact angle and were probably not present (due to evaporation). Three of the contaminants were not detected by the ellipsometer but were detected by SPD or contact angle. Seventeen of the contaminants were detected by SPD. SPD was particularly unsuccessful for processing errors and handling damage. Contact angle measurements detected 15 contaminants, most of which were organic and nonpolar. Contact angle was unsuccessful for the detection of process errors, handling damage and human contamination (except for greasy materials such as fingerprints, lipstick, etc.). In no case did the contact angle detect contamination for which Δ or SPD did not. It is concluded that the best NDI system would include both ellipsometry and SPD. This system would detect essentially all types of contamination. The best single tool is ellipsometry.

SECTION	TABLE OF CONTENTS	PAGE
I.	INTRODUCTION	1
	A. The Contamination Survey	1
	B. The Problem	8
	C. The Solution	8
	1. Task II	8
	2. Task III	9
II.	EXPERIMENTAL	10
	A. Surface Techniques	10
	1. Ellipsometry	10
	2. Surface Potential Difference (SPD)	11
	3. Photoelectron Emission (PEE)	11
	4. Contact Angle (ϕ_{H_2O})	11
	5. Auger Electron Spectroscopy (AES)	12
	B. The Anodizing Process	12
	C. Computerized Mapping	16
III.	EXPERIMENTAL RESULTS	25
	A. Characterization of Anodic Films	25
	B. Sensitivity to Contamination	36
	1. Processing Errors	36
	2. Handling Damage	41
	3. Organic Contamination	47
	4. Aging in Laboratory Air	55
	C. NDI, Automated Computer Mapping	63
	1. Processing Errors	63
	2. Handling Damage	66
	3. Human Contamination	67
	4. Simulated Smog Contamination	67
	5. Reproducibility of the Lowest Level of Contamination	70
	6. Reproducibility of Mapping	71
	7. Scale Up	72

TABLE OF CONTENTS (Cont'd)

SECTION	PAGE
IV. DISCUSSION AND CONCLUSIONS	79
A. Mechanisms	79
B. Surface Tools	84
1. Ellipsometry	84
2. Surface Potential Difference (SPD)	85
3. Photoelectron Emission (PEE)	89
4. Contact Angles	90
C. Conclusions	90
APPENDIX A COMPUTER PLOTS OF CONTAMINATION	94
APPENDIX B COMPUTER PRINTOUTS OF CONTAMINATION	223
REFERENCES	254

LIST OF ILLUSTRATIONS

FIGURE		PAGE
1.	Photograph of the anodizing tank.	14
2.	Photograph of the surface tools.	17
3.	Sensor heads and sample for mapping with computer automated system.	18
4.	Plots of AINTENS vs $\left[A/A_{\max} \right] \times 6$ for various values of C and I.	20
5.	Computer plots of SPD to show the effect of C and I.	23
6.	Computer plots of SPD for panel with thumb print.	24
7.	Δ vs. ψ plot for a theoretical film (curve) of refractive index 1.3 and thickness indicated. The solid circles are experimental data for phosphoric acid anodized Al 1100 that had been previously electropolished to smooth the surface.	26
8.	a. SEM picture of electropolished Al 1100 after anodizing at 10 volts for 22 minutes and bending to reveal hydroxide film edge.	28
	b. SEM picture of Al 2024-T3 after FPL etch and anodizing at 10 volts for 22 minutes then bending.	28
9.	Δ vs. ψ plot for rough Al 7075-T6 and Al 2024-T3 anodized samples (at the indicated voltage for 22 minutes), $\lambda = 6328\text{\AA}$, $\phi = 70^\circ$.	29
10.	Plot of film thickness vs. anodic voltage.	30
11.	Effect of hydroxide film thickness (anodize voltage) on SPD.	40

LIST OF ILLUSTRATIONS (Cont'd)

FIGURE		PAGE
12.	Plot of $-\delta\Delta$, ϕ_{H_2O} , $\delta\psi$ and $\delta(\text{SPD})$ vs. time in the stearic acid-pentane solution.	49
13.	Plot of ϕ_{H_2O} and $\delta(\text{SPD})$ vs. stearic acid film thickness.	51
14.	Auger peak to peak heights (APPH) for C and contact angle ϕ_{H_2O} for contamination.	54
15.	Change of surface parameters with aging of anodized Al 2024-T3.	58
16.	Plot of $\text{APPH}(\text{C})/\text{APPH}(\text{Al } 1390 \text{ ev})$ vs. days of aging anodized Al 2024-T3 in lab air. Left ordinate is estimated fraction of a monolayer (monolayer $\sim 25\text{\AA}$).	59
17.	Sputter profile for sample anodized at 4 volts, 12 min, 5% H_3PO_4 , SET = 15 days, initial oxide thickness 1000 \AA .	61
18.	Sputter profile for sample anodized at 10 V, 22 min, 5% H_3PO_4 , SET = 14 days, initial oxide thickness 2180 \AA .	62
19.	SEM pictures of anodized Al 7075-T6 (from T. P. Remmel, Northrup).	80
20.	SEM pictures of FPL etched AL 2024-T3 after 21 hrs at 100 $^{\circ}\text{C}$ water (boiled dry) (top), 21 hrs, 50 $^{\circ}\text{C}$ water (bottom).	81
21.	SEM pictures of vapor deposited Al after anodizing to 500 \AA then 50 $^{\circ}\text{C}$ water exposure for 150 hrs.	82
22.	Drift of SPD for nickel-gold and nickel-FPL Al 2024-T3 electrode couples.	87
23.	Drift of SPD for various electrode couples.	88
A.1(a) through A.42(d),	Computer Plots, Appendix A	93

LIST OF TABLES

TABLE		PAGE
1	Contamination sources in factory environment.	3
2	Contamination sources in semi-clean room facilities.	3
3	Representative contamination due to various sources.	7
4	Phosphoric acid anodize, Northrup process.	13
5	Effect of pretreatment on anodic film properties.	15
6	Surface properties of aluminum alloys 7075-T6 and 2024-T3 after phosphoric acid anodize from various facilities.	32
7	ESCA results for films on Al 2024-T3.	35
8	Sensitivity of surface tools to processing errors.	37
9	Surface properties of phosphoric anodized Al 7075-T6 after mechanical disturbance with cotton gloves, kraft paper, Al foil and glass wool, etc.	43
10	The effect of surface disturbance of phosphoric acid anodized Al 7075-T6 on lap shear strength	46
11	Change of surface parameters due to adsorption of stearic acid.	48
12.	Auger spectroscopy of contaminated Al 7075-T6 phosphoric acid anodized samples.	53
13	Effect of aging on surface properties.	56
14	Effect of laboratory aging of phosphoric acid anodized Al 2024-T3.	57
15	Surface property map of 1' x 1' x 0.033" panel (#10 from McDonnell Douglas). Production line anodic process.	73

LIST OF TABLES (Cont'd)

TABLE		PAGE
16	Surface property map of 1' x 1' x 0.033" panel (#2 from McDonnell Douglas). Production line anodic process.	74
17	Quality assurance table for production panels from McDonnell Douglas. Acceptance band $141 < \Delta < 144$, $41 < \psi < 43$, $0.2 < \text{SPD} < .4$. $\lambda = 6328\text{\AA}$, angle of incidence 60° , automated ellipsometer.	78
18	Representative contamination due to various sources and surface tool utility.	92
B.1(a) through B.19(c), Computer Printouts, Appendix B		221

SECTION I

INTRODUCTION

Recent emphasis in the USAF on structural integrity and durability has focused attention on the use of adhesive bonding in primary structures as a joining technique. Preliminary estimates of weight and cost savings that would result from utilization of adhesive bonding technology are 15 and 20 percent, respectively. To assure the reliability of this joining method, nondestructive inspection (NDI) tools must be developed to ensure the adequacy of each step in the bonding process.

The program was divided into two tasks. In Task I, a contractor (Northrup Corp. see ref. 1) was to develop a nondestructive inspection technique to determine the surface oxide composition, morphology and thickness of anodized panels.

In Task II a contractor (Rockwell International Science Center) was to develop a nondestructive inspection technique that can be used, just prior to layup, to detect contamination on the aluminum surface.

This report concerns Task II, with a broad interpretation of contamination to include surface damage due to handling and processing errors during surface preparation as well as organic contamination from various sources.

A. Contamination Survey

The type of organic contamination that will be present in a bonding facility will depend upon the precautions taken, ranging all the way from outdoor operations to ultra clean room conditions. The author visited some of our adhesive bonding facilities and found adhesive bonding performed in

normal factory environment and semi-clean room environments. Semi-clean room is somewhere between factory conditions and ultra-clean rooms used for semi-conductor-integrated circuitry facilities. Table 1 is a list of contamination sources found in the factory environments; Table 2 is for a semi-clean room.

The most important sources of contamination are smog, finger prints and possible inadvertent contamination of processing solutions.

1. Smog

We were in a particular advantageous position for identifying the contaminants in smog because the Science Center had just completed an exhaustive study of the constituents of smog for the Air Resources Board State of California². More than ten million bits of data were recorded and examined on the computerized acquisition system, and more than 30,000 chemical determinations were made on aerosol samples.

The interactions were elucidated between particle behavior and reactive gases, including sulfur dioxide (SO_2), nitrogen oxides (NO_x), non-methane hydrocarbons (NMHC), ammonia (NH_3) and water vapor. The analysis and interpretation of observations taken between 1971 and 1973 documented in detail for the first time the great importance in smog of aerosol formation from chemical reactions of SO_2 to form sulfate, NO_x to produce nitrate, and NMHC to generate organic particles. These chemical reactions are very complicated in nature and involve photochemical and non-photochemical processes of the trace gases as well as their interaction

TABLE 1

CONTAMINATION SOURCES IN FACTORY ENVIRONMENT

Industrial smog
 Cigarette smoke
 Oil and grease associated with machinery
 Ink
 Food remnants from lunch boxes (orange peel, banana peel, bread, coffee, etc.)
 Human breath, perspiration and natural body oils (finger prints, women's cosmetics, etc.)
 Clothing lint
 Plasticizers from plastics
 Process solutions

TABLE 2

CONTAMINATION SOURCES IN SEMI-CLEAN ROOM FACILITIES

Industrial smog
 Clothing lint (white smocks are usually used, probably more for psychological effect)
 Human breath, perspiration and natural body oils
 Plasticizers from plastics
 Process solutions

with the suspended particles. Evidence suggests that the natural or quasi-natural constituents of ammonia and water vapor are key ingredients in the evolution of haze in smog; the former appears to be particularly important for nitrate production. The data analysis suggests that more than half of the aerosol sampled over the Los Angeles area was secondary in origin, resulting from atmospheric chemical reactions. Of the remainder, some 10% to 20% consisted of material identified with a natural background of soil, dust and sea salt, with similar contributions coming from primary emissions such as smoke from stationary and transportation sources. The particulate mass concentration in the air over the Los Angeles area is estimated to be heavily influenced by secondary particles from transportation sources combined with primary emissions such as smoke, soot or lead halide from auto exhaust.

The mass concentrations of aerosol particles in California air varies widely during the day, and is heavily influenced by the presence of sulfate, nitrate and non-carbonate or organic carbon. These constituents are identified as products of atmospheric chemical reactions of pollutant gases SO_2 , NO_x and non-methane hydrocarbon vapors. The Los Angeles Basin is exposed to extreme values over two hours of total mass concentrations of more than $450 \mu\text{g}/\text{m}^3$, with (water soluble) sulfate concentrations of $70 \mu\text{g}/\text{m}^3$ or more, (water soluble) nitrate concentrations of $240 \mu\text{g}/\text{m}^3$ or more, and non-carbonate carbon of more than $50 \mu\text{g}/\text{m}^3$. These maximal concentrations are substantially higher than observed twenty-four hour averaged concentrations.

Typically, the aerosol was characterized by a bimodal distribution, with the submicron fraction less than approximately $2\text{ }\mu\text{m}$ diameter dominated by anthropogenic emissions and particles from atmospheric chemical reactions. The supermicron fraction greater than $2\text{ }\mu\text{m}$ was dominated by natural or quasi-natural sources such as sea salt or wind blown or re-entrained soil dust. The chemical composition of the particles was consistent with the source identification.

The aerosol growth accompanying the evolution of photochemical smog was found consistently to be concentrated in the 0.1 to $1.0\text{ }\mu\text{m}$ range. Evidence was found for the contribution of photochemically related reactions to the production of particulate sulfate, nitrate and organics that significantly enhances the formation of these constituents.

The natural or quasi-natural trace gases, ammonia and water vapor have an important influence on the evolution of photochemical aerosol. The sulfate and nitrate anions can be accounted for as ammonium salts, with a minor fraction as sodium salts. Direct measurements of aerosol liquid water content ranged from less than 10% to more than 50% by weight depending on humidity.

The aerosol in Los Angeles Air is identified with different source categories, including secondary material, primary emissions and natural or quasi-natural background. Arguments are given to link sulfate mainly with stationary sources using fuel oil. On the other hand, nitrates and organics are linked with transportation sources using gasoline. More than half the aerosol samples in Los Angeles air came from atmospheric chemical reactions.

The remaining half was roughly equally divided between material of primary origin from stationary or transportation sources, and background material such as soil, dust or seal salt.

From the data in the ACHEX report we can identify the most common contaminants and the order of magnitude concentrations to be expected. Although surfaces prepared for adhesive bonding will be exposed to the smog gases and aerosols, regardless of which surface is facing up or down, the surface facing up is expected to collect additional contamination from gravitational fallout unless protected. An estimate of the range of fallout that might be expected is 19 to 160 μ g/cm²-day. If about 50% is organic, this corresponds to approximately 0.05 to 0.4 monolayers of -CH₂- groups per sec. One monolayer of -CH₂- groups can significantly lower bond strength on FPL etch aluminum. Table 3 is a list of contaminants that were chosen to represent constituents of smog, handling and improper surface preparation, for this study.

TABLE 3

REPRESENTATIVE CONTAMINATION DUE TO VARIOUS SOURCES

Type	Compound or Substance
Processing Errors	Anodize time Anodize voltage Contamination from bath Delay in H_3PO_4 before rinse
Handling Damage	Cotton glove Kraft paper Kimwipe
Human Contamination	Finger prints Cough or sneeze Cigarette smoke Cigarette ashes Food remnants
Representative Constituents of Smog	N Docosane 16-Bromo-9-hexadecanoic acid Dotriacontane Stearic acid Erucic acid Brassicidic acid Decanoic acid Benzoic acid Amino-Benzoic acid 1-12-diamino decane decadiene decacyclene 1 - Eicosene 1 - Hexadecylamine Anthracene Adamantanol 2 - Adamantanane

B. The Problem

The problem is to develop NDI techniques for the types of contamination listed in Table 3. The technique should be one that will inspect all areas of surface treated panels or parts. The need for sophisticated equipment that can scan curved or shaped parts depends on the critical nature of the parts and the number of parts to be inspected. In many factory situations inspection of control samples may be sufficient. This study is limited to flat panels or parts but the techniques described in this report can be adapted to the inspection of shaped or curved parts provided the radii of curvature are not too small.

C. The Solution

1. Task II

The solution to the problem lies in the development of NDI tools that can detect deviations from an acceptable surface condition. The first step involves characterization of an acceptable surface, i.e., to identify the boundaries of signals from surface tools for which the surface is acceptable. The second step involves establishing which tools can detect deviations from the acceptable surface. The third step involves automatic scanning of surfaces with the surface tools to identify regions that deviate from the acceptance band (are contaminated). The type of readout depends on the circumstance and desired spacial resolution. A map of the part, showing contaminated regions, might be desirable. On the other hand automatic scanning with a light or sound warning if a given minimum area deviates from the acceptance band, might be desired. This

study is restricted to automatic mapping with a two dimensional contamination plot and/or averaging the deviation from the acceptance band over selected areas.

2. Task III

It has been understood from the beginning of this program that the decision as to acceptance criteria requires a comprehensive study of the relationship between contamination levels and bond strength and durability. It was decided at AFML to first establish (Task II) the sensitivity of surface tools to anticipated contamination and to develop mapping techniques. Task III would then be a follow-on study if Task II proved successful. Task III involves deliberate contamination of panels followed by surface mapping followed by bonding and durability testing. A correlation should exist between the NDI maps prior to bonding and the failure maps after fracture. The follow-on study will reveal the level of contamination that can be tolerated and thus provide the acceptance band for factory NDI. In this report we have prepared phosphoric acid anodized panels and mapped them prior to deliberate contamination. The acceptance band has been chosen as that in which all of the data fell for clean panels. This is probably more stringent than will be needed after Task III has been performed. For economy and time purposes, it is important that the acceptance band not be unnecessarily stringent so that acceptable parts are being reprocessed or rejected.

SECTION II

EXPERIMENTAL

A. Surface Techniques

1. Ellipsometry

Ellipsometry is nondestructive in that the sample is not touched by the instrument. A beam of polarized monochromatic light is reflected from the surface. Although the incident beam is plane polarized at an azimuth of 45° with respect to the plane of incidence (POI) the reflected beam is elliptically polarized. The parameters measured by the ellipsometer are Δ , the phase shift of light polarized perpendicular to POI with respect to that polarized parallel to POI, and ψ , the arctangent of the reflection coefficients for these components. An advantage of the ellipsometer is that Δ and ψ are absolute values, not dependent on the absolute light intensities but only on the ratio of the intensities. Although ψ is very sensitive to surface roughness, it is relatively insensitive to film thickness. On the other hand, Δ is extremely sensitive to film thickness and relatively insensitive to surface roughness. The phase shift Δ can be used to detect as small as 0.1\AA to as large as 5000\AA of oxide or hydroxide on a properly anodized aluminum surface or a film of contamination on top of the oxide with the same resolution.

Although ellipsometry is usually performed with the null light intensity method, we have invented (previous IR&D study) a technique for very rapid scanning³. Plane polarized light (6328\AA He Ne laser) is reflected from the sample surface. The intensity of the light at $0, 45$

and 90^0 azimuths are logged into the computer as a function of position on the sample. The mini-computer calculates Δ and ψ and records these values as a function of map position.

2. Surface Potential Difference (SPD)

The surface potential difference is the difference between the work function of the sample and that of a reference electrode. The work function of the sample is extremely sensitive to the outer dipole layer and is therefore extremely sensitive to contamination. The SPD can be measured by the Kelvin vibrating electrode technique⁴. The Fokker contamination tester and the Monroe Electronics, Inc. electrostatic voltmeter works on this principle and yield the same information as the radio active electrode. The potential driving the AC capacitive current of the vibrating system is just SPD. For the radio active electrode technique, the radio activity ionizes the air between the electrodes, thus reducing the gap resistance to a point that SPD can be measured with a high impedance electrometer. A description of the radio active technique used in Task II is given in reference 5.

3. Photo-Electron Emission (PEE)

The escape of photo-emitted electrons from metals depends strongly on the oxide film and surface contamination. We use a Pen Ray lamp that gives an intense UV light beam at $\sim 2500 \text{ \AA}$. This light has sufficient energy to emit electrons from aluminum but not oxides of aluminum. A description of this technique is found in Ref. 5.

4. Contact Angle

The contact angle of water on clean oxide covered metals is approximately zero (surface wettable) but becomes large for nonpolar contamination.

Unlike the other surface techniques, the contact angle is sensitive to the type of metal, oxide thickness, etc., but is extremely sensitive to the polar nature of the outermost atomic layer. Consequently, the contact angle measurement (water break test) has been standard for contamination detection for many years. Contrary to the other surface techniques, it is necessary to touch the surface by leaving a drop of water in the spot to be measured. Any contamination in the water or on its surface will deposit on the sample during evaporation. This may or may not be a serious problem depending on the water used and the system.

5. Auger Electron Spectroscopy (AES)

AES is a technique for chemical analysis of the outer 20Å of the surface. Due to the many unknown parameters involved in the shape and size of peaks in the spectrogram, quantitative analysis is not possible. However, the size of the peaks are related to the concentration of a given element and can be used for semi quantitative as well as qualitative analysis. AES (like SEM) is performed in high vacuum and is not amenable to NDI of actual parts but is used as a check on our NDI techniques. A description of our AES is given in reference 6.

B. The Anodizing Process

Although characterization of A11100 and A1 2024-T3 is reported here as well as for A1 7075-T6, AL 7075-T6 was mostly used for the contamination study. In the first part of this study we used Northrup's procedure (see Table 4) for surface preparation, except that in step 1 degreasing was by ultrasonic cleaning in trichloroethane. Later it was found that a degrease

step followed by the anodize step produced satisfactory films. We used a glass jar (see Fig. 1) rather than lead lined tanks as used at Northrup and McDonnell Douglas. Samples were anodized at the Science Center, at Northrup and McDonnell Douglas and then sent to each of the other facilities to be characterized.

TABLE 4

PHOSPHORIC ACID ANODIZE, NORTHROP PROCESS

1. Degrease - Trichloroethane Vapor
2. Alkaline Clean - 10 to 15 minutes
Turco 4215-S - 6-8 oz/gal
Operate at $155^{\circ}\text{F} \pm 10^{\circ}\text{F}$
3. Deoxidize - 5-10 minutes
Amchem 7-2.7 to 3.3 oz/gal
Nitric Acid - 8 to 16% by volume
Operate at R.T.
4. Anodize 20-25 minutes at 10 ± 1 VDC in 11-16 oz/gal phosphoric acid at R.T.
5. Oven dry at 150°F - 160°F

Note: Deionized water used in mixing solutions and rinsing between operations.

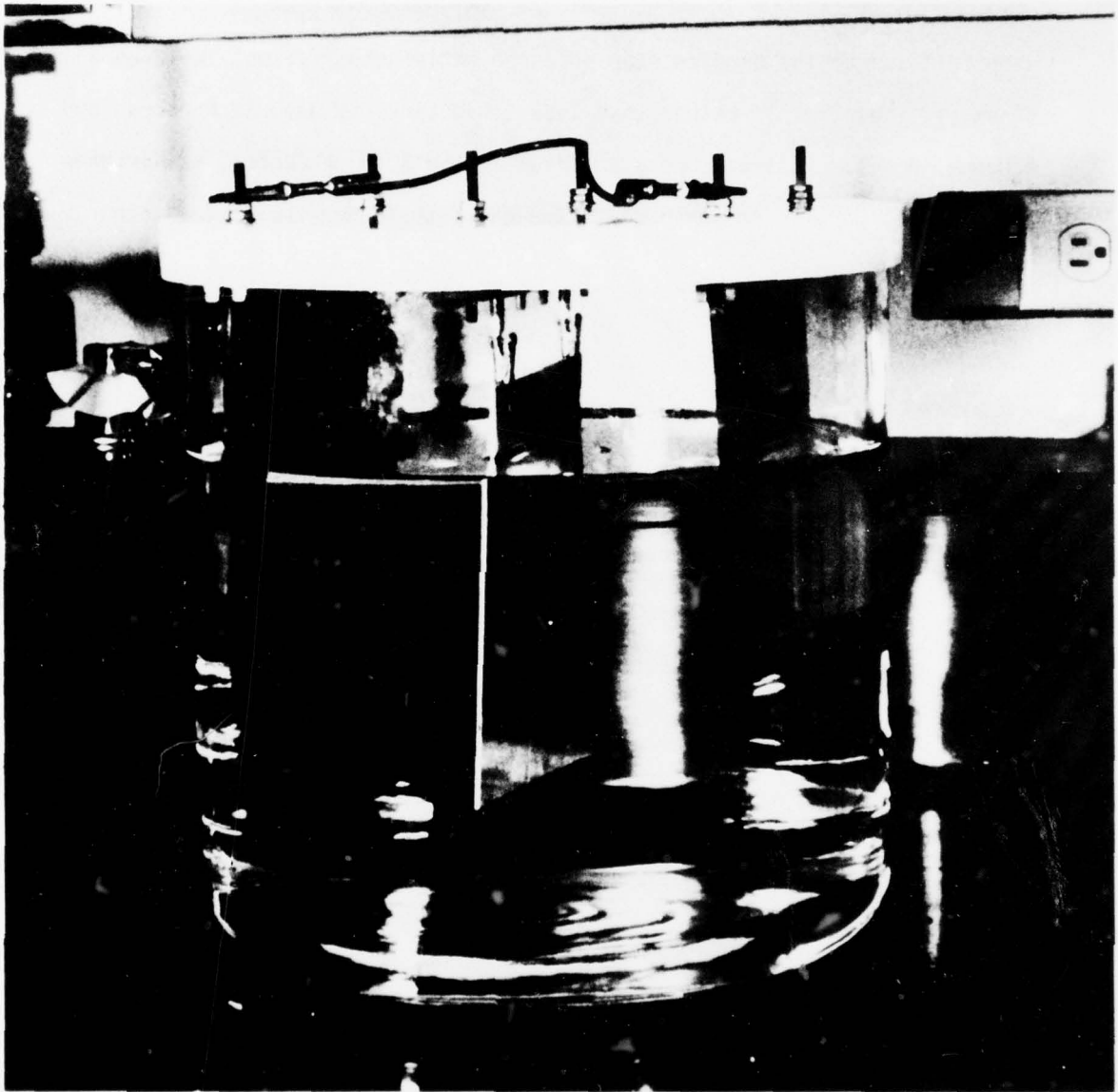


Figure 1 Photograph of the Anodizing Tank

All of the samples proved to be the same in character, indicating that the steps before anodizing need not be precisely the same and some of them can be eliminated. Further evidence for this is given in Table 5, where the surface properties are essentially the same (except for SPD) after anodizing regardless of the surface preparation prior to anodizing. The thickness values in Table 5 were estimated for film refractive index $n_f = 1.6$ for the pretreatment and $n_f = 1.3$ for the anodic treatment.

TABLE 5

EFFECT OF PRETREATMENT ON ANODIC FILM PROPERTIES

Al 2024-T3 $\lambda = 6328\text{\AA}$, $\phi = 70^\circ$

Pretreatment	Δ (deg)	ψ (deg)	Estimated Film Thickness (\AA)	SPD (volts)	PEE amps $\times 10^{11}$	$\phi\text{H}_2\text{O}$ (deg)
<u>Before Anodizing</u> ($n_f \sim 1.6$)						
As received	0.6	52.9	---	0.45	0.8	70
MEK degrease	90.0	34.2	190	0.56	0.1	60
FPL etch	113.6	36.8	120	0.37	28.0	40
<u>After Anodizing 16V, 22 min, 10% H_3PO_4</u> ($n_f \sim 1.3$)						
As received	108.0	44.3	4750	-0.15	1.5	7
MEK degrease	115.0	48.4	4820	-0.23	0.1	6
FPL etch	112.1	44.8	4800	-0.36	0.9	3

C. Computerized Mapping

There may be no need for a computer in the finally chosen NDI instrument but we are using a Data General "Eclipse" MDL S/200 minicomputer to control automatic scanning of the sample under the sensing heads, for data acquisition and data processing. In order to develop a field instrument, our approach is to first establish a signal range or band within which the sample surface is proper. This is done by mapping properly prepared samples and having the computer report the average signal value, the mean deviation from the average value and the maximum and minimum values. After storing the actual signal values for each sample position, we can print out the array and observe the *number map*; or, we can make a map with the X-Y plotter. The map is made by dividing the chosen area on the chart paper into an array of smaller areas and plotting within each small area a number of dots. The number of dots is proportional to the signal amplitude in the corresponding map position. To simulate field use, the computer is programmed to suppress any chosen band of the signal and plot deviation from the band. If the band is chosen as zero, all values that deviate from the mean are plotted. To reveal contamination in greater contrast, the band width is increased so that dots that correspond to proper surface are suppressed. Choice of the proper band width in the factory must await the study of Task III.

Figs. 2 and 3 show the instrument head mounting and closeup of the head, respectively. The numbers on the figures correspond to (1) laser, (2) beam expander, (3) polarizer, (4) analyzer, (5) PEE detector, (6) SPD detector, (7) sample, (8) electrometer, (9) water drop dispenser and detector. The sample is automatically moved under the detector heads.

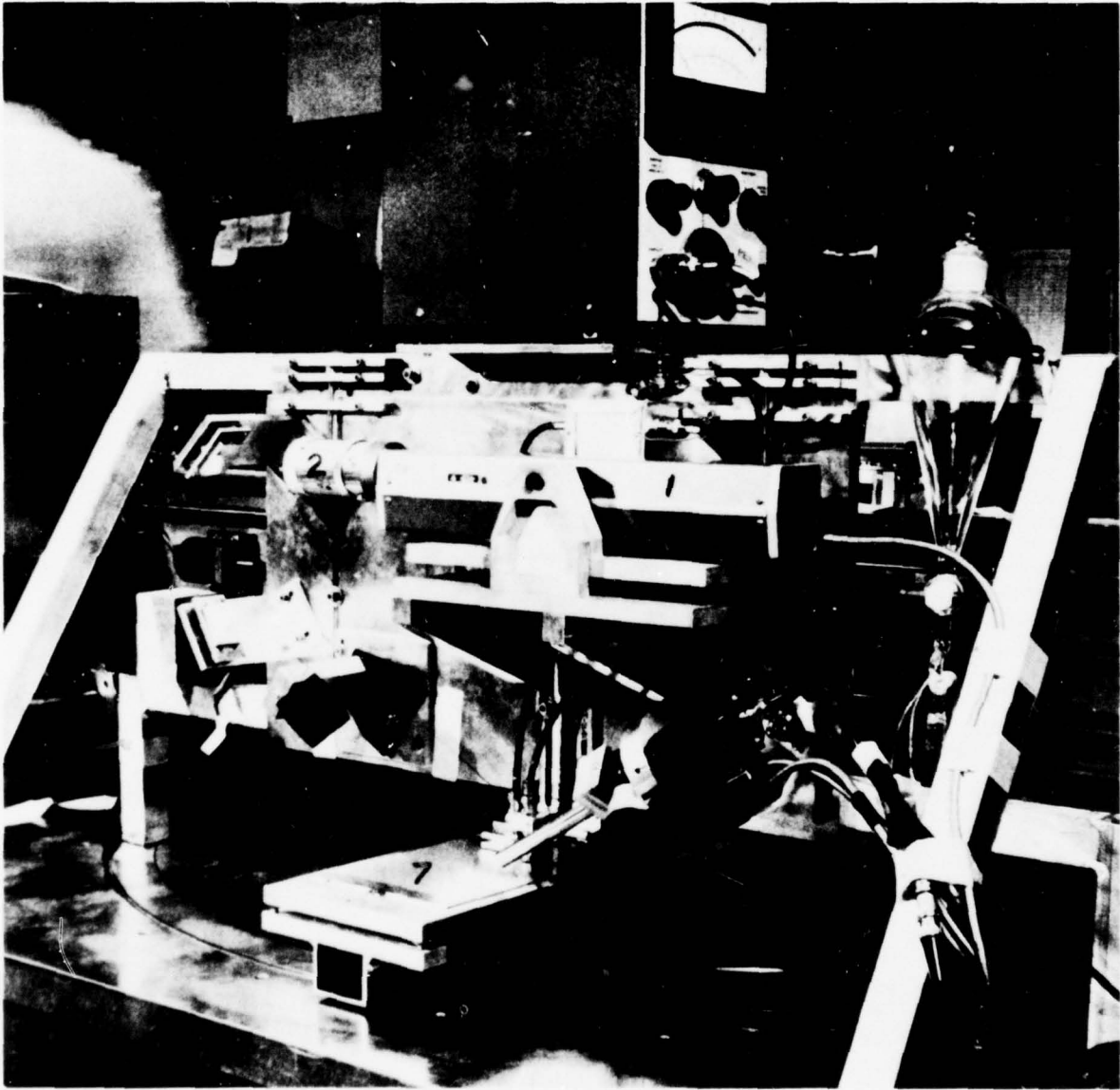
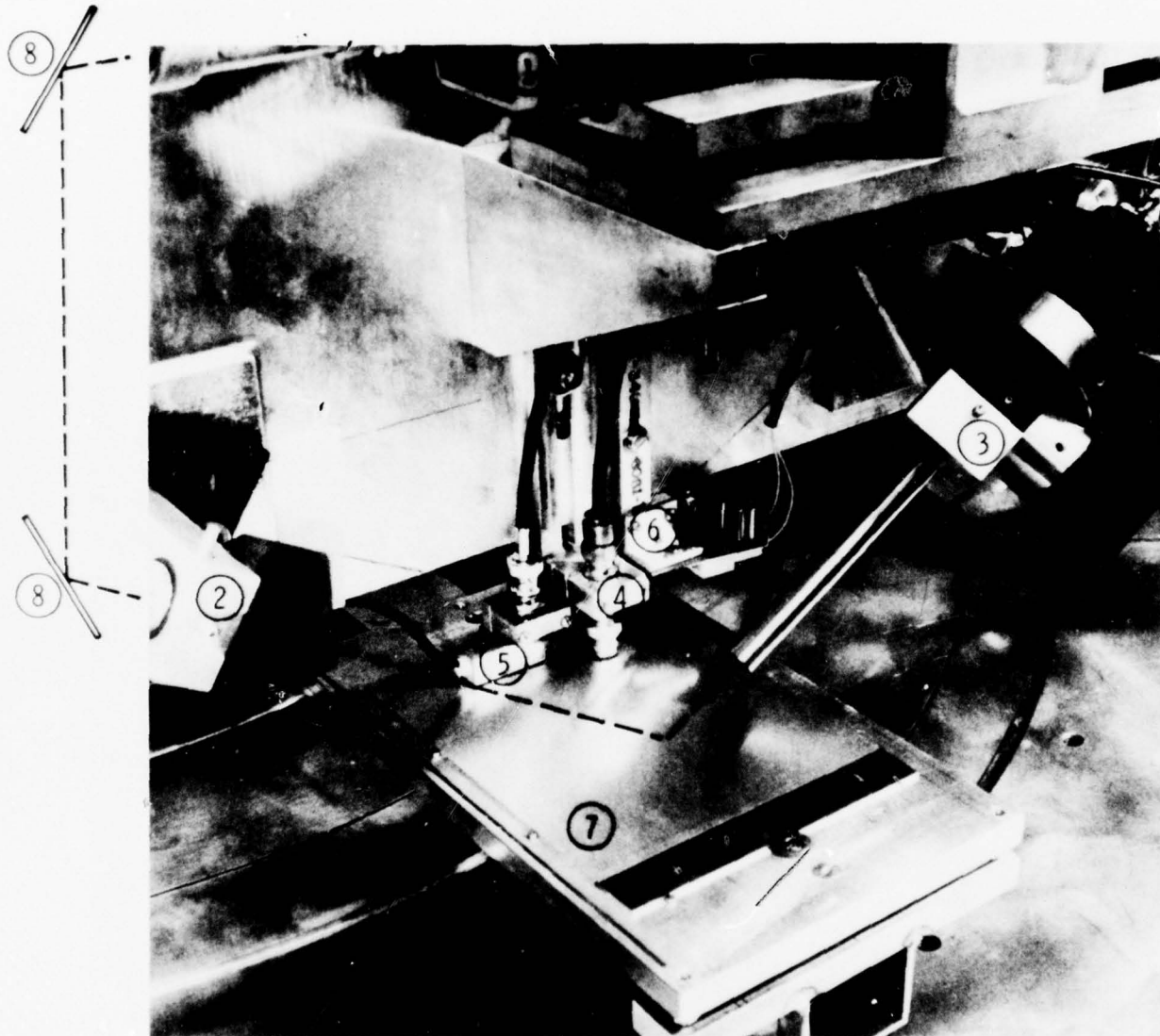


Figure 2 Photograph of the Surface Tools.



- | | | |
|----------------------------|-----------------|-------------------------|
| 1. LASER | } ELLIP SOMETER | 5. PHOTO EMISSION PROBE |
| 2. POLARIZER | | 6. CONTACT ANGLE PROBE |
| 3. ANALYZER | | 7. AL 7075-T6 PANEL |
| 4. SURFACE POTENTIAL PROBE | | 8. MIRRORS |

Figure 3. Sensor heads and sample for mapping with computer automated system

A plotting program was devised to provide two dimensional maps that would reveal areas for which signals deviate from some norm. Qualitatively, the density of dots, in a particular area, is proportional to the deviation of the signal from the norm and therefore proportional to the degree of contamination. The program calls for values of contrast, C , and intensity, I , which allow great flexibility in data portrayed. Fig. 4 illustrates the relationship between the signal amplitude A and the density of dots for the region the signal is monitoring. The abscissa in Fig. 4 scales the amplitude values between 0 and 6. That is, after mapping the area of interest all of the amplitude values are divided by the maximum value, A_{\max} . For each amplitude value (for a particular position in the map) the computer computes a transfer function AINTENS from the equation,

$$(AINTENS - 4) = \left(\frac{6}{6-C} \right) \left[6(A/A_{\max}) - (3 - \frac{I}{2}) \right] .$$

The computer then rounds AINTENS to the lower integer, yielding six possible levels, e.g., AINTENS = 1.99, is rounded to 1 and 3.99 to 3, etc. The computer divides the area that is mapped into a 43 x 43 array of smaller areas and places up to 15 dots in each area. The number of dots placed in unit area depends upon the rounded down value of AINTENS as shown at the left of Fig. 4. Examples of the transfer function for $C = 4$, $I = 0$; $C = 0$, $I = 0$; $C = -5$, $I = 0$, and $C = 0$, $I = -4$ are given in Fig. 4. For a given value of I (which determines the intercept) C determines the slope. The values of I and C are integers between -5 to +5. For illustrative

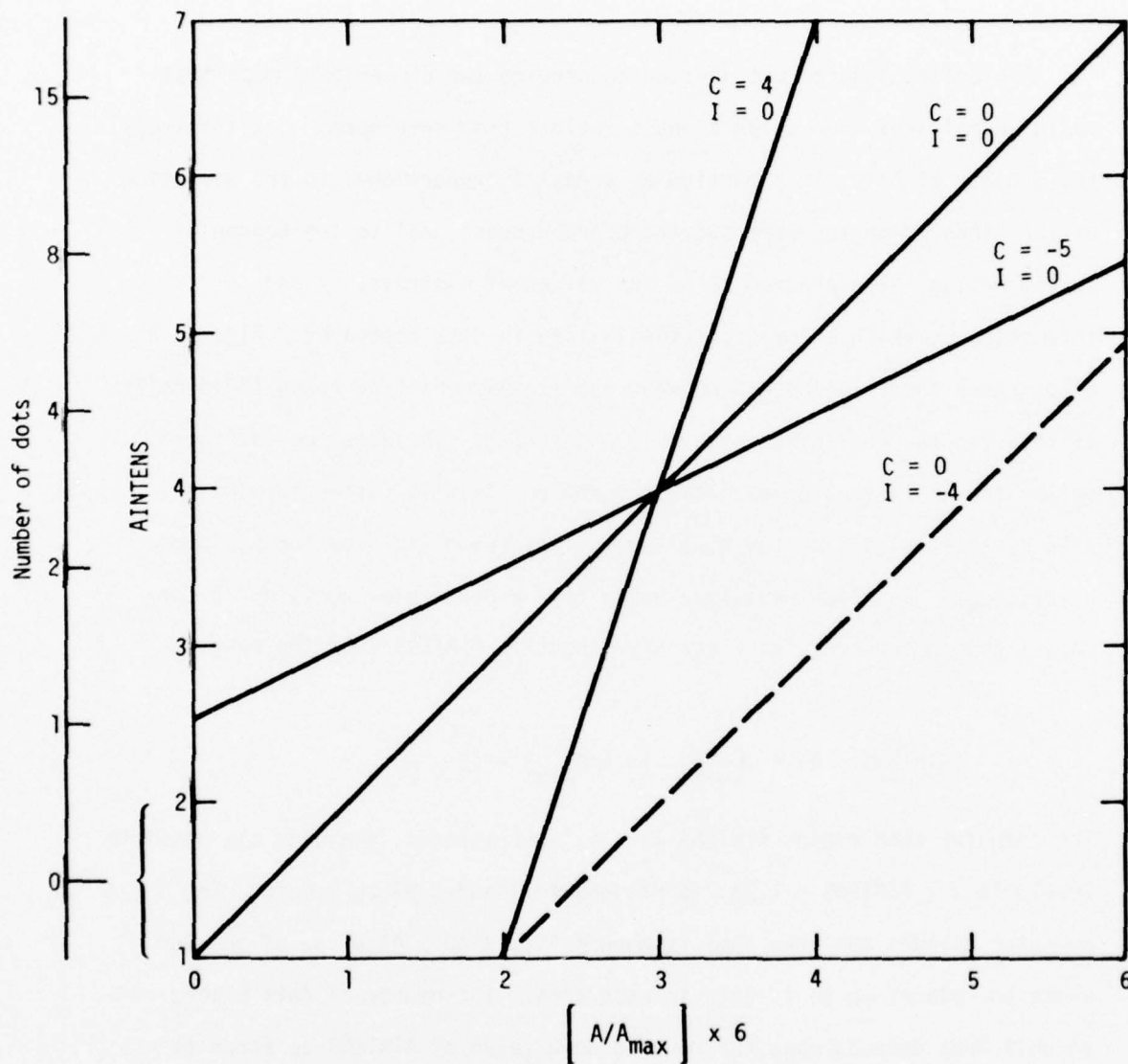


Figure 4. Plots of AINTENS vs. $\left[\frac{A}{A_{\max}} \right] \times 6$ for various values of C and I.

purposes consider the curve for $C = 0$, $I = 0$; if the scaled amplitude $(A/A_{\max})^6$ is between 0 and 1, AINTENS is between 1 and 2 and will be rounded to 1 and zero dots will be mapped for the unit area, if the scaled amplitude is between 5 and 6, 15 dots will be mapped. The exponential relationship between AINTENS and the number of dots, relates to the inability of the eye to distinguish differences in dot density at high density as compared to low density. Increasing contrast C suppresses low values of A and enhances high values of A . For a given value of C , I translates the curve along the horizontal axis, e.g., compare $C = 0$, $I = 0$, and $C = 0$, $I = -4$. Increasing I increases the density of dots for a given value of A .

The program is also devised to suppress or include only the data in a particular amplitude range. For example suppose a Δ map yields values of

$$\Delta_{\max} = 170$$

$$\Delta_{\min} = 150$$

for a contaminated sample and

$$\Delta_{\max} = 165$$

$$\Delta_{\min} = 155$$

for uncontaminated control samples. All values between $155 < \Delta < 165$ can be mapped as zero dots. Values of $165 < \Delta < 155$ can be given values of $A_a - 165$ and $155 - A_b$, where the subscript a refers to above 165 and b to below 155. In this case A_{\max} would be 5 and A would vary between 0 and 5. For

$A = A_{\max}$ (i.e. $\Delta = 170$ or 150), fifteen dots would be plotted in unit area, for $\Delta = 168$ or 153 , four dots would result, if $C = 0$, $I = 0$. On the other hand, all of the values between any two values of A can be included in the plot and all values outside suppressed.

Maps of SPD are given in Figs. 5 and 6 to illustrate the effect of C , I and the suppression band. The map is for an Al 7075-T6 anodized panel that had a thumb print in the top left corner and contamination along the edges. The relationship between the values of A and SPD in Figs. 5 and 6 is $SPD \approx A \times 10^{-4}$.

Figs. 5a and b show the effect of changing the C , I values from $C = 4$, $I = 4$ to $C = 0$, $I = 0$, for a given band of 3000 to 3500. The maps include all values between 3000 and 3500 and suppress all others. There is little difference in the appearance of a and b in Fig. 5.

Figs. 5c and d show the effect of changing the suppression band. Fig. 5c plots all values, whereas d plots only values outside 4700 to 6600. The thumb print is beginning to show in Fig. 5c. Fig. 5c plots only data inside 2480 to 3000 and Fig. f all data above 2480. The effect of using these two bands is to produce pictures similar to a negative and positive photograph. Figs. 6a to f show maps for various C , I and suppression bands. All of them reveal the contamination, but the parameters for Fig. 6b appear to give the best map in terms of exposing the contamination but suppressing background. It is a simple matter to try various combinations of C , I and band width that will produce a map that reveals known contamination and then continue to use these optimum parameters for unknown contamination.

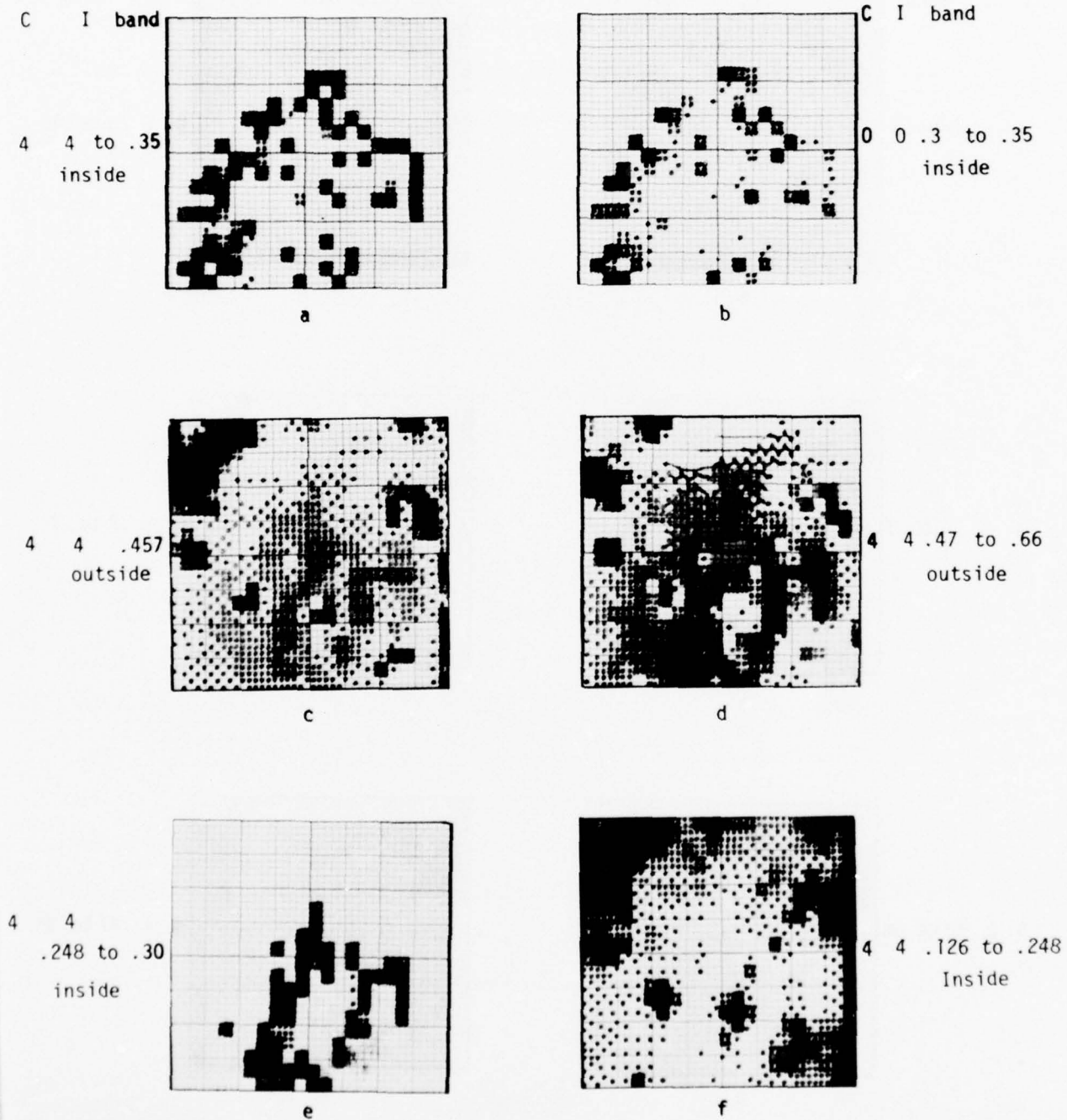


Figure 5. Computer plots of SPD to show the effect of C and I.

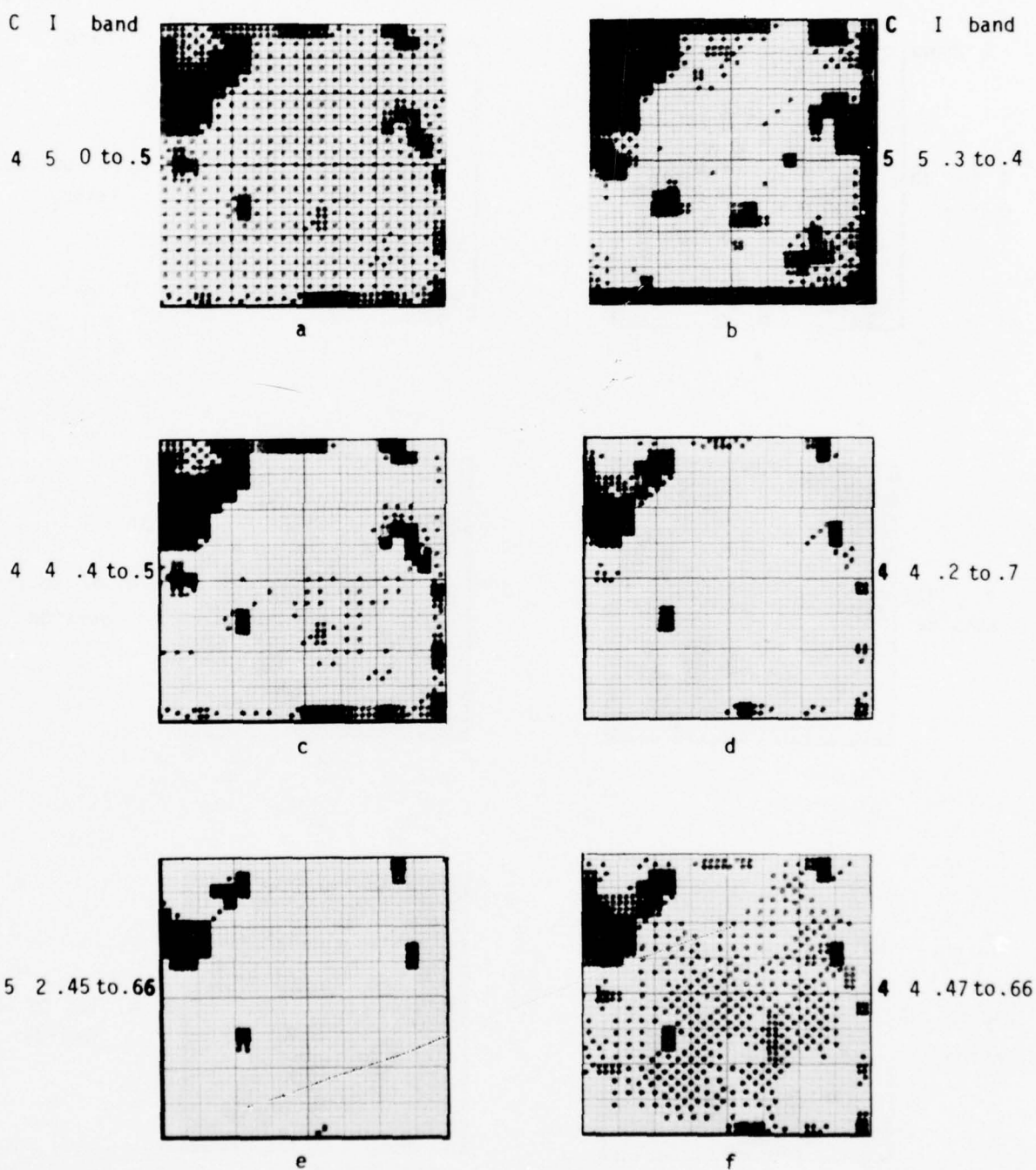


Figure 6. Computer plots of SPD for panel with thumb print.

SECTION III

EXPERIMENTAL RESULTS

A. Characterization of Anodic Films

At first, small 1" x 4" x 1/10" Al 7075-T6 samples were anodized to check the physical properties and reproducibility of the anodic films. Ellipsometric, SPD, and contact angle measurements were made in six positions on each of 44 anodized samples. From the 264 measurements, average values of $\Delta = 167.9 \pm 3.8$, $\psi = 36.8 \pm 1.0$ were obtained for $\lambda = 6328 \text{ \AA}$ and an angle of incidence of 70° . These samples were anodized at different times over a period of two months. Measurements of SPD averaged -0.057 ± 0.005 volts for some of the samples during one period and $+0.075 \pm .020$ volts for other samples at another time, yielding an average value of about $0.010 \pm .01$ volts for all of them. Measurement of the water contact angle averaged 5.1° , the samples all being quite wettable. For PEE the relatively thick anodic films attenuate the emission current to very low values as compared to FPL etched samples. For example the PEE current averages about $2-4 \times 10^{-11}$ amps for the phosphoric acid anodic films as compared to about 30×10^{-11} amps for FPL etched films. In order to interpret ellipsometric data for films $>2000\text{\AA}$, it is necessary to track Δ and ψ as the film thickens. Also, it has been shown⁷ that surface roughness primarily affects ψ whereas film thickness primarily affects Δ . Therefore, ellipsometric measurements were made as a function of anodic voltage for fairly smooth electropolished Al 1100 then for rough FPL etched Al 7075-T6 and for rough FPL etched Al 2024-T3 for comparison. The curve in Figure 7 is a plot of the theoretical values of Δ vs ψ for films of refractive index $n = 1.3$ on perfectly smooth aluminum with complex refractive index $\hat{n}_s = n_s (1 + iK_s)$ where $n_s = 1.43$ and $K_s = 5.17$ for wave

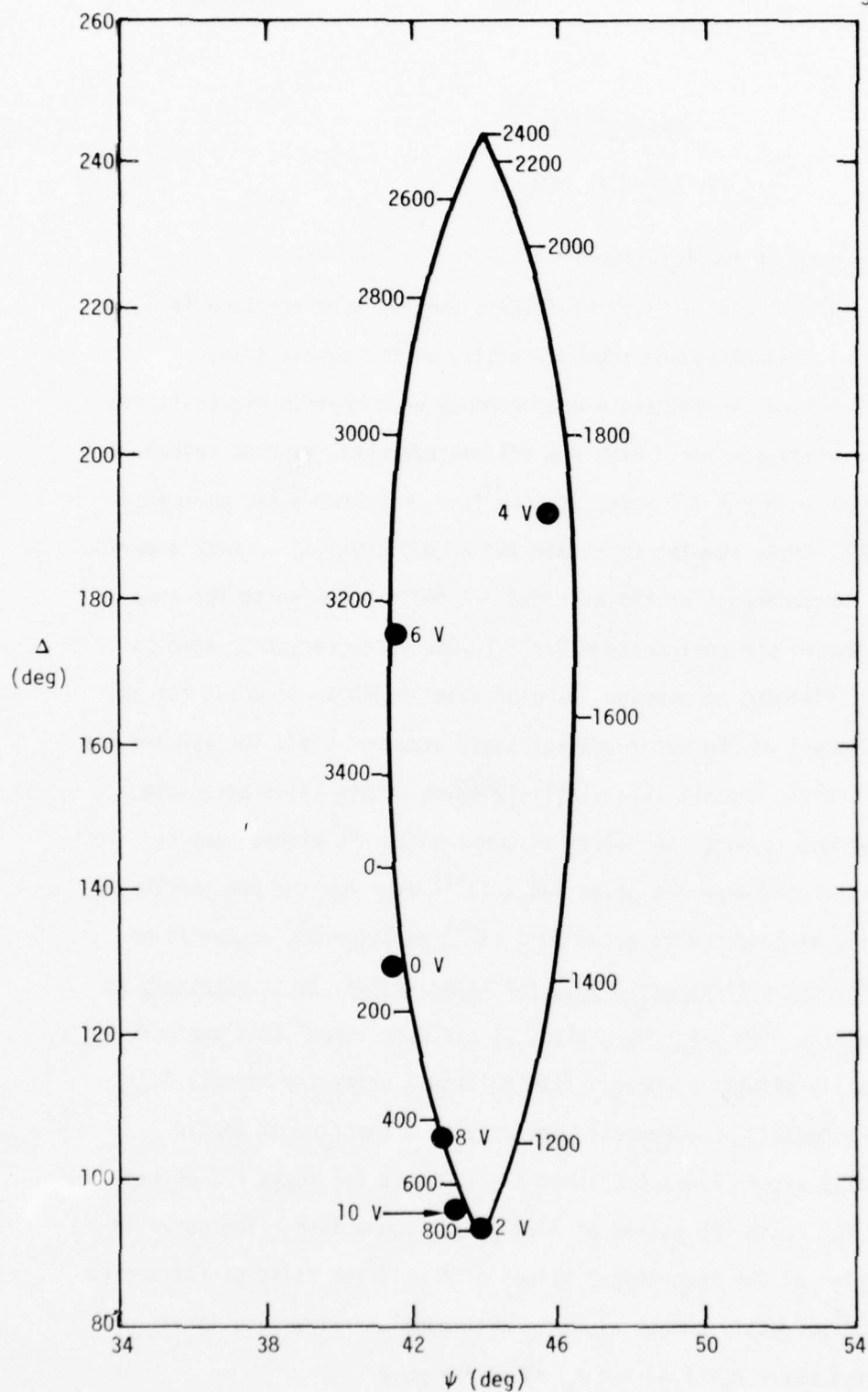


Figure 7. Δ vs. ψ plot for a theoretical film (curve) of refractive index 1.3 and thicknesses indicated. The solid circles are experimental data for phosphoric acid anodized Al 1100 that had been previously electro-polished to smooth the surface.

length $\lambda = 6328\text{\AA}$ and angle of incidence 70° . The solid circles in Fig. 7 are experimental data for the electropolished Al 1100. The numbers along the loop in Fig. 7 are film thickness in Angstroms. The black circles are labelled with the anodic voltage. The initial film thickness after electropolishing is about 120\AA ending at 4250\AA at 10 volts. To check this number the sample was bent to fracture the metal and expose an edge view of the hydroxide film. Fig. 8a reveals the film is $4290\text{\AA} \pm 500\text{\AA}$, in close agreement with the ellipsometer.

Values of Δ vs ψ for rough FPL etched Al 7075-T6 (solid circles) and Al 2024-T3 (circle with \otimes) are plotted in Fig. 9. As for previous experiments⁽⁷⁾, the effect of roughness is to broaden the range of ψ . Estimates of film thickness from Δ values alone vs anodic voltage is given in Fig. 10 for the various samples. An SEM check on the Al 2024-T3 sample anodized at 10 volts for 22 min is given in Fig. 8b. The hydroxide can be seen scattered over the surface, but due to the brittle nature of the alloy the type of fracture that clearly reveals the film edge (as in Fig. 8a) is not obtained. No interpretable SEM results for Al 7075-T6 was obtained. An estimate of the film thickness for Al 2024-T3 in Fig. 8b is $\sim 3000 \pm 1000\text{\AA}$ in agreement with the ellipsometric result in Fig. 9. The average increase in film thickness per volt is above 300\AA for the alloys and about 400\AA for the Al 1100. These values are much larger than $14\text{\AA}/\text{volt}$ when aluminum is anodized in borate solutions and form barrier type films. The much greater rate of film growth with voltage is due to the porous nature as is the low index of refraction. Barrier aluminum oxide or hydroxide films have a refractive index of about 1.6-1.7 as compared to 1.3 for the phosphoric acid anodic films. Assuming



Figure 8a. SEM picture of electro-polished Al 1100 after anodizing at 10 volts for 22 minutes and bending to reveal hydroxide film edge.



Figure 8b. SEM picture of Al 2024-T3 after FPL etch and anodizing at 10 volts for 22 minutes then bending.

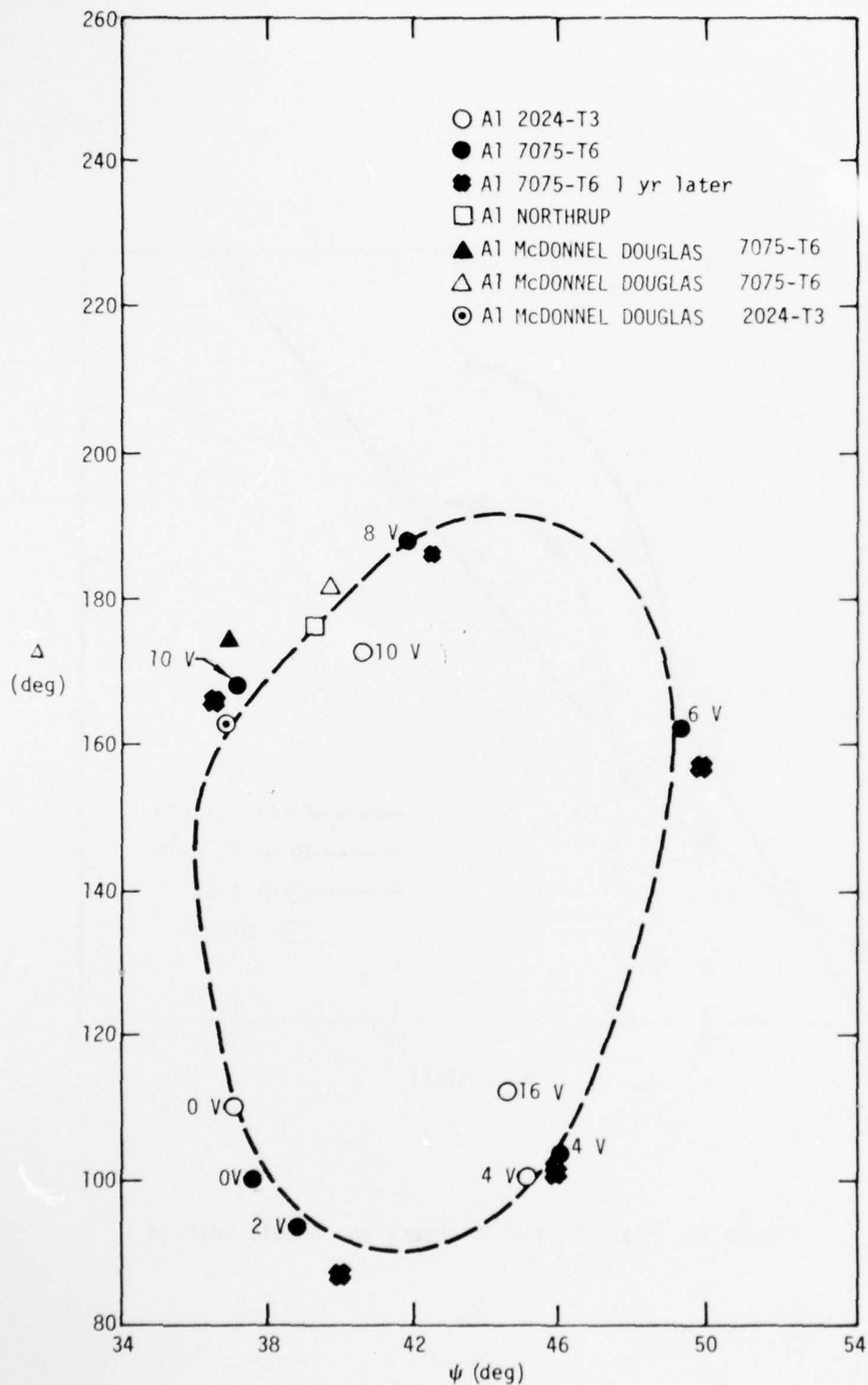


Figure 9. Δ vs. ψ plot for rough Al 7075-T6 and Al 2024-T3 anodized samples (at the indicated voltage for 22 minutes), $\lambda = 6328 \text{ \AA}$, $\phi = 70^\circ$

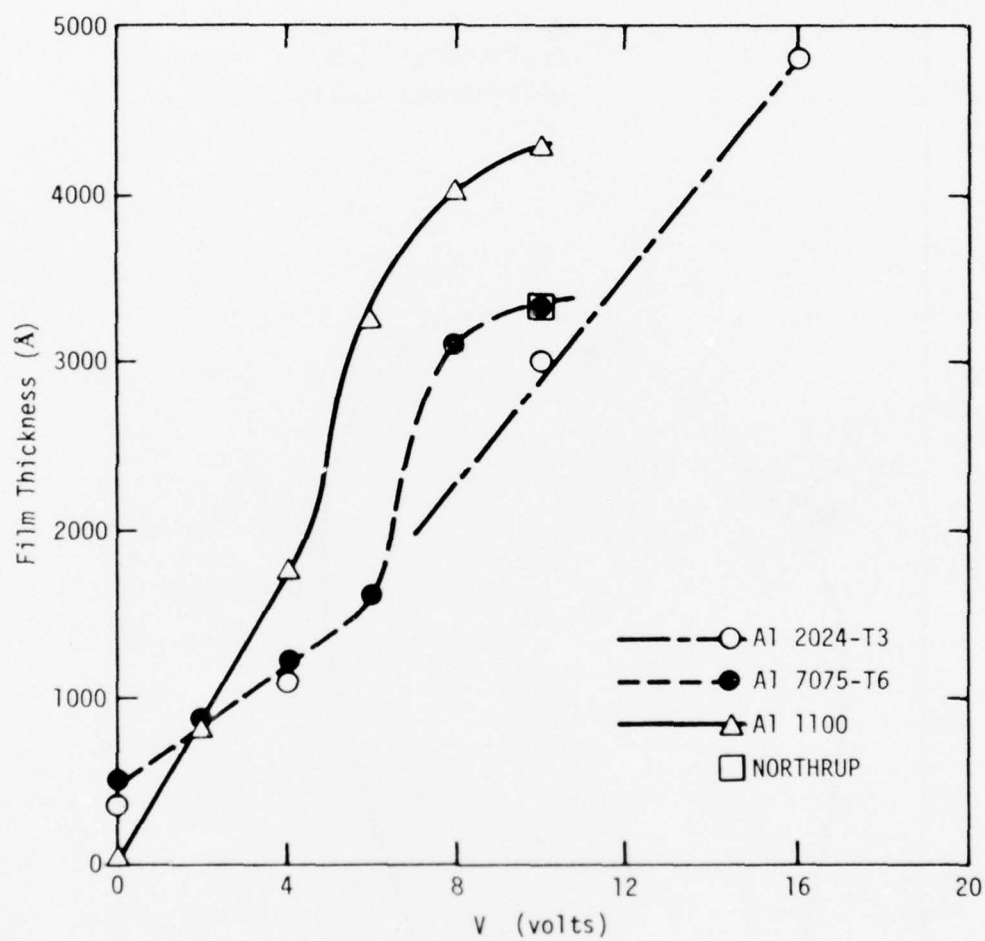


Figure 10. Plot of Film Thickness vs. Anodic Voltage

a linear relation between refractive index and film density (porosity) the phosphoric acid anodic films are about 20% porous.

A comparison of the ellipsometric parameters Δ and ψ as well as SPD, PEE and water contact angle ϕ_{H_2O} for samples from various facilities is given in Table 6. Samples with dimensions about 1" x 4" x 1/10" and panels of about 6" x 6" x 1/6" and 6" x 6" x 1/8" have been studied after the standard phosphoric acid anodic treatment (10V, 20 to 22 min). The standard anodic treatment yields $\Delta \sim 170-180^\circ$ and $\psi \sim 38^\circ$ regardless of the originating facility. It should be noted that the same Δ and ψ values correspond to a film about 2000Å thick if the index is 1.7 as for nonporous alumina. The SEM results confirm the thickness to be between 3000 and 4000Å.

All of the fresh samples (within 2 or 3 days) were water wettable with $\phi_{H_2O} \sim 0$ to 5 degrees. Samples Md1, 2, MD3, 4, MD5, 6 and MD7, 8 from McDonnell Douglas but sent to us by Northrup, were much older and had been wrapped in brown paper. The contact angles were near 100° indicating contamination.

The surface potential difference (SPD) changes from day to day but is useful for comparing samples at a given time. The SPD is about 0.3 for clean samples and 0.45 for contaminated samples on the day of measurement for Table 6. A corresponding decrease in PEE is noted for contaminated samples. Clean samples yielded ~ 14 to 18×10^{-11} amps as compared to 7 to 11×10^{-11} amps for contaminated samples.

TABLE 6

SURFACE PROPERTIES OF ALUMINUM ALLOYS 7075-T6 AND
2024-T3 AFTER PHOSPHORIC ACID ANODIZE FROM VARIOUS FACILITIES

H_3PO_4 10V 22 Min

Facility* and No.	Sample Dimensions	Δ (deg)	ψ (deg)	Thickness		ϕ_{H_2O} (deg)	SPD Volts	PEE amps x 10 ⁻¹¹
				from Δ Å	from SEM Å			
Al 7075-T6								
SC	1"x4"x1/16"	168±4	37±1	3300	3000± 1000	5	0.3	
SC	5"x7"x1/16"	179.8±4	38±1	3200		5	0.3	14±1
NC	1"x4"x'/16"	175±4	39±1	3250	3500	6	0.29	
MD 1-2	~5"x4"x1/16"	171	35	3280	4400	100	0.45	11
MD 7-8	~5"x4"x1/16"	183	38	3220	4200	100	0.45	8
MD	6"x6"x1/8"	182±3	40±1	3210		2	0.27	18
Al 2024-T3								
SC	1"x4"x1/16"	172±4	41±1	3260		5		
		if $n_f = 1.7$		2000				
MD 3, 4	5"x4"x1/16"	172	37	3260	3000- 4000	100	0.35	7
MD 5, 6	5"x4"x1/16"	190	40	3120	3300	100	0.48	7

* SC - Science Center
NC - Northrop Corp
MD - McDonnell Douglas

Table 7 gives a summary of the chemical properties (ESCA) of FPL etched Al 2024-T3, sample, a 10 volt, 10 min phosphoric acid anodize sample and a similar anodic film after boiling in water. The results indicate that phosphoric acid anodized hydroxide film on AL 2024-T3 has about 60% of the water content of boehmite and that the oxide on FPL etched Al 2024-T3 is stoichiometrically much closer to alumina than boehmite. An alumina crystal was used as a standard of known oxygen to aluminum ratio. The carbon impurity 1S 1/2 peak was adjusted to 284.3 ev in each case to correct for charging. The binding energies are therefore relative to the carbon peak. The column labelled chem. shift gives the difference in binding energy between the oxygen and aluminum of the oxide films and the oxygen and aluminum of the standard Al_2O_3 . The relative peak heights were obtained by multiplying the maximum number of divisions on the recorder paper for a particular peak, by the number of counts per division and by dividing by the number of scans and the cross section for the particular element. The relative concentration was obtained by dividing the relative peak height by the total of all the relative peak heights. This procedure is incorrect but gives a first order approximation for the relative concentration of the impurities. For example the ratio of the relative concentrations for O and Al in the standard Al_2O_3 should be 1.5 as compared to 3.3 from Table 7. Therefore the formulas on the right of Table 7 for the hydrates are derived from the ratio of the relative concentration of O to Al but multiplied by the correction factor $1.5/3.3 = 0.45$.

All of the oxide films show a chemical shift of ~ 0.7 to 0.9 ev for oxygen and 0.4 to 0.9 ev for the aluminum in spite of the fact that the relative concentrations indicate that the FPL and anodic films are only partially hydrated. It was noted that the O/Al ratio decreased with time in the vacuum system for

the FPL Al 2024-T3 sample and therefore the hydration number may be low. On the other hand aluminum boiled in water is known to produce a boehmite film ($\text{Al}_2\text{O}_3(\text{H}_2\text{O})$) and the ESCA results confirm this. It follows that if the FPL and anodic films are boehmite they are not as stable in vacuum as that produced in boiling water.

TABLE 7

ESCA Results for Films on Al 2024-T3

Sample	Element	Photoline	Relative Peak height	Relative Conc.	Binding Energy	Chem Shift	Oxide or Hydroxide
Standard Al_2O_3	O	2S $\frac{1}{2}$	7,500	0.614	530.3		Al_2O_3 Alumina
	Al	1S $\frac{1}{2}$	2,273	0.186	118.1		
	C	1S $\frac{1}{2}$	2,444	0.200	284.3		
			<u>12,217</u>				
FPL etch Al 2024-T3	O		13,750	0.751	531.2	0.9	$Al_2O_3 \cdot (H_2O)_{0.2}$
	Al		3,864	0.211	118.7	0.6	
	C		<u>685</u>	0.037	284.3		
			<u>18,299</u>				
Anodic film 2024-T3 10V, 10 min ↓ boiled in water	O		20,892	0.670	531.0	0.7	$Al_2O_3 \cdot (H_2O)_{0.6}$
	Al		5,342	0.171	119.0	0.9	
	C		4,474	0.143	284.3		
	P	2S $\frac{1}{2}$	313	0.010	192.0		
	Si	2S $\frac{1}{2}$	128	0.004	154.0		
	Mn	3P $\frac{1}{2}, 3/2$	43	0.001	50.0		$Al_2O_3 \cdot (H_2O)$ Boehmite
	O		6,000	0.621	531.1	0.8	
	Al		1,364	0.141	118.5	0.4	
	C		1,852	0.192	284.3		
	P		145	0.015	191		
	N	1S $\frac{1}{2}$	50	0.005	399.5		
	Cl	2S $\frac{1}{2}$	256	0.026	269.2		

B. Sensitivity to Contamination

1. Processing Errors

The sensitivity of the surface tools to processing errors of three types were considered, i.e., wrong anodizing voltages, times and post anodizing exposure to phosphoric acid. Table 8 gives the ellipsometric, SPD and PEE results. Estimated film thickness from the manual ellipsometric results indicates about 300Å per volt. It should be noted that for Table 8 the manual ellipsometric data were taken at an angle of incidence $\phi = 60^{\circ}$ rather than 70° to coincide with the automated ellipsometer. As noted in the experimental section the automated values of Δ and ψ are different from the manual mulling technique due to surface roughness.

TABLE 8

SENSITIVITY OF SURFACE TOOLS TO PROCESSING ERRORS

Anodic Parameters			Ellipsometry, $\lambda = 6328, \phi = 60^0$							
			Automated		Manual		SPD		PEE	
Potential	Anodize Time	Post Anodize Time	Δ	ψ	Δ	ψ	Esti- mated Thick.			
(volts)	(min)	(min)	(deg)	(deg)	(deg)	(deg)	Å	(Volts)	(amps x 10 ⁻¹¹)	
<u>Anodize</u>								Fresh	Aged 6 Mo.	
5	20	0	160	45	152	45.5	1400	0.5	0.3	6
10	20	0	158	40	153	40.8	3300	0.3	0.2	6
15	20	0	162	40	157	46.1	4650	0.2	0.2	6
20	20	0	145	45	135	42.3	5900	0.06	0.1	6
25	20	0	166	39	170	41.0	7200	-0.1	-.2	6
<u>H₃PO₄ Exposure</u>										
10	20	0	167	44	170	42.0	1475	0.2		4
10	20	2.5	155	44	152	45.0	1375	0.5		5
10	20	5.0	144	40	122	41.0	225	0.7		20
10	20	7.5	144	38	124	38.7	225	0.7		120
10	20	10.0	141	35	117	36.0	270	0.7		160

Figure 11 is a plot of SPD vs hydroxide thickness (anodic voltage) for fresh Al 7075-T6 and Al 2024-T3 and aged (6 months) Al 7075-T6. The water contact angle ϕ_{H_2O} for freshly anodized aluminum is near zero whereas that for the aged (contaminated) aluminum $\phi_{H_2O} \sim 50^\circ$. In each case the SPD decreases approximately linearly with film thickness. The relative position of the curves are ambiguous due to drift in the reference electrode; however, the slopes of the lines are significant and indicate that the hydroxide on Al 2024-T3 is different than that on Al 7075-T6. SEM pictures indicate that at a given voltage the hydroxide film on Al 2024-T3 is thinner (and perhaps more dense) than for that on Al 7075-T6.

FPL etched aluminum alloys have a film thickness of about 100\AA and PEE of about 30×10^{-11} amps. Anodic films of 1400\AA or greater (Table 8) yield about 6×10^{-11} amps. The constancy of PEE with thickness indicates that photo emission may be from the outer region of the hydroxide film rather than from the substrate metal. However, this is unlikely because alumina does not emit until the photo energy is of the order of 9 eV as compared to 5 eV used in these measurements. Another possibility is that the hydroxide is essentially transparent to electrons in the porous outer film but are attenuated by the inner barrier layer.

Data at the bottom of Table 8 reveal that exposure to H_3PO_4 after anodizing decreases the film thickness about 100\AA in the first 2.5 minutes and about 1150\AA in the next 2.5 minutes. Further exposure leaves about 225\AA of film but roughens the surface with etch time. The increased roughness is indicated by the decrease in ψ and the increase in PEE.

These results demonstrated that the ellipsometer and SPD are sensitive to film thickness but that PEE and water contact angle are not. For small changes in film thickness ($<200\text{\AA}$) Δ changes by about $1\text{deg}/10\text{\AA}$. The SPD changes by about $-1\text{ mv}/10\text{\AA}$ for Al 7075-T6 and $-2.4\text{ mv}/10\text{\AA}$ for Al 2024-T3.

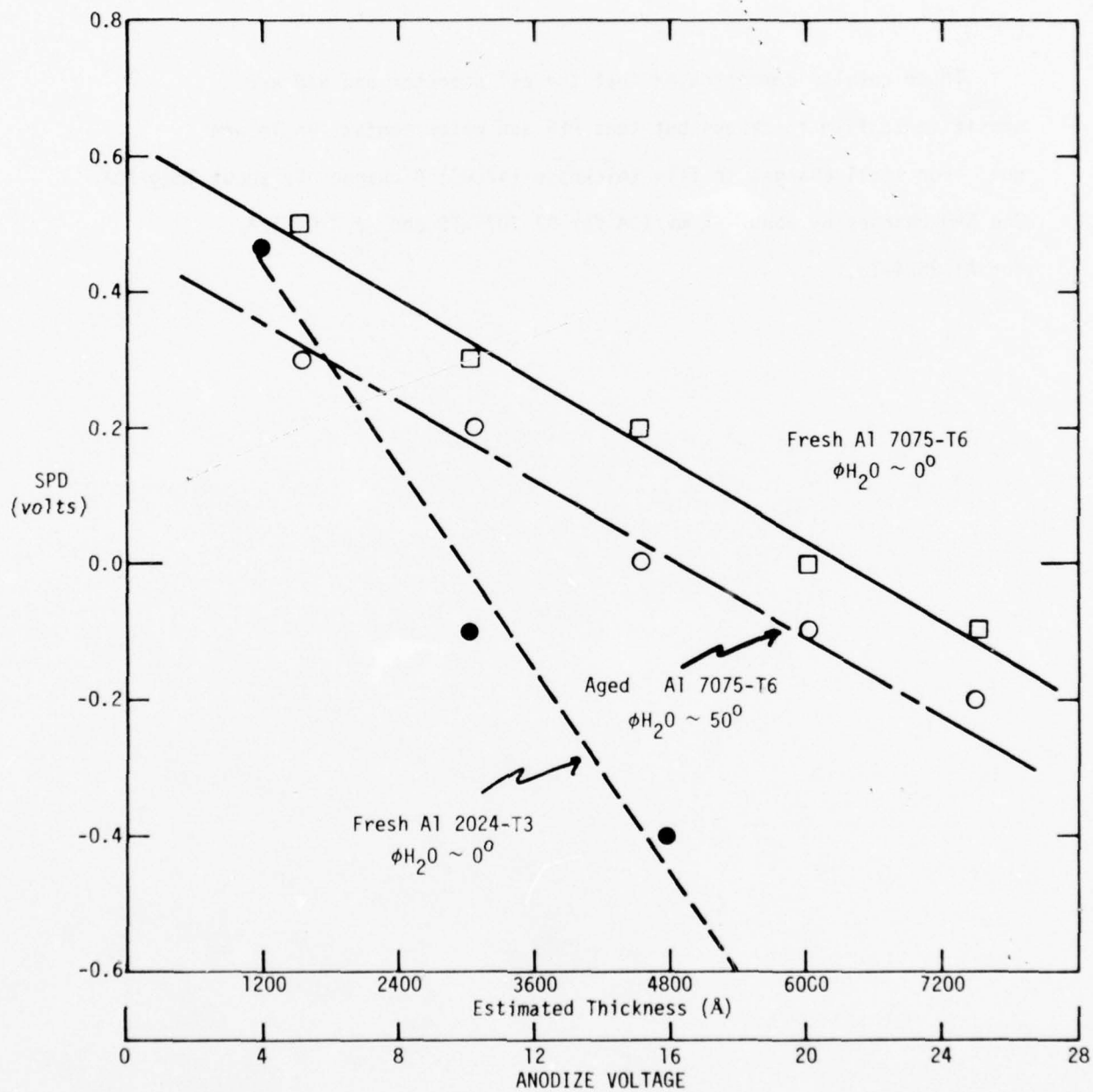


Figure 11. Effect of hydroxide film thickness (anodize voltage) on SPD.

2. Handling Damage

It was discovered at McDonnell Douglas by M. Danforth, that rubbing a phosphoric acid anodized Al 7075-T6 surface with a clean cotton glove or Kraft paper would degrade the surface with respect to bond endurance by the wedge test. Table 9 is a report of change in surface properties due to rubbing with various materials. Samples of Al 7075-T6 that had been anodized at McDonnell Douglas (referred to as MD) along with samples anodized at the Science Center (referred to as SC) were rubbed with very light pressure, medium pressure and hard pressure. Prior to and after rubbing, the samples were measured with ellipsometry (Δ and ψ), SPD, PEE and water contact angle (ϕ_{H_2O}). Under the pressure column in Table 9, control, refers to measurements prior to the rubbing.

All of the control samples, except SC #3, had similar surface properties; i.e., $\Delta \sim 182$ to 188 deg, $\psi \sim 41$ to 43 deg, SPD ~ 0.2 volts, PEE 8×10^{-11} amps and $\phi_{H_2O} \sim 0$. SC #3 was anodized in phosphoric acid solution that had been contaminated by anodizing an as-received sample without prior degreasing. It is important to note that the surface properties after anodizing in contaminated solution are quite different than after anodizing in clean solution, i.e., the surface tools would easily detect that something was wrong during processing.

The low value of ϕ_{H_2O} for #3 indicates that although the contaminated solution drastically changed the hydroxide film, it did not contaminate the surface with organic material.

The effect of rubbing the anodized surface with cotton, Kraft paper, Kimwipe paper tissue, is about the same, i.e., increase Δ , decrease ψ , increase SPD, and increase ϕ_{H_2O} , with little change in photoelectric emission (PEE). To see if rubbing with material that was contamination free would affect surface parameters, the surface of SC #3 was rubbed with quartz wool. The cleanliness of the quartz wool was checked by allowing single wool fibers to touch water. The fibers were immediately wetted indicating they were clean. The surface property trends are the same for rubbing #3 (end of Table 9) with contamination free material as for all the other materials, indicating that the changes are not due to contamination but due to some mechanical disturbance of the hydroxide film.

To deliberately contaminate a surface with a low energy material, SC #1 was rubbed with a clean Teflon bar. Δ decreased by 10^0 rather than increase, SPD increased from 0.13 to 0.3, PEE decreased from 12×10^{-11} amps to 8×10^{-11} amps and ϕ_{H_2O} increased from 0 to 50 deg. It was also thought that if contamination particles were deposited by rubbing with the different materials, that heating the sample might cause the contamination to spread. A sample MD 7075-T6 #12 was heated with a hot air gun after rubbing with Kraft paper (3rd area of #12, Table 9). The only property to change appreciably was SPD from 1.1 to 0.5 volts. Again, it was concluded that contamination is not the cause of change in surface properties.

TABLE 9

SURFACE PROPERTIES OF PHOSPHORIC ANODIZED Al 7075-T6 AFTER MECHANICAL DISTURBANCE WITH COTTON GLOVES, KRAFT PAPER, Al FOIL AND GLASS WOOL, ETC.

$$\lambda = 6328, \theta = 70^\circ$$

No.	Sample	Treatment	Pressure	Δ (deg)	ψ (deg)	SPD (volts)	PEE ($\times 10^{-4}$ amps)	Contact Angle ϕ_{H_2O} (deg)
12	MD7075-T6 6"x6"x1/8"	Cotton Glove	Control	184	43	0.25	6	0
			Light	184	43	0.23	7	3
			Medium	196	40	--	8	5
			Hard	214	37	1.1	7	25
12	MD7075-T6 Corner diagonal to 7075 Scratch	Cotton Glove	Control	182	42	0.31	10	0
			Light	184	42	0.82	12	0
			Medium	214	42	0.70	12	12
			Hard	222	38	1.15	8	36
12	MD7075-T6 Corner next to 7075 Scratch	Kraft Paper	Control	182	43	0.20	7	0
			Light	192	42	1.00	7	11
			Medium	204	42	0.75	11	24
			Hard	214	40	1.10	11	30
		Heat Gun		217	41	0.50	8	25
1	SC 4"x1"x1/16"	Kraft Paper	Control	188	42	0.13	12	0
			Medium	197	35	0.20	12	20
		Cotton Glove	Medium	190	33	0.20	15	20
		Kimwipe	Medium	204	32	0.30	12	20
2	SC	Teflon	Medium	177	31	0.30	8	50
		FPL Etch Al Foil	Control	187	41	0.16	14	0
			Hard	186	39	0.16	13	2
			Hard	188	40	0.46	15	2
			Hard	186	40	0.44	12	4
			Hard	184	40	0.40	17	4
			Hard	186	37	0.21	14	4
			Hard	188	40	0.17	13	2

TABLE 9
(Continued).SURFACE PROPERTIES OF PHOSPHORIC ANODIZED Al 7075-T6 AFTER MECHANICAL
DISTURBANCE WITH COTTON GLOVES, KRAFT PAPER, Al FOIL AND GLASS WOOL, ETC.

$$\lambda = 6328, \theta = 70^\circ$$

No.	Sample	Treatment	Pressure	Δ (deg)	ψ (deg)	SPD volts	PEE x10" amps)	Contact Angle ϕ_{H_2O} (deg)
12	MD7075		Control	187	42	0.19	8	8
1.	6"x6"x1/8"	Al Foil	Hard	187	42	1.10	13	8
			Control	189	43	0.20	8	9
2.		Al Foil	Hard	190	41	1.10	14	18
10	MD7075		Control	187	42	0.20	8	0
1.		Al Foil	Hard	190	42	0.75	18	14
			Control	186	42	0.16	8	2
2.		Al Foil	Hard	188	41	0.72	10	11
			Control	187	41	0.12	8	2
		Rub with Al Foil		194	51	1.00	1400	10
3	SC	Contami- nated H_3PO_4	Control	156	34	0.08	17	2
		Cotton Glove	Light	--	--	0.30	12	3
		Cotton	Hard	--	--	0.2	--	40
			Control	147	32	0.16	11	8
		Clean Quarts Wool	Light	152	24	0.72	10	23
		44 min later				0.40		20

To check the effect of pressure, without rubbing against the sample, aluminum foil was placed between the sample and the cotton glove and the foil was rubbed with hard pressure. Sample SC #2 in Table 10 shows that this procedure has little effect on the surface parameters, except that in some cases SPD increases. The foil used for SC #2 was FPL etched and checked for zero contact angle before use. An area of sample #2 was also pressed using clean platinum foil (see bottom of Table 9). No changes in surface properties occurred. Samples 12 and 10 of MD 7075-T6 were pressed with foil that was not properly cleaned. In these cases, SPD, PEE and ϕH_2O increased.

MD 7075-T6 #10 was rubbed with aluminum foil. The increase of PEE from 8×10^{-11} to 1400×10^{-11} amps indicates the large amount of abrasion exposing fresh aluminum with very thin oxide.

Samples 1 to 6 in Table 10 were anodized in the contaminated H_3PO_4 solution and 7 to 12 in fresh solution. Samples 7 to 12 were treated as indicated at the bottom of Table 10 prior to bonding with 3M 2214 adhesive. Bonds were made with samples 1 and 7, 2 and 8, etc. The surface parameters after treatment and the corresponding lap shear bond strength are given at the bottom of Table 10. All except the Teflon contaminated sample gave strengths about the same as the control, i.e., ~ 4400 psi and all except the Teflon sample failed entirely cohesively within the adhesive. These results show that mechanical distortion of the hydroxide film does not degrade the static shear strength even though the surface properties were dramatically changed. The lap shear results are consistent with results reported by Danforth at McDonnell Douglas. However, he found that the durability, as measured by the wedge

TABLE 10

THE EFFECT OF SURFACE DISTURBANCE OF PHOSPHORIC
ACID ANODIZED AL 7075-T6 ON LAP SHEAR STRENGTH

Sample	Treatment	Δ	ψ	SPD	PEE $\times 10''$	ϕH_2O	σ
<u>Contaminated Solution</u>							
1	None	157.4	34	0.34	16	2	
2	"	142.4	30	0.08	16	2	
3	"	146.4	29.4	0.10	16	2	
4	"	158.0	32.8	0.08	18	2	
5	"	155.6	33.2	0.12	16	2	
6	"	150.8	31.3	0.15	16	2	
<u>New Solution H_3PO_4 14 oz/gal</u>							
7	None	177.0	39.0	0.17	17	2	
8	"	168.0	33.9	0.35	14	2	
9	"	175.2	37.0	0.24	15	2	
10	"	168.4	36.1	0.18	16	2	
11	"	169.6	33.2	0.16	16	2	
12	"	173.4	37.5	0.21	18	2	
8	Hard Quartz Wool	238	36.4	0.72	50	15	4300
9	Hard Cotton Gloves	174.8	20.7	0.56	8	32	4500
9	Hard Kraft	189.4	26.6	0.43	10	19	4300
10	Clean Foil	174.2	35.2	0.55	12	5	4300
11	Teflon	169.6	25.7	-1.8 to 0.27	0	50	3700
12	Control	173.2	37.2			0	4400

All cohesive failure except Sample 5-11 with Teflon

test, is greatly reduced by the mechanical disturbance. The cause of the degradation in durability is not understood as yet, but it is clear that our tools will detect the disturbance.

As noted for #11 in Table 10, Teflon rubbing caused SPD to become -1.8 volts which then drifted back to 0.27 volts in a few minutes. It was also noted that the large increase from 0.2 to ~1.0 volt caused by rubbing with cotton, paper, etc., would slowly decay back towards 0.2 with time. These results indicate the rubbing process is charging the surface which then can discharge with time. It will be interesting to see (in Task III) if the bond durability is related to the time of discharge.

3. Organic Contamination

To establish the sensitivity of the surface tools to the presence of organic contamination, measurements were made on samples dipped through monolayers on water and samples exposed to aerosols of pentane containing larger molecules in solution. These two types of sources simulate contamination during the removal of panels from the phosphoric acid solution after anodizing, and exposure to smog, respectively.

Samples were dipped into pentane that contained 5×10^{-5} g of stearic acid per ml. One sample was repeatedly dipped for six sec and measurements made after the sample had dried after each dip. Another sample was left in for 36 sec, dried and measured, then for another 144 sec, dried and measured. The changes in Δ , ψ , SPD and ϕ_{H_2O} are given in Table 11 and plotted in Fig. 12. The refractive index of stearic acid is 1.66 and the approximate change in $\delta\Delta$ per Angstrom is calculated to be $\sim 1.4^0/10\text{\AA}$. The lower plot of $-\delta\Delta$ vs time

TABLE 11

CHANGE OF SURFACE PARAMETERS DUE
TO ADSORPTION OF STEARIC ACID

Exposure Time (sec)	$\delta\Delta$ (deg)	$\delta\psi$ (deg)	$\delta(\text{SPD})$ (volts)	$\delta(\phi\text{H}_2\text{O})$ (deg)	δd (Å)
<u>Sample #3</u>					
0	0	0	0	0	0
6	-0.4	-0.35	0.015	3	-2.8
12	2.4	0.85	0.017	66	16.8
18	4.8	1.25	0.028	79	33.6
24	8.6	1.75	0.035	85	60.2
30	8.2	1.45	0.045	87	57.2
36	8.0	1.45	0.054	112	56.0
42	9.6	1.75	0.060	105	67.0
48	8.8	2.45	0.065	105	62.0
54	8.8	2.95	0.073	107	62.0
60	10.0	2.15	0.078	115	70.0
66	8.8	2.75	0.081	115	62.0
72	10.4	2.55	0.086	117	73.0
78	10.3	2.15	0.081	117	73.0
84	10.8	2.65	0.097	117	76.0
90	10.3	2.35	0.093	117	73.0
<u>Sample #1</u>					
0	0	0	0	0	0
36	4.2	1.0	0.032	98	28
180	9.4	1.8	0.113	100	66

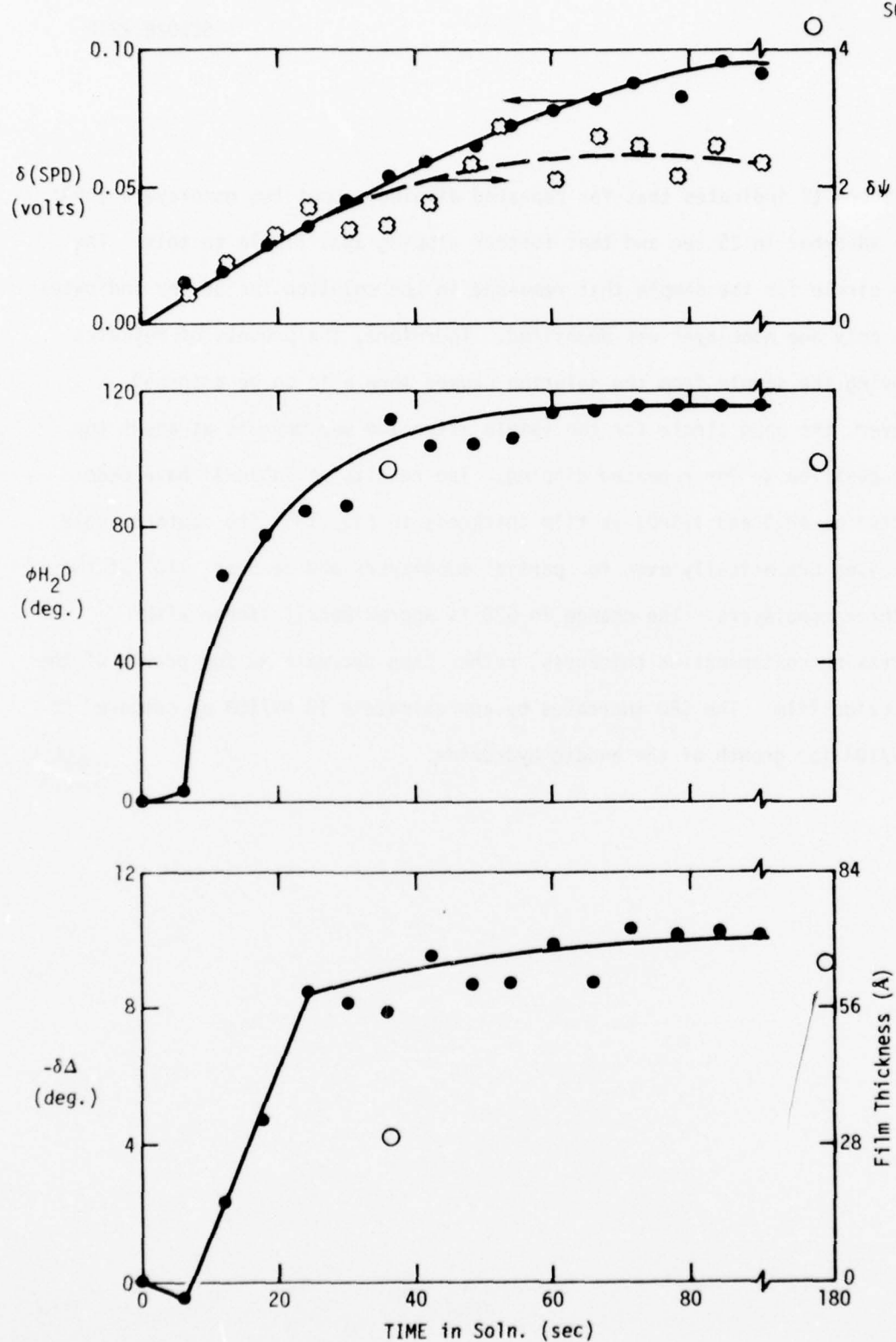


Figure 12. Plot of $-\delta\Delta$, $\phi_{\text{H}_2\text{O}}$, $\delta\psi$ and $\delta(\text{SPD})$ vs. Time in the Stearic Acid-Pentane Solution

in Figure 12 indicates that for repeated dipping, about two monolayers (56Å) have adsorbed in 25 sec and that further dipping adds little to this. The open circle for the sample that remained in the solution for 36 sec indicates that only one monolayer was deposited. Therefore, the process of repeated removing the sample from the solution causes more acid to be adsorbed. However, the open circle for the sample after 144 sec more is at about the same position as for repeated dipping. The results of Table 11 have been plotted as ϕ_{H_2O} and $\delta(\text{SPD})$ vs film thickness in Fig. 13. The contact angle increases dramatically even for partial monolayers and reaches $\sim 110^\circ$ at two or three monolayers. The change in SPD is approximately linear with increasing contamination thickness, rather than decrease as for growth of the hydroxide film. The SPD increases by approximately 10 mV/10Å as compared to -1mV/10Å for growth of the anodic hydroxide.

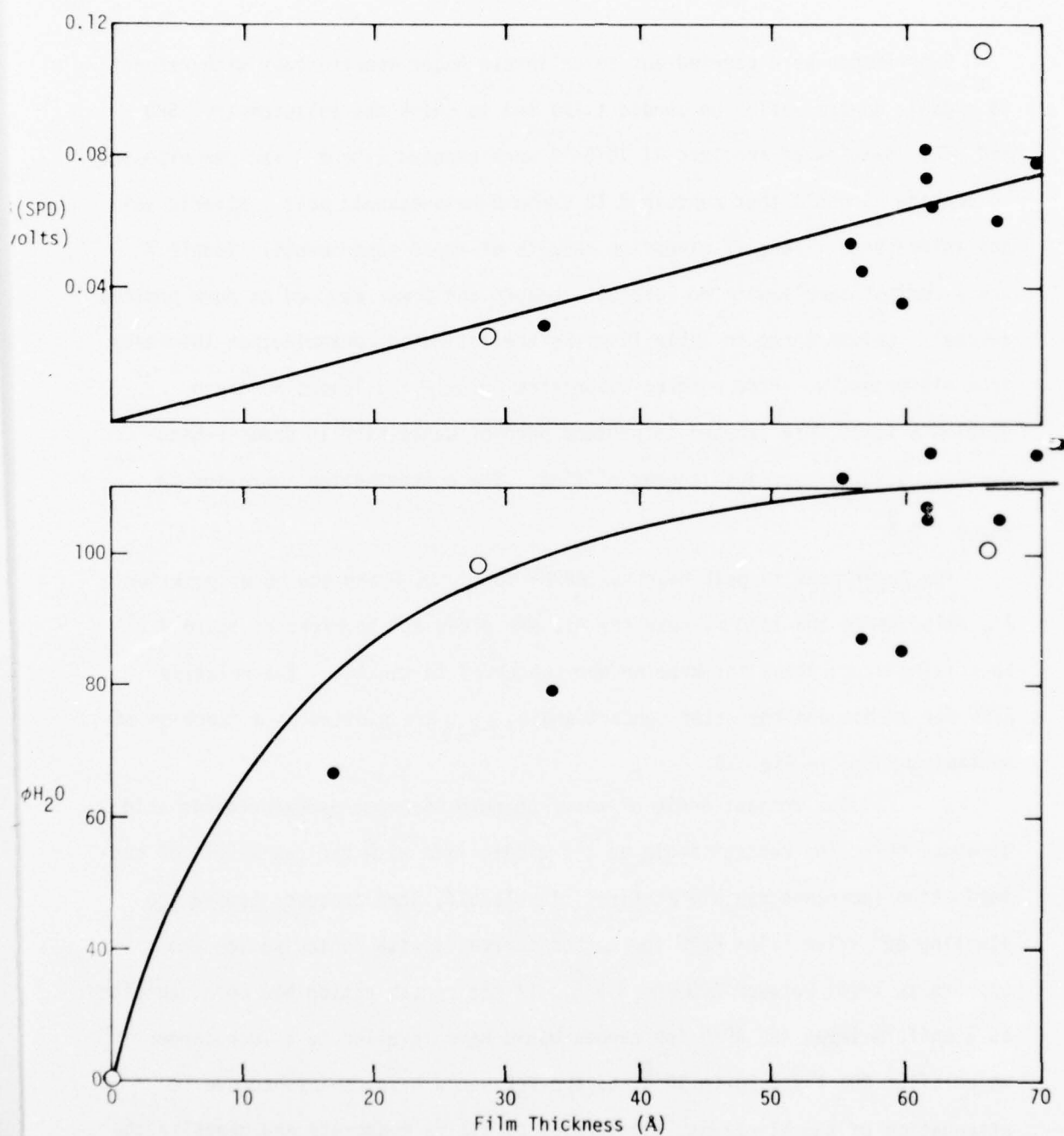


Figure 13. Plot of $\phi_{\text{H}_2\text{O}}$ and $\delta(\text{SPD})$ vs. Stearic Acid Film Thickness

Experiments were carried out to calibrate Auger spectroscopy with respect to organic contamination on anodic films and to check the ellipsometry, SPD and PEE. Samples of anodized Al 7075-T6 were exposed (about 3 sec per exposure) to pentane aerosols that contained 16 bromo-9-hexadecanoic acid, stearic acid and anthracene. Table 12 gives the results of these experiments. Sample 1 was a control sample with no aerosol exposure and 2 was exposed to pure pentane aerosol. Column three in Table 12 gives the estimated contamination thickness from ellipsometry. Pure pentane evaporates quickly and leaves no trace. Samples 5 to 10 were exposed to pentane aerosol containing 16 bromo-9-hexadecanoic acid for various lengths of time. The contamination increased to about 279 \AA .

The Auger peak to peak heights (APPH) for C, O, P and the 55 ev peak for Al, relative to the 1390 ev peak for Al, are given at the right of Table 9. Surprisingly, no peaks for bromine were observed in the AES. The relative APPH for carbon and the water contact angle $\phi_{\text{H}_2\text{O}}$ are plotted as a function of contamination in Fig. 14.

The contact angle of water on pure 16 bromo-9-hexadecanoic acid is about 50° . The contact angle on the anodic film with various levels of contamination increases rapidly at first, levels off, then proceeds toward the limiting 50° value. The APPH for carbon increases with contamination and appears to level between 200 and 300 \AA . If the contamination had been deposited as a uniform layer the APPH for carbon would have levelled to a much larger value after the first 20 to 50 \AA and the PEE would have diminished due to attenuation of the electrons. The aerosol particles evaporate and deposite the hydrocarbon as particulate precipitates so that the electron beam sees hydroxide as well as contamination even though the average effective thickness is 280 \AA .

TABLE 12
Auger Spectroscopy of Contaminated Al 7075-T6 Phosphoric Acid Anodized Samples

Sample	No. of Aerosol Exposures	Contamination Thickness	SPD	PEE	ϕH_2O	APPH/APPH(Al 1390 ev)			
						C	0	P	Al(55 ev)
(Å) volts $\times 10^4$ (deg.) 16 Bromo-9-Hexadecanoic Acid in Pentane									
1,2	0	0	0.91	5.6	4	0.4	6.0	0.4	0.7
5	1	2.8	0.89	5.4	14	0.6	10.0	0.6	2.2
6	2	34	0.91	4.7	25	0.9	6.1	0.3	1.7
7	3	113	0.88	4.4	25	1.5	7.1	0.4	1.8
8	4	158	1.10	4.4	26	2.2	7.4	0.4	1.8
9	5	225	0.90	4.2	30	5.0	5.6	0.2	0.8
10	6	279	0.90	3.9	36	5.3	5.4	0.2	0.9
Stearic Acid in Pentane									
3	1	22	0.80	4.8	36	1.5	5.6	0.3	1.0
Anthracene in Pentane									
4	1	10	0.74	7.8	5	0.9	12.3	0.7	2.5
Degreased Sample									
VI,0	0		0.92	25	58	2.7	6.2	0	1.2

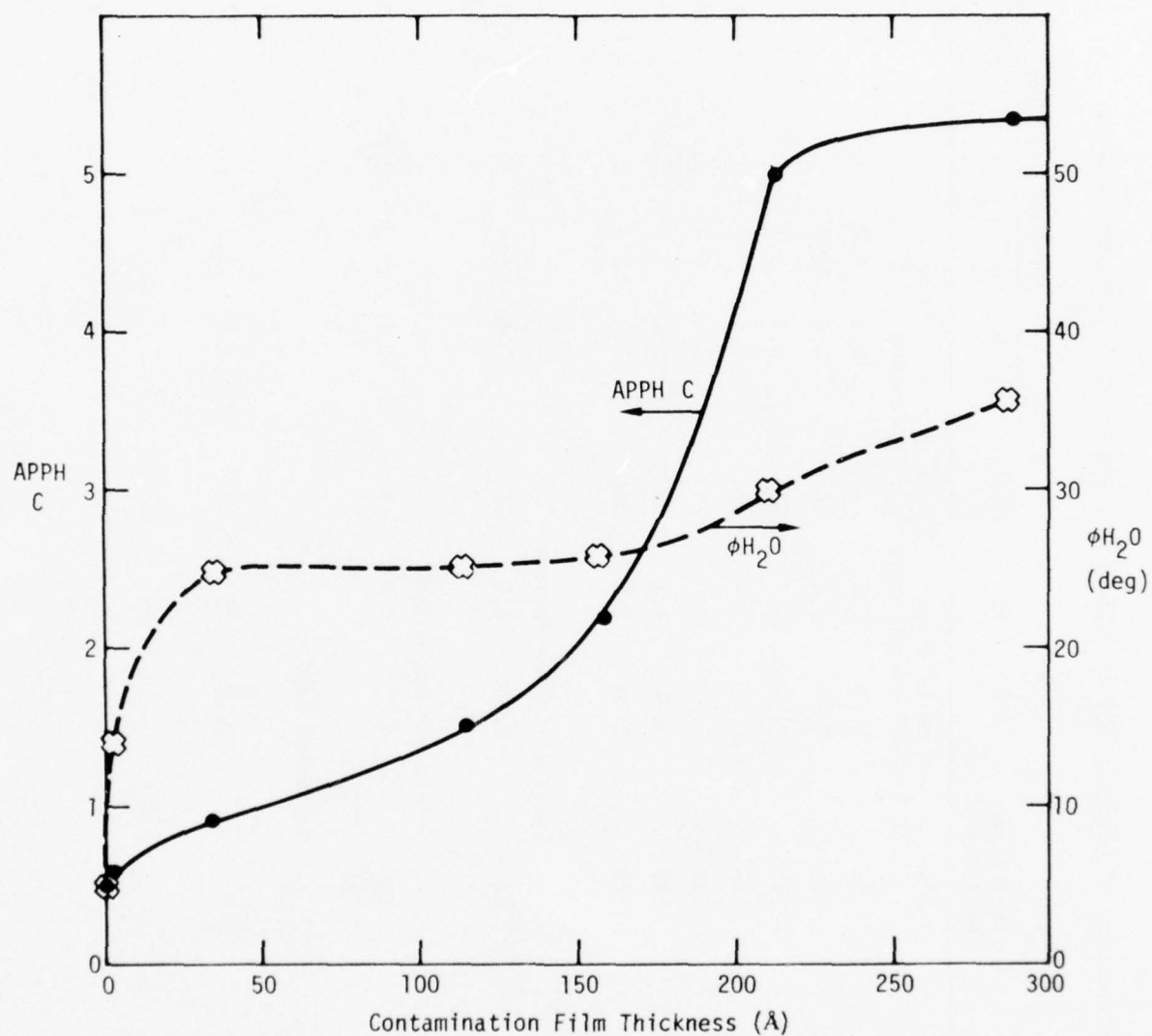


Figure 14. Auger peak to peak heights (APPH) for C and contact angle ϕ_{H_2O} for contamination.

One exposure to aerosol containing anthracene deposits about 10 \AA^0 but doubles APPH(C) (with respect to the control) and leaves the surface wettable. One exposure to aerosol with stearic acid leaves about 22 \AA^0 which increases ϕ_{H_2O} to about 36° and is detected by AES (1.5 vs. 0.4 for the control). The last sample in Table 12 had been degreased but not anodized. Due to approximately a monolayer of contamination that is left SPD remains high, $\phi_{H_2O} \sim 58^\circ$ and APPH(C) ~ 2.7 . The PEE is about five times as large as for anodized samples due to a much thinner oxide layer.

4. Aging in Laboratory Air

Table 13 shows the effect of laboratory aging of an Al 2024-T3 panel that had been anodized at McDonnell Douglas. Tracking in two positions (13 and 27) on the panel reveals a slow decrease in Δ , increase in ψ , decrease in PEE and increase in SPD as seen in Fig. 15. The open circles with a cross are for position 13, the solid dots are for position 27. Values of SPD and PEE are almost identical for the two positions as a function of aging. Values of Δ and ψ differ slightly for the two positions. All of the surface tools indicate growth of contamination during aging, but at the extremely low rate of about $1 \text{ \AA}^0/\text{day}$ or a monolayer (25 \AA^0) in about 25 days. This can be compared to contamination of FPL etched Al 2024-T3, of about 1 monolayer in 10 hrs. Table 14 gives AES data for aged Al 2024-T3. Table 14 confirms the contamination to be carbonaceous and that the rate is approximately $1 \text{ \AA}^0/\text{day}$. This estimate is made by comparing the APPH for carbon in Table 14 with that for a monolayer of stearic acid ($\sim 25 \text{ \AA}^0$ for molecules erect). A plot of the estimated fraction of a monolayer (of equivalent stearic acid) for laboratory aging is given in

TABLE 13

EFFECT OF AGING ON SURFACE PROPERTIES

Days After Anodize	Position 13				Position 27			
	Δ^* Deg.	ψ Deg.	SPD Volts	PEE Amps x 10"	Δ^* Deg.	ψ Deg.	SPD Volts	PEE Amps x 10"
5	122.4	38.8	0.50	3.3	126.4	36.6	0.34	3.0
7	123.6	38.6	0.04	2.0	120.4	38.2	0.04	2.0
8	123.4	38.3	0.07	3.0	119.2	38.9	0.06	3.0
9	121.6	38.3	0.10	3.5	119.2	38.6	0.10	3.6
12	121.6	37.8	0.18	4.0	119.2	38.3	0.15	4.0
14	122.6	38.2	0.28	2.2	118.6	38.6	0.25	2.2
19	122.8	38.2	-	-	118.6	38.4	-	-
20	122.4	38.1	0.38	1.8	118.4	38.4	0.36	1.3
21	121.8	38.2	0.73	1.7	119.6	39.9	0.73	1.6
26	120.4	38.4	0.78	1.6	117.0	39.4	0.78	1.4
28	121.8	38.8	0.93	2.8	115.8	39.6	0.95	2.6
30	120.6	38.3	0.82	1.2	116.4	39.3	0.82	1.2
33	119.6	39.0	0.33	1.4	115.6	39.0	0.30	1.5
* $\lambda = 6328\text{\AA}$, Angle of Incidence = 70°								

TABLE 14
Effect of Laboratory Aging of Phosphoric Acid Anodized Al 2024-T

Age (Days)	Anodize Voltage	Film Thickness	APPH/APPH (Al 1390 ev)					
			C	O	P	Al(55 ev)	Si	S
1	15	4500	0.10	7.4	0.25	1.9	0.20	0.00
2	15	4500	0.25	7.5	0.45	2.1	0.15	0.00
7	10	3000	0.25	7.4	0.45	1.7	0.20	0.00
8	10	3000	0.50	7.3	0.50	1.8	0.20	0.10
14	10	3000	0.50	7.0	0.45	1.8	0.15	0.15
14	5	1300	0.50	7.5	0.45	1.8	0.20	0.25
15	5	1300	0.70	7.0	0.40	1.7	0.20	0.20

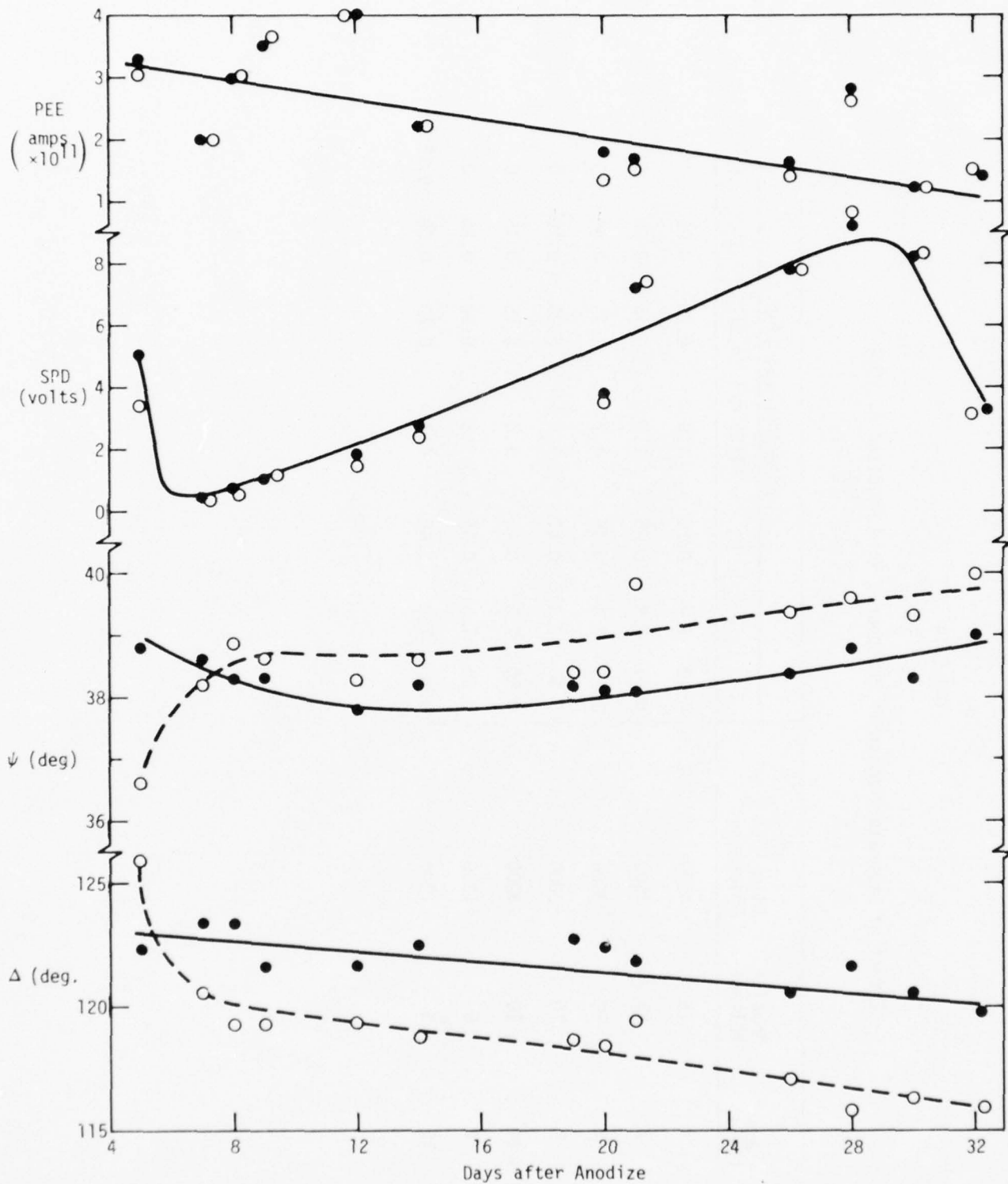


Figure 15. Change of surface parameters with aging of anodized Al 2024-T3.

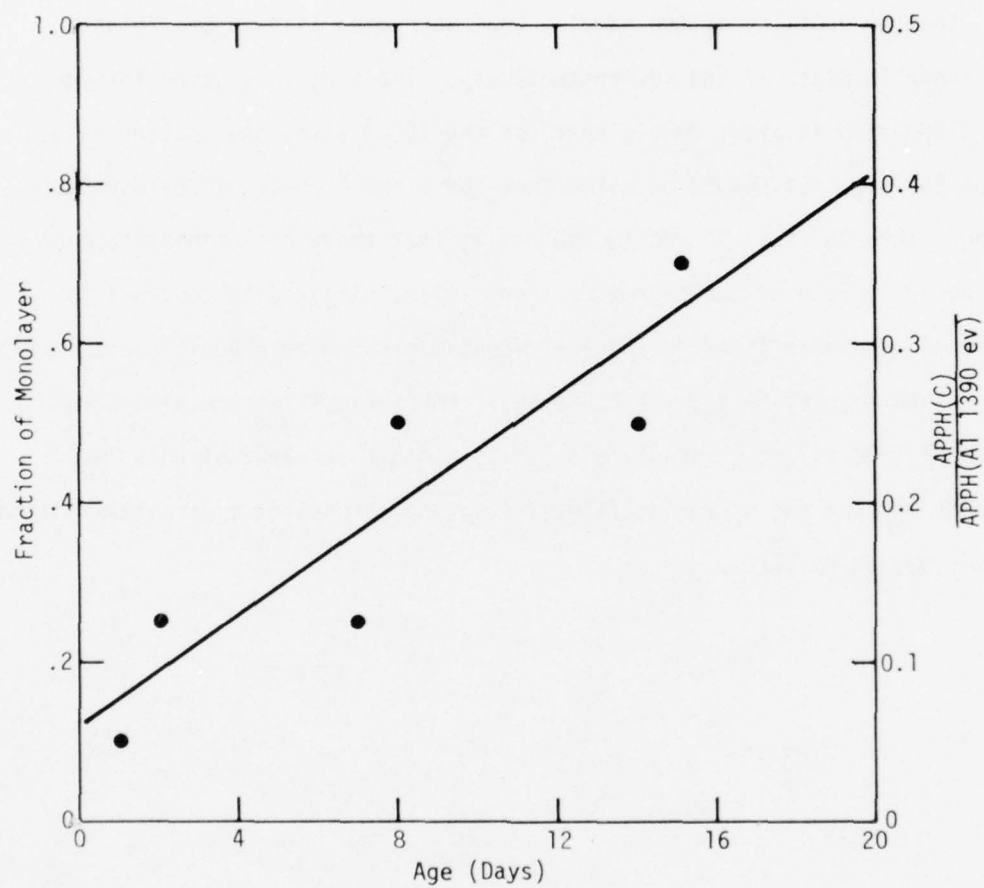


Figure 16. Plot of $\text{APPH(C)}/\text{APPH(A1 1390 ev)}$ vs. days of aging anodized Al 2024-T3 in lab air. Left ordinate is estimated fraction of a monolayer (monolayer $\sim 25 \text{ \AA}$)

Fig. 16. In spite of the carbonaceous contamination the water contact angle remains near 5° for all of the aged samples.

Sputter profiles of the samples that were aged 14 days and 15 days are shown in Figs. 17 and 18, respectively. The time to sputter through the 2180Å film is about double that for the 1000Å film, the sputter rate about 25Å/min. It should be noted that the C and P peaks decrease rapidly to near zero in Figs. 17 and 18 indicating that these contaminants are at the outer surface of the hydroxide anodic film. This is in contrast to profiles of anodic films deliberately contaminated with organic contamination in pentane aerosol (e.g., see Table 12). For these films the high APPHC/ (APPH A1 1390 ev) of 5 rapidly dropped to 0.8 but remained at this level through most of the hydroxide film, indicating the presence of contamination in the hydroxide pores.

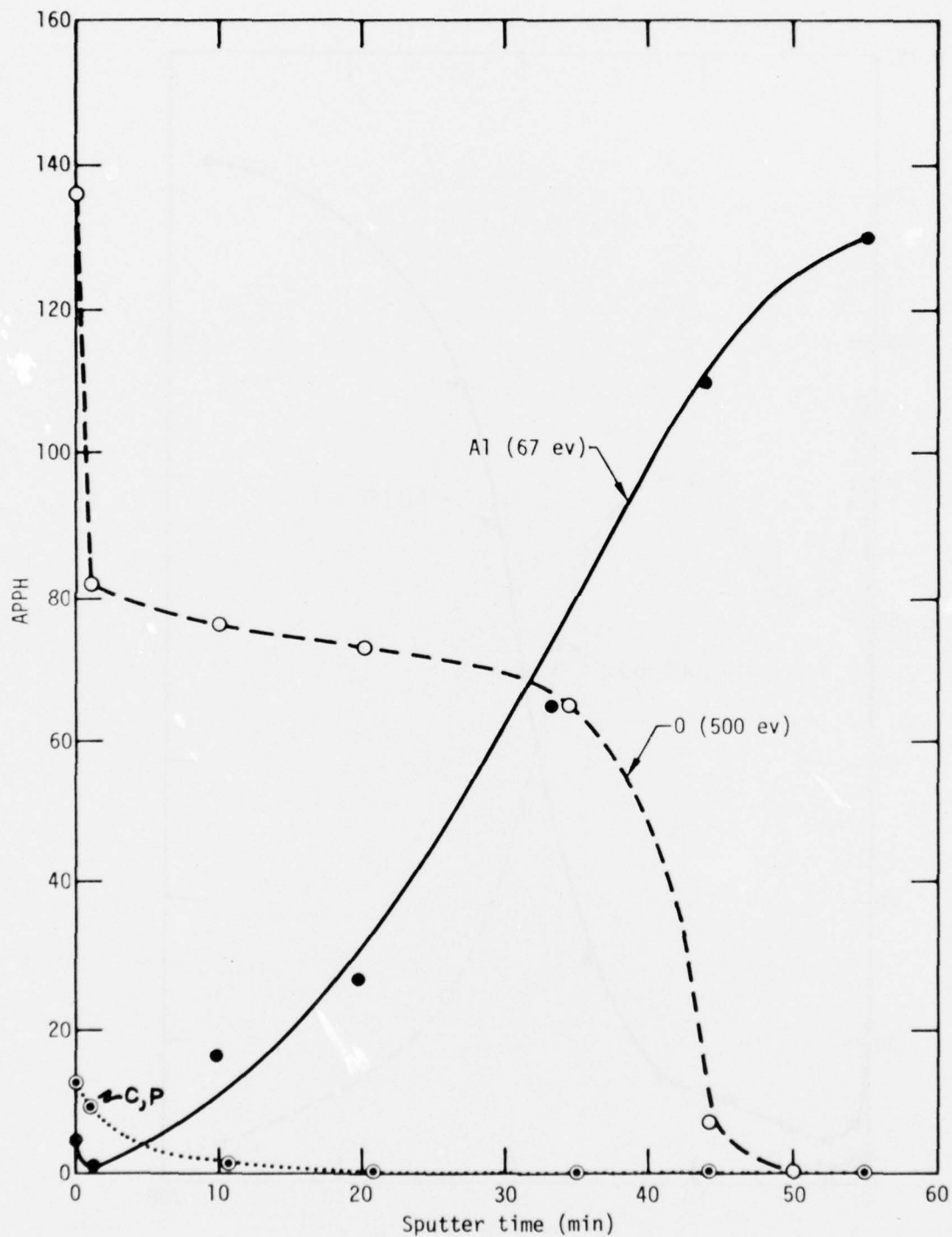


Figure 17. Sputter profile for sample anodized at 4 volts, 12 min, 5% H_3PO_4
 SET = 15 days, initial oxide thickness 1000 Å .

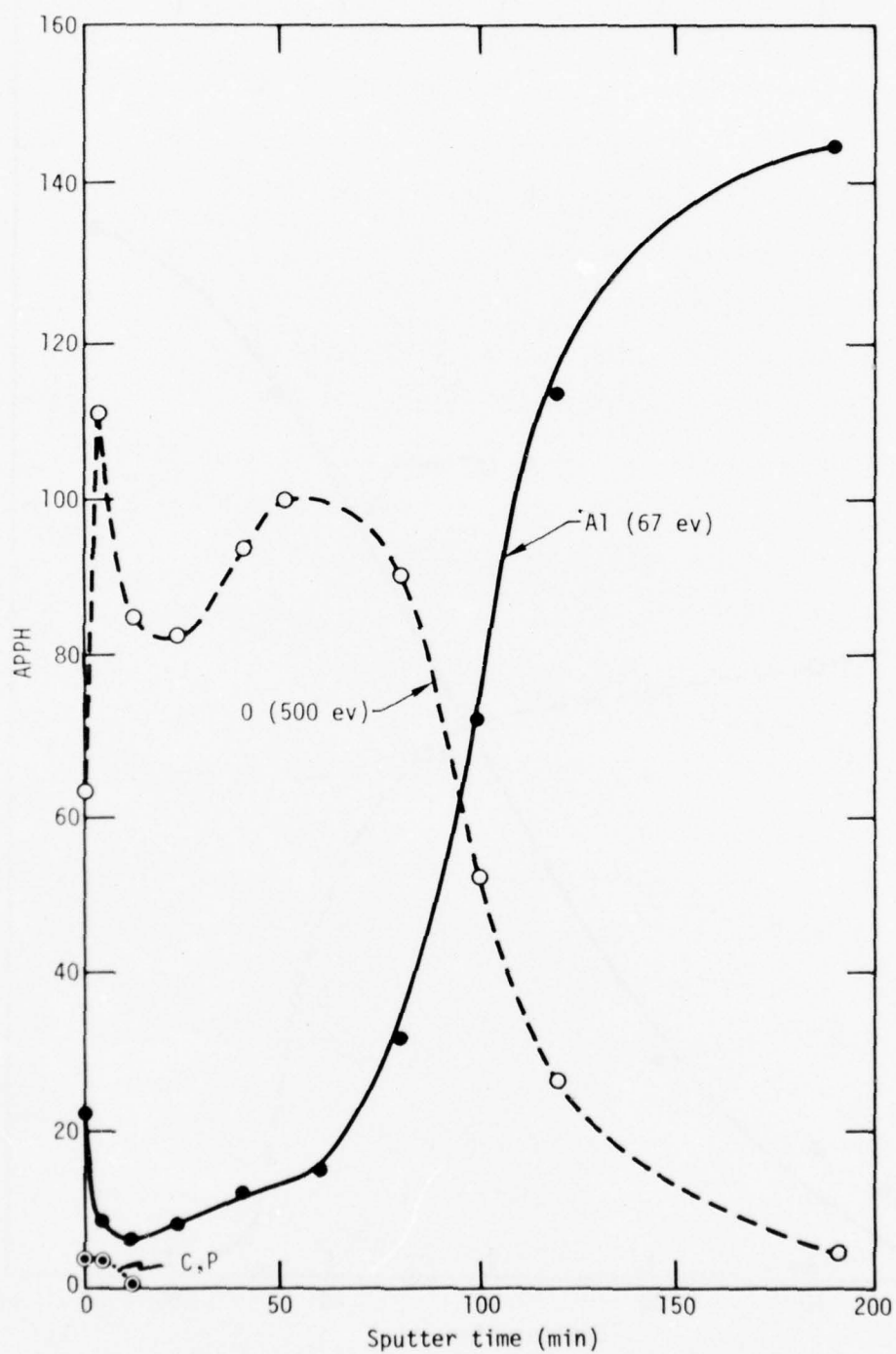


Figure 18. Sputter profile for sample anodized at 10 V, 22 min. 5% H_3PO_4
SET \approx 14 days, initial oxide thickness 2180 Å.

C. NDI, Automated Computer Mapping

All computer maps are found in Appendix A at the end of the text and are labelled with an A, a number and the letter a, b, c or d for Δ , ψ , SPD or ϕH_2O , respectively. Corresponding printouts are found in Appendix B for some of the figures.

1. Processing Errors

First the uniformity of panels within the acceptance window is shown, then it is shown that if the band (window) is suppressed the panel appears clean (blank map). Next is shown the effect of possible processing errors such as anodizing for the wrong period of time, at the wrong voltage and leaving in the acid bath after completion of anodizing.

To show the uniformity of a phosphoric acid anodized sample that had been aged in Kimwipes in a plastic bag for four months, computer plots were made of Δ , ψ and SPD. Fig. A.1(a)(pg. 93) is a Δ plot for all the data that deviate from the average value by not more than 1.5° . Fig. A.1(a)(pg. 94) is a Δ plot for the data that fall outside the 3° window ($163^\circ < \Delta < 160^\circ$). Fig. A.1(b)(pg. 95) is a ψ plot of data that deviate from the average by not more than 1° and Fig. A.1(b)(pg. 96) is for data that fall outside the 2° window ($42^\circ < \psi < 40^\circ$). Fig. A.1(c)(pg. 97) is an SPD plot data that fell within a window (0.45 to 0.65) and Fig. A.1(c)(pg.98) is outside of this window. These data indicate that after four months the anodic film remains within the band used for the calibration sample, $\sim 3^\circ$ for Δ , $\sim 1^\circ$ for ψ , and ~ 0.2 for SPD.

To show the reproducibility of the computerized plotting instrument Tables B.1(a)(pgs. 222-224), B.1(b)(pgs. 225-227) and B.1(c)(pgs.228,229) are three plots of the same sample. Tables B.1(a)(pg.223), B.1(b)(pg.226) and B.1(c)(pg. 229) are for plots made immediately after (a)(pg. 222), (b)(pg.225) and (c)(pg.228). Tables B.1(a)(pg.224) and B.1(b)(pg. 226) are

for plots made three weeks earlier. Although the reproducibility is not exact, it is very close. Three weeks have caused a drift of about 1^0 in Δ and ψ .

Figs. A.2(a), (b) and (c) are computer plots of Δ , ψ and SPD for a panel that had been anodized for various lengths of time (5, 10, 15, 25, and 30 minutes) to simulate possible anodizing problems. Above 15 minutes the data fall within the band for the standard preparation (20 mins.). This is consistent with Northrup's SEM results which revealed that after 10 mins. the film thickness remained essentially constant.

In Fig. A.2(c) it is noted that deviations from the window (.2 to .4) fall along the boundaries between zones. The reason for this is not known. The correspondence between Δ measurements made 3 weeks apart (Tables B.2(a) (pg. 230) and B.2(a)(pg. 231)) are considered to be good, especially with respect to relative values within a map. It is clear that a single calibration sample would not be adequate for indefinite periods of time. It will be necessary to periodically check samples that are known to be properly prepared and calibrate the instrument with these samples. However, the periodic calibration may be as long as a month.

Figs. A.3(a), (b) and (c) show computer plots for a panel that was cut into five strips and anodized at 5, 10, 15, 20 and 25 volts to show the effect of improper anodizing. The Δ plot (Fig. A.3(a)) distinguishes between five levels, as does the SPD plot. The ψ plot can only distinguish the 5 and 20V levels from the others. This is a case for which the Δ values are very close for two very different film thicknesses (1200Å at 5V and 2400Å at 10V) due to the cyclic nature of Δ with thickness. However, there is no ambiguity

because ψ very strongly distinguishes between 5 and 10V in Fig. A.3(b). As expected from Fig. 11, the SPD plot (Fig. A.3(c)) distinguished between voltage regions.

Figs. A.4(a), (b) and (c) are Δ , ψ and SPD plots for a panel that was anodized in a bath that was deliberately contaminated by dropping cigarette ashes, a hair and some table top dust on the bath surface. The Δ and ψ plots reveal contamination over a large portion of the panel. The SPD only reveals contamination in one spot. Figs. A.5(a), (b) and (c) are Δ , ψ and SPD plots for a panel that was anodized in the same contaminated bath as Figs. A.4(a), (b) and (c), but with a particle of stearic acid added. The Δ and ψ plots reveal more contamination.

Figs. A.6(a), (b) and (c) show Δ , ψ and SPD plots for a panel that had been left in the phosphoric acid for 0, 2.5, 5.0, 7.5 and 10 minutes after the anodic process. Except for SPD the plots show strong deviation from the proper area (0 min.) with increasing time in H_3PO_4 .

Δ and ψ values in Tables B.6(a) and (b) that correspond to Figs. A.6(a) and (b) indicate that most of the film is removed in the first five minutes and that the final exposure (5-10 mins.) etches the surface (see bottom of Table 8).

The water contact angle is near zero and completely insensitive to film thickness as long as the surface has not been contaminated.

It is clear that gross processing errors, that result in large deviations of hydroxide film thickness from the proper value, will be detected very well by ellipsometry, fairly well by SPD in the case of anodizing voltage, but not good for exposure to acid after anodizing and not at all by water contact angle.

2. Handling Damage

Figs. A.7 and A.8 demonstrate the great sensitivity of the ellipsometer to surface damage on a phosphoric acid anodized Al 7075-T6 panel. The mapped area is 4" x 5". Tables B.7(a)(pgs. 236-238) and B.8(a)(pgs. 242-244) and B.7(b)(pgs. 239-241) and B.8(b)(pgs. 245-247) give the printout values of Δ and ψ that correspond to the plots in Figs A.7 and A.8. Table B.7(a)(pg. 236) shows that prior to surface damage, the surface is very uniform, $\Delta = 161$ to 162 , $\psi = 40$ to 41 . In Figs. A.7 and A.8 these values of Δ and ψ were suppressed. Values that fall outside these bands were plotted as previously described. In Fig. A.7-a and b a Kimwipe had been lightly passed over the area indicated by the arrow. Both Δ and ψ strongly reveal this area. In Fig. A.7-a' and b' a Kimwipe was pressed hard against the surface and passed from one side of the panel to the other. The computer program scales the plot to the largest deviation from the suppressed band so that region 2 becomes the heavy plot relative to region 1. In region 3 a cotton glove was lightly passed over the surface. This region is detected by Δ but not by ψ . Region 4 in Fig. A.8-a was a hard press wipe across the panel with the cotton glove. Both Δ and ψ reveal this region dramatically. In region 5 a thumb smudge was made with a cotton glove on. This region is revealed by Δ and ψ . Fig. A.9 is a plot of SPD after the various treatments corresponding to Figs. A.7 and A.8. The SPD is very poor for revealing surface damage probably because the time between damaging and mapping allowed the surface to discharge as in Table 9. Table B.9 is the computer printout of the SPD values scaled between 0 and 999 to show relative values. These figures and tables show that five levels of surface damage, that might be caused by handling of panels, are easily detected by Automatic Scanning Ellipsometry but not by SPD.

3. Human Contamination

Fig. A.10 shows the areas of an anodized sample that had been contaminated by fingerprints and exposure to moisture from a cough, cigarette smoke, cigarette ashes and food remnants (bread, banana peel). Figure A.11(a) is a Δ map which reveals contamination in areas 2 (banana peel), 13 (fingerprint after placing finger on forehead) 14 (after wetting finger with saliva), 15 (after running finger through hair), 17 (placing finger in 3 in 1 oil then wiping with Kimwipe). The ψ plot of Fig. A.11(b) is unrevealing, but the SPD plot of Fig. A.11(c) reveals contamination in regions 17, 14 and 11. Region 11 was contaminated with fresh cigarette ashes. Fig. A.12(a) is a Δ map after storing a sample in a plastic bag containing cigar smoke for three days. A map of SPD is given in Fig. A.12(c) after exposure to cigar smoke. There is a general observed contamination in each case.

4. Simulated Smog Contamination

For simulated smog contamination phosphoric acid anodized panels of Al 7075-T6 have been divided into three zones. The middle zone has been left clean as a control area, the top and bottom zones were contaminated to eight levels with pentane aerosol containing various constituents of smog. The attempt was to contaminate the top and bottom zone in an identical way. Since replotting the same zone always gives the same map, different maps indicate differences in contamination. Figs. A.13 through A.18 show Δ , ψ and SPD plots for decanoic acid, erucic acid, brassidic acid, N-docosane, 16-bromo-9-hexadecenoic acid and dotriacontane, respectively. Although mapping at top and bottom is not identical, because of the difficulty in reproducible contamination, the maps are very similar at the top and bottom of each panel for Δ plots. Only the brassidic acid gave a reasonable SPD plot. As usual ψ plots are very bad.

In Figure A.19, except for the middle zone labelled "clean", each 1" x 1" area was exposed to aerosol by masking the sample except for a 1" diameter hole in the mask in the area of interest. By exposing different areas to more or less aerosol by spraying in the vicinity of the panel different levels of contamination were obtained. The level of contamination was roughly estimated and related on a relative scale of 1 to 8. That is, the level "L" of 8 is for an area exposed roughly to 8 times that at $L = 1$. The contamination level L , and the ellipsometric parameters Δ and ψ , that were measured manually by the null technique, are listed in each area in Figure A.19. The corresponding estimate of contamination average film thickness is listed as $d(\text{\AA})$ for levels 1 to 6. Although levels 7 and 8 have more contamination, it is difficult to estimate film thickness without carefully following as the contamination is layed down because of the cyclic nature of Δ and ψ with increasing film thickness. It is, therefore, possible to have thick contamination without detecting it with the ellipsometer at discrete levels for which Δ and ψ fall within the band for clean panels. However, the probability of passing through the 5° window in Δ out of 360° , is only 1.4% and if the contamination were thick enough to pass through the second cycle the film could easily be observed visually. Fig.A.19(a) shows that a computer plot of Δ that fell outside the band $162 < \Delta < 160$ reveals levels 4, 5, 6, 7 and 8 for 1-Hexadecylamine but only levels 7 and 8 for 1-Eicosene. Fig.A.19(c) shows that SPD reveals 1-Hexadecylamine very strongly but no 1-Eicosene. Similar data for anthracene aminobenzoic acid, and 1, 12 diaminododecane are given in Figs. A.20, A.20(a) and (b) and A.21, A.21(a),(b) and (c). The molecules, eicosene, anthracene and benzoic acid are not observed by the automated system because they

evaporated before measurement. These type molecules will probably not be a contamination problem due to their high vapor pressure, but tests in Task III are necessary to demonstrate this.

The mapped values of Δ with the computerized system, that correspond to Fig. A.19(a), are found in Table B.19(a). It will be noted by comparing region 6 in Table B.19(a) with region 6 in Fig. A.19 that the low value of Δ is 150, as compared to 140, respectively. The discrepancy between manual observations by the null method and the light intensity method used with the computer, caused us to make a careful study with these two systems. We discovered that for smooth samples both methods yield the same values of Δ and ψ where as rough samples do not. It is apparent that rough samples scatter light of different polarization in a way that does not correspond to smooth surfaces. It should also be noted that the null method is about twice as sensitive to contamination as the intensity method. The need for utilizing a nulling ellipsometer will be revealed in our follow-on study to discover the level of contamination that significantly affects bond strength and durability.

Fig. A.22(a)(pg.152) is a Δ map of a panel that was contaminated with stearic acid by dipping the top left corner in a solution of stearic acid in pentane. Fig. A.22(a)(pg.153) is of the same panel but with a larger suppression band to suppress the acceptable area. Fig. A.22(d) is a water contact angle map of the same panel. No tables were printed for this panel.

Fig. A.23(a) is a Δ plot and is labelled in areas 1, 2, 3, 4 and 5 in order of increasing exposure to pentane aerosol containing stearic acid. The rest

of the panel was clean. The stearic acid contaminated ranges from 0 in the clean areas to about 150Å in area 5. Plots of ψ do not reveal any contamination nor does an SPD plot. The clean panel was very uniform with respect to Δ and ψ .

Figure A.24 shows the areas of an anodized panel that were contaminated with aerosol containing decadiene, decacyclene and adamantanol. The Δ plot in Fig. A.24(a) reveals level 4 and 5 of decacyclene and levels 3, 4 and 5 of adamantanol but does not reveal decadiene which has evaporated. The ψ plot in Fig. A.24(b) only reveals level 5 of adamantanol. The SPD plot in Fig. A.24(c) reveals all levels of adamantanol but does not reveal the other two contaminants. The Δ and ψ maps are very uniform.

5. Reproducibility of the Lowest Level of Contamination

To show that the NDI techniques can reproducibly reveal contamination at the lowest level, panels were divided into five regions. Two top regions and two bottom regions were contaminated and the center region was left uncontaminated as a control. The contamination regions were divided into four areas and each of the four areas was exposed to the same minimum aerosol exposure to test the NDI reproducibility. Figs. A.25 through A.29 show Δ , ψ , SPD and water contact angle plots for various types of contamination found in smog.

As usual for organic contamination ψ plots are not revealing. Note that in Fig. A.25(a) the Δ plot reveals all contamination except stearic acid in spots 1, 2 and 3 starting from the bottom left corner. The SPD also reveals all contamination except the stearic acid. The SPD is more sensitive to N-docosane than was Δ but less sensitive to the acids. The water contact angle wettability plot reveals all contamination including stearic acid. In Fig. A.26(a) the Δ plot reveals all contamination including stearic acid but is not very sensitive to dotriacontane. The SPD is more sensitive to the alkane than the acids as before. Again the wettability map in Fig. A.26(d) reveals all contamination. The blank regions in the top row are misleading and reveal a problem with the drop dispenser in some cases. If the drop does not detach from the dispenser it is dragged along and not detected by the probe. This is easily corrected by using a nonwetting dispenser rather than the metallic tube we have used. The Δ plot in Fig. A.27(a) is insensitive to 1-adamantane carbonitrile and anthracene. The SPD sees the nitrile but not the anthracene and 1-adamantane carboxylic acid. The wettability map sees everything except the anthracene. It is concluded that most of the anthracene has evaporated. It is apparent that both Δ and SPD sensors are needed and will detect nearly all types of contamination. Task III will reveal whether all significant contamination can be detected.

6. Reproducibility of Mapping

To further show the reproducibility of the NDI techniques, panels that had been contaminated and mapped months before were remapped. The remaps are seen in Figs. A.30 to A.36 and are almost identical to the original maps. Each remap is identified with the figure number of the original map for comparison.

7. Scale Up

We received 1' x 1' x 0.033" production anodized panels of Al 2024-T3 from M. Danforth at McDonnell Douglas. The uniformity of the anodic film has been checked by mapping panels 2 and 10 with ellipsometry, SPD, PEE and water contact angle. All of the positions on the panels were wettable ($\phi_{H_2O} \sim 5^\circ$). The anodic films are estimated to be about 3700 to 3800 Å with index of refraction about 1.3 (i.e., about 20% porous). Table 15 gives surface properties for 23 positions on each side of panel 10 and Table 16 gives properties of each side of panel 2. The average values of Δ were 121.6 ± 1.2 , 127.2 ± 1.3 , and 116.1 ± 1.3 . These values correspond approximately to an average variation of 14 Å over one side of a panel, 35 Å from one side of a panel to the other and 100 Å from one panel to another. The average surface potential difference (SPD) values proved to be 0.27 ± 0.03 , 0.29 ± 0.04 , 0.26 ± 0.03 for measurements on one day and 0.15 ± 0.02 and 0.16 ± 0.02 for measurements on the next day. This change is due to drift of the reference electrode. The photo electron emission values averaged 2.3 ± 0.2 , 2.3 ± 0.1 , 2.0 ± 0.2 on one day and 2.6 ± 0.2 on the next (units of 10^{-11} amps). There was little difference between values of SPD and PEE from one side to the other and from one panel to the other. The uniformity in each case was within $\pm 10\%$ of the average value.

TABLE 15

SURFACE PROPERTY MAP OF 1' X 1' X 0.033" PANEL
 (#10 from McDonnell Douglas)
 PRODUCTION LINE ANODIC PROCESS

Sample	One Side of Panel				Other Side of Panel			
	Δ	ψ	SPD	PEE	Δ	ψ	SPD	PEE
	Deg.	Deg.	Volts	Amps x 10"	Deg.	Deg.	Volts	Amps x 10"
1	121.8	38.9	0.27	3.0	126.6	37.2	0.25	2.2
2	122.4	39.4	0.23	2.2	127.2	37.7	0.25	2.2
3	121.6	38.6	0.27	3.0	127.6	37.7	0.31	2.4
4	122.4	39.0	0.30	2.1	126.4	36.9	0.32	2.2
5	121.2	38.5	0.23	2.2	128.6	37.1	0.27	2.2
6	122.2	38.1	0.25	2.0	127.8	36.7	0.34	2.6
7	120.0	40.0	0.30	2.6	126.4	37.7	0.34	2.3
8	122.8	38.2	0.23	2.3	126.8	37.1	0.25	2.2
9	120.0	38.4	0.32	2.1	129.0	37.3	0.38	2.3
10	124.6	38.6	0.22	2.3	129.0	37.1	0.22	2.2
11	122.8	38.8	0.36	2.1	128.4	36.4	0.40	2.1
12	123.4	38.5	0.23	2.3	130.6	36.5	0.23	2.7
13	123.2	37.8	0.24	2.4	128.4	36.0	0.26	2.3
14	123.2	38.3	0.26	2.6	123.6	38.2	0.31	2.5
15	121.6	37.5	0.22	2.4	125.6	37.6	0.26	2.6
16	120.6	38.9	0.26	2.2	128.4	37.0	0.28	2.2
17	120.4	39.7	0.26	8.0	125.6	36.8	0.28	2.4
18	120.4	39.2	0.30	2.1	126.4	36.6	0.34	2.2
19	120.6	38.4	0.34	2.3	126.4	36.4	0.34	2.1
20	120.6	38.9	0.30	2.1	125.6	36.1	0.31	2.1
21	119.4	39.2	0.23	2.0	128.0	36.2	0.25	2.0
22	119.8	37.6	0.31	2.5	-	-	0.26	2.4
23	120.6	38.8	0.23	2.1	-	-	0.28	2.2
Avg.	121.6	39.0	0.27	2.3	127.2	37.0	0.29	2.3
\pm	1.2	0.5	0.03	0.2	1.3	0.5	0.04	0.1

TABLE 16

SURFACE PROPERTY MAP OF 1' X 1' X 0.033" PANEL
 (#2 from McDonnell Douglas)
 PRODUCTION LINE ANODIC PROCESS

Position	One Side of Panel				Next Day		Other Side of Panel	
	Δ	ψ	SPD	PEE	SPD	PEE	SPD	PEE
	Deg.	Deg.	Volts	Amps x 10"	Volts	Amps x 10"	Volts	Amps x 10"
1	113.6	40.8	0.21	3.6				
2	113.6	40.3	0.11	1.7	0.07	3.0	0.14	3.0
3	113.2	40.9	0.28	1.7				
4	114.4	41.2	0.22	1.7				
5	114.8	40.7	0.26	1.7	0.18	3.0	0.16	2.8
6	114.4	40.8	0.26	1.7				
7	116.0	40.8	0.30	2.0				
8	116.8	40.0	0.28	1.7	0.16	2.8	0.16	2.8
9	116.2	40.5	0.26	1.7				
10	117.8	40.0	0.28	1.7				
11	116.8	40.2	0.21	1.7	0.17	2.5	0.18	2.5
12	117.4	40.3	0.28	2.0				
13	117.4	40.6	0.32	2.1				
14	117.2	40.4	0.30	2.0	0.18	2.7	0.18	2.6
15	117.6	39.8	0.29	1.9				
16	116.6	40.4	0.31	2.0				
17	116.8	40.3	0.29	1.9	0.18	2.5	0.17	2.5
18	116.8	40.4	0.20	2.0				
19	117.2	39.8	0.33	2.0				
20	116.4	40.7	0.30	2.0	0.16	2.6	0.22	3.0
21	117.2	39.9	0.29	2.0				
22	113.2	39.9	0.29	2.3				
23	114.0	40.3	0.26	2.0	0.12	2.4	0.18	2.8
24	113.6	40.7	0.27	5.0				
25	115.6	40.8	0.29	2.4				
26	115.8	40.1	0.27	2.0	0.15	2.8	0.15	2.3
27	115.4	40.2	0.27	2.2				
28	118.2	38.4	0.28	2.0				
29	117.6	39.4	0.29	2.0	0.15	2.5	0.16	2.4
30	117.2	39.1	0.27	2.0				
31	117.4	39.0	0.29	2.0				
32	117.6	39.1	0.25	2.2	0.15	2.4	0.12	2.5
33	116.8	40.2	0.26	2.0				
34	116.8	39.8	0.28	2.1				
35	118.0	39.3	0.25	2.0	0.18	2.5	0.17	2.2
36	115.6	39.1	0.24	1.9				
37	116.0	38.7	0.27	2.0				
38	117.2	38.8	0.24	1.9	0.17	2.5	0.20	2.2
39	117.8	40.1	0.25	2.0				
Avg. ±	116.1	40.1	0.26	2.0	0.15	2.6	0.16	2.6
	1.3	0.5	0.03	0.1	0.02	0.2	0.02	0.2

Six of the panels from McDonnell Douglas were mapped with respect to Δ , ψ and SPD. Figures A.37(a), (b) and (c) to A.41(a), (b) and (c) are Δ , ψ and SPD maps of panels MD1, 3, 4, 5 and 6. In the figure maps (A.37(a), (b), (c) to A.41(a), (b), (c)) all of the panels appeared fairly contamination free (i.e., most of the data falls within the acceptance bands and are therefore suppressed) except panel MD1 and MD5. Panel MD1 had a light colored streak in the position indicated in Fig. A.37(a) and panel MD5 had two lighter regions as indicated in Fig. A.40(a). These regions were caused by the sanding or buffing process used to remove letters printed on the aluminum panels, prior to anodizing. The three degree window for Δ suppresses most of the data but does reveal the damaged areas for MD1 and 5. The ψ and SPD plots (Figs. A.37(b) and (c)) do not reveal the streaks for MD1. The ψ plot (Fig. A.40(b)) does reveal the damaged areas but the SPD plot (Fig. A.40(c)) does not. A six degree window would have suppressed almost all of the data and all of the Δ plots would have been blank (appeared clean or undamaged). Whether the buffed regions have any effect on bond strength or durability is not known at this time.

Panel MD4(Figs.A.39(a),(b),(c)) for which almost all of the data fell within the chosen acceptance bands, was divided into 2" x 2" squares for deliberate contamination. Every other square was contaminated, according to the pattern in Fig. A.42. Contamination included coffee (wetted and dried), soda pop (wetted and dried), smudge with clean cotton glove, finger prints, 3 in 1 oil, hand lotion, lipstick, ink, human cough, cigarette smoke (after filtering through a human lung) and smog constituents docosane, hexadecylamine and stearic acid in pentane aerosol. The Δ plot in Fig.A.42(a) reveals all contamination but cigarette smoke and the cough, consistent with Fig.A.11(a). The ψ plot (Fig.A.42(b)) reveals all contamination but stearic acid cigarette smoke and the cough. The SPD plot (Fig.A.42(c)) reveals all contamination except the cough and just barely the cigarette smoke. The water contact angle plot (Fig.A.42(d)) reveals the stearic acid, hexadecylamine, docasane, lipstick, hand lotion, 3 in 1 oil and fingerprints but not the cigarette smoke, cough, ink, cotton smudge, soda pop or coffee.

Finally the test of the automated NDI technique with ellipsometry and SPD is shown in table 17 for production panels from McDonnell Douglas. The average value of Δ , ψ and SPD computed by the computer for 100 sq. inches of each panel is recorded in Table 17. The acceptance bands for Δ , ψ and SPD have been chosen as $141 < \Delta < 144$, $41 < \psi < 43$ and $.2 < \text{SPD} < .4$. Panel 4 was rotated 90° and replotted to see the effect of the aluminum roll direction. The average value of Δ increased by 2° while ψ and SPD changed very little. The change in Δ is due to the difference in light scattering with the direction of roughness. The difference is small enough to be neglected in terms of the acceptance band. It would be useful in practice to scan all panels with the grain in the same direction but probably not necessary.

The average values of Δ and ψ fall outside the acceptance band for Panel 5. On the production line a warning signal would result and panel 5 would be reinspected. Panel 6 passed Δ and ψ criteria but not SPD. Panel 4-1C fails Δ , ψ and SPD tests. Visual inspection would indicate that panels 1, 3, 4 and 6 are acceptable whereas panel 5 is damaged and 4-1c is contaminated.

It is a simple matter to program the computer to average over different areas and compare the average with the acceptance band. It might be appropriate to use higher spacial resolutions in critical areas (along edges, around holes, etc.) than others. It might also be appropriate to increase or decrease the acceptance band for different areas of the panel. Decisions as to the size of contaminated areas that can be accepted and acceptance band width must await task III. An example of the effect of spacial resolution is given at the bottom of Table 17. The average values of Δ and ψ in region of the damage for panel 1 (see Figure A.37(a)) prove to be 137 and 41, respectively. This region fails the acceptance band. If the spacial resolution was such that averaging took place for each square inch rather than each 100 sq. inches panel 1 would be reinspected rather than accepted (at the top of Table 17).

The automated NDI tools can be used to signal for reinspection if any specified area exceeds the acceptance band. If the signals are mapped the region of contamination is identified.

TABLE 17

Quality Assurance Table for Production Panels from
McDonnell Douglas. Acceptance Band $141 < \Delta < 144$,
 $41 < \psi < 43$, $0.2 < \text{SPD} < .4$. $\lambda = 6328 \text{ \AA}$, Angle of
Incidence 60° , Automated Ellipsometer.

Panel	Automated NDI Average Values			Pass Acceptance Band	Reinspect	Visual Inspection
	Δ	ψ	SPD			
MD 1	142	42.5	0.30	yes		OK
3	144	42.4	0.32	yes		OK
4	142	42.0	0.33	yes		OK
rotate 4 , 90°	144	42.1	0.32	yes		OK
5	146	40.1	0.35	no	x	damage
6	141	42.0	0.45	no	x	OK
contaminated 4-1C	136	38.0	0.47	no	x	deliberate contamination
region 5	137	41.0	-	no	x	damage
region 3,5	147	39.3	-	no	x	damage
region 11-12,5	148	39.0	-	no	x	damage

SECTION IV

DISCUSSION AND CONCLUSIONS

In this section we discuss possible mechanisms by which anodic films are stable, strong and durable, the utility and limitations of each surface tool and the conclusions as to the general utility of the final combination of NDI surface tools.

A. Mechanisms

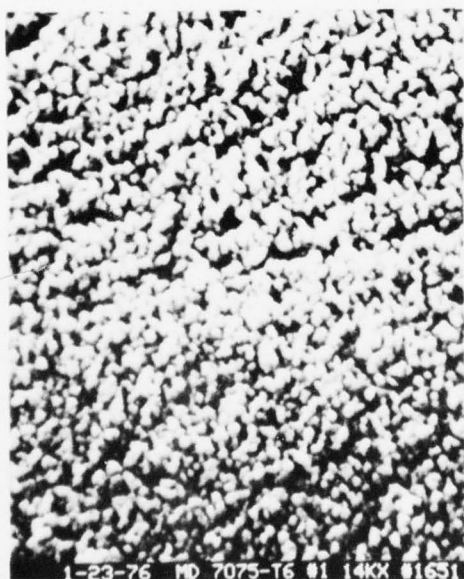
Some speculation as to the physical and chemical properties that account for the excellent bonding character of the phosphoric acid anodized aluminum surfaces is in order. Figure 19 shows different SEM magnifications of an anodized Al 7075-T6 sample. These pictures were taken at Northrup and sent to the Science Center by T. P. Remmel. Figures 19a, b and c are of an unbent area and Fig. 19d is of a bent area. The striking feature of the anodic films is the hedge row appearance. The hydroxide is topologically very rough and very porous. The exposed surface area on and within the film must be very large. The porous open structure (which acts like a blotter) and the polar nature of the outer surface (covered with hydroxyl ions) probably accounts for the wettability of the surface by water and by adhesive primer even in the presence of some contamination. If a monolayer of organic matter is transferred from the anodizing bath surface, it probably stretches over the hydroxide roughness as a continuous film (see ref. 8). However, this film is very fragile and would be broken into small fragments upon spray rinsing or priming. In the case of contamination from smog aerosol, the aerosol particles deposit contamination in discrete spots rather than as a uniform layer. In either type of contamination the surface is heterogeneous, much of it is left uncontaminated. These properties, plus mechanical interlocking of adhesive that



a



b



c



d

Figure 19. SEM pictures of anodized Al 7075-T6 (from T. P. Rimmel, Northrup).

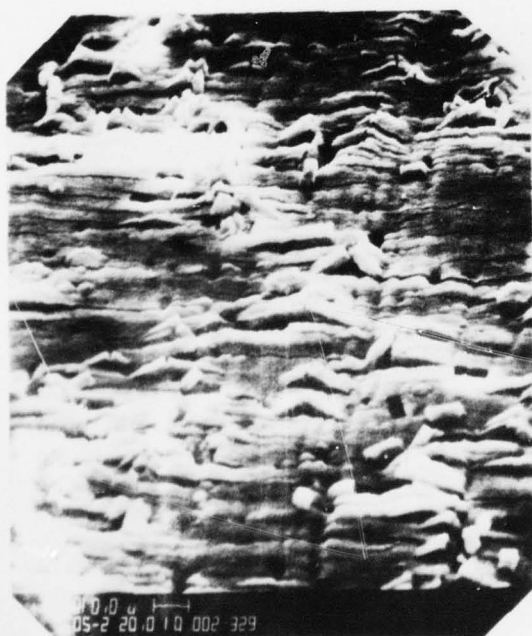
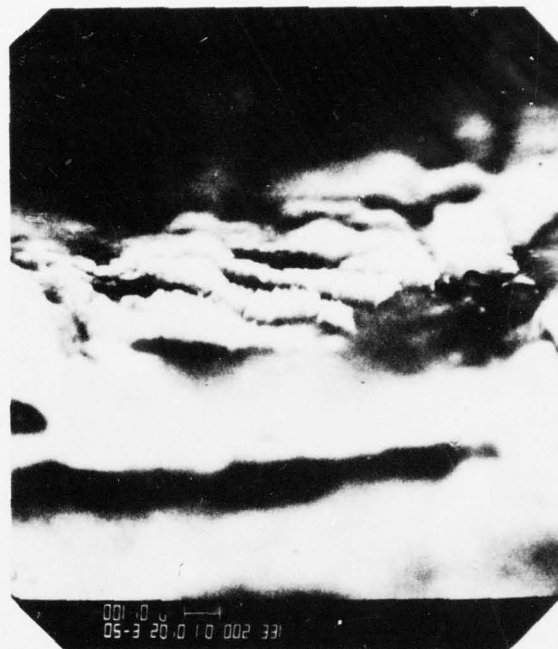
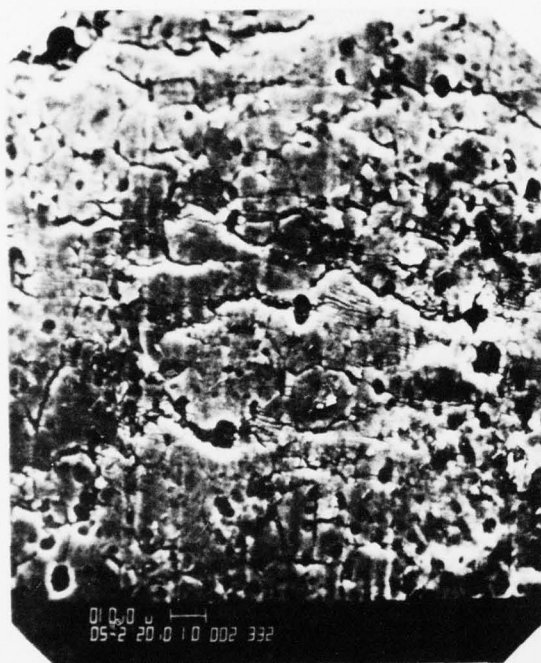


Figure 20. SEM pictures of FPL etched AL 2024-T3 after 21 hrs at 100°C water (boiled dry) (top), 21 hrs., 50°C water (bottom).

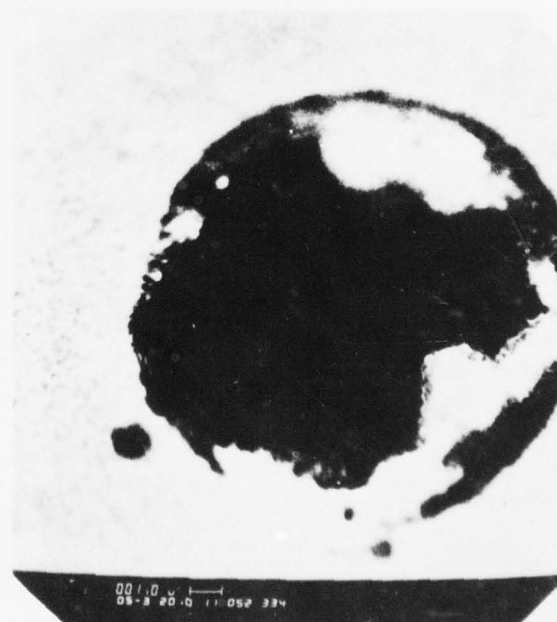
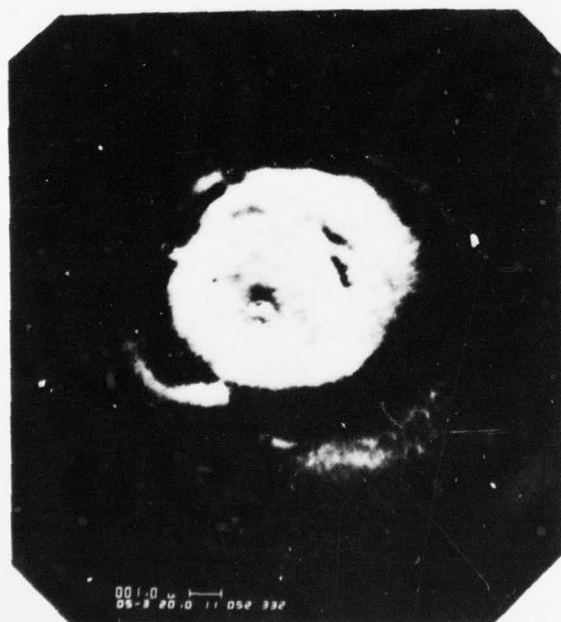
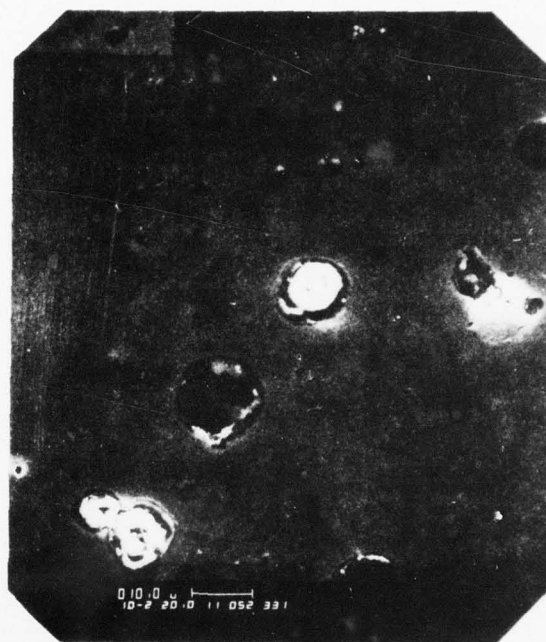
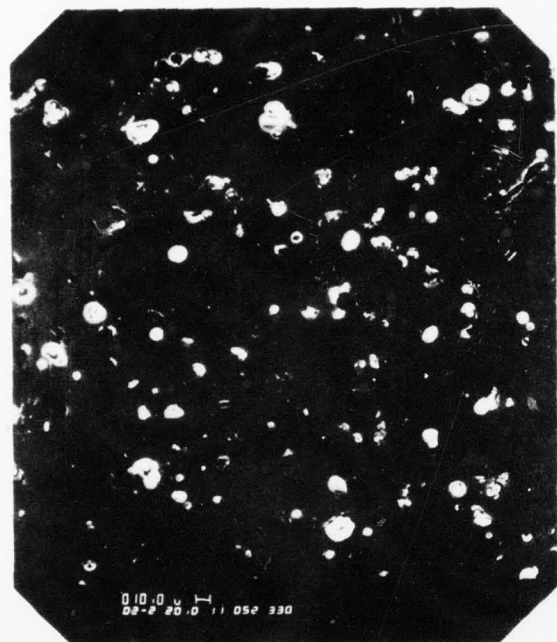


Figure 21. SEM pictures of vapor deposited Al after anodizing to 500 Å then 50°C water exposure for 150 hrs.

penetrates into the porous film, account for the excellent bonding character of the anodic surface. There is probably little cohesion between adjacent columns of hydroxide and they separate with little fracture along the column when the metal is bent (see Fig. 19d). On the other hand the columns are chemically bonded to a barrier layer on the substrate and each column may be a single crystal giving high strength in a direction perpendicular to the surface. Compare the anodic pseudo boehmite in Fig. 19 with that formed in hot water at the top of Fig. 20 and with bayerite at the bottom of Fig. 20. The water formed hydroxides are very cellular (see Fig. 21) and fail in the oxide when adhesively bonded and stressed to failure.

Surface damage, caused by handling with cotton gloves, Kimwipes, etc., has been shown (at McDonnell Douglas with AES) to increase slightly the carbon peak on the hydroxide surface. From experience, at the Science Center, of deliberate contamination followed by AES, ESCA and then the small amount of hydrocarbon necessary to produce C peaks reported by McDonnell Douglas, bonding is considered insufficient to degrade the bond. In addition, our results with clean quartz wool indicates that the surface changes occur in the absence of contamination.

It is reported⁹ that if the outer atomic layers of oxide are covered with polar hydroxyl ions the surfaces are very wettable with water and polar adhesives whereas if the outer atomic layer is oxygen the surface is not polar or wettable. It is postulated that surface damage by cotton gloves, etc. shears the hydroxide film exposing planes of oxygen as well as hydroxyl and probably leaves the surface electrically charged. This type of surface is thermodynamically metastable and will revert to an uncharged hydroxyl outer

layer when exposed to moisture. This process of conversion at the bond line is believed to cause separation during the wedge test. This hypothesis is consistent with the increase in water contact angle and large temporary increase in SPD on damaged anodic films (see Table 9). It can be further tested by exposing the damaged surface to water and then drying prior to bonding. A return to the hydroxylated state should restore durability to the bond.

B. Surface Tools

1. Ellipsometry:

The ellipsometer is sensitive to the anodic film thickness and structure as well as to contamination. Since the light beam does not change or contaminate the surface, ellipsometry is truly nondestructive and very useful for detecting all forms of contamination, such as incorrect film thickness from processing errors, damaged films from handling and contamination from the various sources. It has been shown in this report that Δ is in the range of 80° to 110° and ψ in the range of 37° to 46° for anodic films less than 1000 \AA , whereas properly prepared anodic films ($\sim 3000 - 4000 \text{ \AA}$) have a range of $\Delta \sim 160^\circ$ to 180° and $\psi \sim 37^\circ$ to 41° . Therefore ellipsometric results (as SEM) can easily detect if the film is below 1000 \AA (in the danger region). However, the high sensitivity to film thickness is a disadvantage with respect to detecting surface contamination because small changes in film thickness might be interpreted as contamination, whereas small changes in film thickness is probably inconsequential with respect to bond strength or durability. The maximum Δ window experienced in this work for a particular alloy and specific anodizing conditions is about 6° degrees ($\sim 40 \text{ \AA}$) and from panel to panel about 12° degrees ($\sim 80 \text{ \AA}$). For example, if a panel had an anodic film of thickness near the top of the Δ window, plus 80 \AA of organic contamination the panel would pass the acceptance test. Considering the fact that some organic contamination does not change the wettability, it is conceivable that the 80 \AA of organic contamination

AD-A044 241

ROCKWELL INTERNATIONAL THOUSAND OAKS CALIF SCIENCE --ETC F/G 11/6
NONDESTRUCTIVE INSPECTION OF PHOSPHORIC ACID ANODIZED ALUMINUM --ETC(U)
APR 77 T SMITH

UNCLASSIFIED

SC5026.22TR

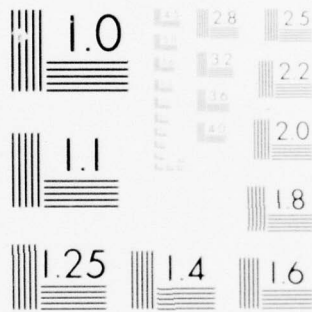
AFML-TR-77-42

NL

2 OF 3

AD
A044241





MICROCOPY RESOLUTION TEST CHART
NATIONAL BUREAU OF STANDARDS-1963-A

would not be detrimental to bond strength or durability. This information must be discovered in Task III.

The automated intensity ellipsometer, used for mapping panels, is extremely fast since there are no moving parts and the photodetectors have time constants in the nanoseconds. Therefore the speed of mapping depends upon the speed of the computer data acquisition and the speed of movement of the sensing head with respect to the panel surface. We have shown that an automated nulling ellipsometer would be about twice as sensitive to contamination due to the effect of surface roughness. Although this type of ellipsometer would be much slower than the intensity type, it may well be adequate for most applications. Due to the absolute measurement (phase shift and amplitude ratio of the components of polarized light) the ellipsometer does not suffer from a stability problem. However, due to changes in processing parameters it is necessary to periodically calibrate with control samples.

2. Surface Potential Difference (SPD)

Although the surface potential difference between the reference electrode and the surface of interest is directly related to the anodic film thickness ($\sim -1 \text{ mv}/10 \text{ \AA}$) it is much more sensitive to permanent and induced dipoles associated with organic contamination on the surface ($\sim +10 \text{ mv}/10 \text{ \AA}$). SPD can be very useful for film thickness as well as contamination. The prime difficulty with SPD is that the reference electrode is unstable with time. This problem is equally important for vibrating or oscillating systems (e.g. Fokker contamination tests and ISO probe) as for our radio active system. This is because each system is measuring the work function difference between two electrodes. The drift of the reference electrode is usually not great over a

one day period and therefore measurements comparing different surfaces the same day are very revealing. Figure 22 shows SPD between our nickel foil reference electrode and gold vapor deposited on aluminum. The upper curve in Fig. 22 is SPD between our nickel foil electrode and an FPL etched Al 2024-T3 sample for the same time period. The fact that the two curves have different shapes is indication that the fluctuations of at least one of the couples is not due to the common reference electrode. The SPD between the nickel and gold is more stable and averages about $- .18$ volts with maximum deviations of about ± 0.07 volts over a period of 50 days. The data at the right of Fig. 22 was taken about a year later. The fact that both the FPL etched and gold have shifted up about 0.09 volts indicates that the shift is probably due to a change in the work function of the nickel reference electrode. To use SPD as a NDI tool frequent calibration (perhaps daily) will be needed. As yet we have not found a surface, in our laboratory or referred to in the literature, that can be demonstrated to be completely stable (e.g. to ± 20 mv) for more than a day or so. We have tried anodized aluminum and anodized aluminum sprayed with a teflon type spray (FLUO-Kem) as well as gold and platinum, etc. Figure 23 shows SPD between our reference electrode and the gold electrode for 200 hrs. SPD varies between 0 and 0.1 volts. The SPD between the nickel reference electrode and the anodized aluminum have much larger changes over the 200 hr period. There is no correlation between the nickel-gold couple and the nickel and aluminum electrodes, whereas there is a correlation between the aluminum electrodes. Since the nickel and gold are not expected to follow each other with respect to work function the stability of the nickel reference electrode has settled to at least ± 0.05 volts. The correlation between the aluminum electrodes indicates these electrodes are changing in a similar way, with or without the teflon spray.

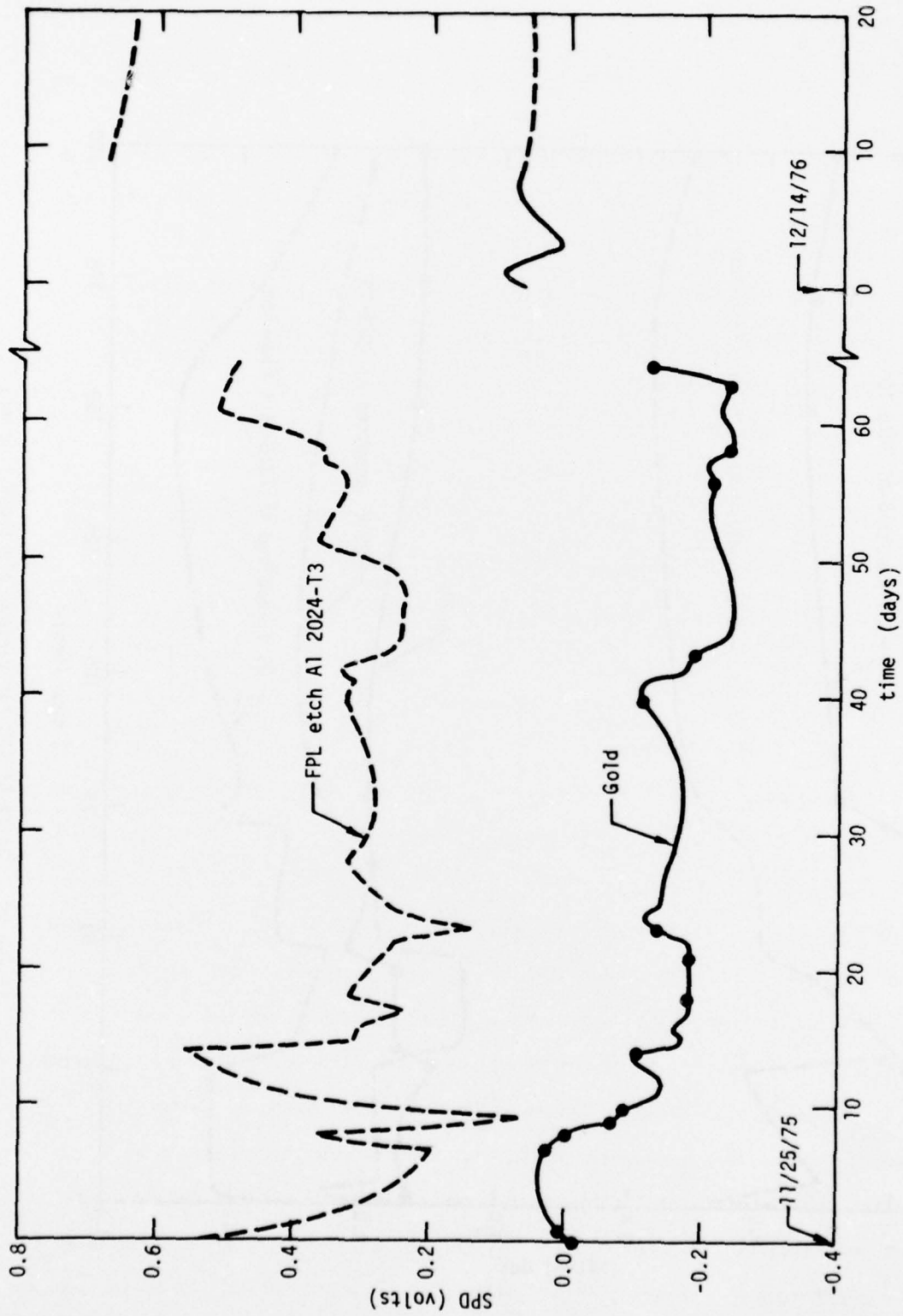


Figure 22. Drift of SPD for a Nickel-Gold and Nickel-FPL Al 2024-T3 electrode couples

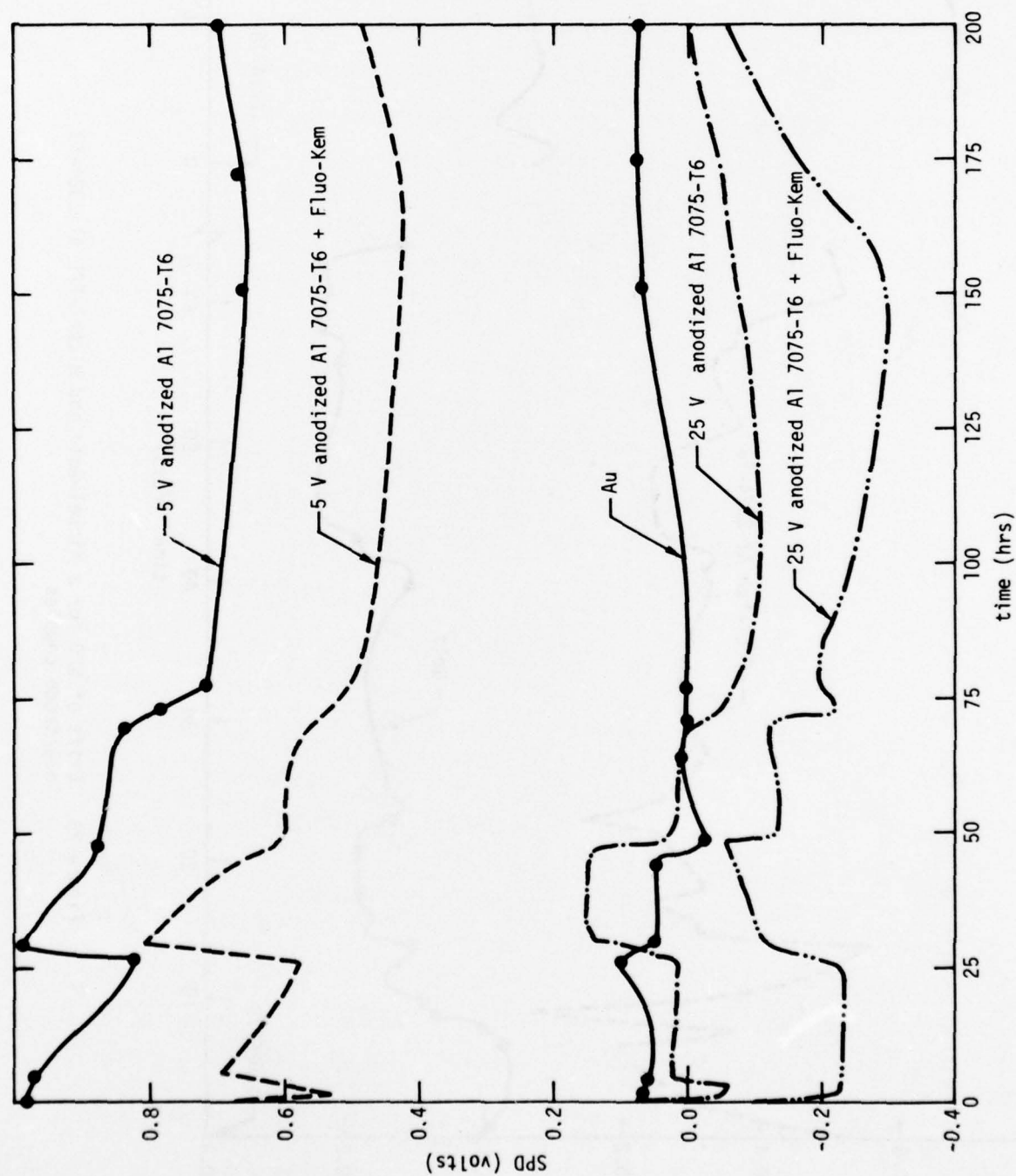


Figure 23. Drift of SPD for various electrode couples.

According to Fig. 13 an increase of 0.08 in SPD could be interpreted as two monolayers of contamination when in fact there is none, but the reference electrode has changed by this much. In order to calibrate the SPD tool it will be necessary to prepare a surface of constant work function. The best surface for this purpose thus far is a freshly anodized aluminum surface.

3. Photoelectron Emission (PEE)

The PEE is driven by a constant voltage source (45 volt battery in our instrument) much larger than the SPD and therefore is not sensitive to reference electrode drift as with SPD. The emission of electrons from aluminum with UV light of 2500 \AA is primarily from the substrate metal and depends on the surface roughness and the attenuation of the hydroxide film. Due to the porous nature of the phosphoric acid anodic films the PEE is almost independent of film thickness. The porous outer film is approximately transparent to emitted electrons as they pass along the open channels. Attenuation does occur with respect to a barrier layer at the bottom of the pores. For example the PEE for a 5 volt film ($\sim 1500 \text{ \AA}$) on Al 7075-T6, was measured eight times over a period of 10 days. The average value of PEE proved to be $3.8 \pm 0.6 \times 10^{-11}$ amps. This can be compared to $5.9 \pm 0.7 \times 10^{-11}$ amps for a 25 volt film ($\sim 7500 \text{ \AA}$) and about 50×10^{-11} amps for an FPL etched ($\sim 200 \text{ \AA}$ film) sample. The thicker 25 volt film must either have a less attenuating barrier layer or a thinner barrier layer than the 5 volt film. Due to the thickness and nature of the anodic films the PEE is near background and is insensitive to mechanical damage or contamination. It has been shown to be very useful for other surface preparations of aluminum and titanium.^{10,11}

4. Contact Angles

The water contact angle measurement has the advantage that it is sensitive only to the outer atomic layers and thus is extremely sensitive to non-polar organic contamination. It has the disadvantages that the surface must be contacted (increasing the chance of contamination) and is not sensitive to polar contamination that can decrease bond strength and durability (see ref. 5).

C. Conclusions

Examination of all of the contamination maps has been made to establish if the particular surface tool can or cannot detect the contamination near the minimum levels for this study. Table 18 gives the list of contaminants and a y or N below each surface tool. The y indicates (yes) the surface tool is considered to successfully detect the contamination and N (No) the surface tool is not considered to successfully detect the contamination. The ellipsometric parameter Δ is considered successful for 25 of the 32 contaminants. Four of the contaminants not detected by Δ were not detected by SPD or contact angle and were probably not present (due to evaporation). Three of the contaminants were not detected by the ellipsometer but were detected by SPD or contact angle. Seventeen of the contaminants were detected by SPD. SPD was particularly unsuccessful for processing errors and handling damage. Contact angle measurements detected 15 contaminants, most of which were organic and nonpolar. Contact angle was unsuccessful for the detection of process errors, handling damage and human contamination (except for greasy materials such as finger prints, lipstick, etc.). The spaces left blank under the contact angle column were not tested. In no case did the contact angle detect contamination for which Δ or SPD did not. It is concluded that the best NDI system would include

SC5026.22TR

both ellipsometry and SPD. This system would detect essentially all types of contamination. The best single tool is ellipsometry.

TABLE 18
REPRESENTATIVE CONTAMINATION DUE TO VARIOUS SOURCES
AND SURFACE TOOL UTILITY

Type	Compound or Substance	Ellipsometry (Δ)	SPD	Contact Angle
Processing Errors	Anodize time	y	N	N
	Anodize voltage	y	y	N
	Contamination from bath	y	N	N
	Delay in H_3PO_4 before rinse	y	N	N
Handling Damage	Cotton glove	y	N	N
	Kraft paper	y	N	N
	Kimwipe	y	N	N
Human Contamination	Finger prints	y	y	y
	Cough or sneeze	N	N	N
	Cigarette smoke	N	N	N
	Cigarette ashes	N	y	N
	Food remnants	y	y	N
Representative Constituents of Smog	N Docosane	y	y	y
	16-Bromo-9-hexadecanoic acid	y	y	y
	Dotriacontane	y	y	y
	Stearic acid	y	N	y
	Erucic acid	y	y	y
	Brassicidic acid	y	y	y
	Decanoic acid	y	N	y
	Benzoic acid	y	y	y
	Amino-Benzoic acid	y	y	y
	1,1,2 diamino dodecane	y	y	y
	1-12-diamino decane	y	y	
	decadiene	N	N	
	decacyclene	y	N	N
	1-Eicosene	y	N	y
	1-Hexadecamine	y	y	y
	Anthracene	N	N	N
	Adamantanol	y	y	N
	2-Adamantanone	y	y	N
	1-Adamantone carbonitrile	N	y	y
	1-Adamantane carbonylic acid	y	N	y

APPENDIX A

Computer plots of anodized aluminum surfaces with controlled contamination. The computer printouts that correspond with some of the figures have the same number in Appendix B.

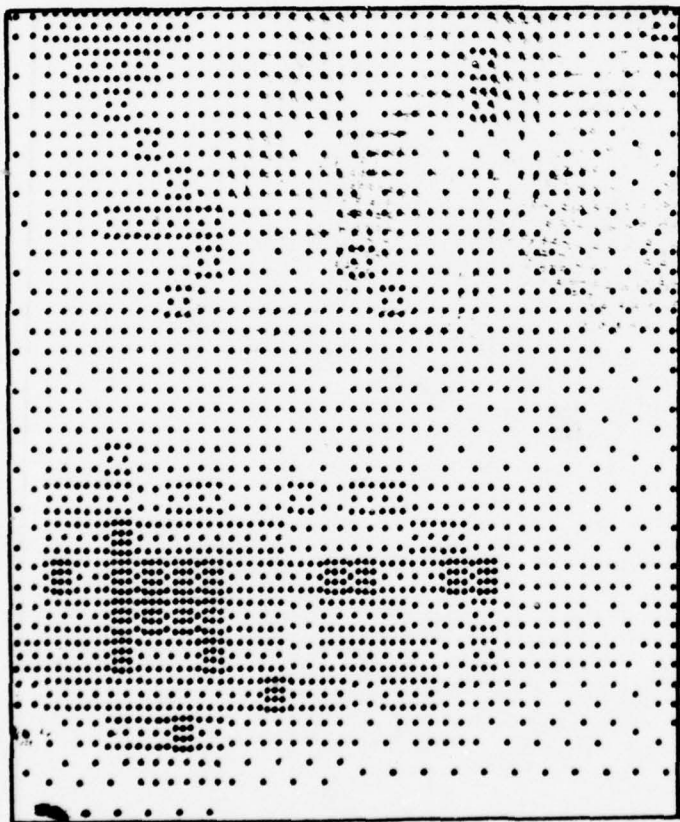


Figure A.1(a). Computer plot of Δ within the band ($160 < \Delta < 163$) for the calibration sample

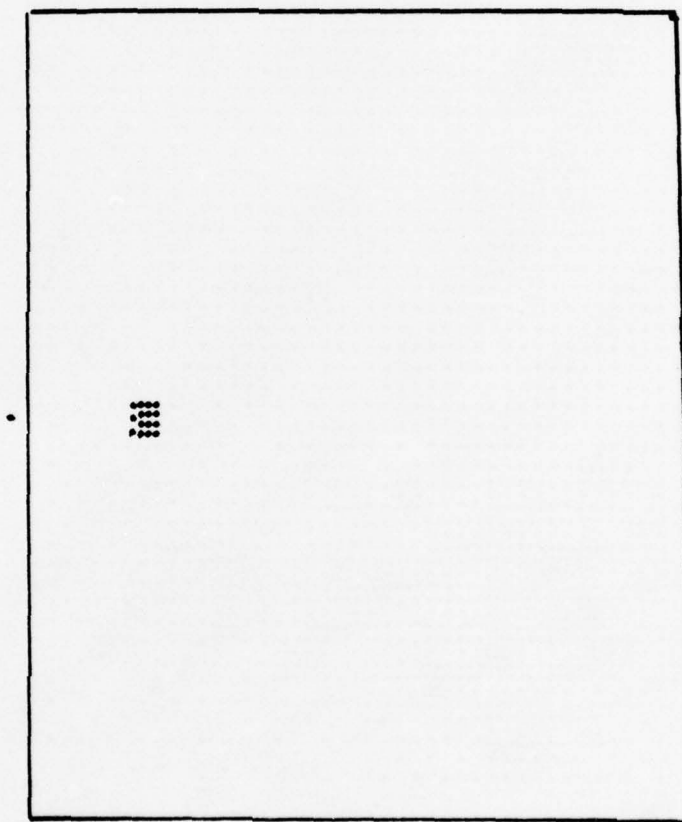


Figure A.1(a). Computer plot of Δ outside the band ($163 < \Delta < 160$)
(cont'd) for the calibration sample.

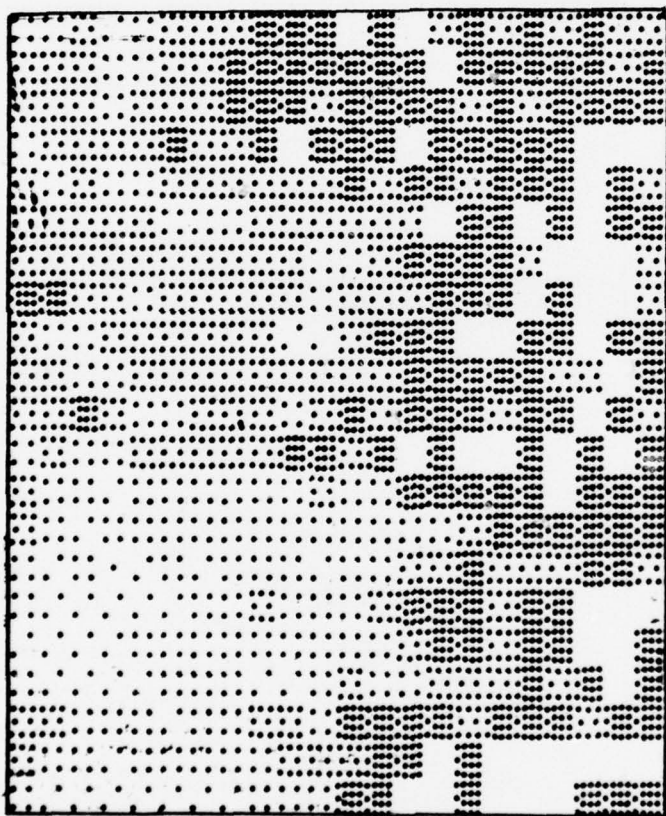


Figure A.1(b). Computer plot of ψ within the band ($40 < \psi < 42$) for the calibration sample.

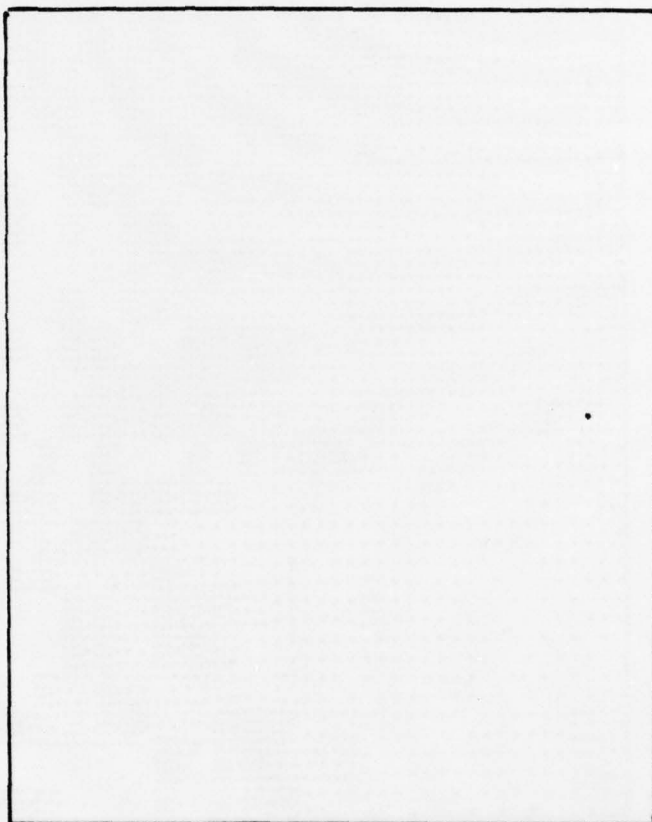


Figure A.1(b). Computer plot of ψ outside the band ($42 < \psi < 40$) for the
(cont'd) calibration sample.

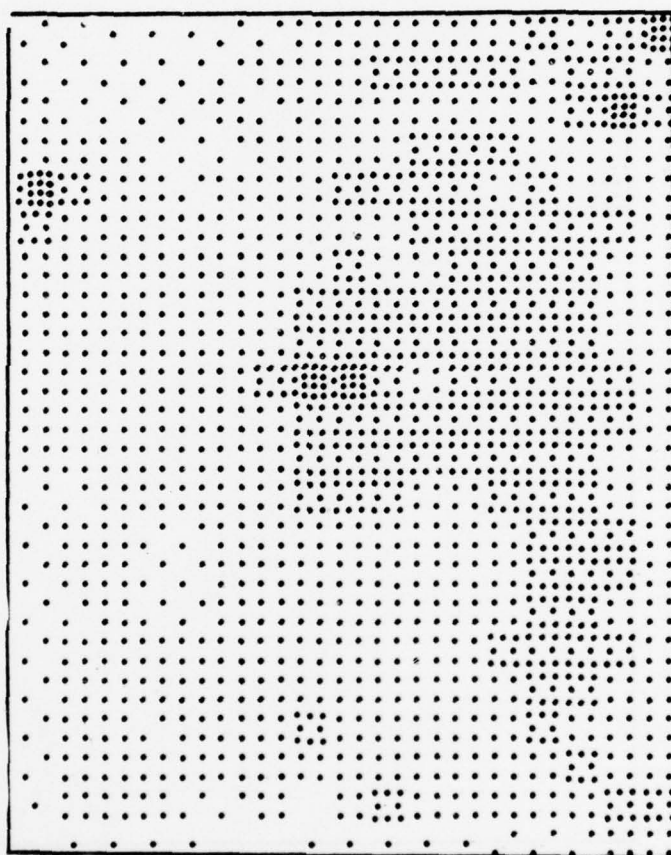


Figure A.1(c). Computer plot of SPD within the band $(.47 < \text{SPD} < .65)$ for the calibration sample

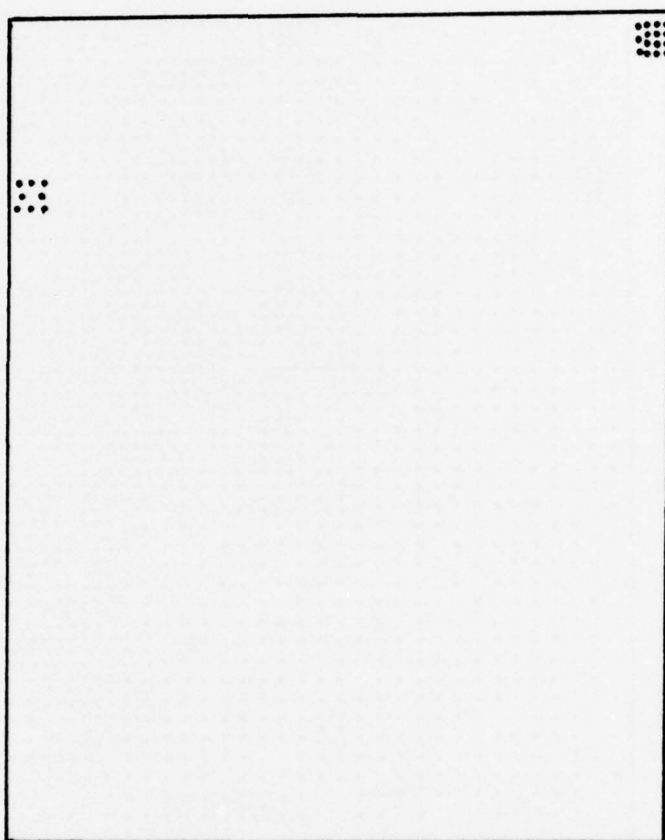


Figure A.1(c). Computer plot of SPD outside the band ($.65 < \text{SPD} < .47$)
(cont'd) for the calibration sample.

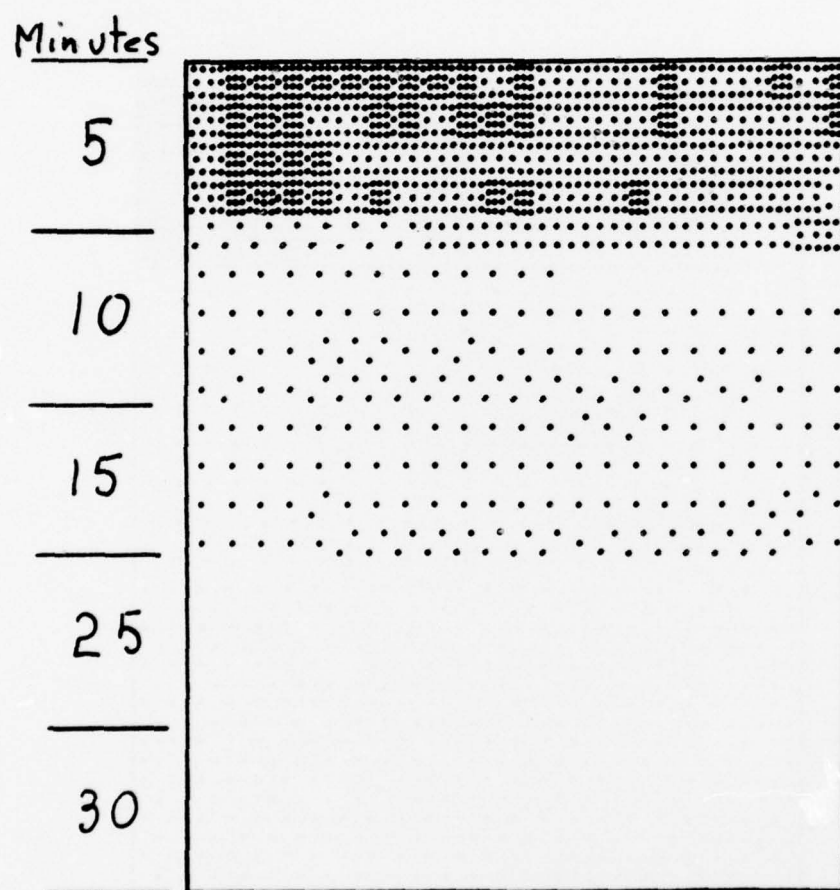


Figure A.2(a). Computer plot of Δ outside the band ($164 < \Delta < 162$) for a sample that was anodized for 5, 10, 15 and 30 minutes in the indicated areas

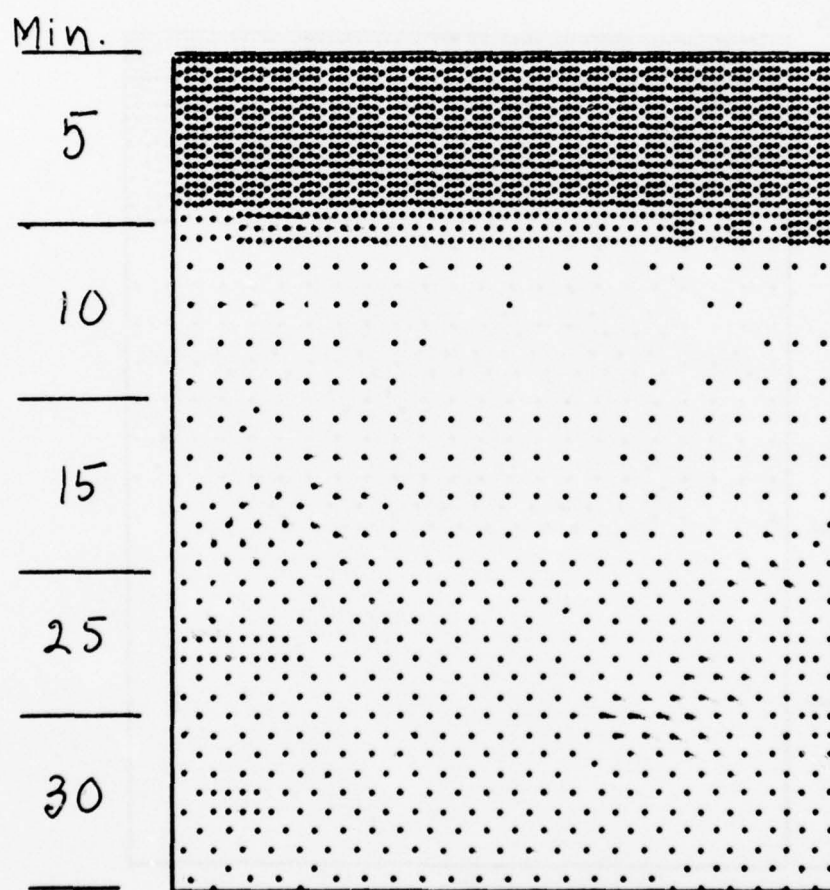


Figure A.2(b). Computer plot of ψ outside the band ($42 < \psi < 41$) for a sample that was anodized for 5, 10, 15, 25, and 30 minutes in the indicated areas.

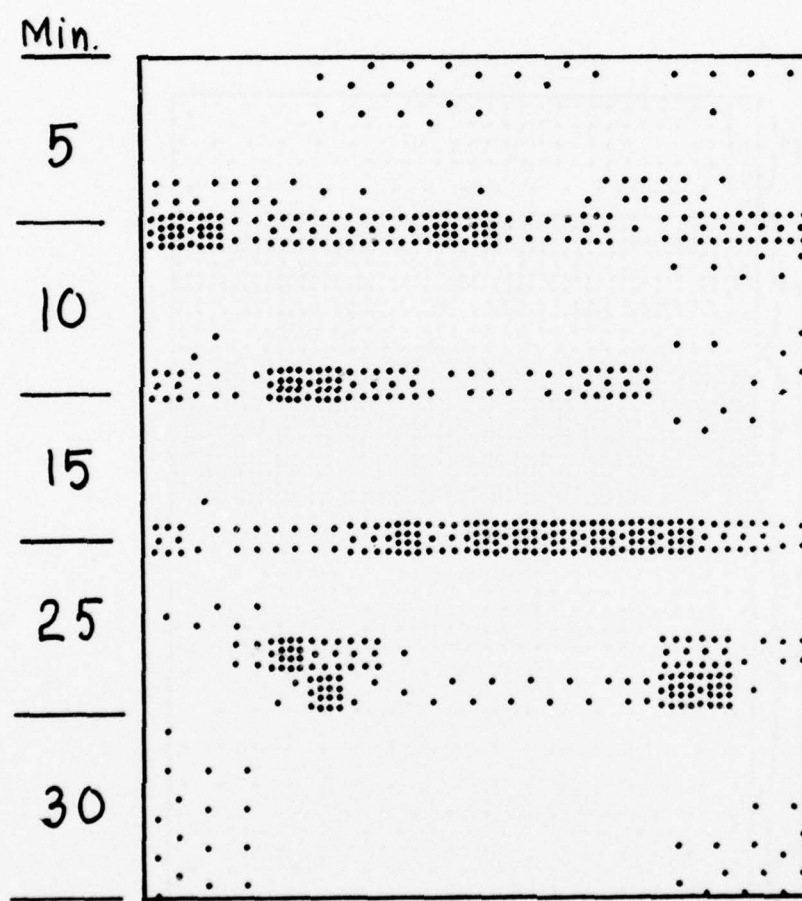


Figure A.2(c). Computer plot of SPD outside the band ($0.4 < \text{SPD} < 0.2$) for a sample that was anodized for 5, 10, 15, 25 and 30 minutes in the indicated areas.

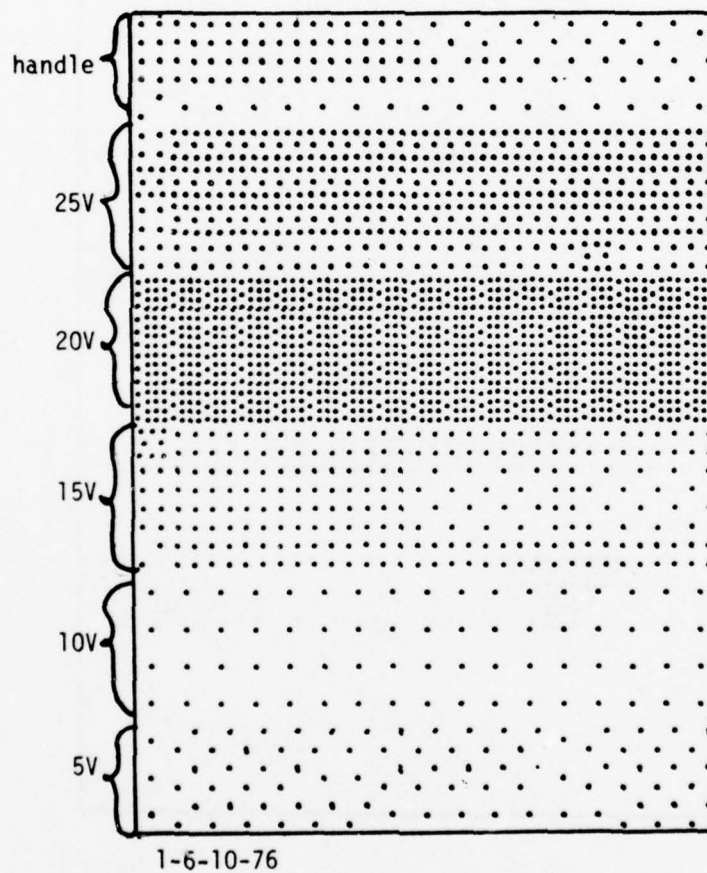


Figure A.3(a). Computer plot of Δ ($159 < \Delta < 156$) for a panel that was anodized at 5, 10, 15, 20 and 25 volts.

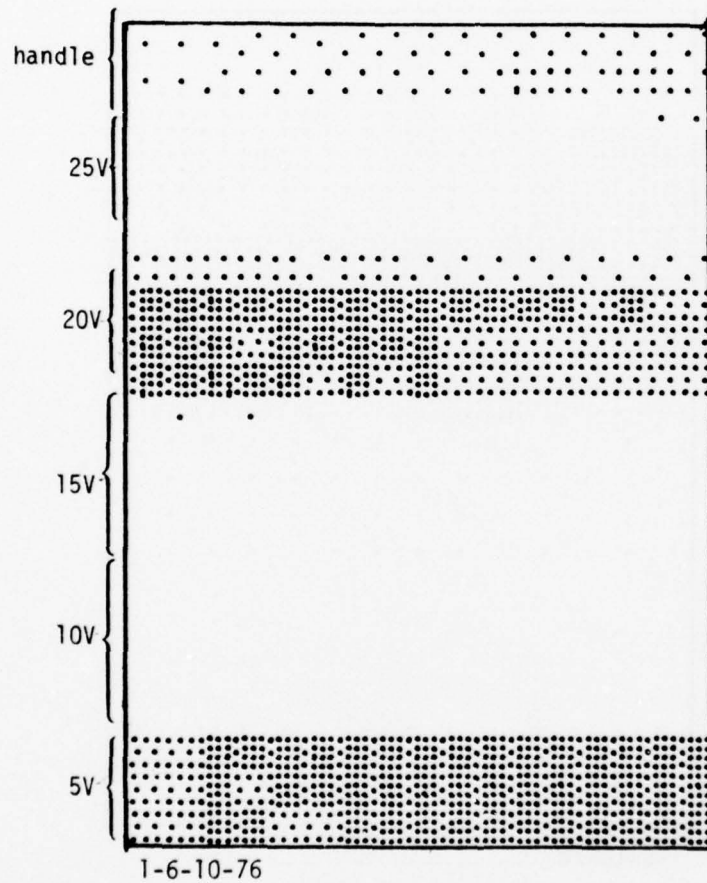


Figure A.3(b). Computer plot of ψ ($41 < \psi < 40$) for 5, 10, 15, 20 and 25 volts.

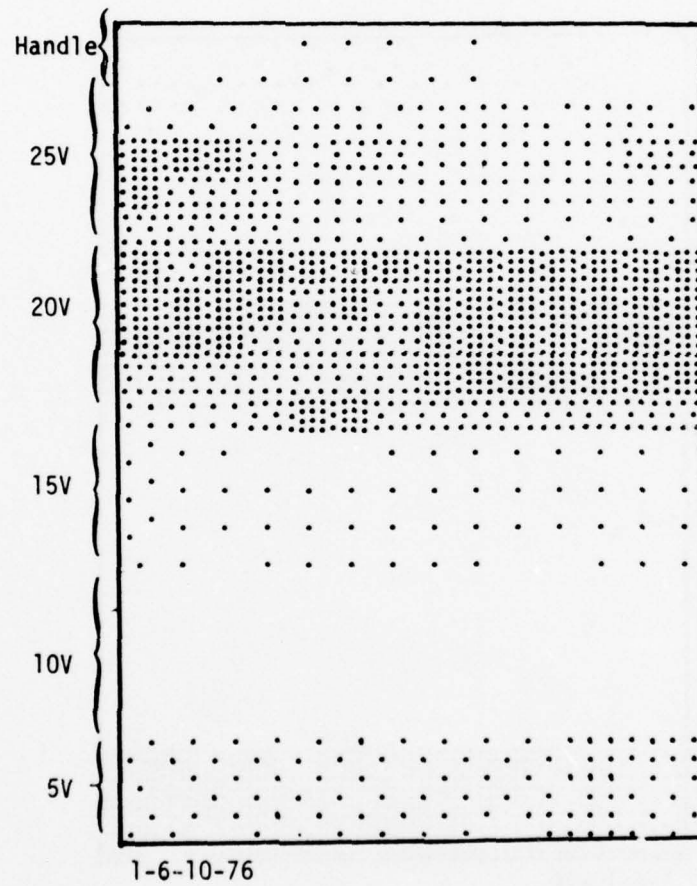
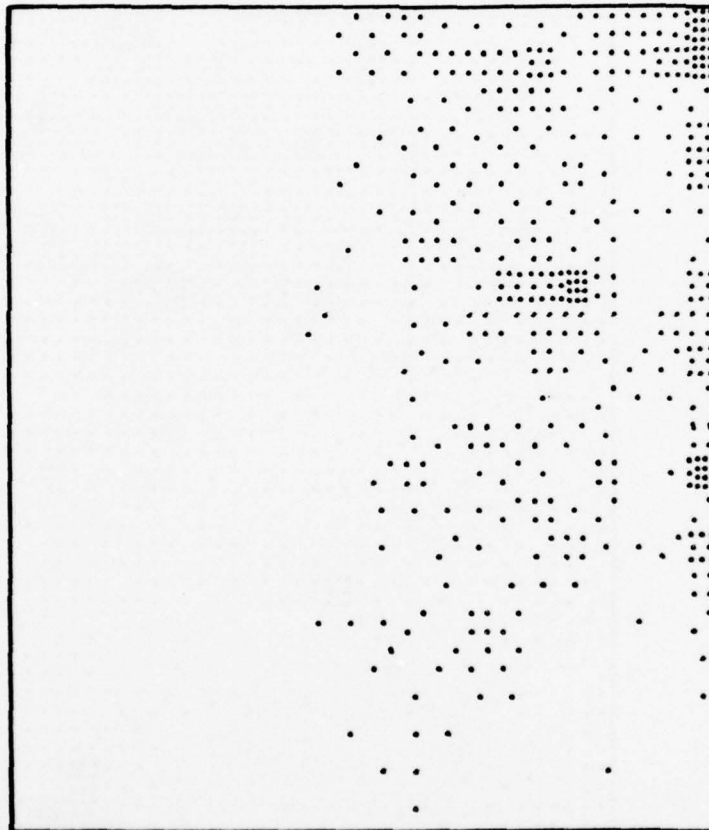
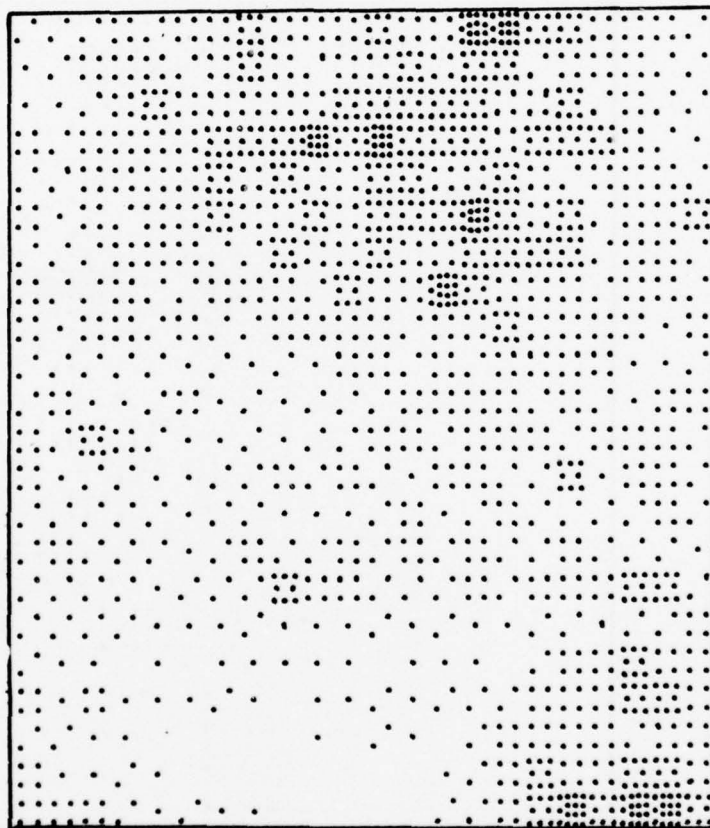


Figure A.3(c). Computer plot of SPD ($.4 < \text{SPD} < .3$) for 5, 10, 15, 20 and 25 volts.



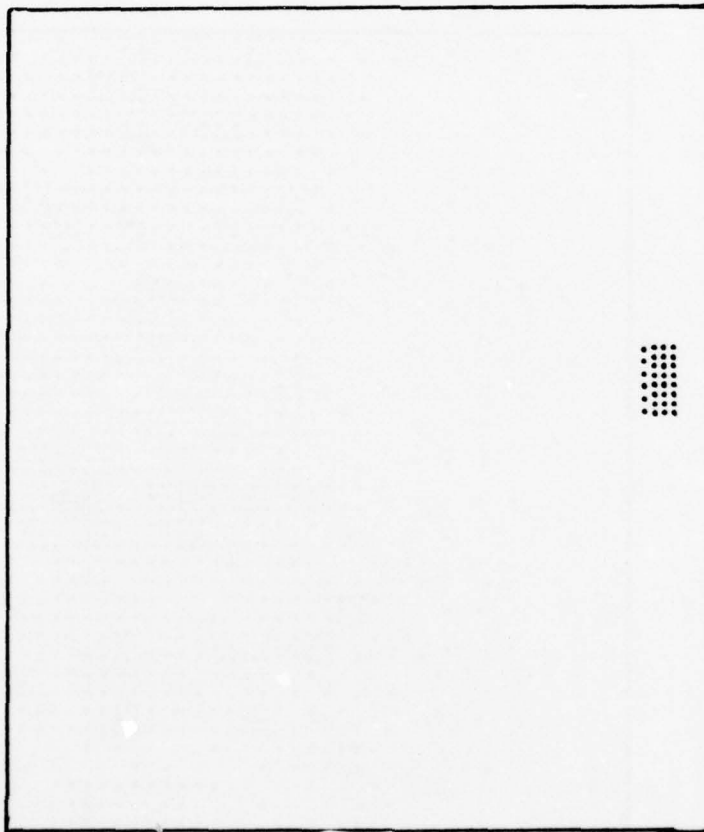
2-6-10-76

Figure A.4(a). Computer plot of Δ ($164 < \Delta < 162$) for a panel anodized in a bath contaminated with cigarette ashes, hair and dirt.



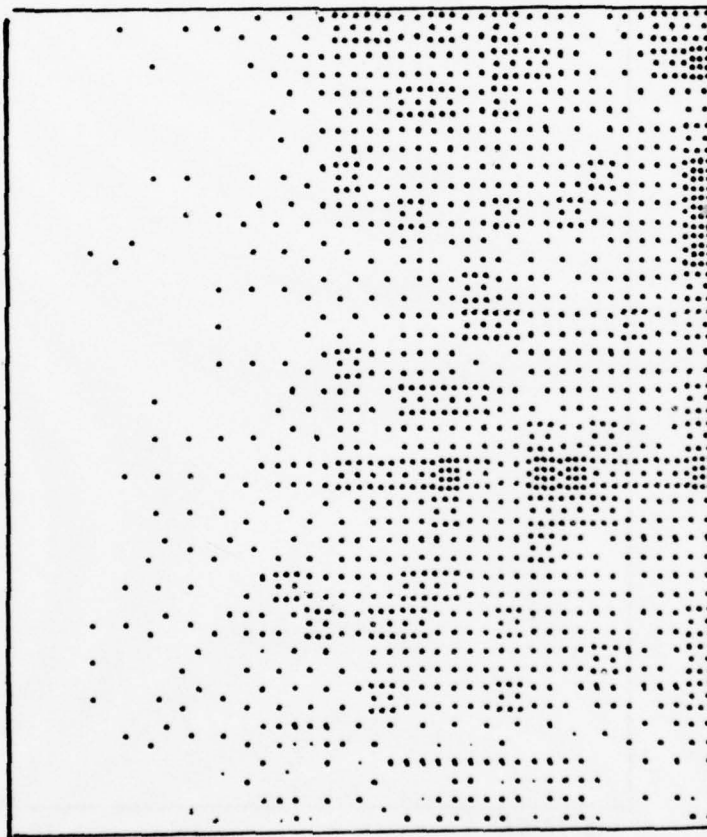
2-6-10-76

Figure A.4(b). Computer plot of ψ ($42 \leq \psi \leq 41$) for a panel anodized in a bath contaminated with cigarette ashes, hair and dirt.



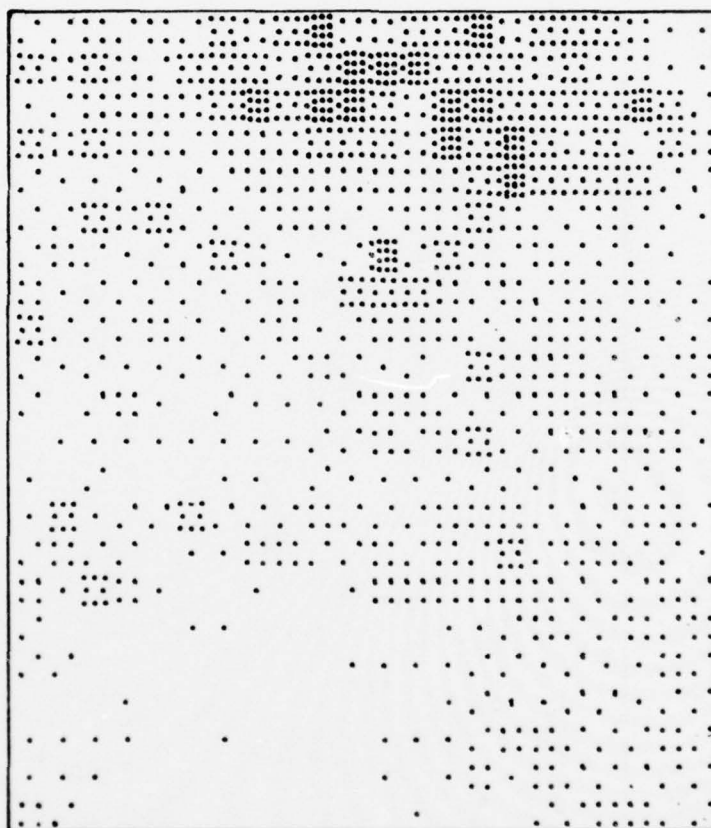
2-6-10-76

Figure A.4(c). Computer plot of SPD ($.4 < SPD < .2$) for a panel anodized in a bath contaminated with cigarette ashes, hair and dirt.



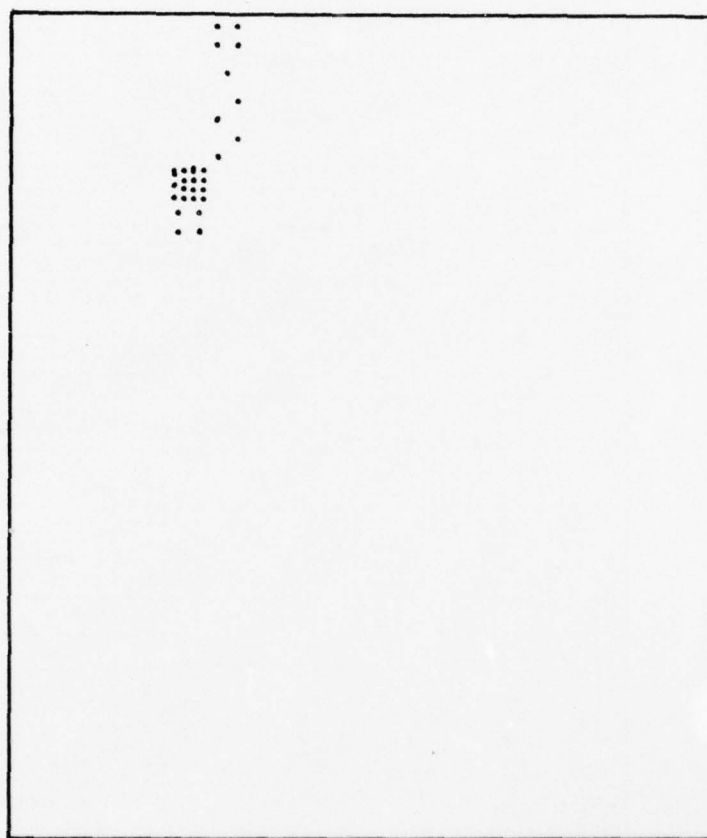
3-6-10-76

Figure A.5(a). Computer plot of Δ ($164 < \Delta < 162$) for a panel anodized in bath contaminated with cigarette ashes, hair, dirt and a particle of stearic acid.



3-6-10-76

Figure A.5(b). Computer plot of ψ ($42 < \psi < 41$) for panel anodized in bath contaminated with cigarette ashes, hair, dirt and a particle of stearic acid.



3-6-10-76

Figure A.5(c). Computer plot of SPD ($.5 \leq \text{SPD} < .3$) for panel anodized in bath contaminated with cigarette ashes, hair, dirt and a particle of stearic acid.

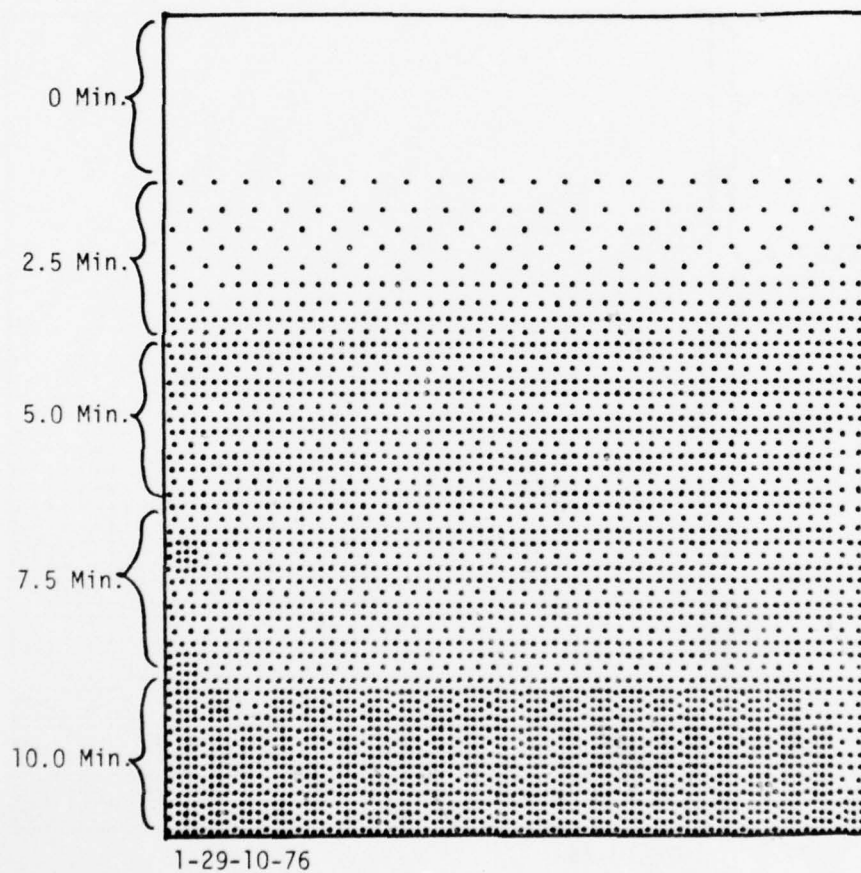


Figure A.6(a). A Δ plot ($168 < \Delta < 165$) of a panel that was left in the acid bath for various lengths of time before rinsing.

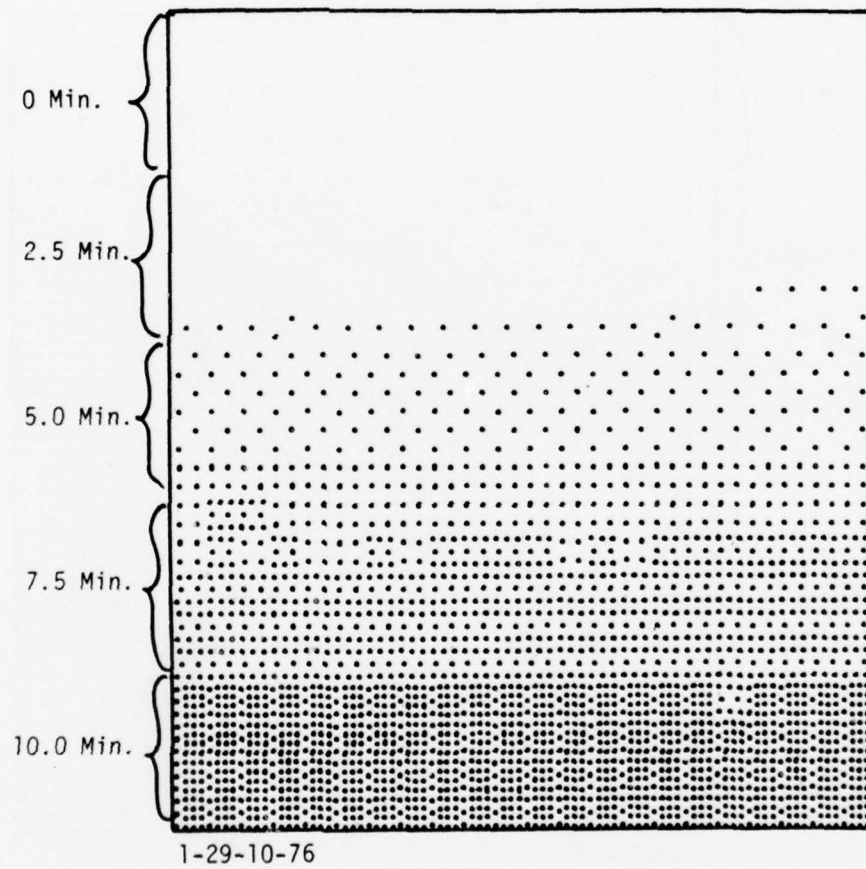


Figure A.6(b). A ψ plot ($45 < \psi < 44$) of a panel that was left in the acid bath for various lengths of time before rinsing.

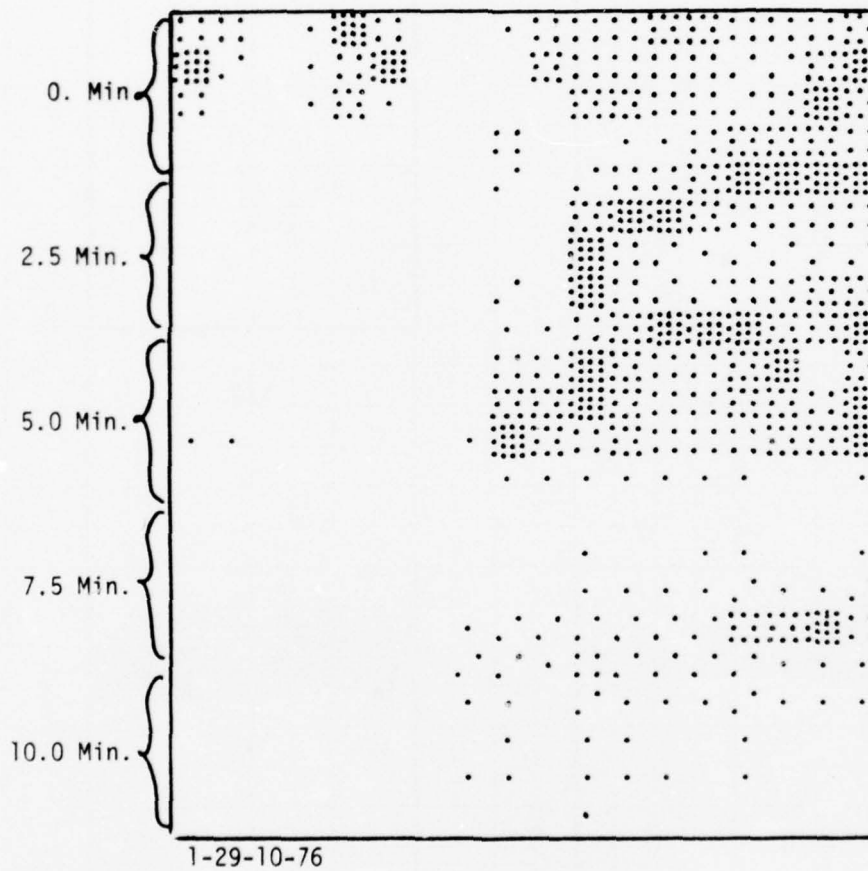
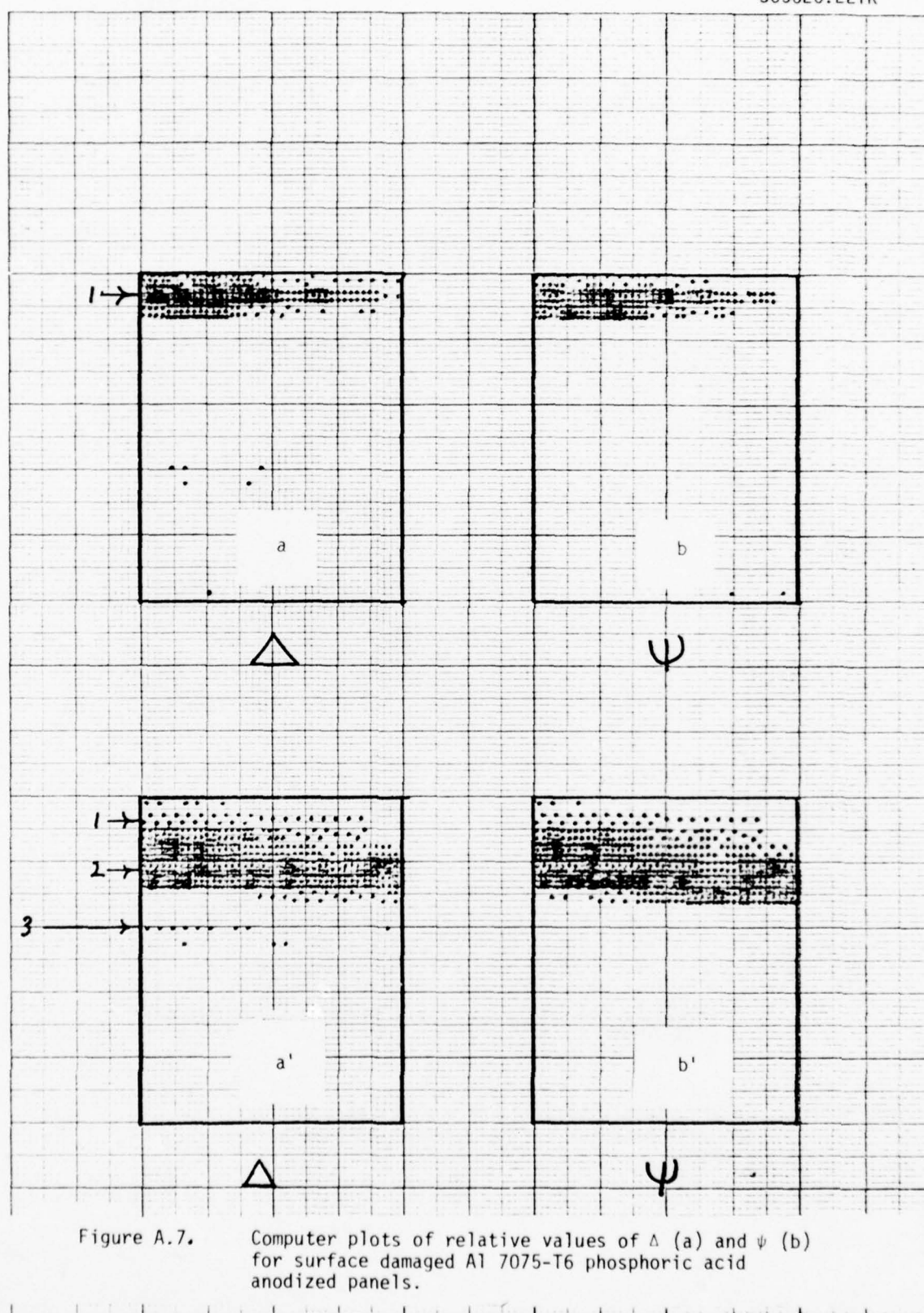
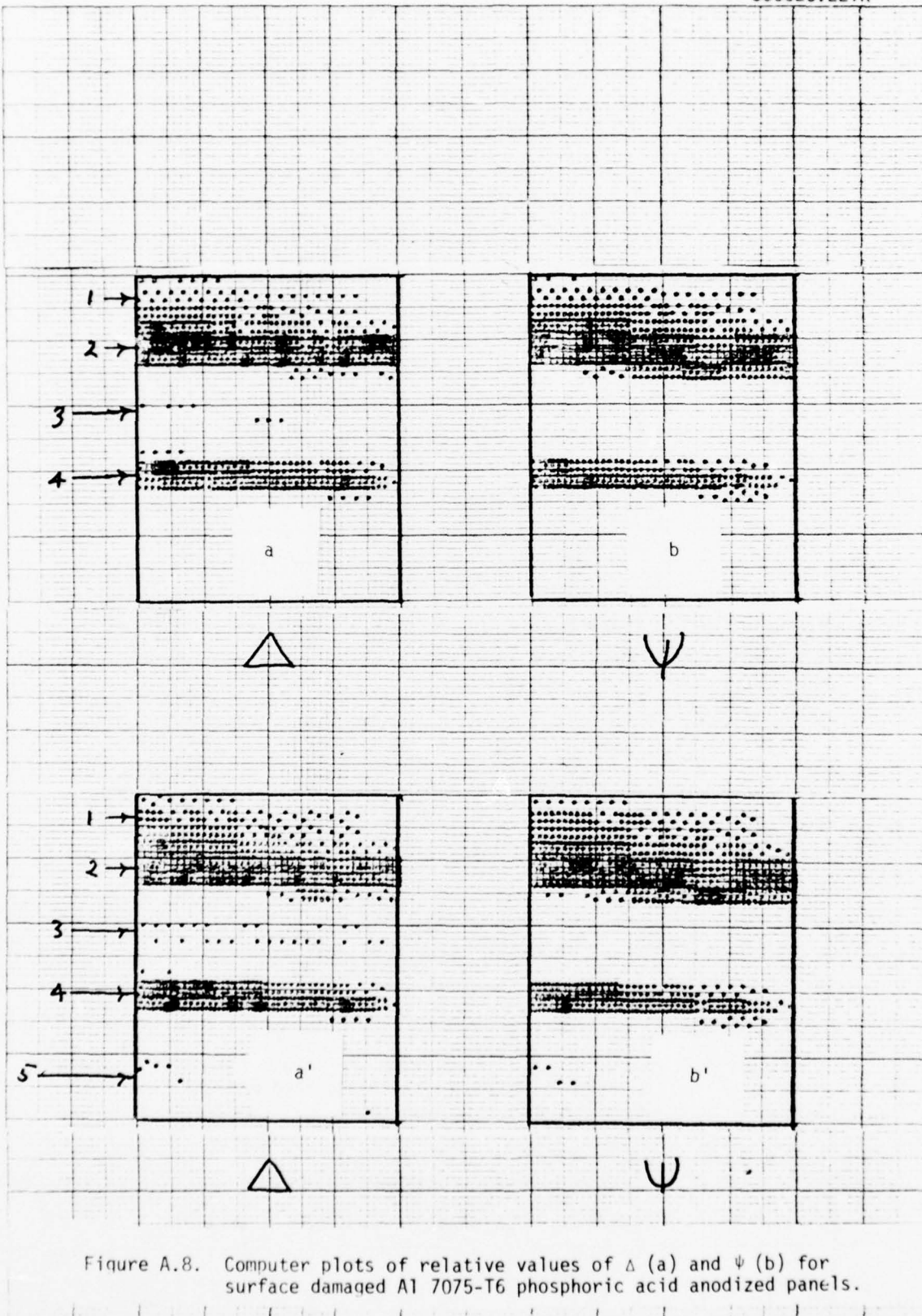


Figure A.6(c). An SPD plot ($.4 < \text{SPD} < .2$) of a panel that was left in the acid bath for various lengths of time before rinsing.





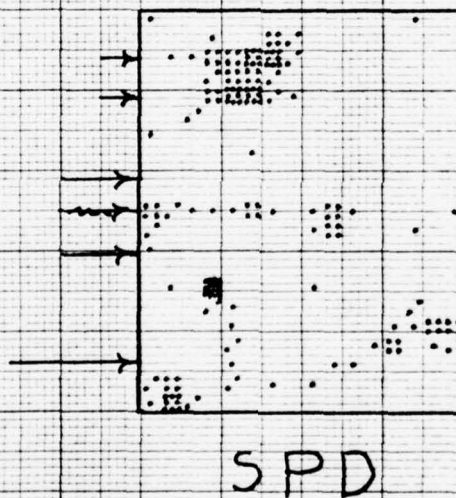
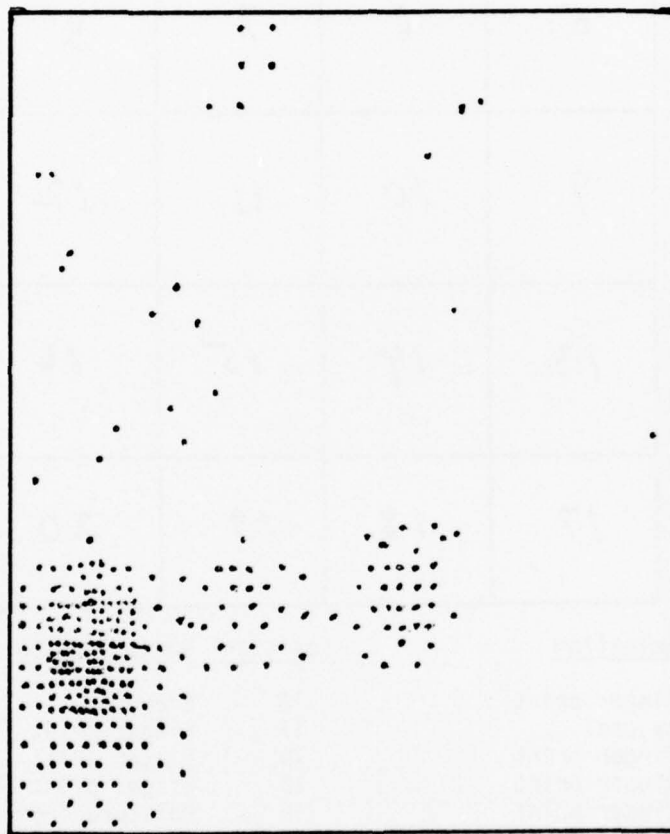


Figure A.9. Computer plot of relative SPD values for surface damaged Al 7075-T6 phosphoric acid anodized panels.

1	2	3	4
5	6	7	8
9	10	11	12
13	14	15	16
17	18	19	20

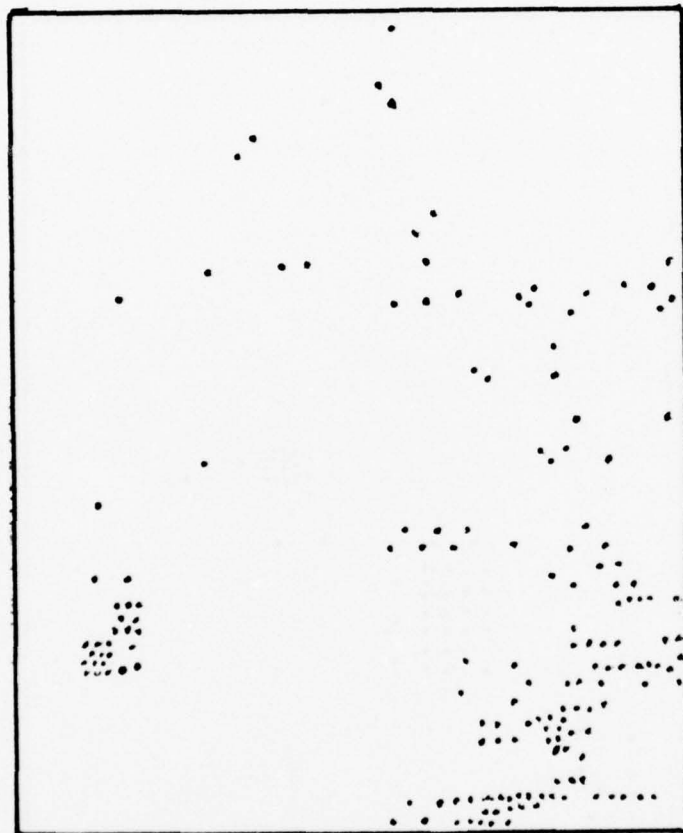
<u>Position</u>	<u>Contamination</u>	<u>Position</u>	<u>Contamination</u>
1	Dry finger print	12	Bread
2	Banana peel	13	Finger print (touch forehead)
3	Dry finger print	14	Finger print (touch wet saliva)
4	Dry finger print	15	Finger print (touch hair)
5	Dry finger print	16	Moisture from cough
6	Dry finger print	17	Finger print (touch finger 3 in 1 oil, wipe with Kimwipe)
7	Dry finger print	18	Finger print (washed)
8	Dry finger print	19	Finger print (washedalconox)
9	Cigarette smoke	20	Finger print (washed acetone)
10	Cigarette ashes (stale)		
11	Cigarette ashes (fresh, hot)		

Figure A.10. Regions of an anodized sample that have been contaminated according to the listing.



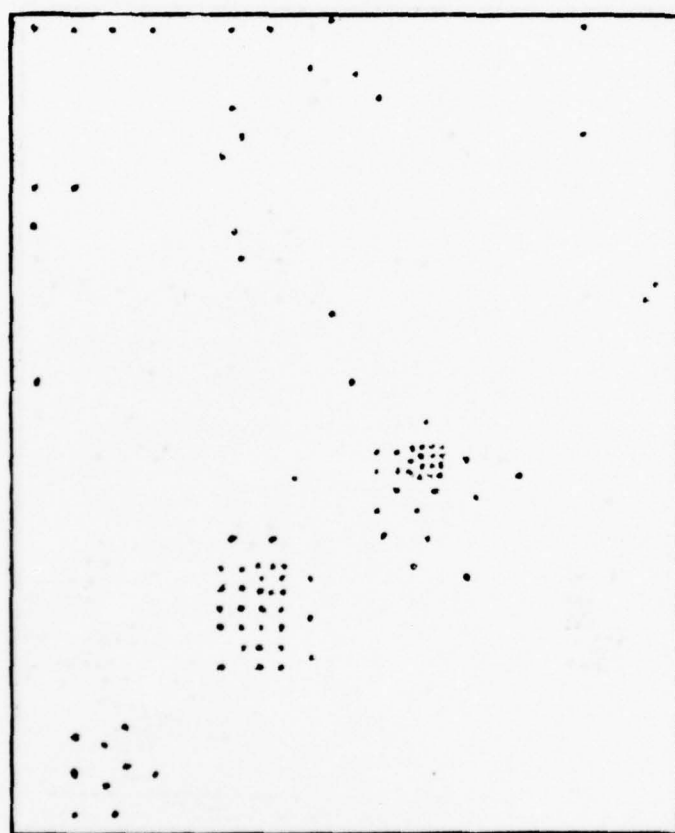
7-21-4-76

Figure A.11(a). A Δ plot for $163 < \Delta < 160$ for a panel contaminated as in Figure A.1(a).



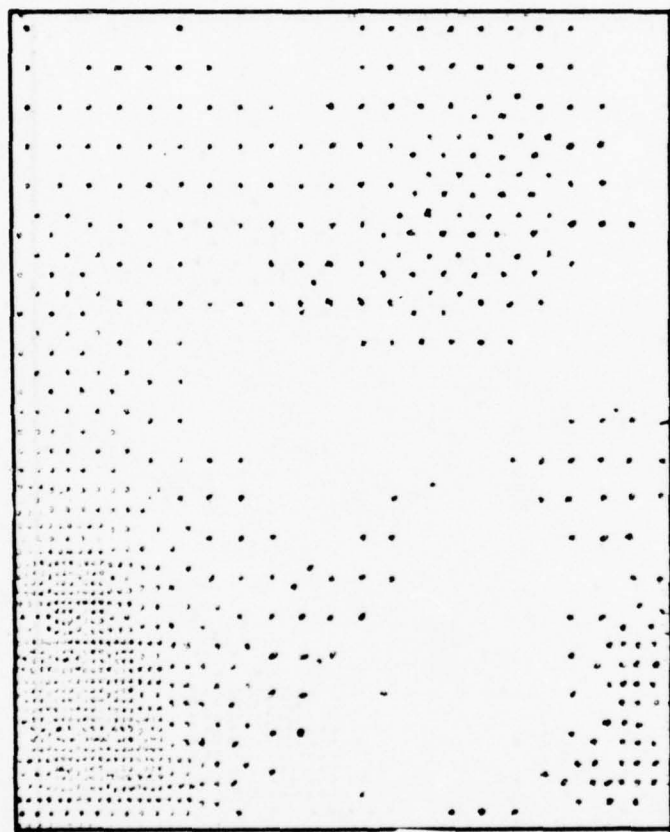
7-21-4-76

Figure A.11(b). A ψ plot for $43 < \psi < 41$ for panel for Figure A.1(a).



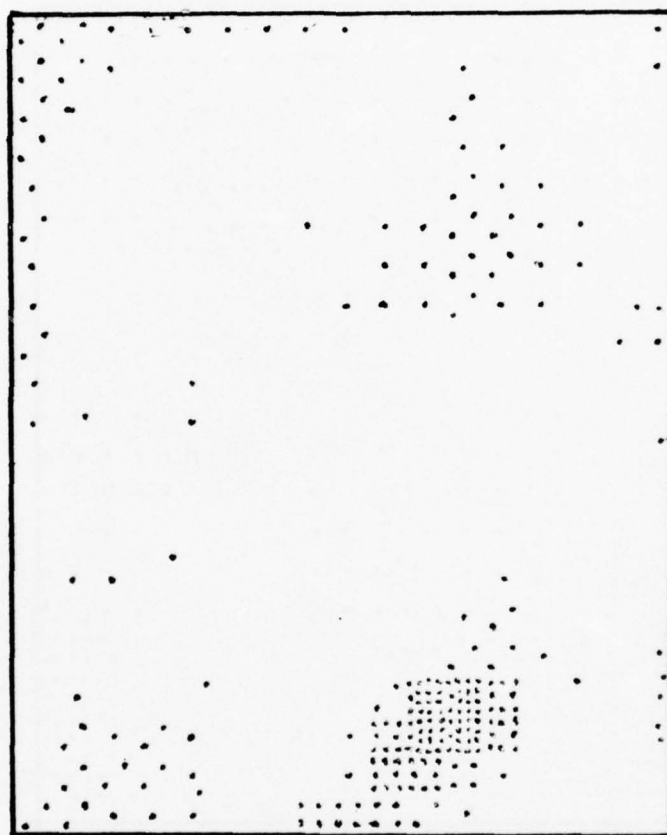
7-21-4-76

Figure A.11(c). An SPD plot for $.49 < SPD < .45$ for panel of Figure A.1(a).



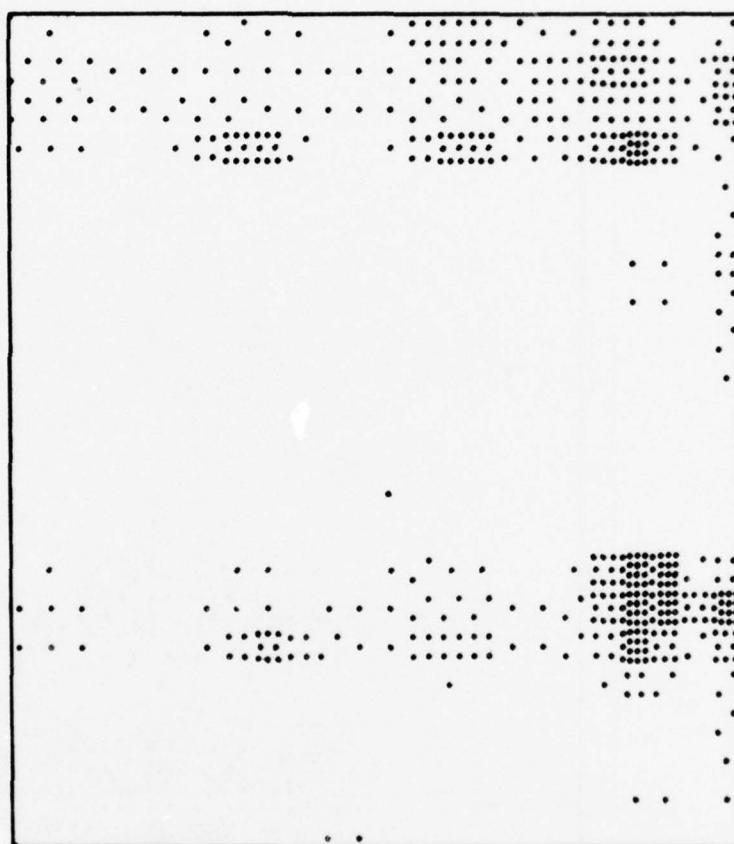
9-21-4-76

Figure A.12(a). A Δ plot for $163 < \Delta < 160$ for a panel exposed to cigar smoke for 3 days.



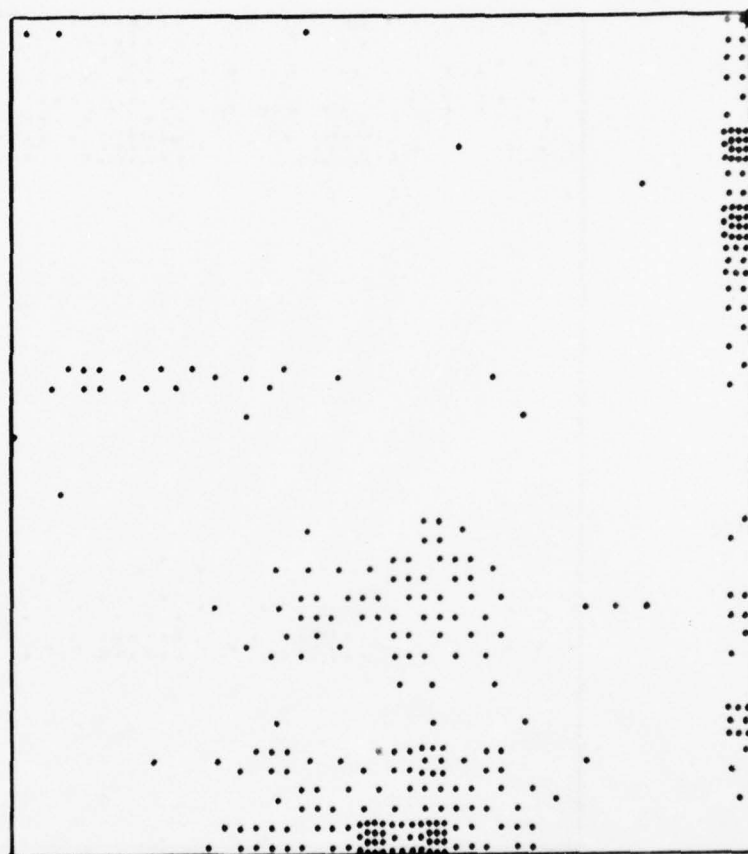
9-21-4-76

Figure A.12(c). An SPD plot for $.61 < SPD < .59$ after exposure to cigar smoke.



3-10-5-76

Figure A.13(a). A plot of Δ ($164 < \Delta < 162$) for a panel contaminated (top and bottom) with pentane aerosol containing decanoic acid.



3-10-5-76

Figure A.13(b). A ψ plot ($42 < \psi < 41$) for a panel contaminated (top and bottom) with pentane aerosol containing decanoic acid.

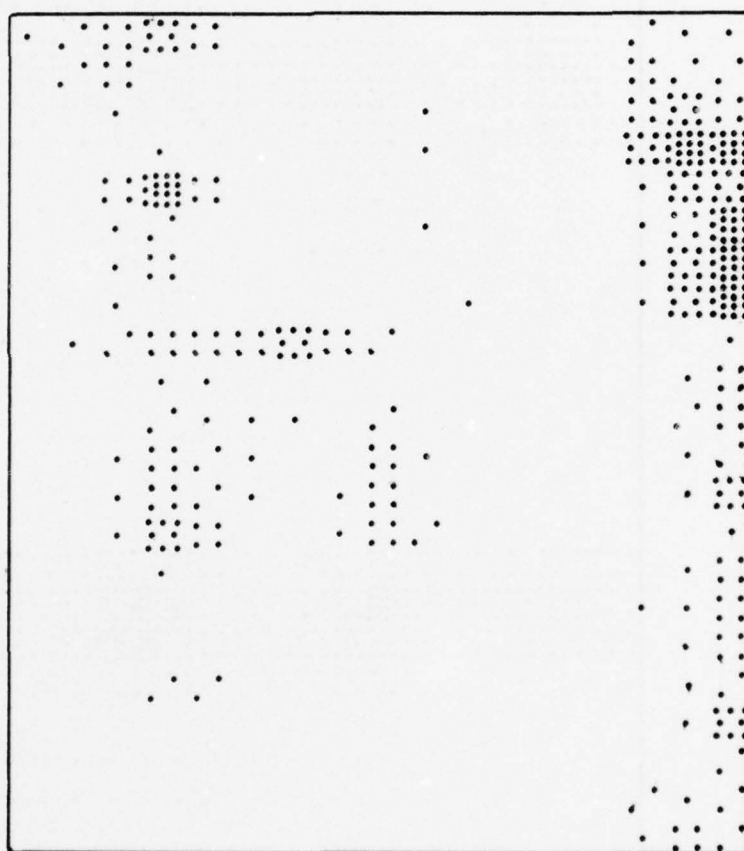
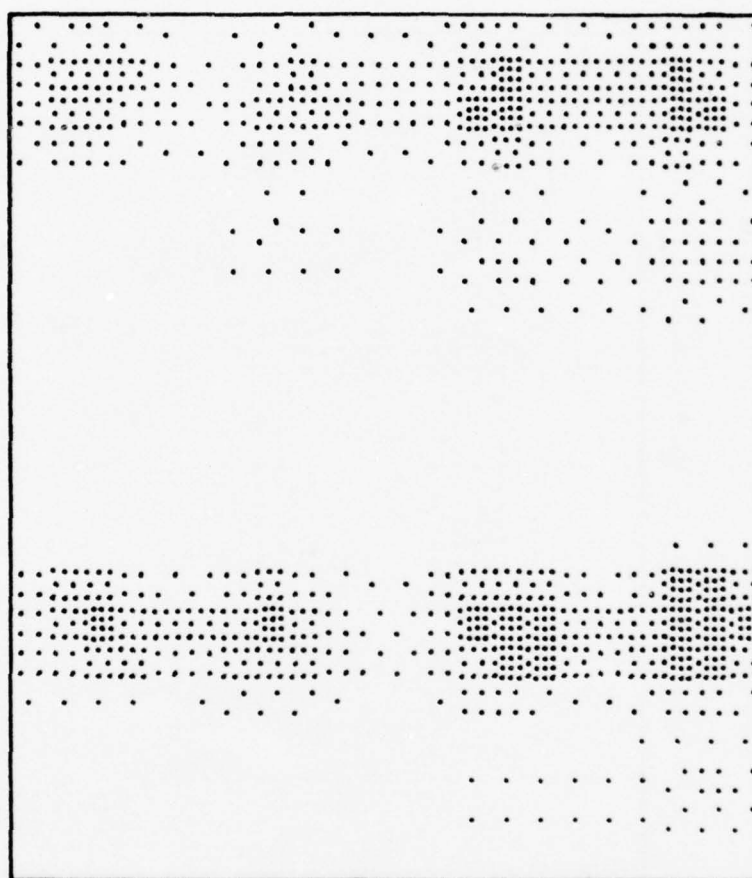
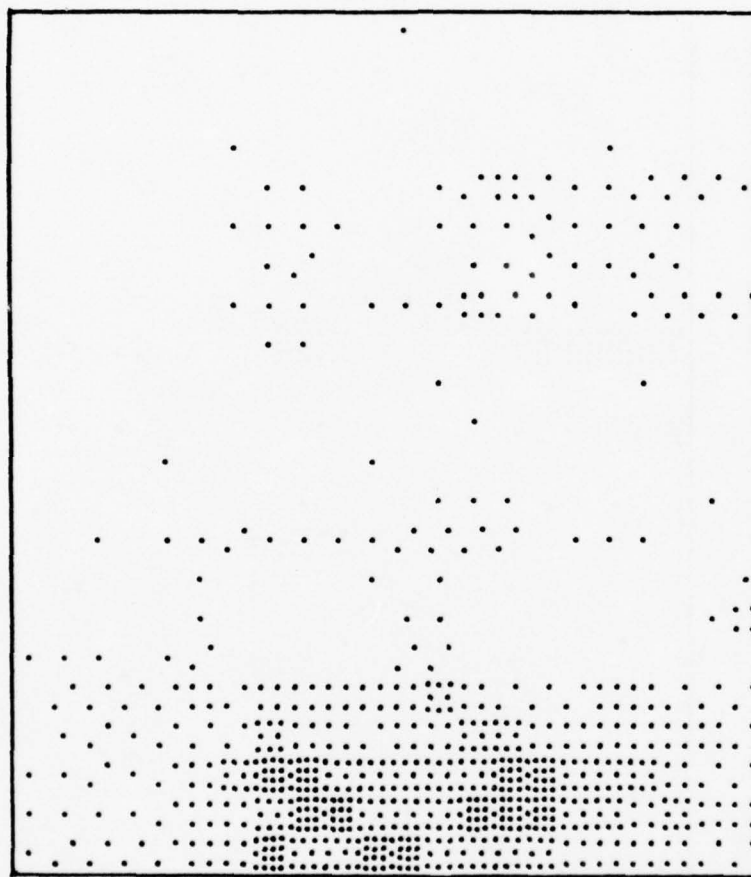


Figure A.13(c). An SPD plot ($.44 < \text{SPD} < .34$) for a panel contaminated (top and bottom) with pentane aerosol containing decanoic acid.



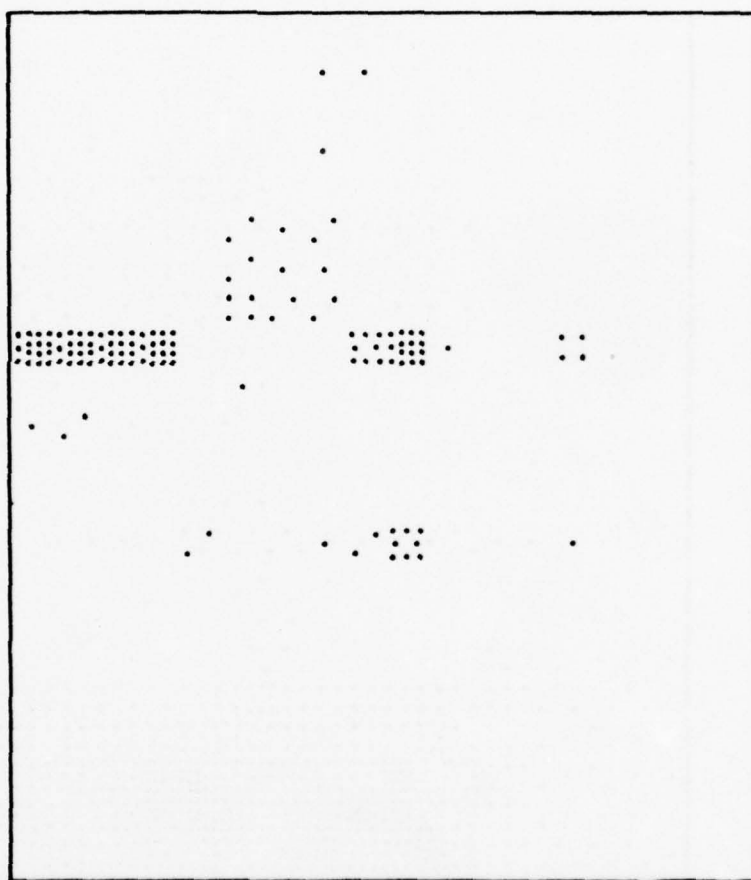
4-10-5-76

Figure A.14(a). A Δ plot ($164 \leq \Delta \leq 162$) for a panel contaminated (top and bottom) with pentane aerosol containing erucic acid.



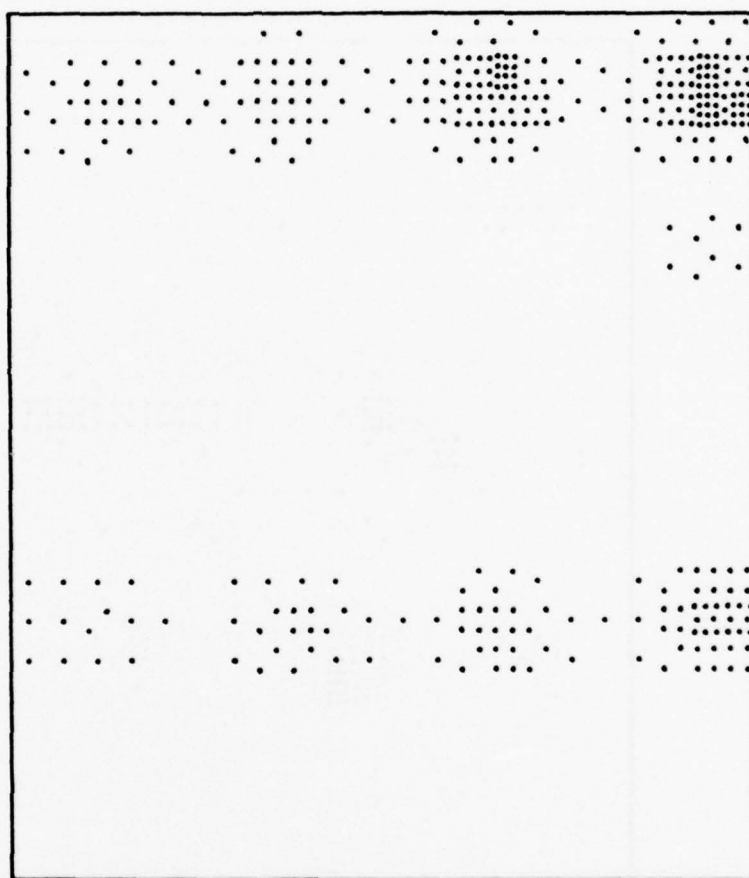
4-10-5-76

Figure A.14(b). A ψ plot ($44 < \psi < 42$) for a panel contaminated (top and bottom) with pentane aerosol containing erucic acid.



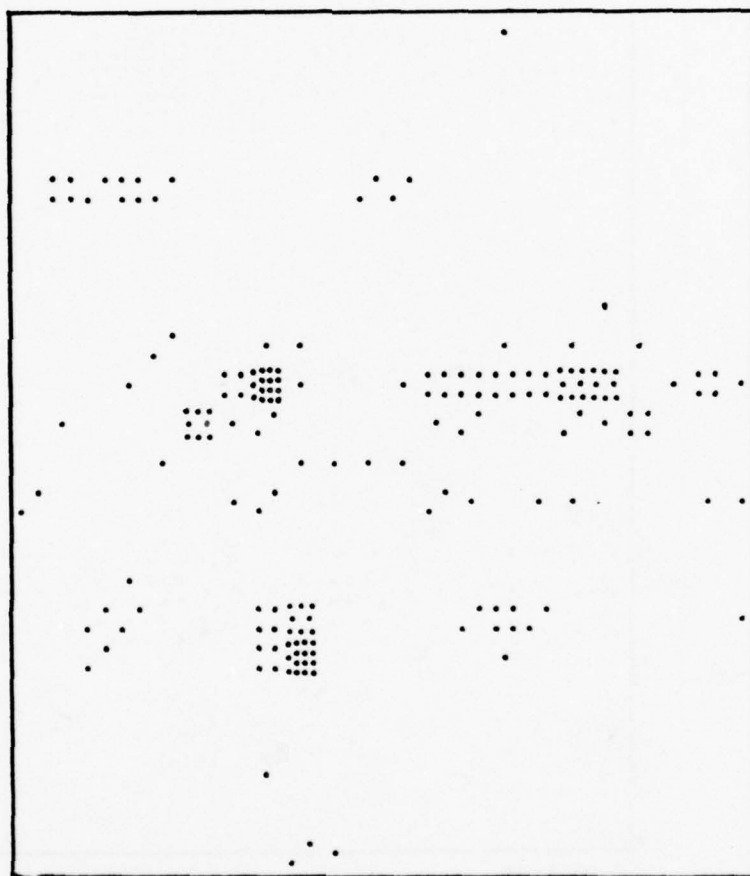
4-10-5-76

Figure A.14(c). An SPD plot ($.55 < SPD < .45$) for a panel contaminated (top and bottom) with pentane aerosol containing erucic acid.



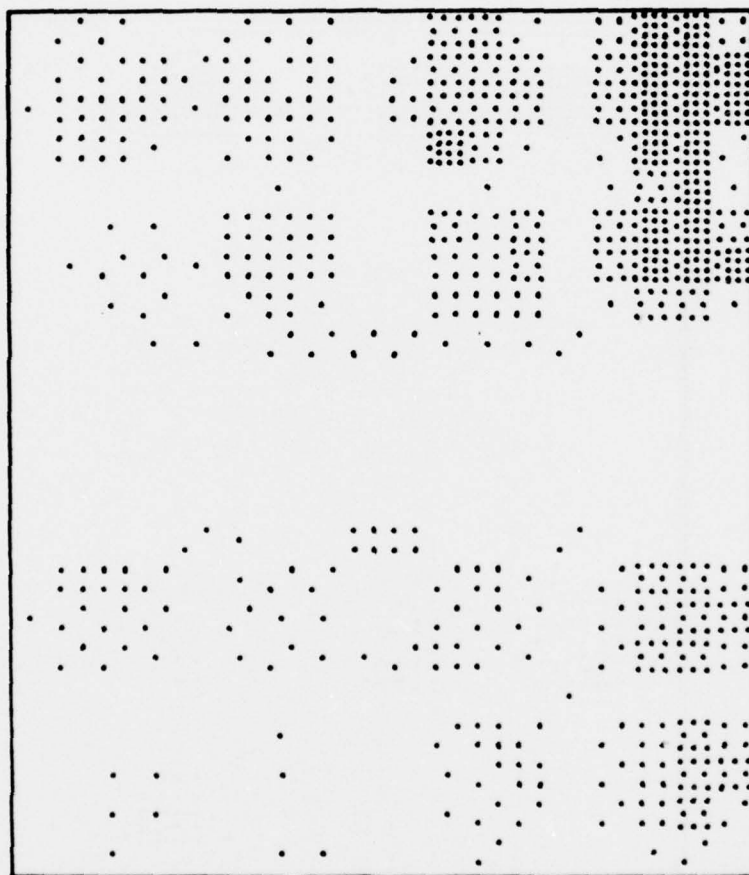
1-27-7-76

Figure A.15(a). A Δ plot ($169 < \Delta < 167$) for a panel contaminated (top and bottom) with pentane aerosol containing brassidic acid.



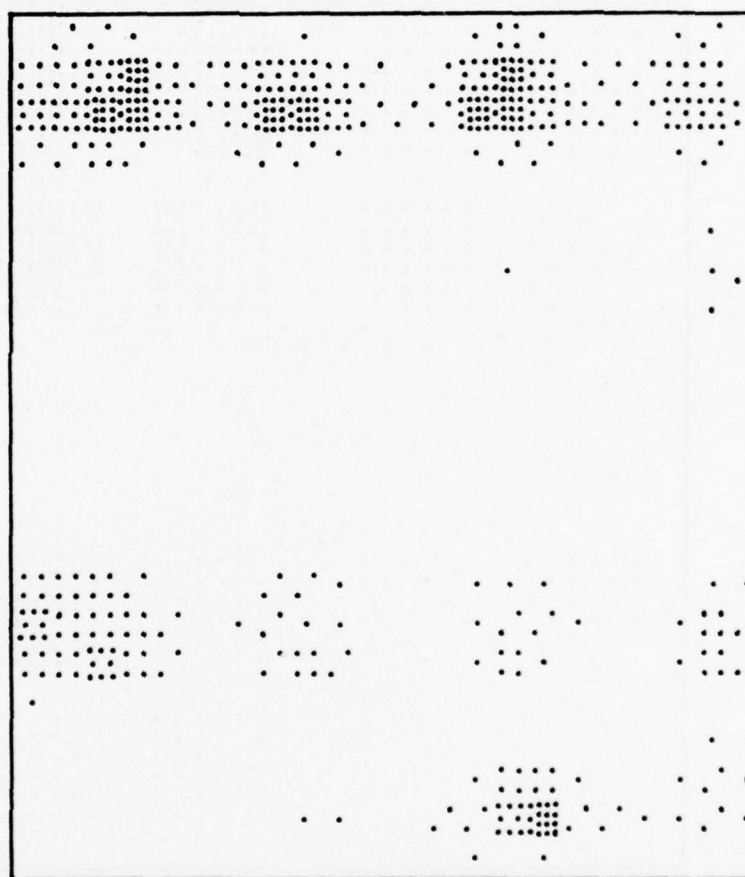
1-27-7-76

Figure A.15(b). A ψ plot ($44 < \psi < 42$) for a panel contaminated (top and bottom) with pentane aerosol containing brassidic acid.



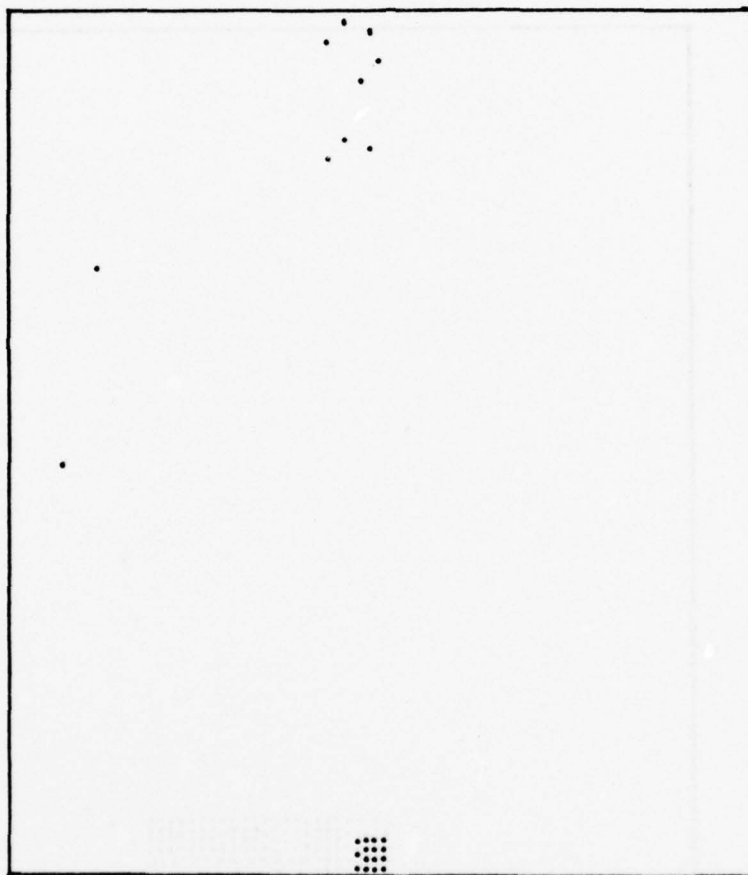
1-27-7-76

Figure A.15(c). An SPD plot ($.50 < \text{SPD} < .40$) for a panel contaminated (top and bottom) with pentane aerosol containing brassidic acid.



3-27-7-76

Figure A.16(a). A Δ plot ($165 < \Delta < 163$) for a panel contaminated (top and bottom) with pentane aerosol containing N-docosane.



3-27-7-76

Figure A.16(b). A ψ plot ($43 < \psi < 41$) for a panel contaminated (top and bottom) with pentane aerosol containing N-docosane.

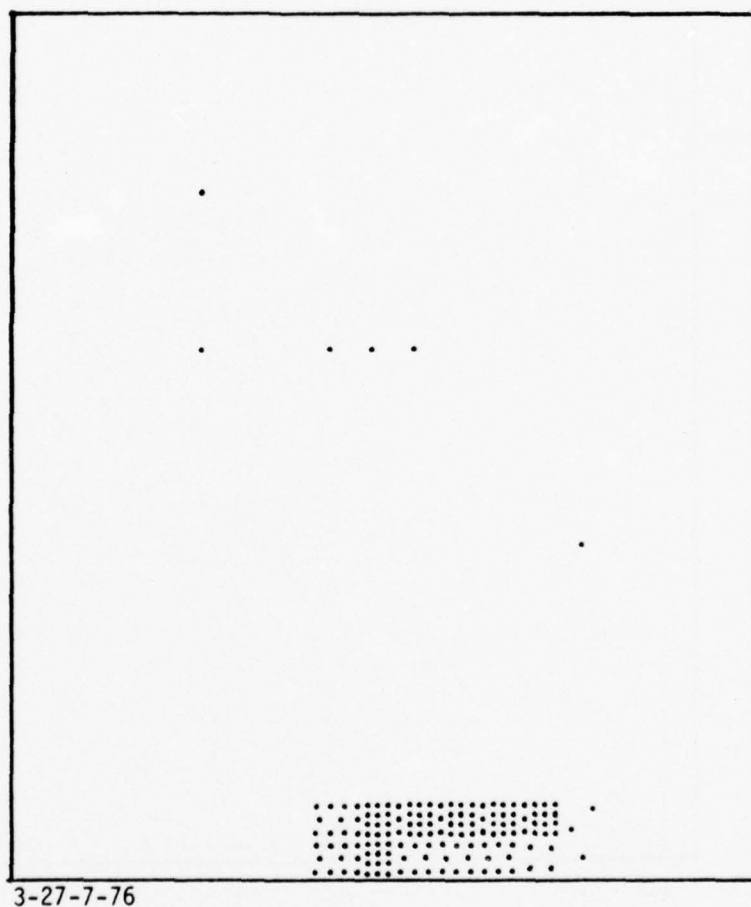
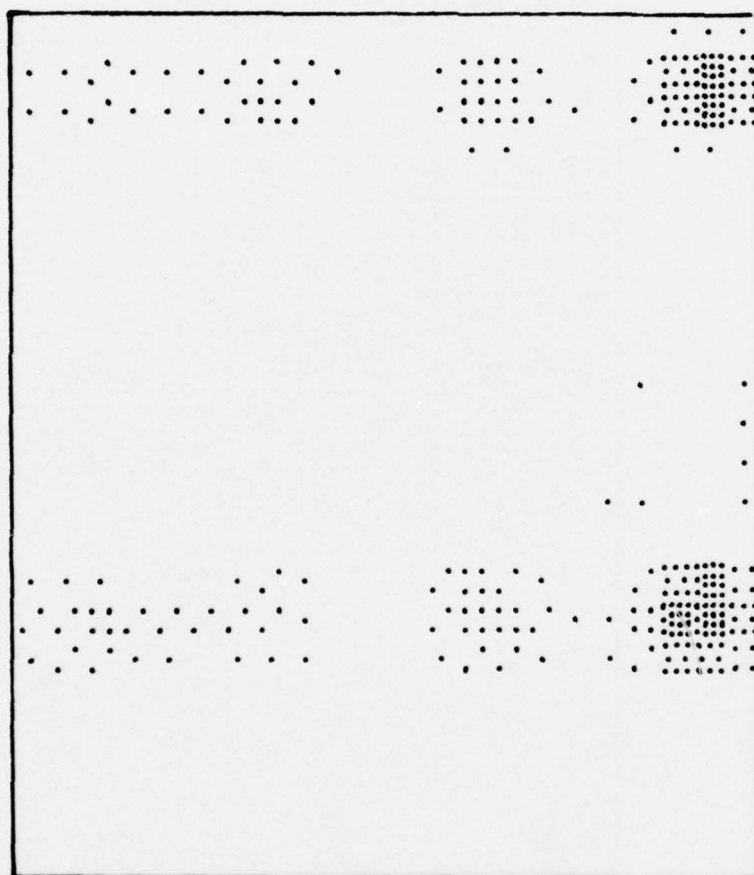
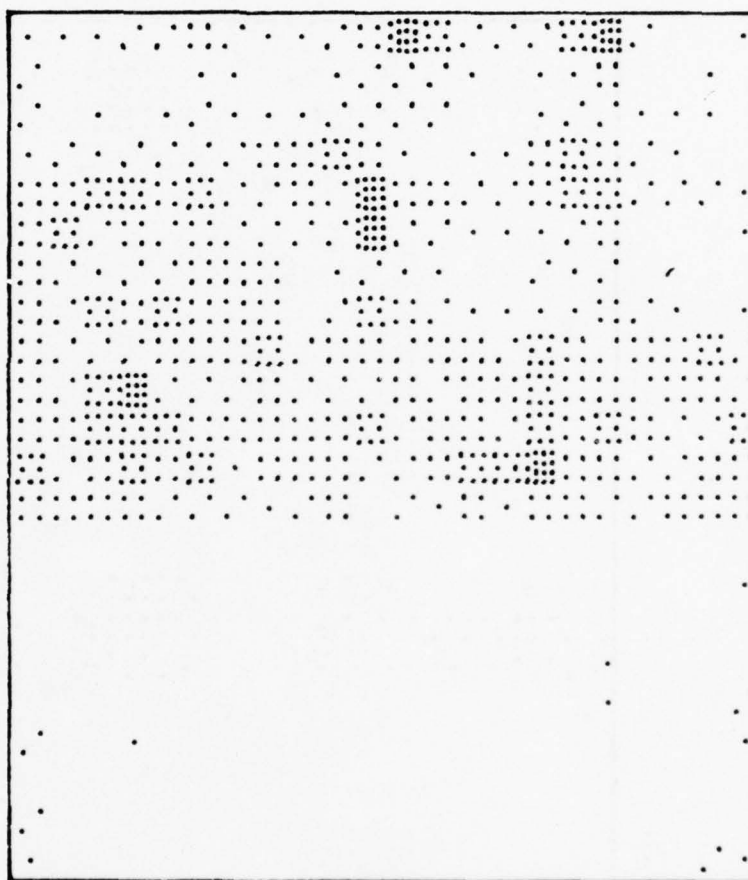


Figure A.16(c). An SPD plot ($.40 < \text{SPD} < .20$) for a panel contaminated (top and bottom) with pentane aerosol containing N-docosane.



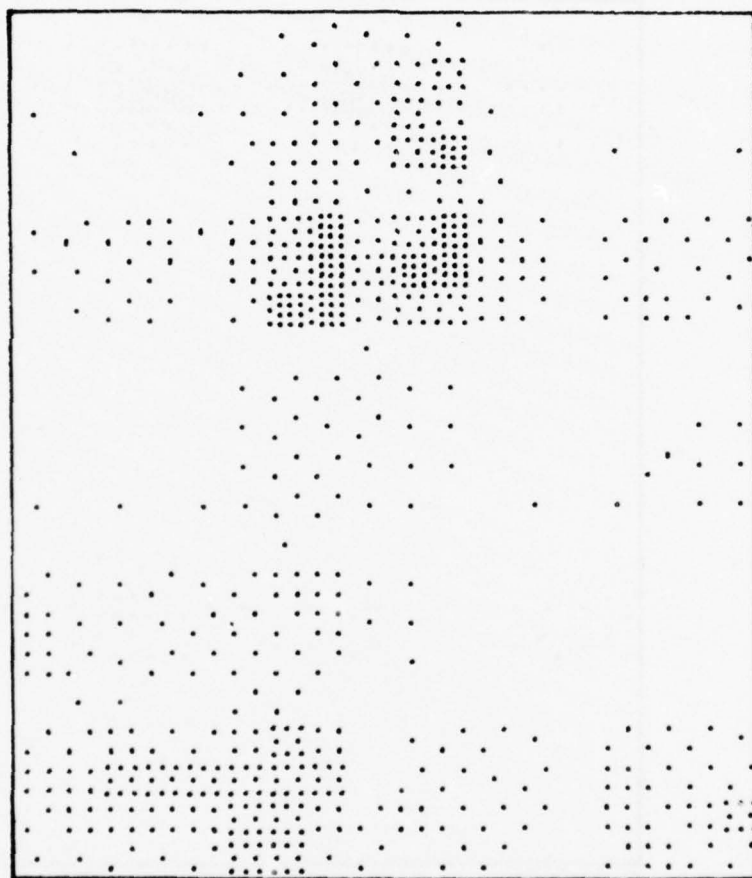
4-27-7-76

Figure A.17(a). A Δ plot ($164 < \Delta < 162$) for a panel contaminated (top and bottom) with pentane aerosol containing 16-bromo-9-hexadecenoic acid.



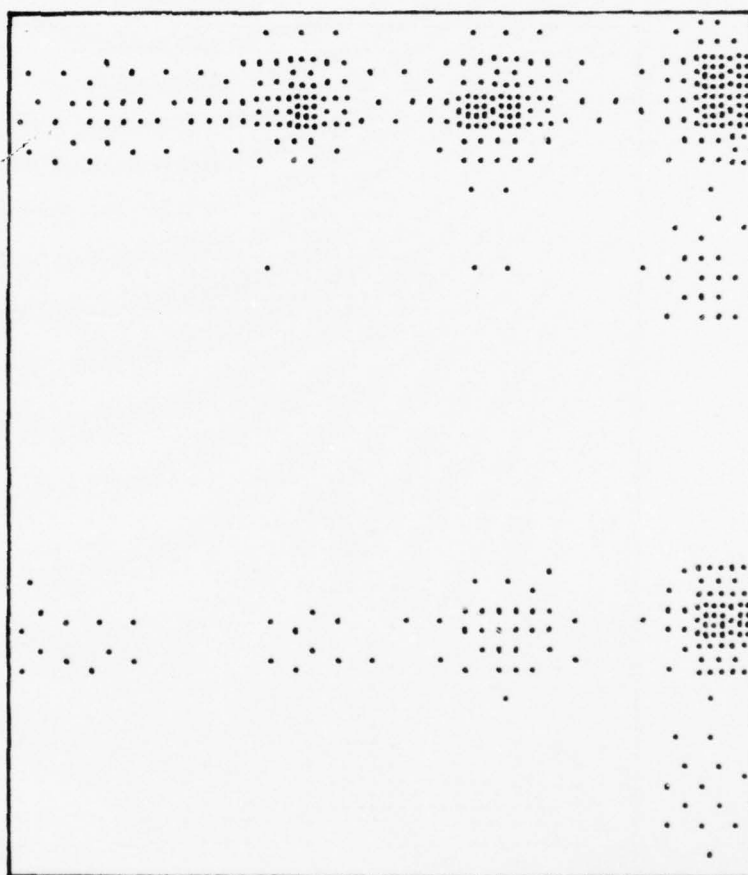
4-27-7-76

Figure A.17(b). A ψ plot ($42 < \psi < 41$) for a panel contaminated (top and bottom) with pentane aerosol containing 16-bromo-9-hexadecenoic acid.



4-27-7-76

Figure A.17(c). An SPD plot ($.35 < \text{SPD} < .25$) for a panel contaminated (top and bottom) with pentane aerosol containing 16-bromo-9-hexadecenoic acid.



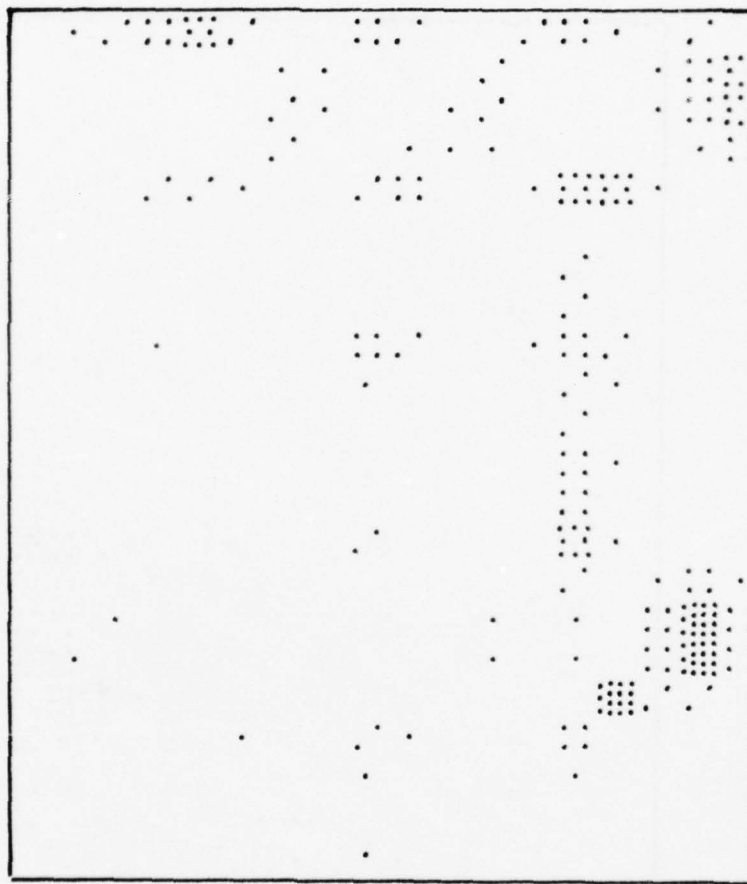
2-28-7-76

Figure A.18(a). A Δ plot ($165 < \Delta < 163$) for a panel contaminated (top and bottom) with pentane aerosol containing dotriacontane.



2-28-7-76

Figure A.18(b). A ψ plot ($43 < \psi < 41$) for a panel contaminated (top and bottom) with pentane aerosol containing dotriacontane.



2-28-7-76

Figure A.18(c). An SPD plot ($.30 < \text{SPD} < .20$) for a panel contaminated (top and bottom) with pentane aerosol containing dotriacontane.

L	6	7	8	1	1-Eicosene
Δ	156	152.6	141.6	160	
ψ	41.7	41.8	42.7	42.2	
d(Å)	86	82	169	22	
L	2	3	4	5	Clean
Δ	159	158	158.8	158.8	
ψ	42.2	42	41.8	42.0	
d(Å)	30	38	32	32	
L		162.8			1-Hexadecylamine
Δ		42.2			
ψ		0			
d(Å)					
L	5	6	7	8	1-Hexadecylamine
Δ	150	140	145	173	
ψ	42	43.5	45.3	44.1	
d(Å)	102	182	?	?	
L	1	2	3	4	1-Hexadecylamine
Δ	157.6	158.8	157.0	150.5	
ψ	41.2	42.1	41.6	41.4	
d(Å)	42	32	46	98	

6-21-4-76C

Figure A.19. Regions on a phosphoric acid anodized Al 7075-T6 panel with various contamination levels. Top: 1-Eicosene
Middle: Clean Bottom: 1-Hexadecylamine

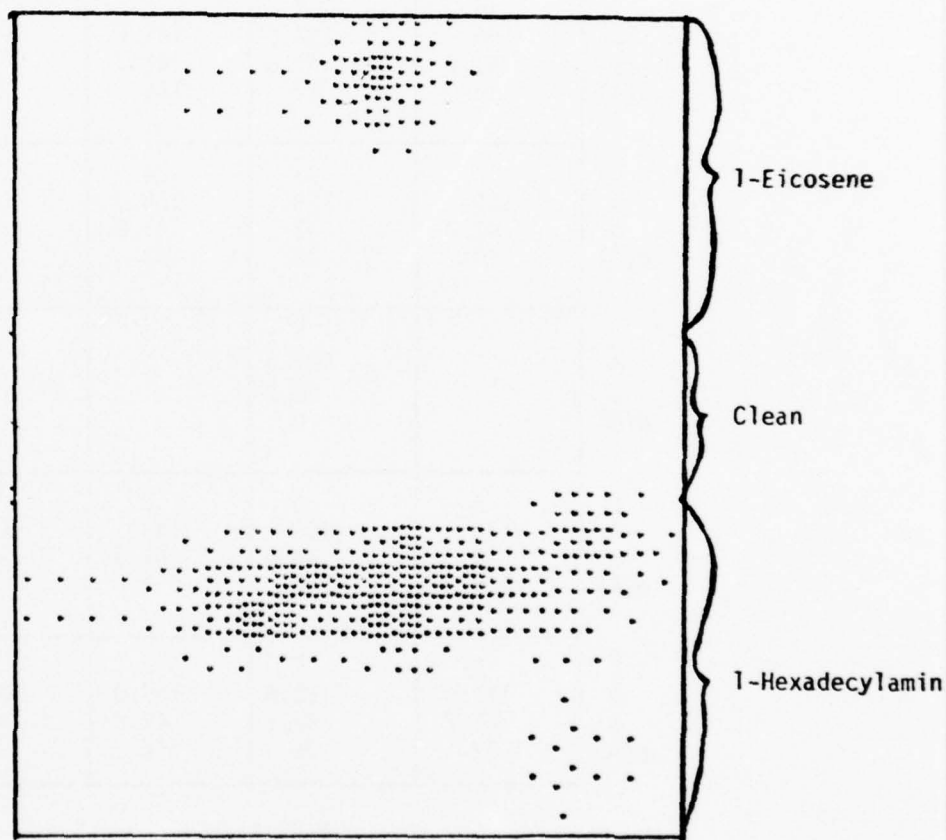


Figure A.19(a). Computer plot of $162\Delta 160$ for contamination.
Top: 1-Eicosene Middle: Clean Bottom: 1-Hexadecylamine

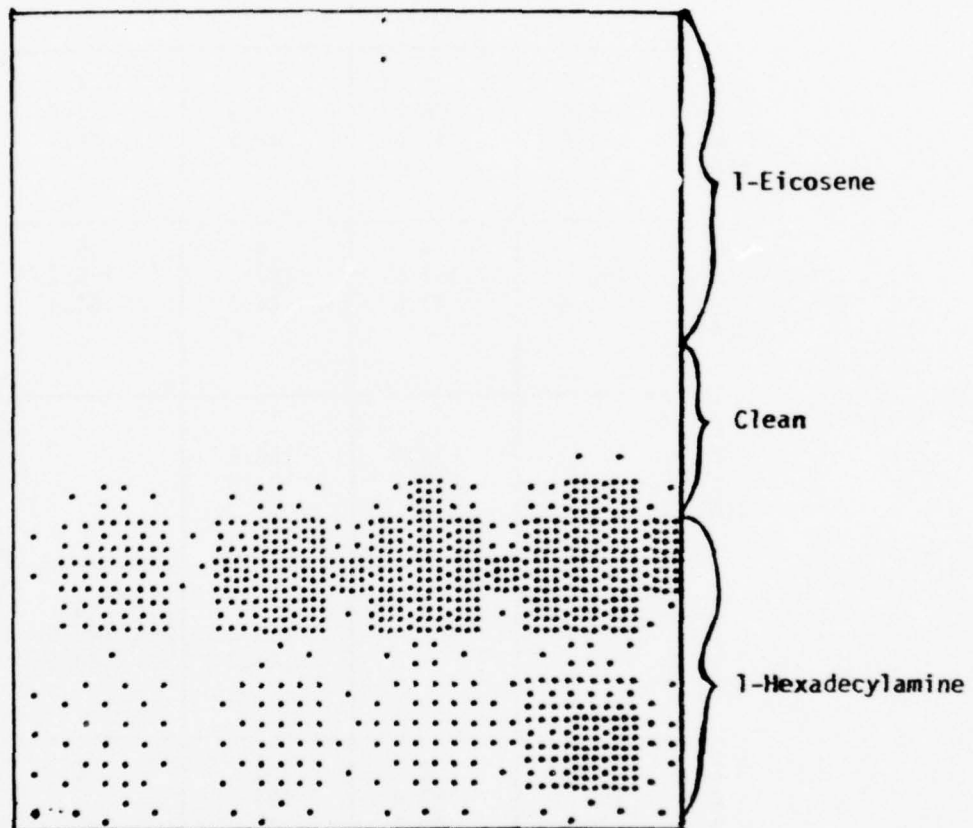


Figure A.19(c). Computer plot of $.8 < \text{SPD} < .6$. Top: 1-Eicosene
Middle: Clean Bottom: 1-Hexadecylamine

L Δ ψ d(Å)	1 156.5 41.8	6 156.2 41.6	7 153.8 41.5	1 155.4 41.4	} Anthracene
L Δ ψ d(Å)	2 158 41.6	3 157.5 41.6	4 157 41.2	5 156.2 41.4	
L Δ ψ d(Å)		158.4 41.8	156.5 41.8		} Clean
L Δ ψ d(Å)	5	6	7 151.8 41.3	8 149.6 40.9	
L Δ ψ d(Å)	1 152 40.2	2 153.4 40.9	3 154 41.1	4	} Amino benzoic acid

4-21-4-76C

Figure A.20. Regions on a Phosphoric Acid Al 7075-T6 anodized panel with various contamination levels. Top: Anthracene, Middle: Clean, Bottom: Amino benzoic acid.

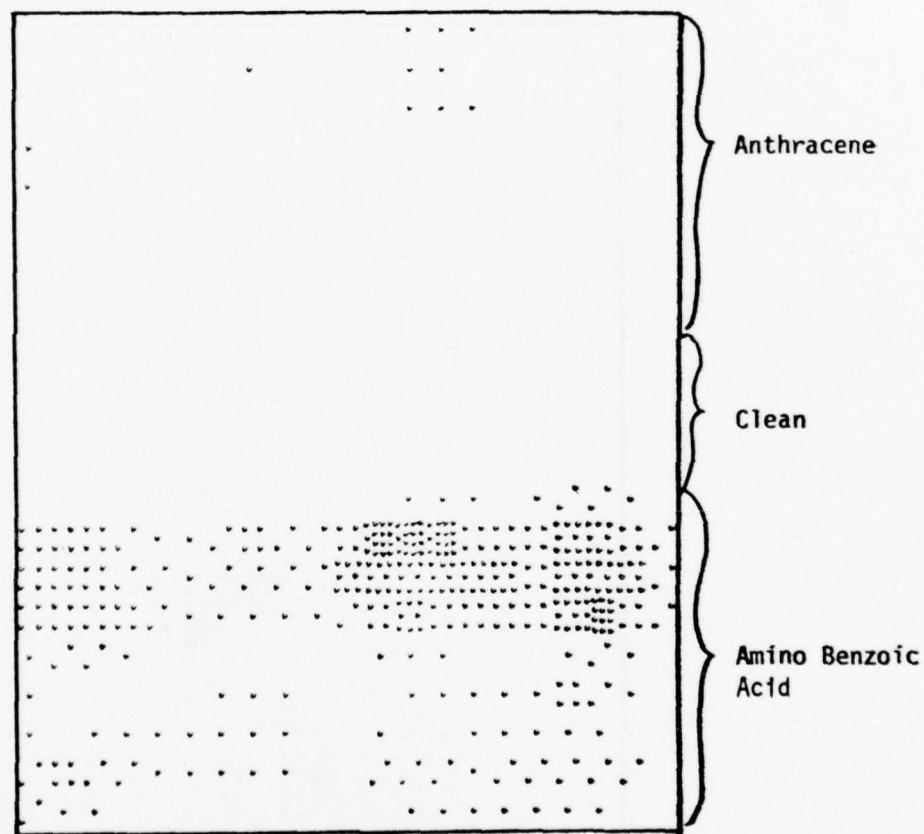


Figure A.20(a). Computer plot of $162 < \Delta < 159.5$. Top: Anthracene
Middle: Clean Bottom: Amino Benzoic Acid

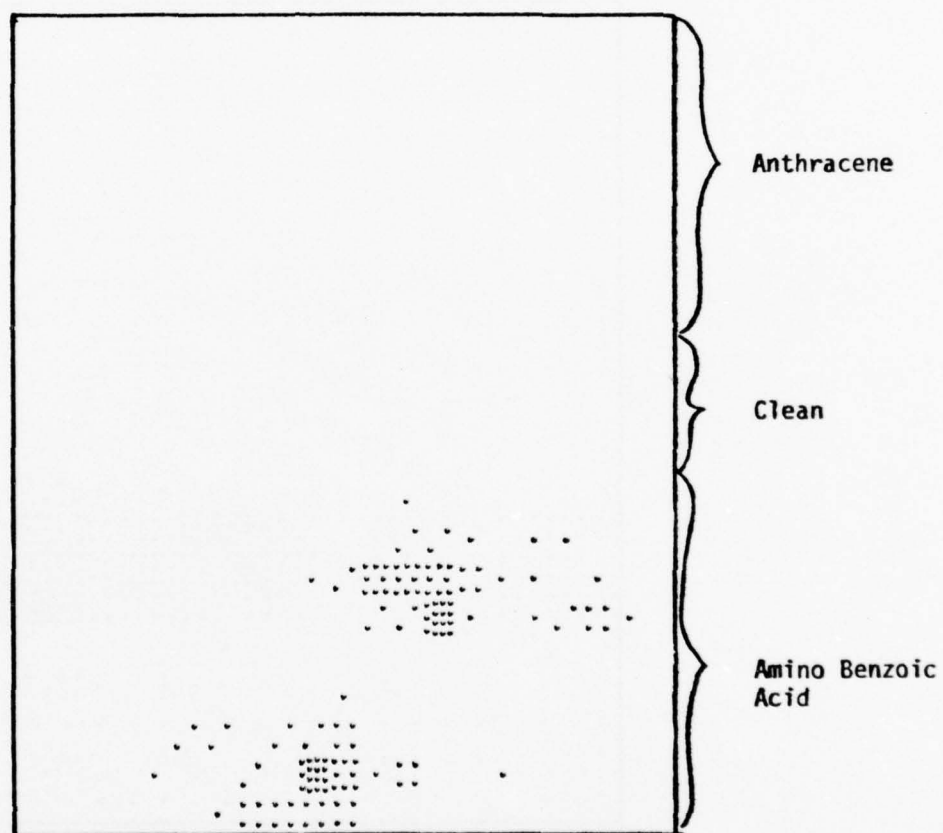


Figure A.20(b). Computer plot of $43.5 < \psi \leq 41.5$.

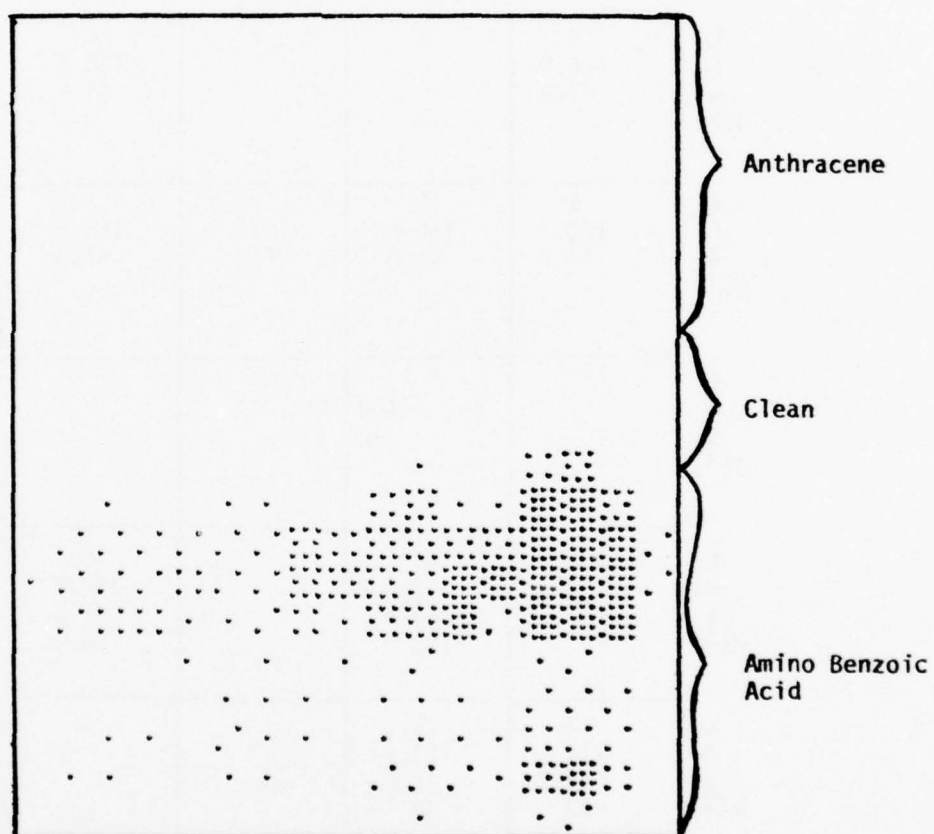


Figure A.20(c). Computer plot $.8 < \text{SPD} < .6$.

L Δ ψ d(Å)	5 156.6 41.9	6	7	8 156.6 41.8	Benzoic Acid
L Δ ψ d(Å)	1 160 41.7	2 156.6 41.8	3 157 42	4 156.8 41.8	
L Δ ψ d(Å)		160 .4 42 .1			Clean
L Δ ψ d(Å)	5	6 147.6 43.4 102	7	8 156.0 41.5 35	1,12.Diaminododecane
L Δ ψ d(Å)	1 157 41.2 27	2 154.6 41.5 46	3	4	

5-21-4-76C

Figure A.21. Regions on a phosphoric acid anodized Al 7075-T6 panel with various contamination. Top: Benzoic Acid
Middle: Clean Bottom: 1,12.Diaminododecane

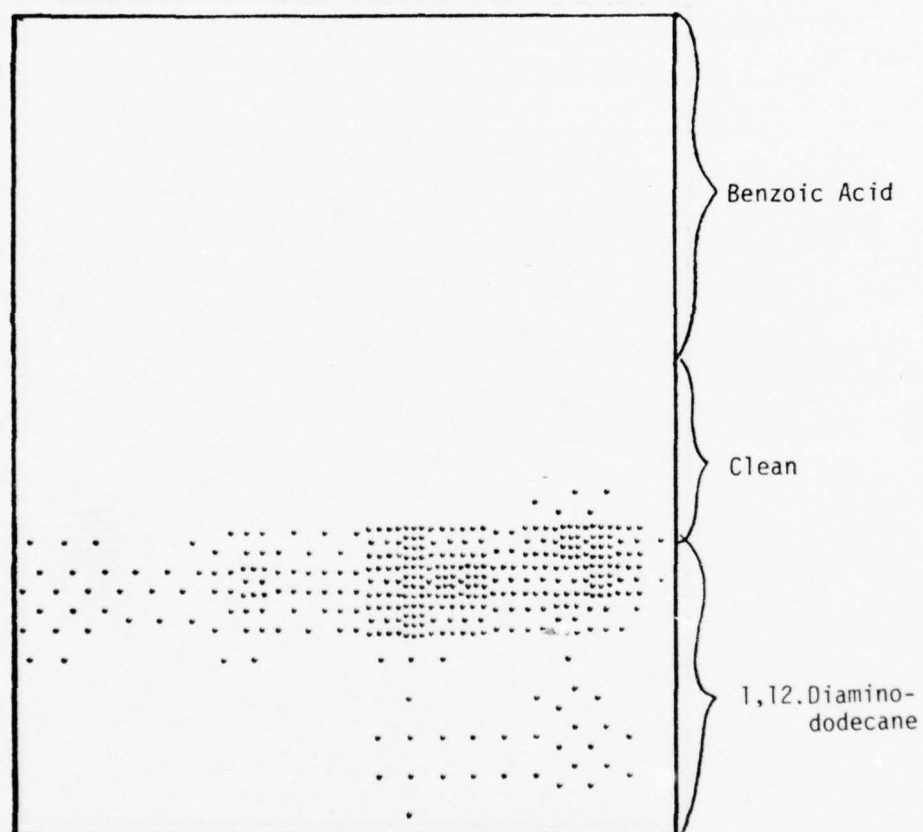


Figure A.21(a). Computer plot $162 < \Delta < 159.5$.

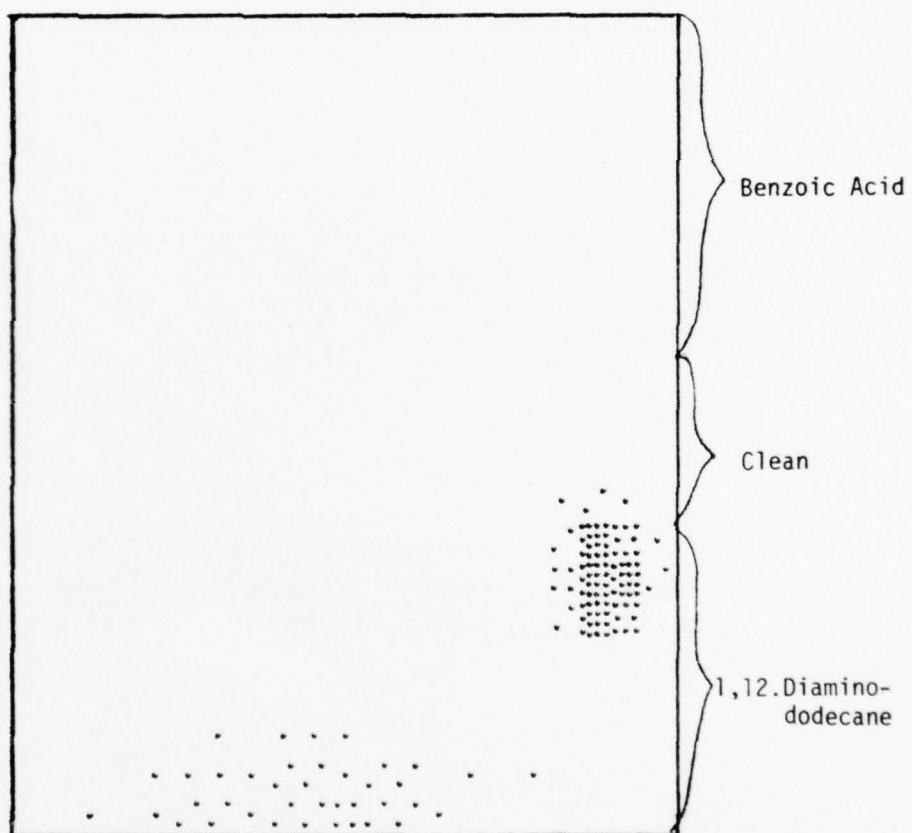


Figure A.21(b). Computer plot $43.5 < \psi < 41.5$.

SC5026.22TR

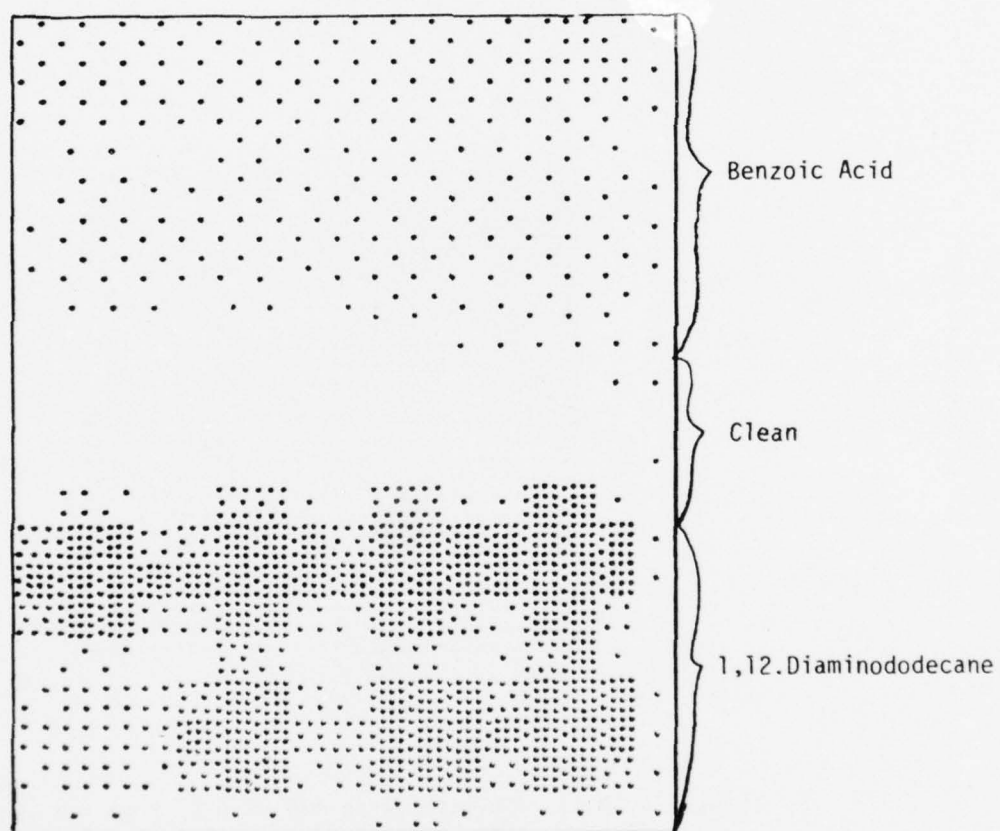


Figure A.21(c). Computer plot $.8 < \text{SPD} < .6$.

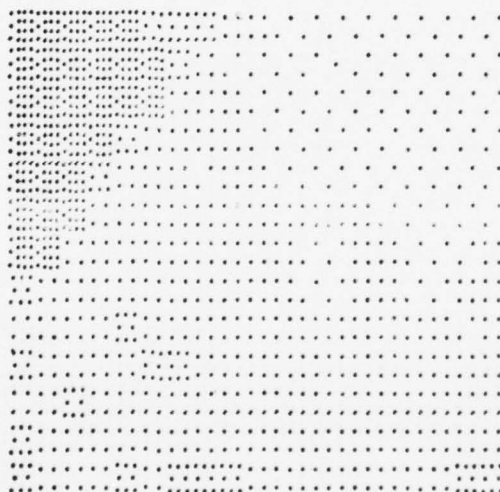


Figure A.22(a). Ellipsometric map of $(\Delta_{av} + \delta) < \Delta < (\Delta_{av} - \delta)$ for a stearic acid contaminated (top left corner) surface.

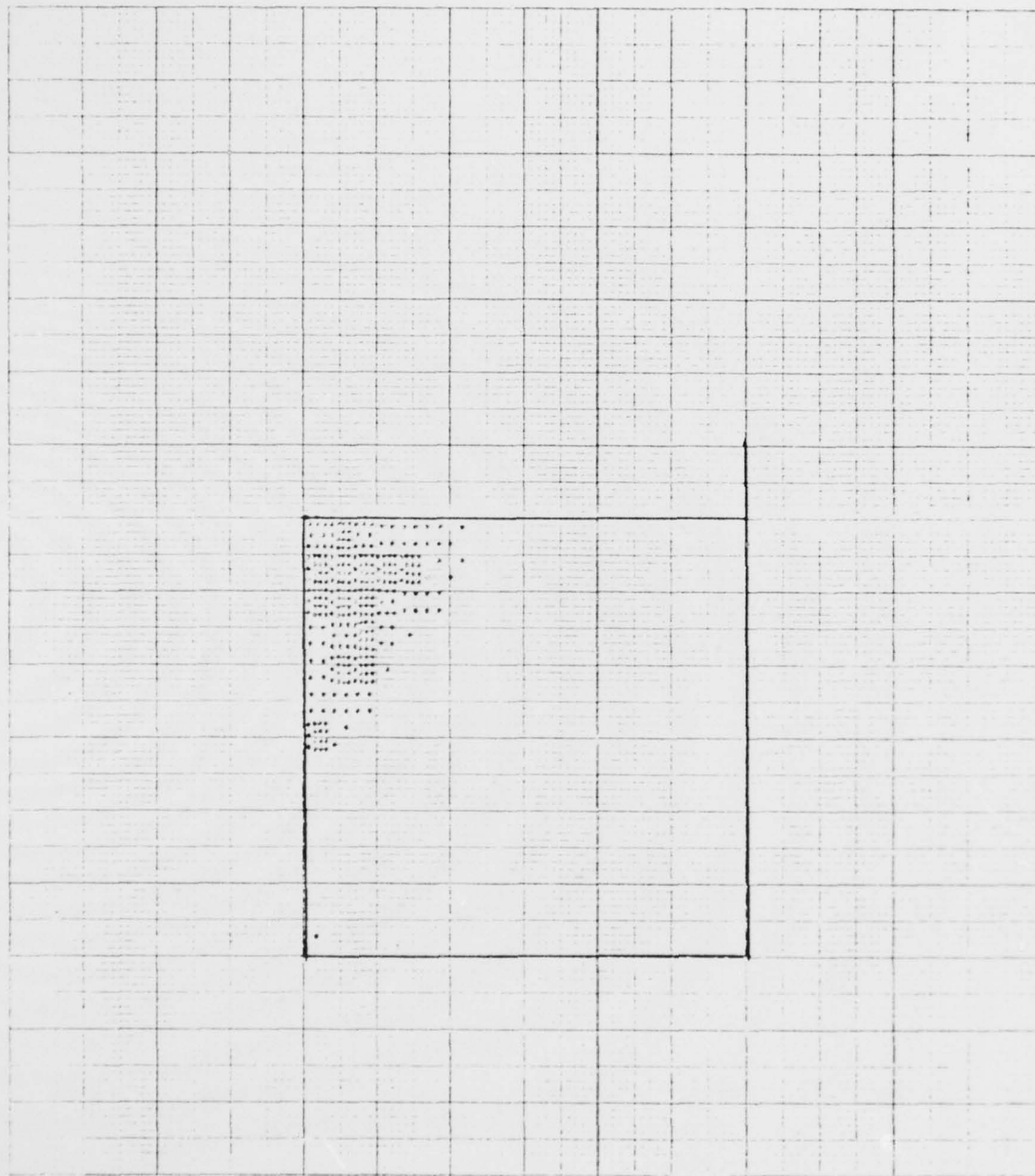


Figure A.22(a). Ellipsometric map with greater suppression.
(cont'd)



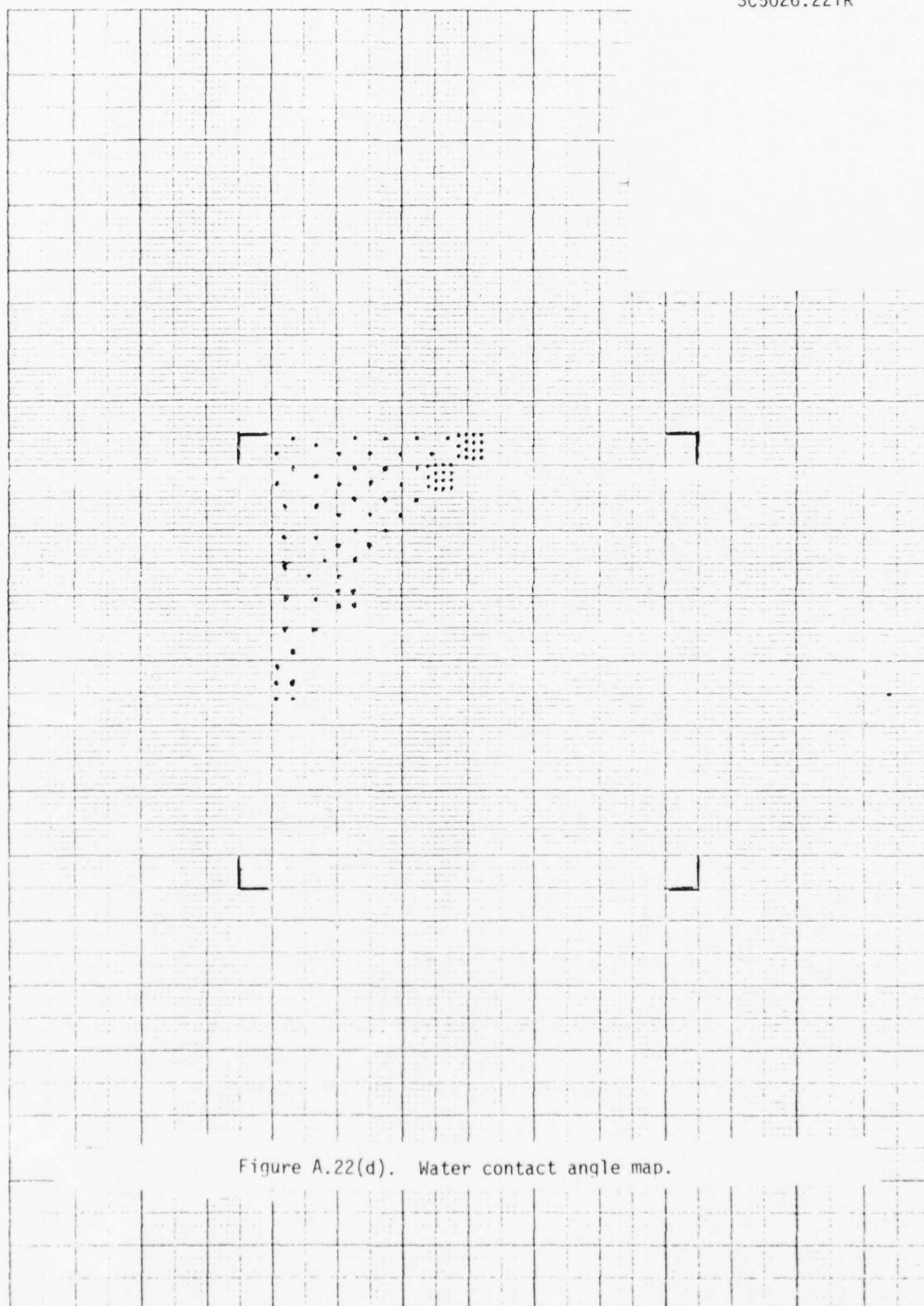


Figure A.22(d). Water contact angle map.

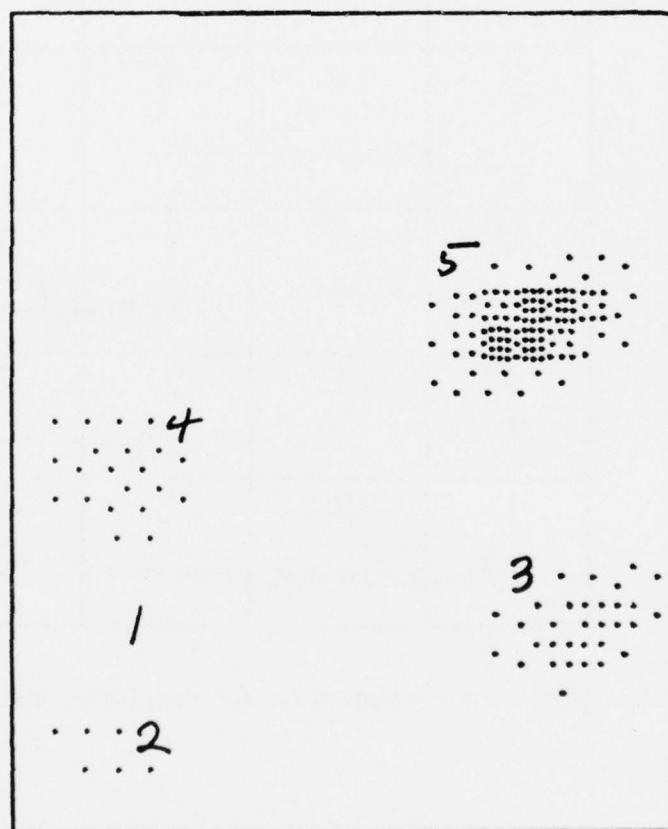


Figure A.23(a). Computer plot of $161 < \Delta < 164$ for stearic acid in pentane aerosol, levels 1 through 5.

3	4	5	
—		→	
4	5	1	2
—	→	Adamantanol	
5	1	2	3
→	Decacylene	→	
1	2	3	4
Decadiene		→	

Figure A.24. Regions of contamination for decadiene, decacylene and adamantanol.

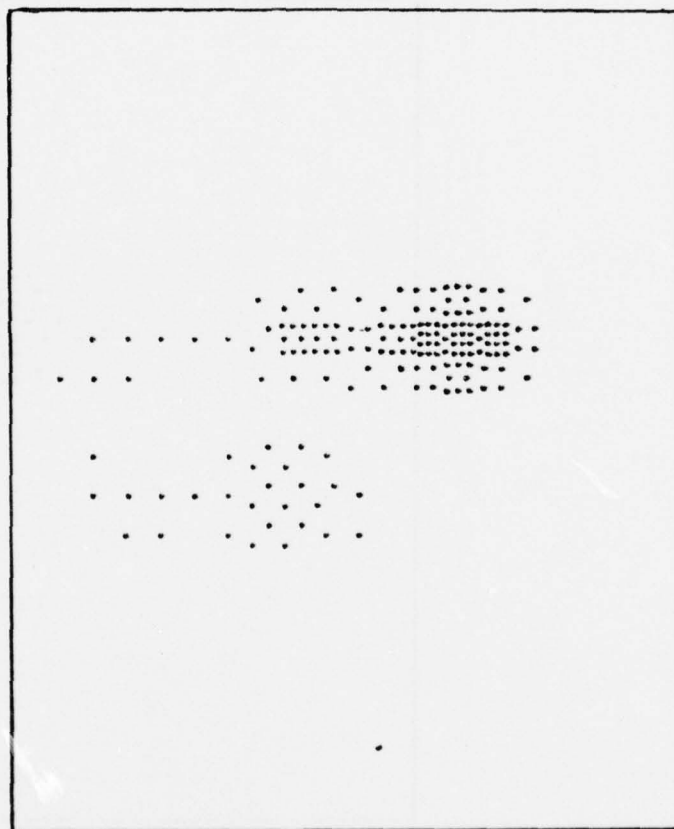


Figure A.24(a). Computer plot of $164\Delta 161$ for decadiene, decacyclene and adamantanol.

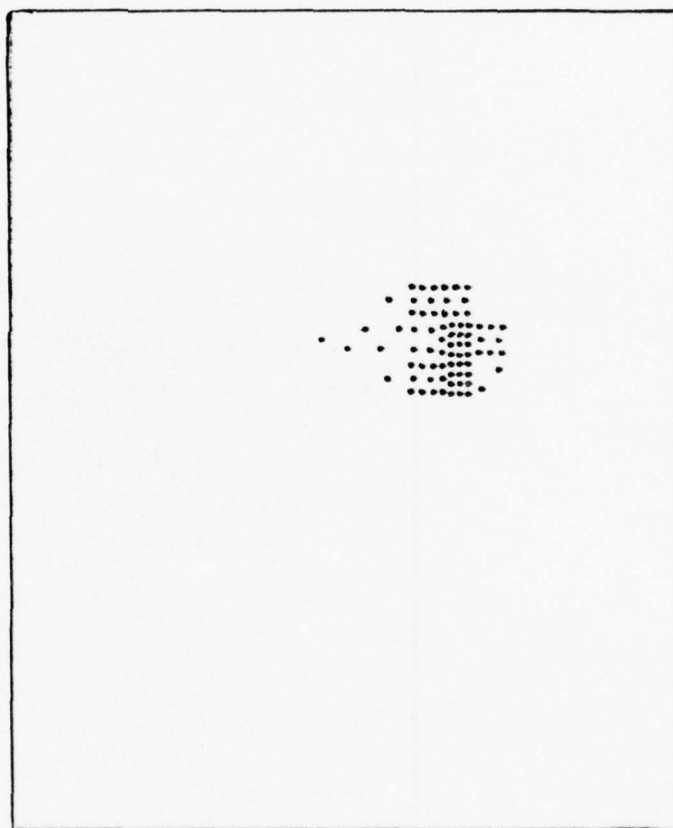


Figure A.24(b). Computer plot of $44 < \psi < 42$ for decadiene, decacyclene and adamantanol.

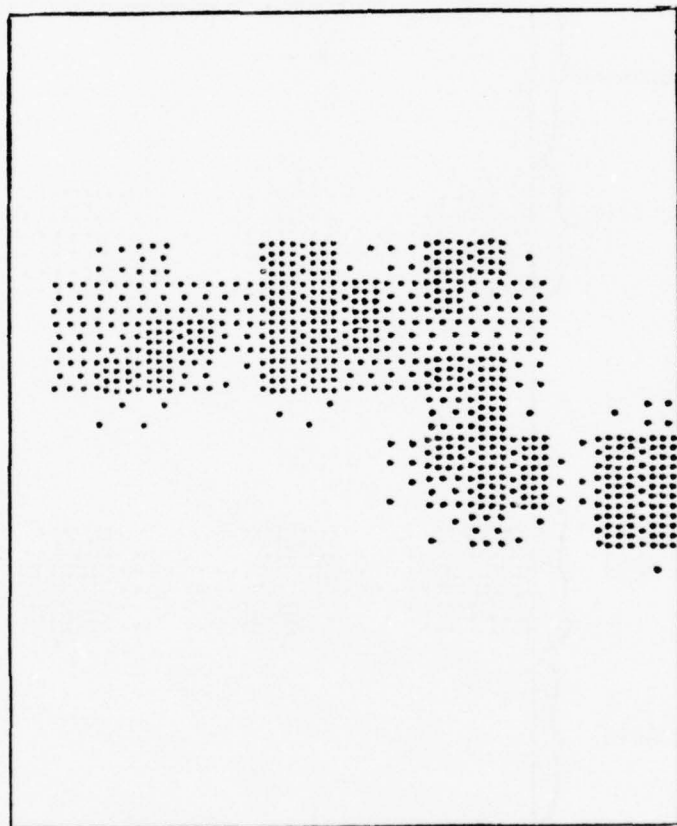


Figure A.24(c). Computer plot of $.24 < SPD < .15$ for decadiene, decacyclene and adamantanol

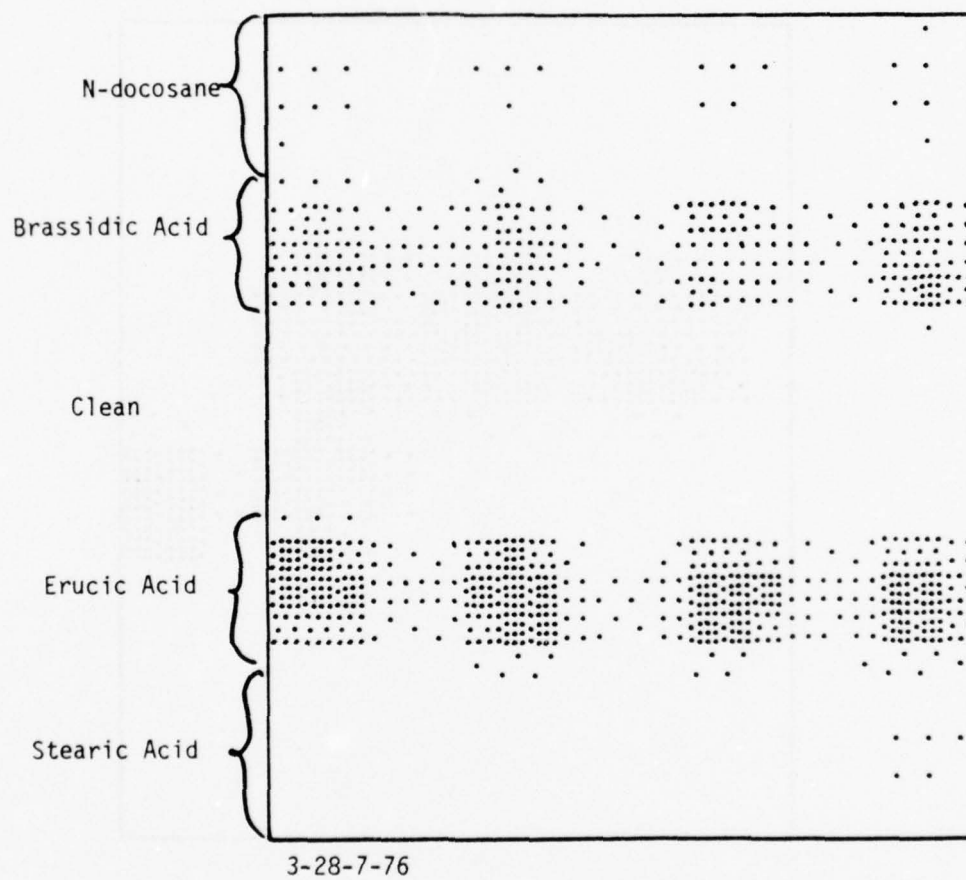


Figure A.25(a). A Δ plot ($165 < \Delta < 163$) for a panel that was contaminated in four regions but left clean in the center region.

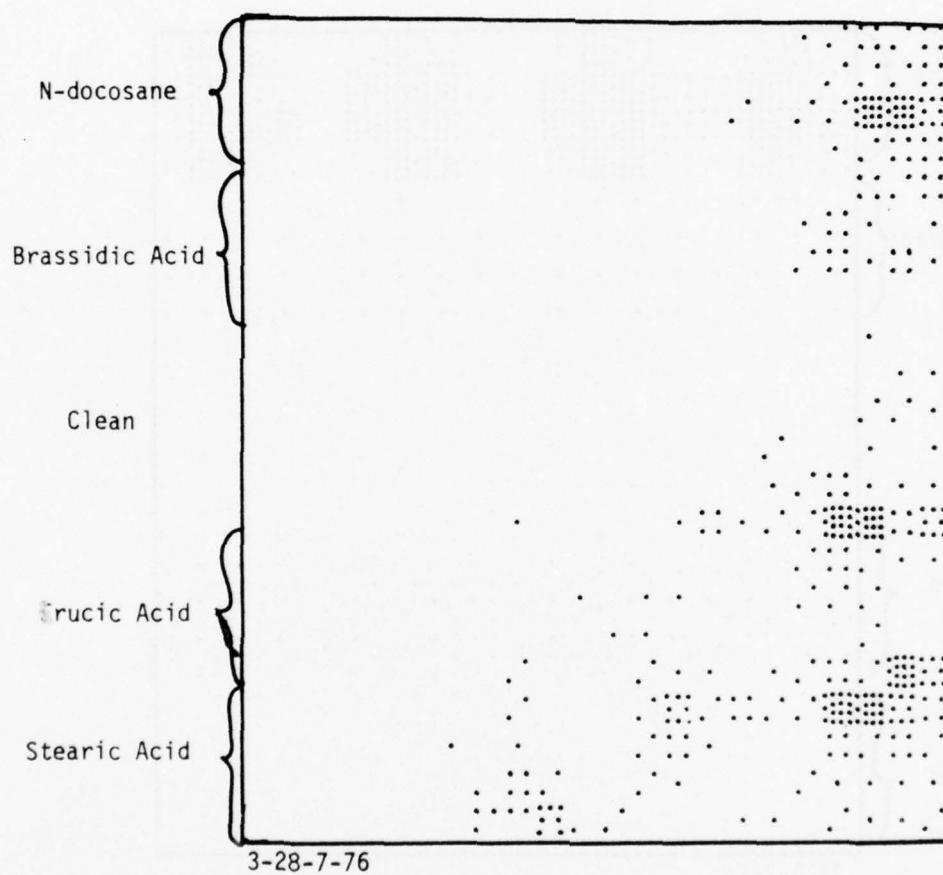


Figure A.25(b). A ψ plot ($43.5 < \psi < 41.5$) for a panel that was contaminated in four regions but left clean in the center region.

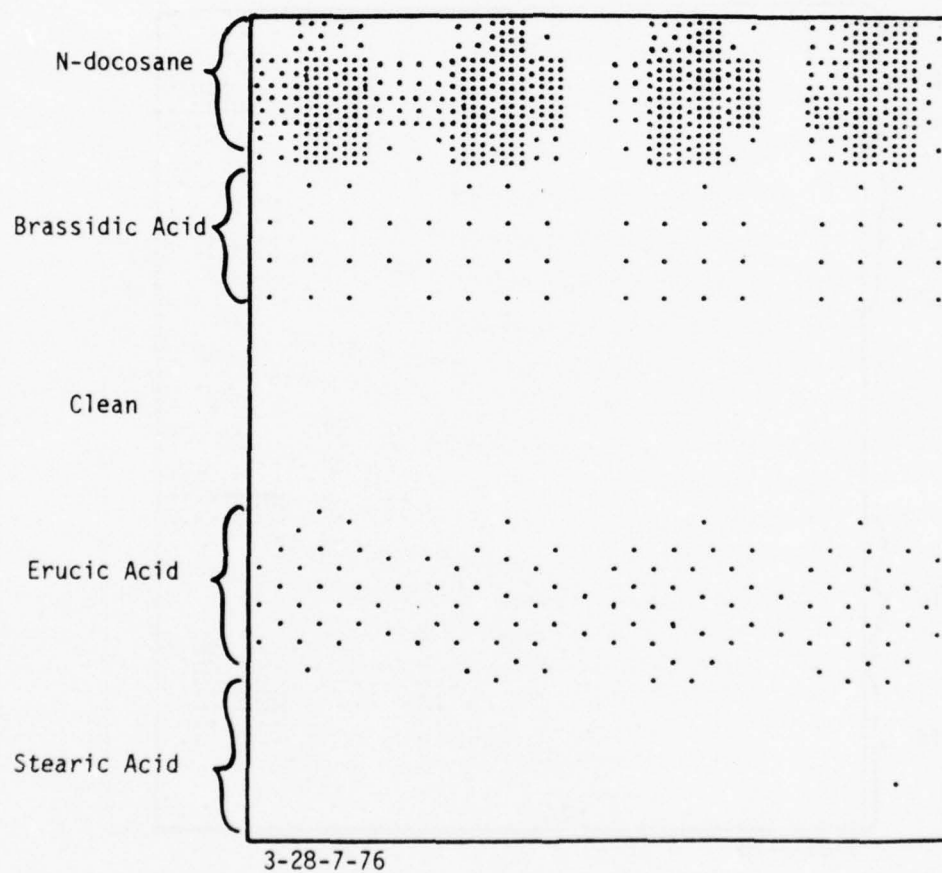


Figure A.25(c). An SPD plot ($.32 < \text{SPD} < .22$) for a panel that was contaminated in four regions but left clean in the center region.

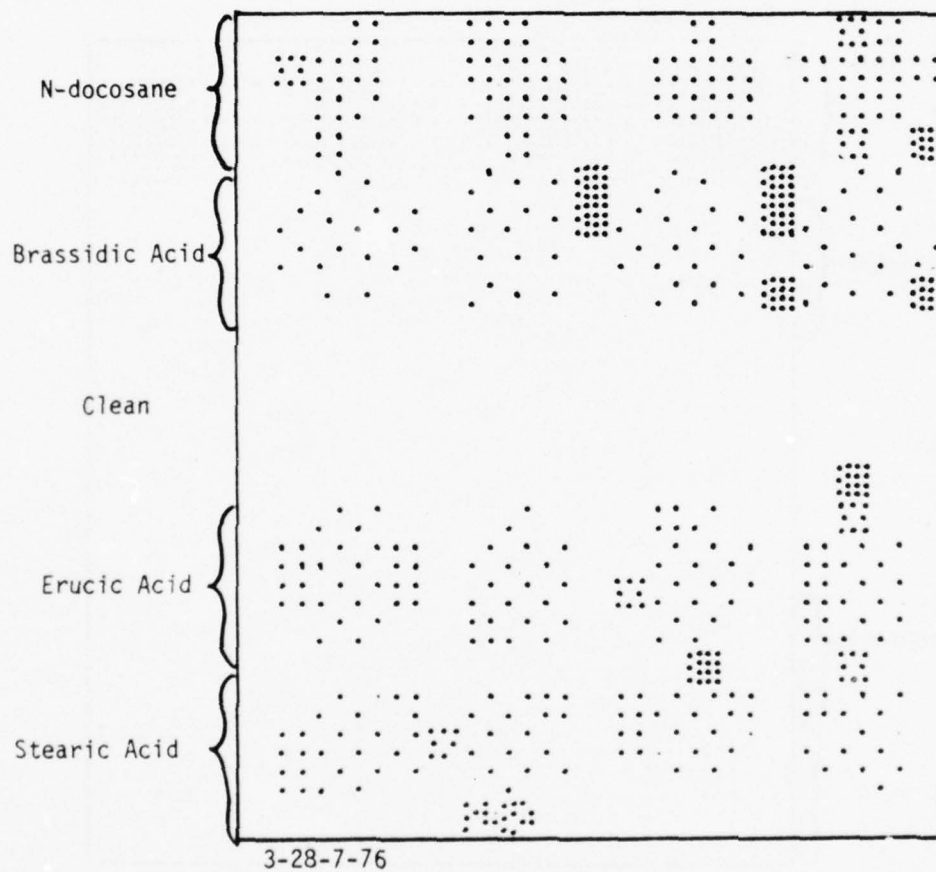


Figure A.25(d). A wettability plot for a panel that was contaminated in four regions but left clean in the center region.

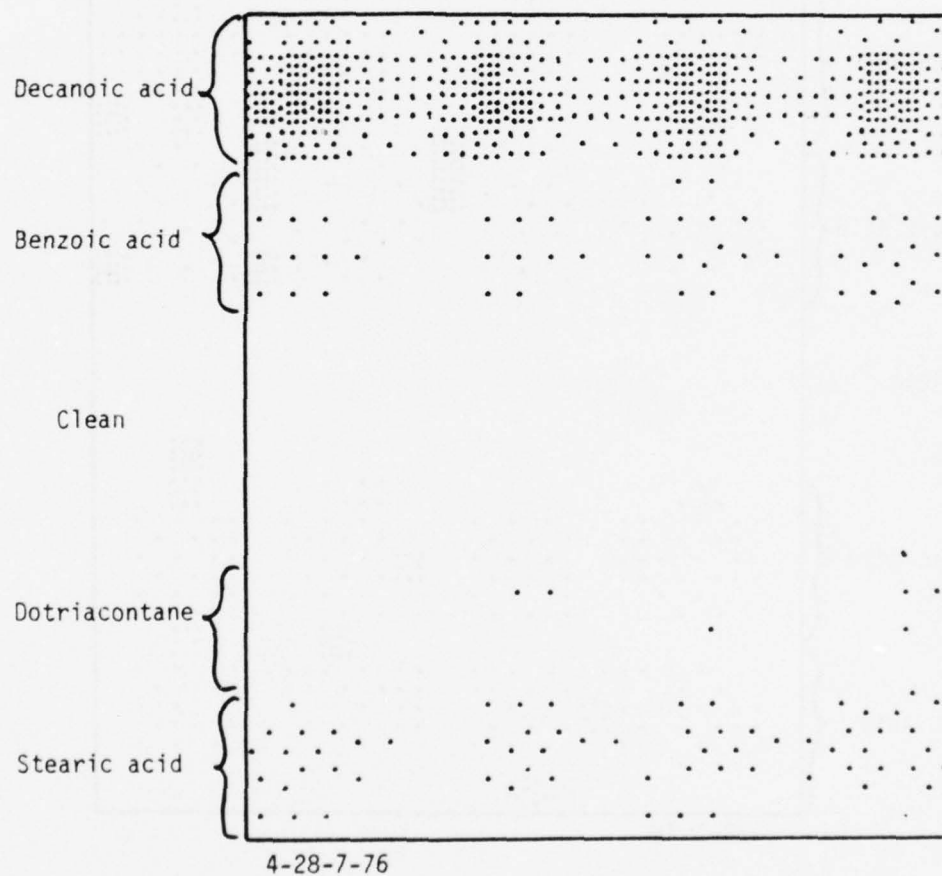


Figure A.26(a). A Δ plot ($165 < \Delta < 163$) for a panel that was contaminated in four regions but left clean in the center region.

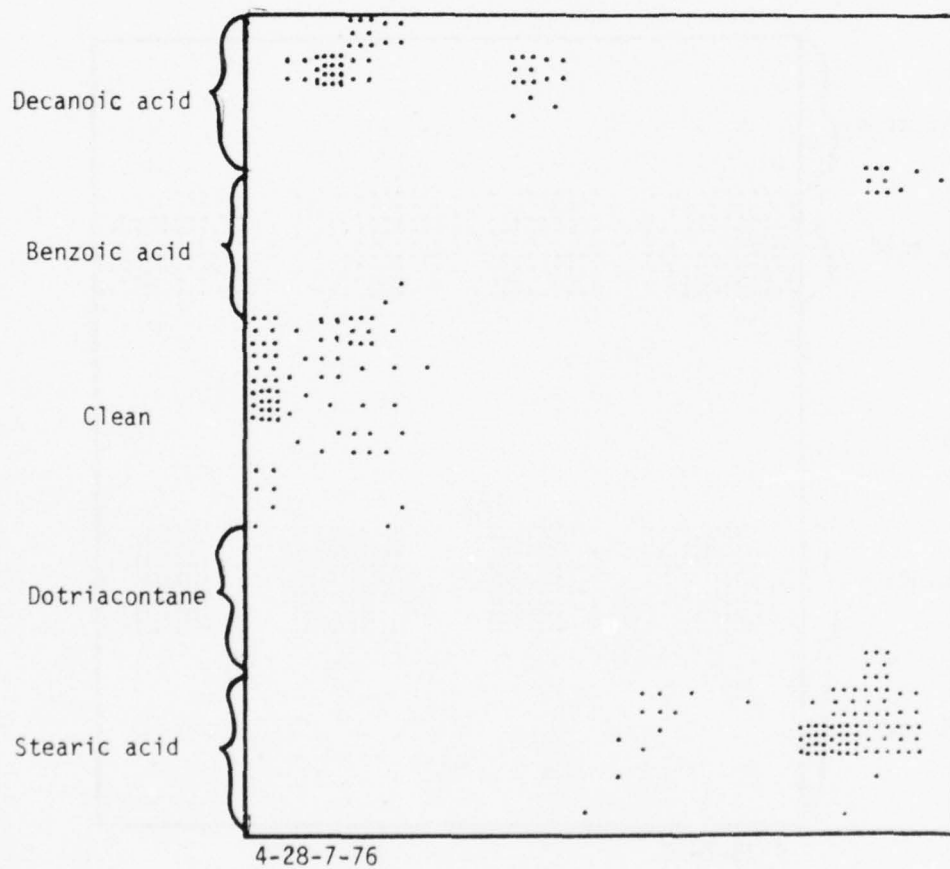


Figure A.26(b). A ψ plot ($43 < \psi < 41$) for a panel that was contaminated in four regions but left clean in the center region.

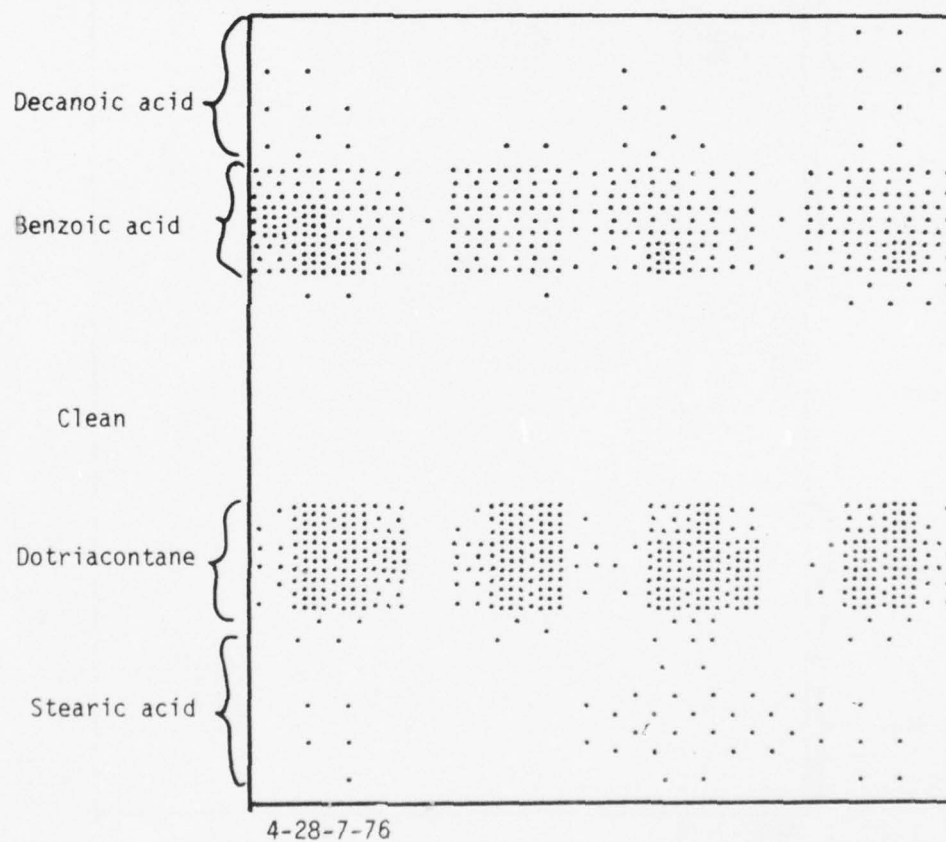


Figure A.26(c). An SPD plot ($.25 < \text{SPD} < .05$) for a panel that was contaminated in four regions but left clean in the center region.

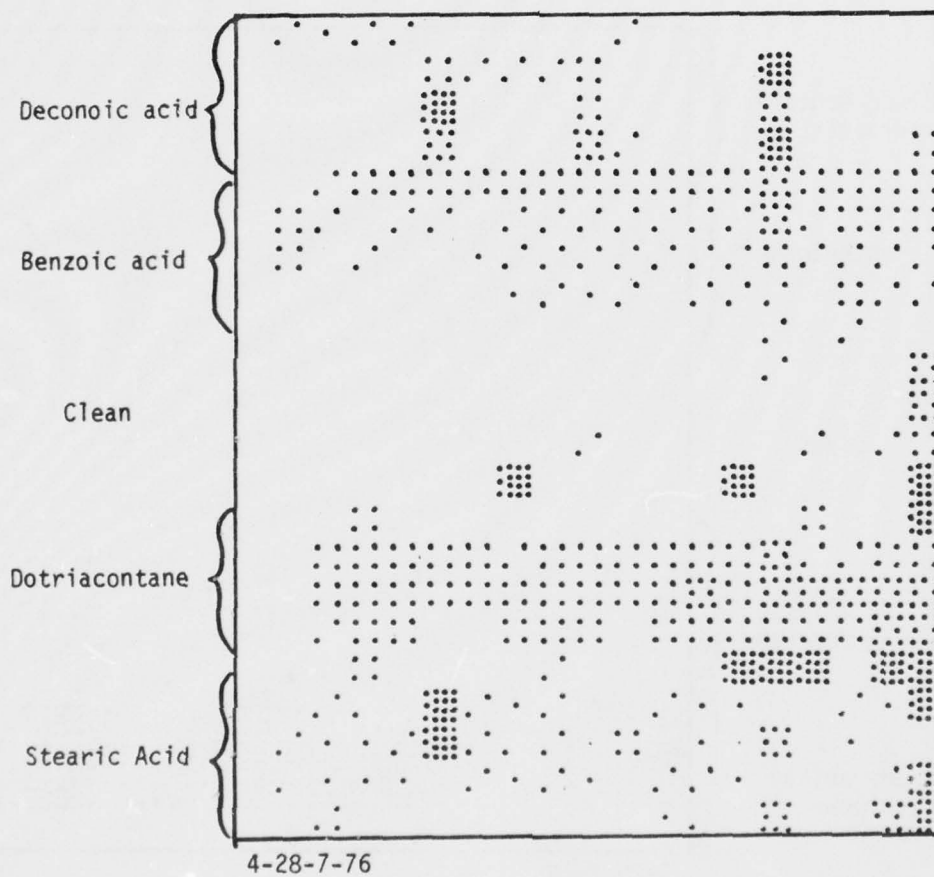


Figure A.26(d). A wettability plot for a panel that was contaminated in four regions but left clean in the center region.

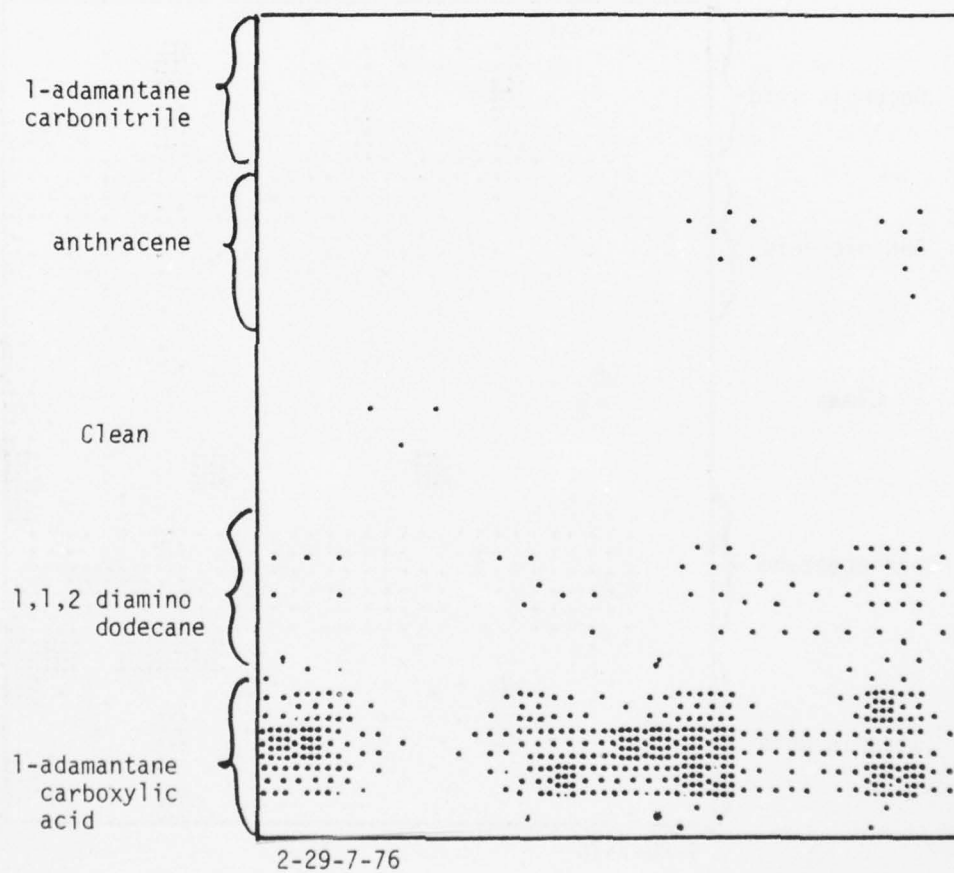


Figure A.27(a). A Δ plot ($160 < \Delta < 158$) for a panel that was contaminated in four regions but left clean in the center region.

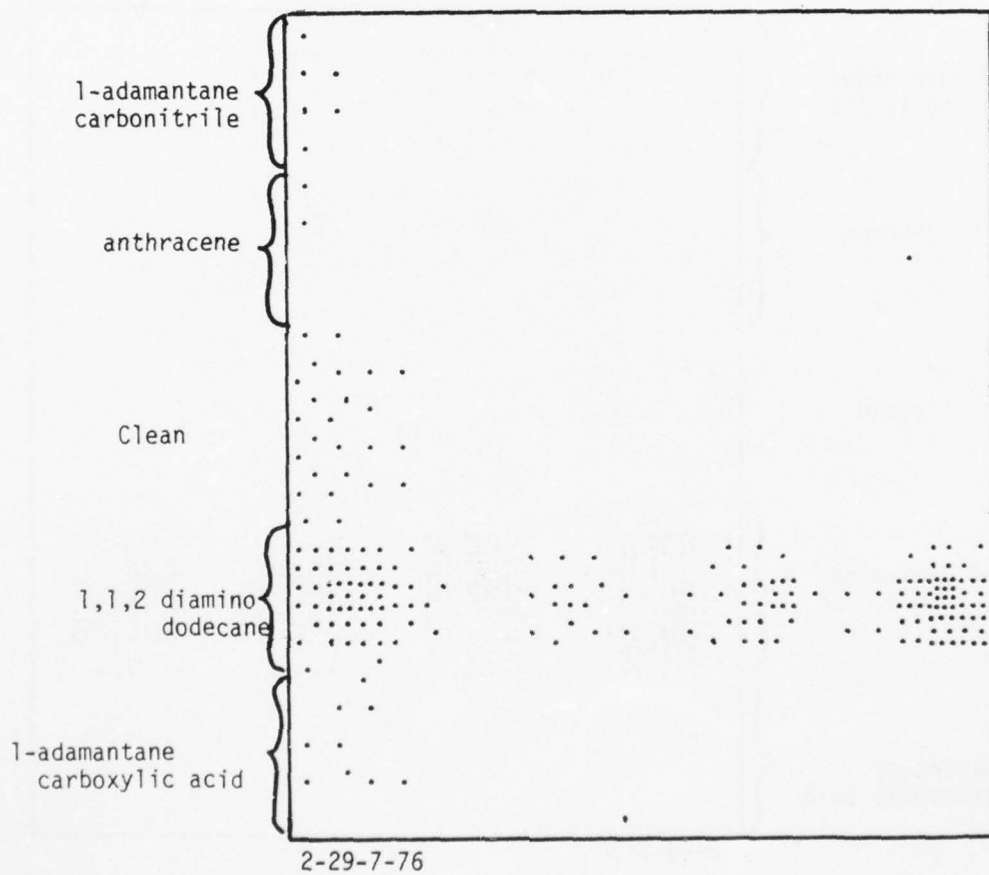


Figure A.27(b). A ψ plot ($41 < \psi < 40$) for a panel that was contaminated in four regions but left clean in the center region.

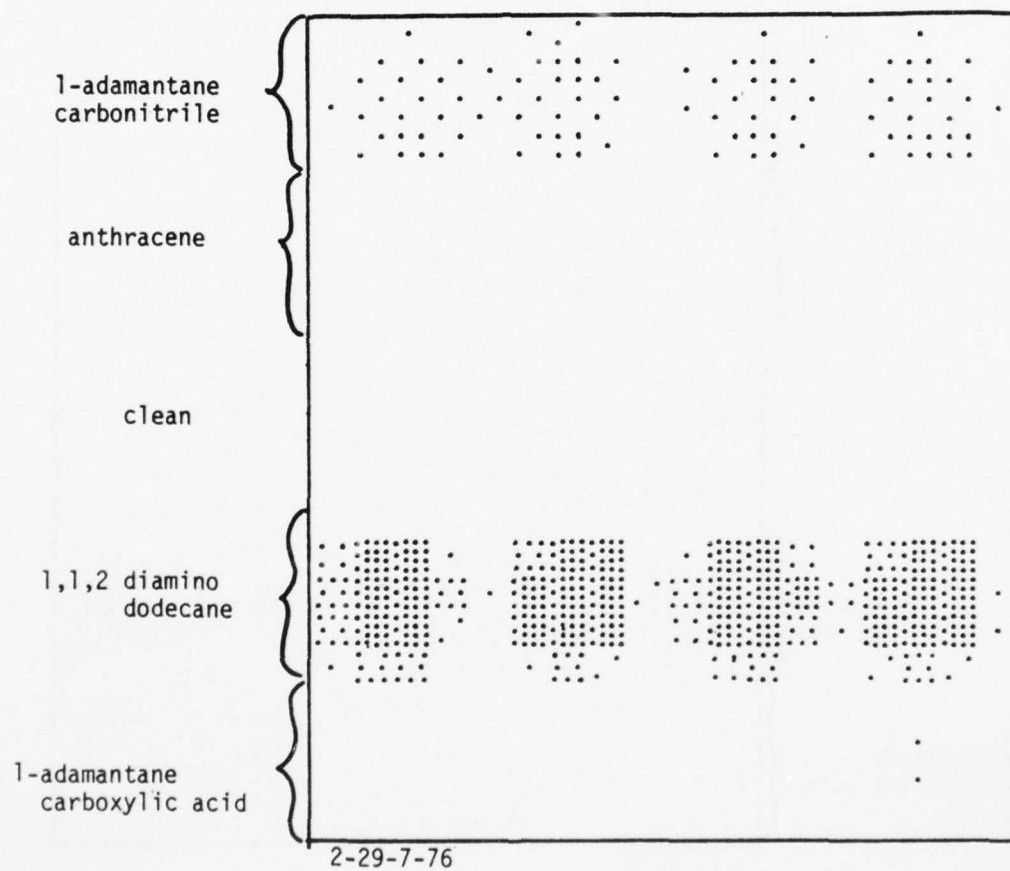


Figure A.27(c). An SPD plot ($.35 < \text{SPD} < .15$) for a panel that was contaminated in four regions but left clean in the center region.

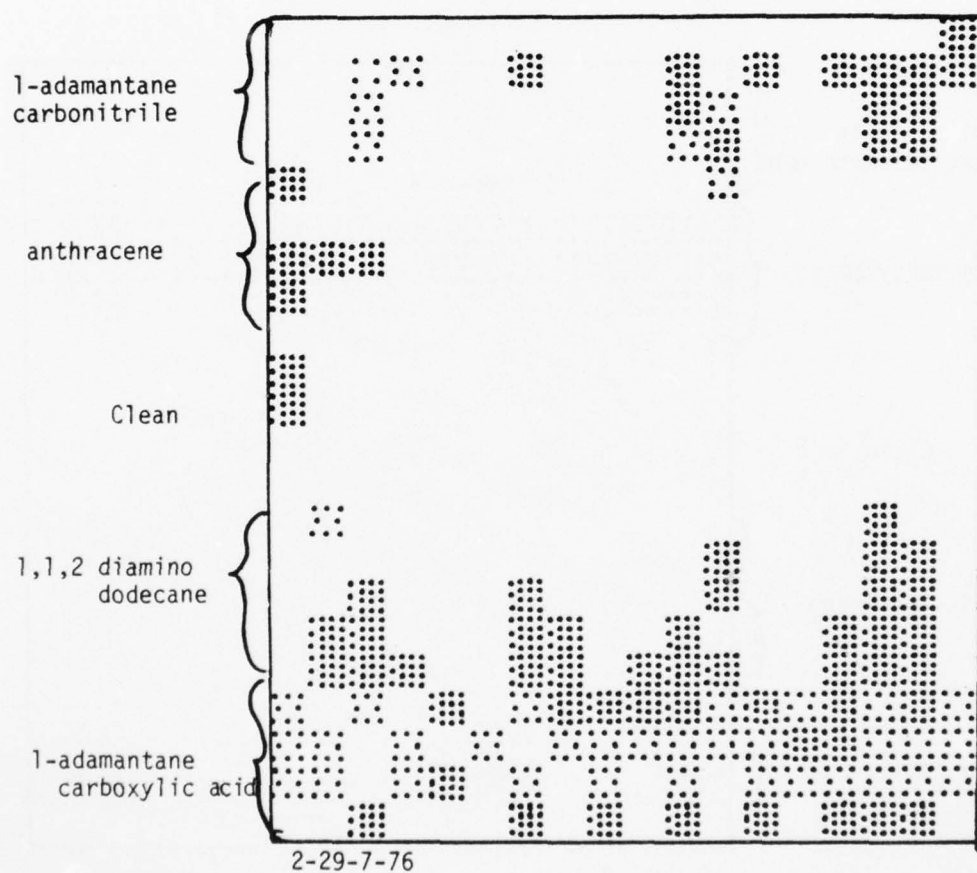


Figure A.27(d). A wettability plot for a panel that was contaminated in four regions but left clean in the center region.

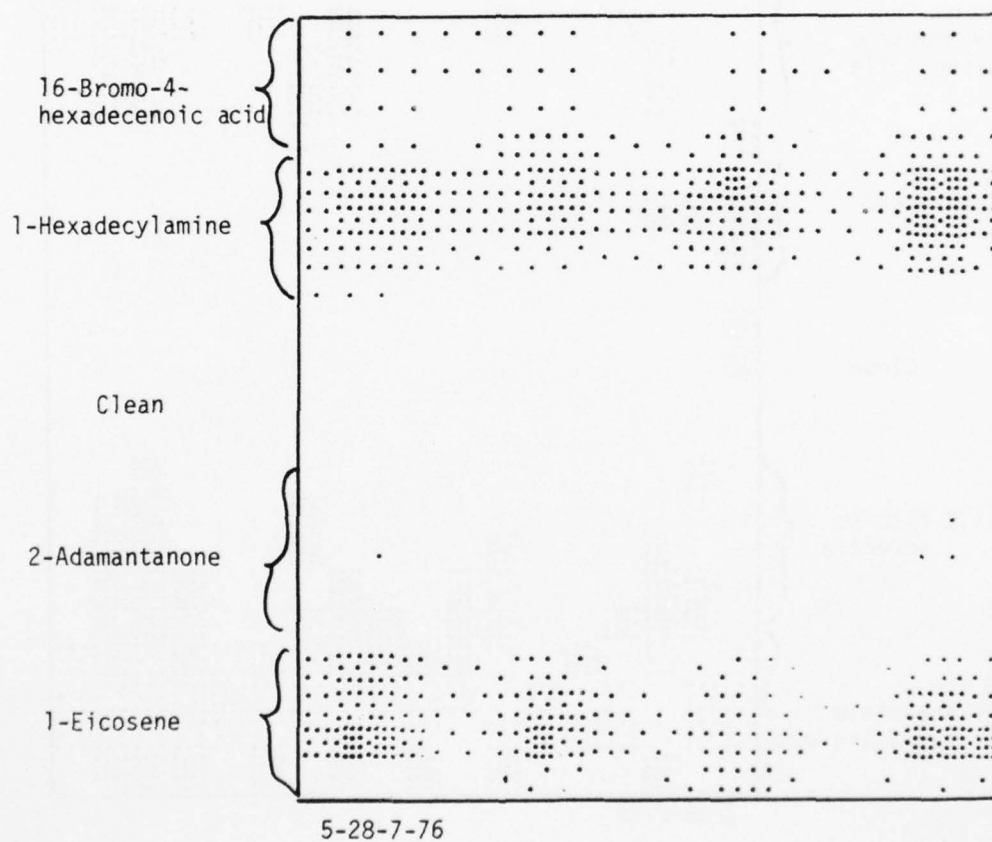


Figure A.28(a). A Δ plot ($165 < \Delta < 163$) for a panel that was contaminated in four regions but left clean in the center region.

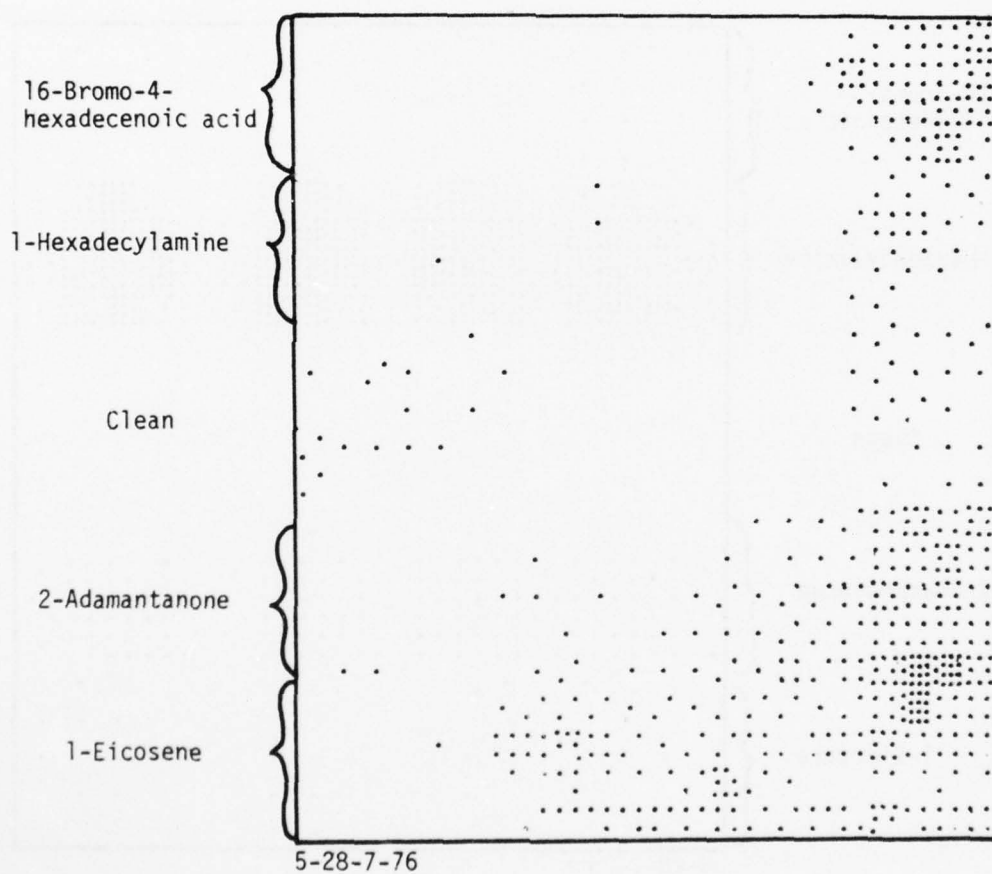


Figure A.28(b). A ψ plot ($43 < \psi < 42$) for a panel that was contaminated in four regions but left clean in the center region.

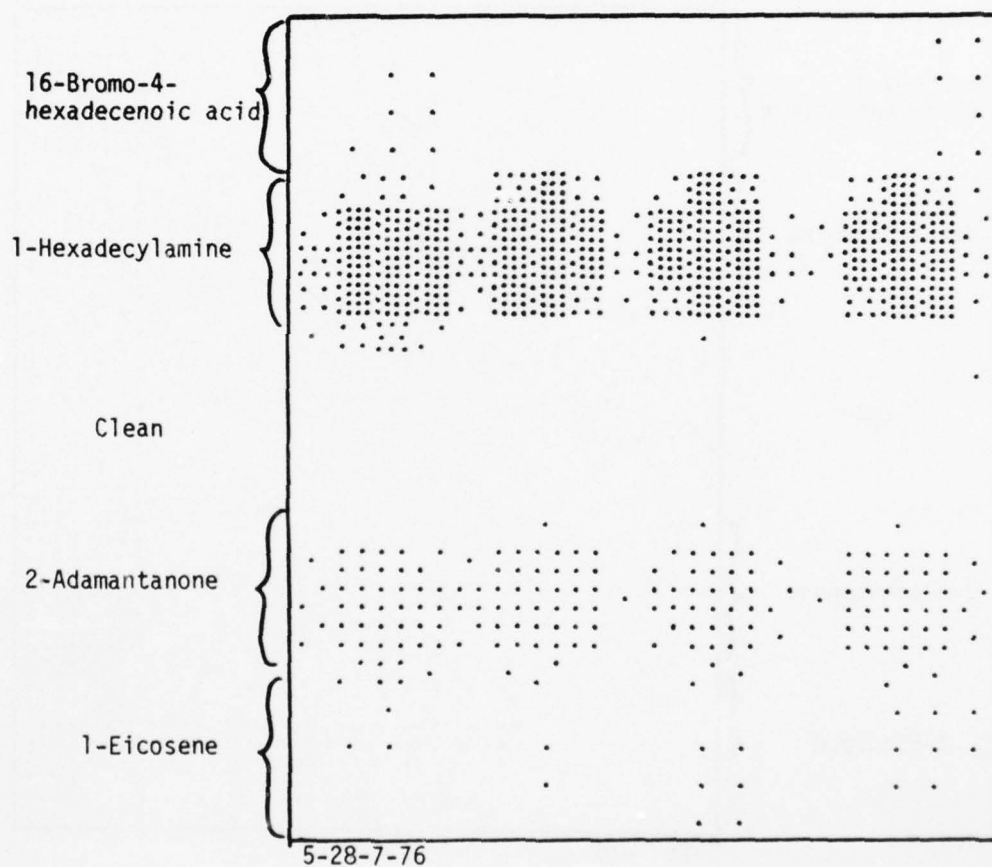


Figure A.28(c). An SPD plot ($.17 < \text{SPD} < .15$) for a panel that was contaminated in four regions but left clean in the center region.

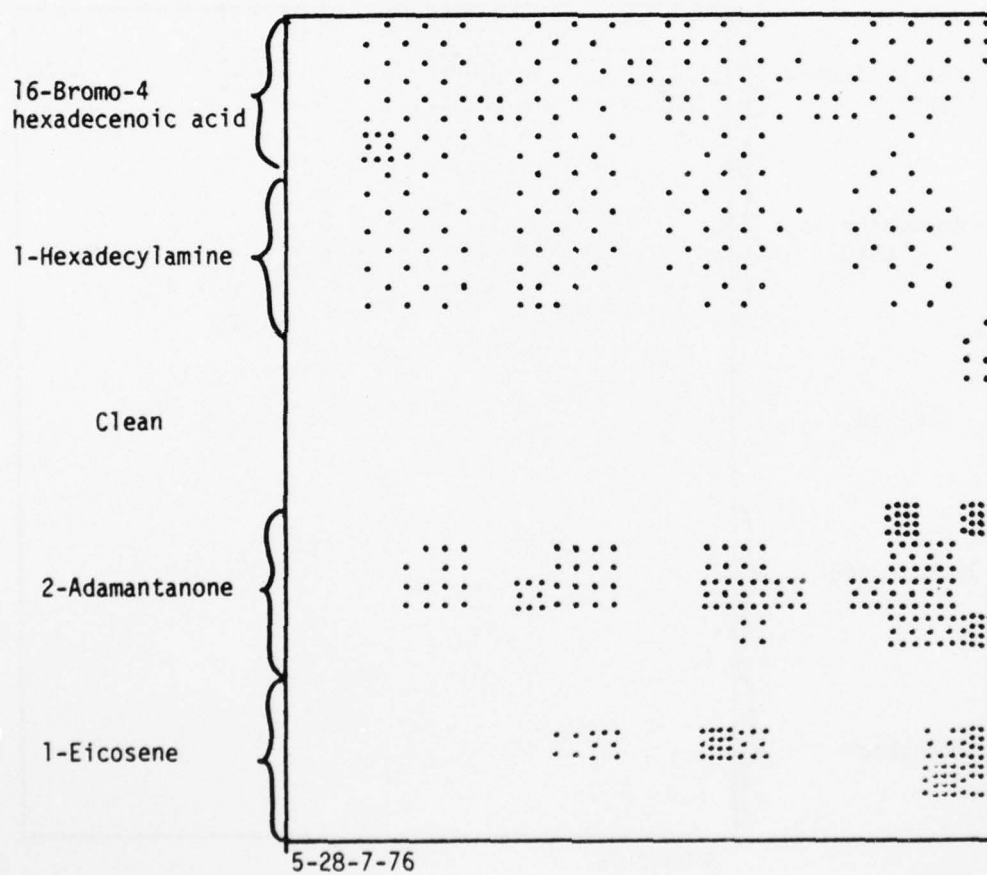


Figure A.28(d). A wettability plot for a panel that was contaminated in four regions but left clean in the center region.

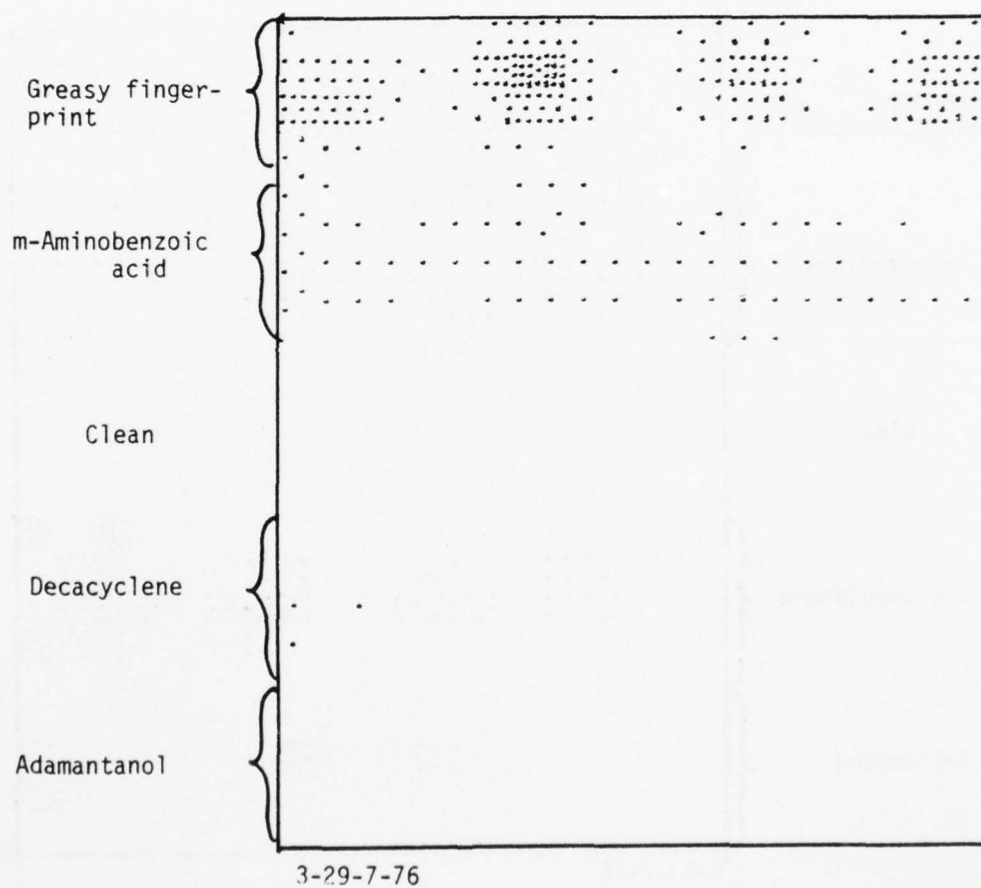


Figure A.29(a). A Δ plot ($163 < \Delta < 161$) for a panel that was contaminated in four regions but left clean in the center region.

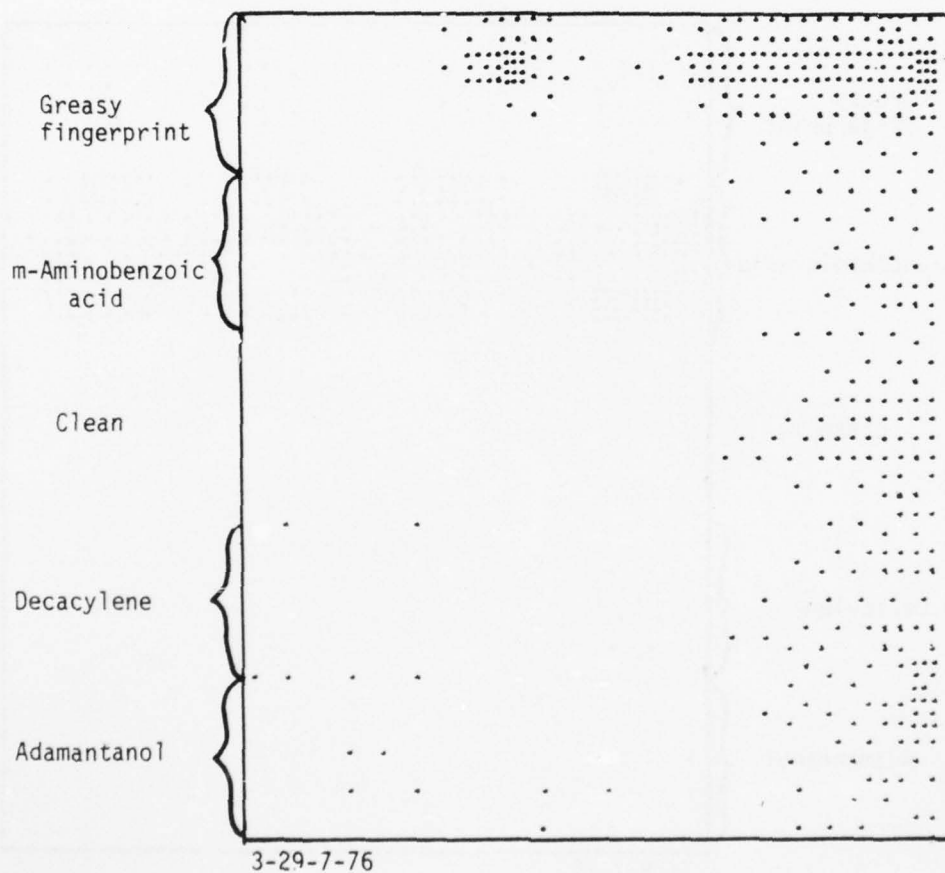


Figure A.29(b). A ψ plot ($41 < \psi < 40$) for a panel that was contaminated in four regions but left clean in the center region.

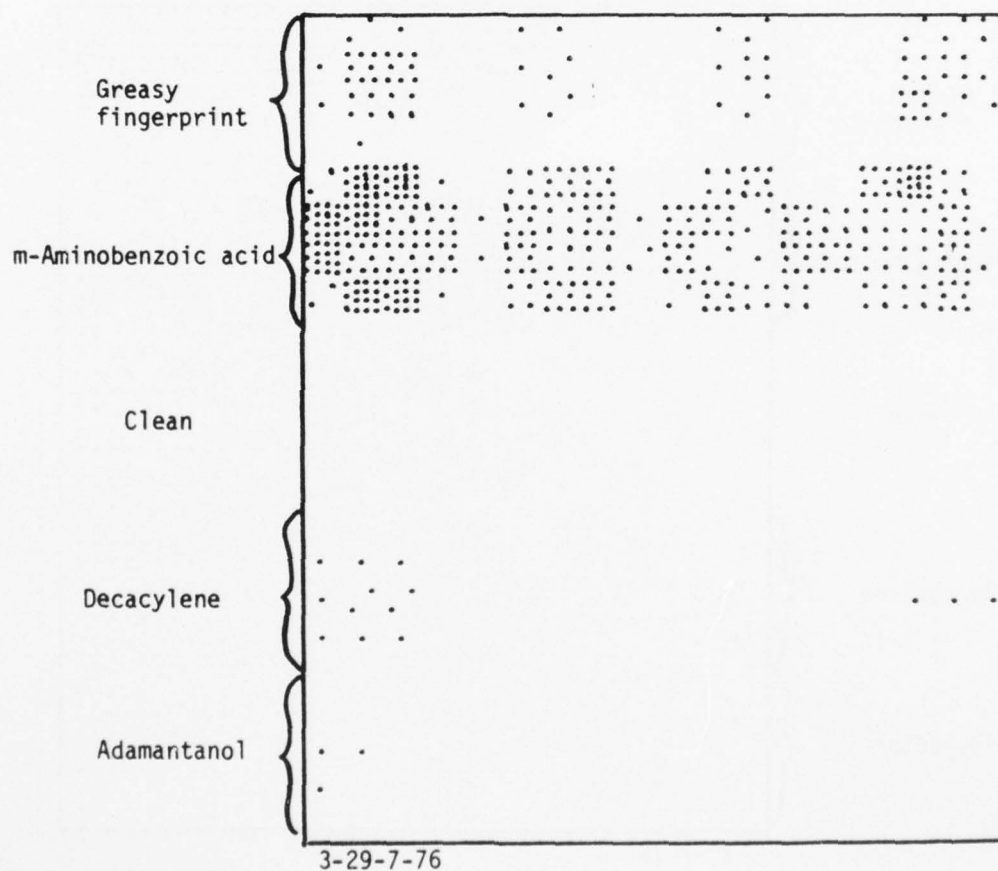


Figure A.29(c). An SPD plot ($.25 < \text{SPD} < .05$) for a panel that was contaminated in four regions but left clean in the center region.

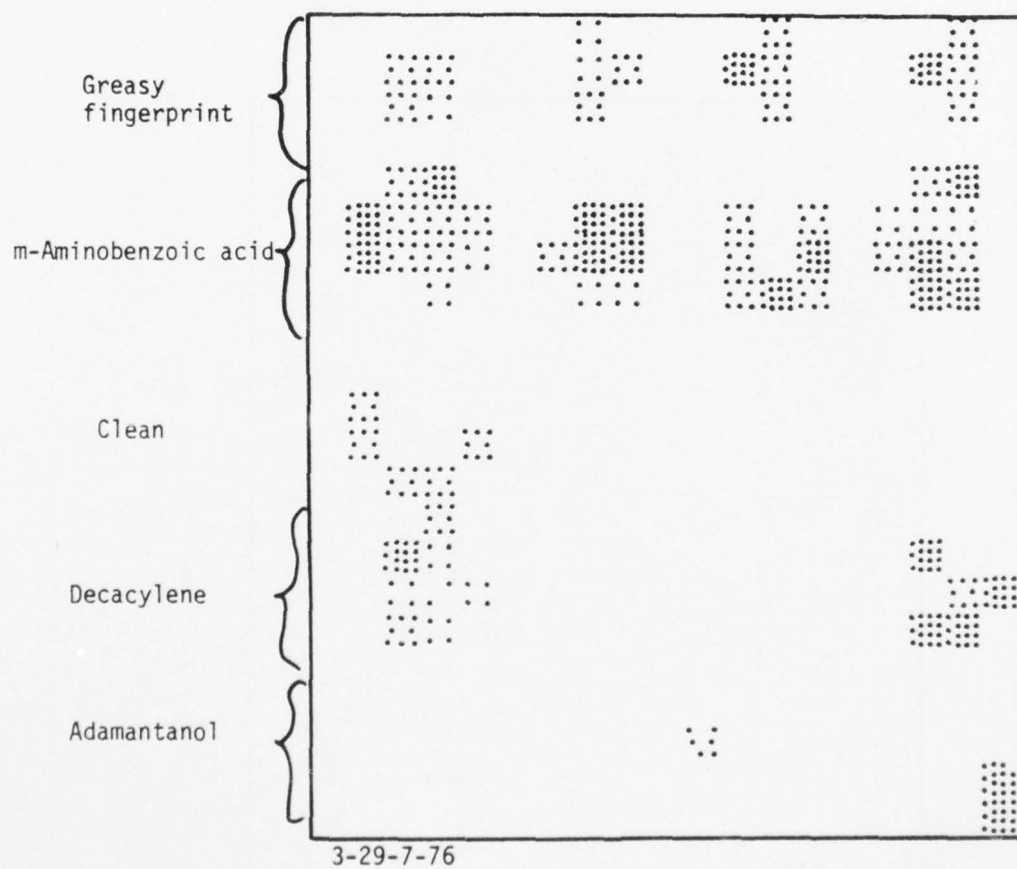
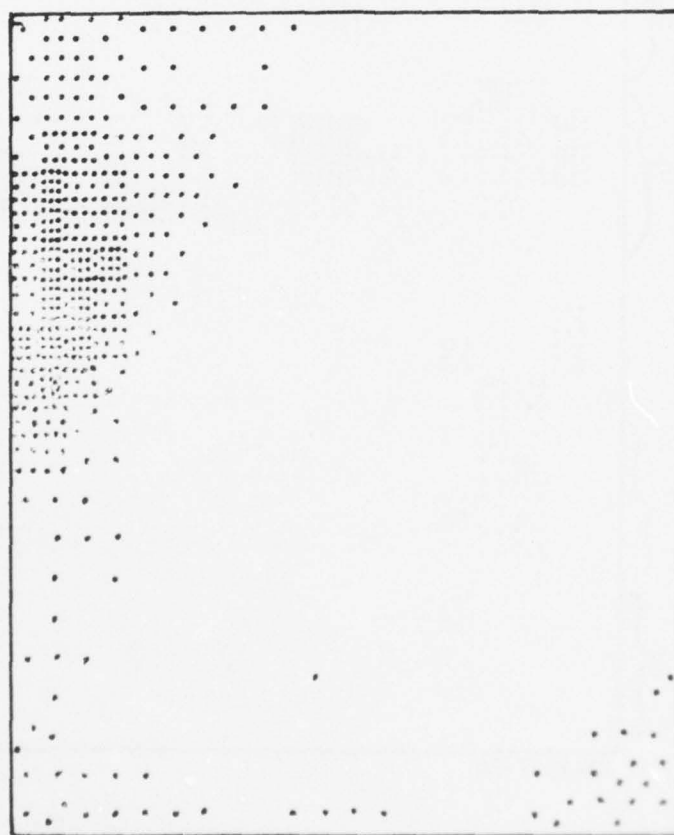


Figure A.29(d). A wettability plot for a panel that was contaminated in four regions but left clean in the center region.



10-16-75-2

Figure A.30(a). A Δ replot for $166 \leq \Delta \leq 162$ of a panel with steady-state contamination, same panel as Figure A.27(a) (lower left).

AD-A044 241

ROCKWELL INTERNATIONAL THOUSAND OAKS CALIF SCIENCE --ETC F/G 11/6
NONDESTRUCTIVE INSPECTION OF PHOSPHORIC ACID ANODIZED ALUMINUM --ETC(U)
APR 77 T SMITH

UNCLASSIFIED

SC5026.22TR

AFML-TR-77-42

F33615-75-C-5235

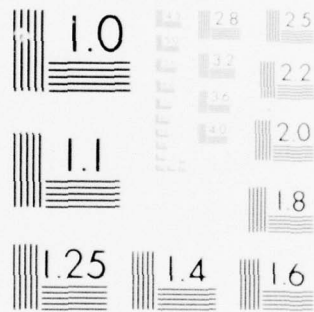
NL

3 OF 3

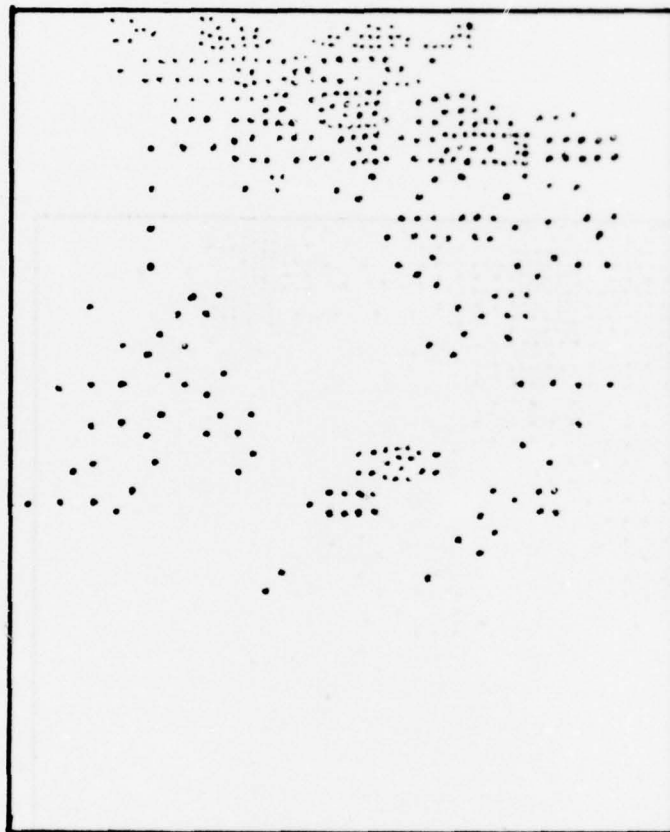
AD
A044241



END
DATE
FILMED
10-77
DDC

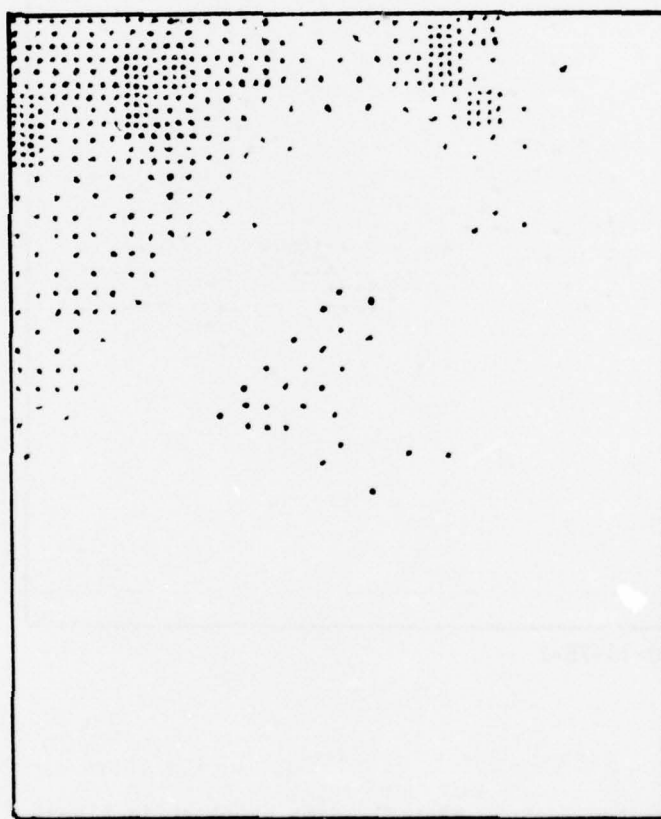


MICROCOPY RESOLUTION TEST CHART
NATIONAL BUREAU OF STANDARDS-1963-A



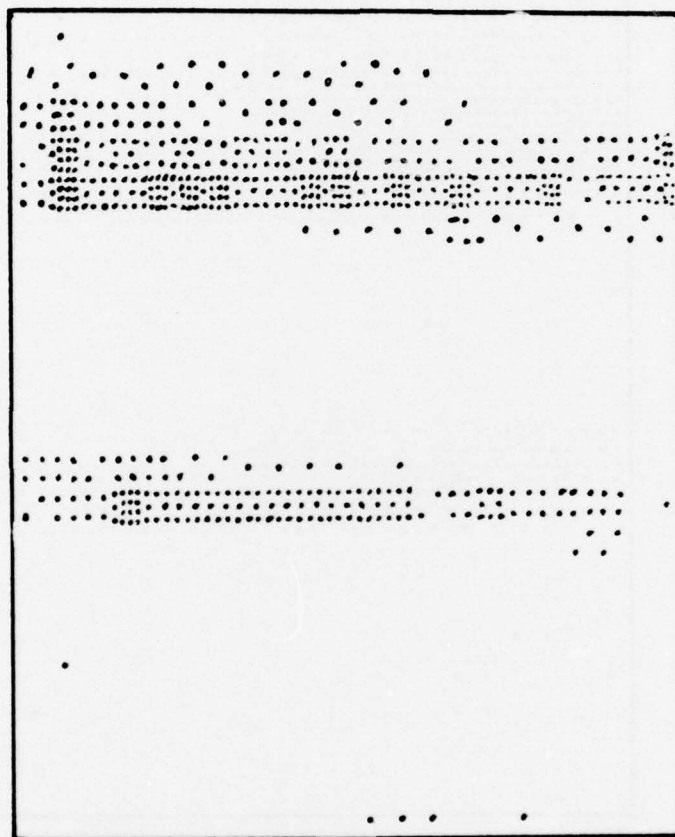
10-16-75-2

Figure A.30(b). A ψ replot, $43 < \psi < 41$, same panel as in Figure A.22(a).



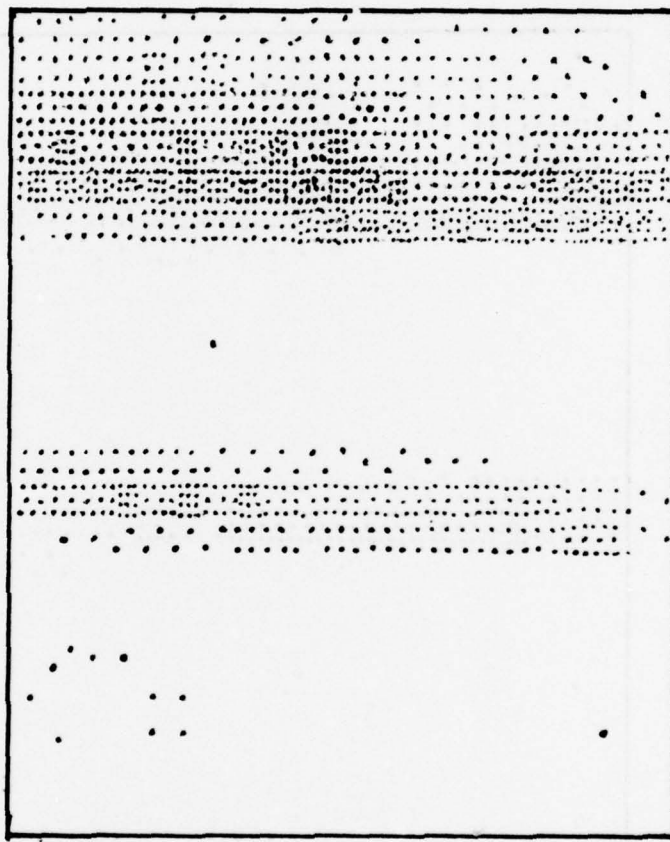
10-16-75-2

Figure A.30(c). An SPD plot $.43 < \text{SPD} < .35$, same panel as in Figure A.22(a)



2-26-2-76

Figure A.31(a). A Δ replot, $164 < \Delta < 161$, for a surface damaged panel, same as Figure A.8(a')



2-26-2-76

Figure A.31(b). A ψ replot, $43 < \psi < 41$, same as Figure A.8(b').

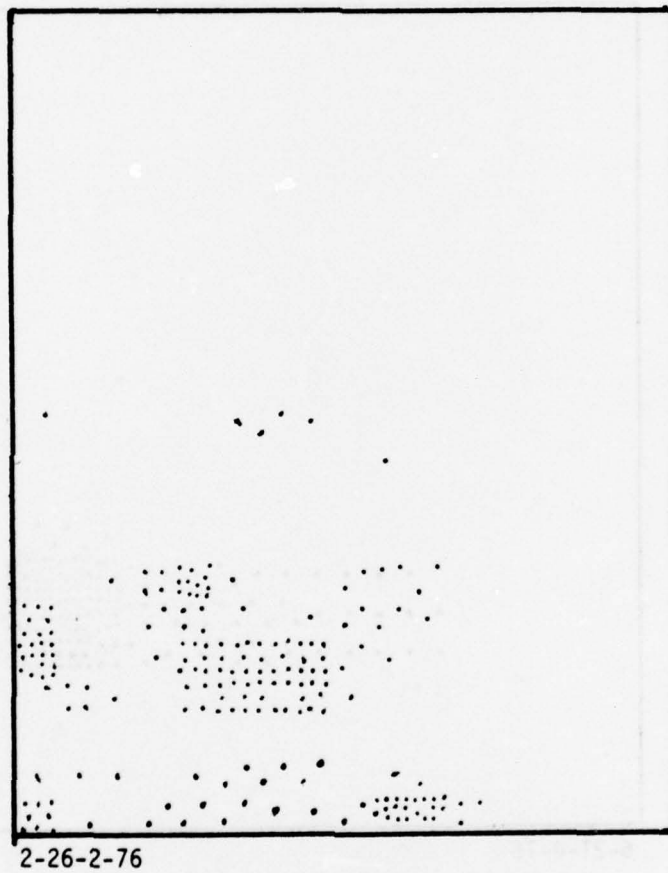


Figure A.31(c). An SPD replot, $.43 < \text{SPD} < .35$, same as Figure A.9.

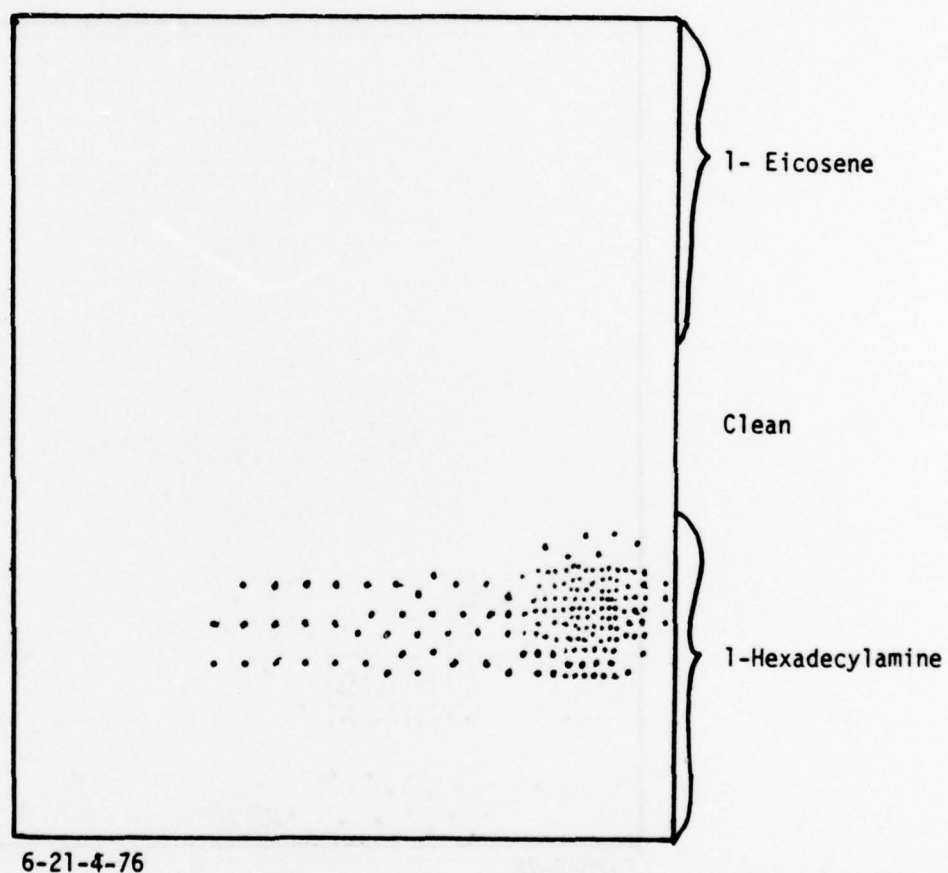


Figure A.32(a). A Δ replot, $162 < \Delta < 160$, same as Figure A.19(a).
1-Eicosene and 1-Hexadecylamine.

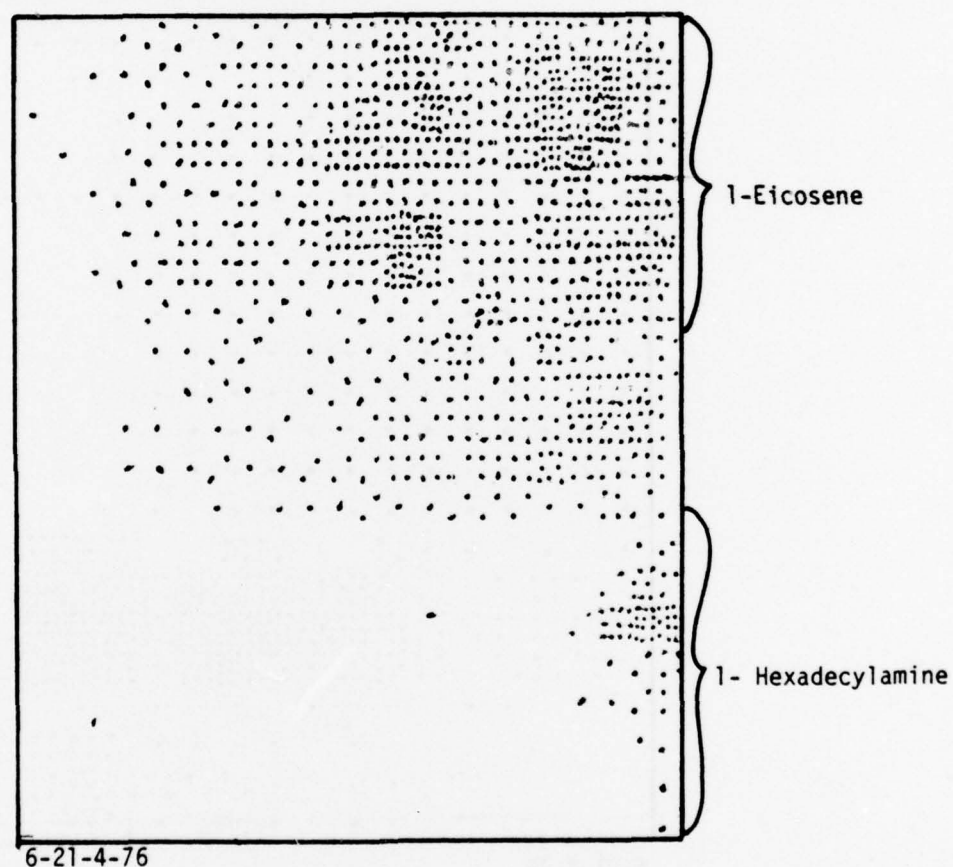


Figure A.32(b). A ψ replot, $43 < \psi < 41$, same as for sample Figure A.19(d).

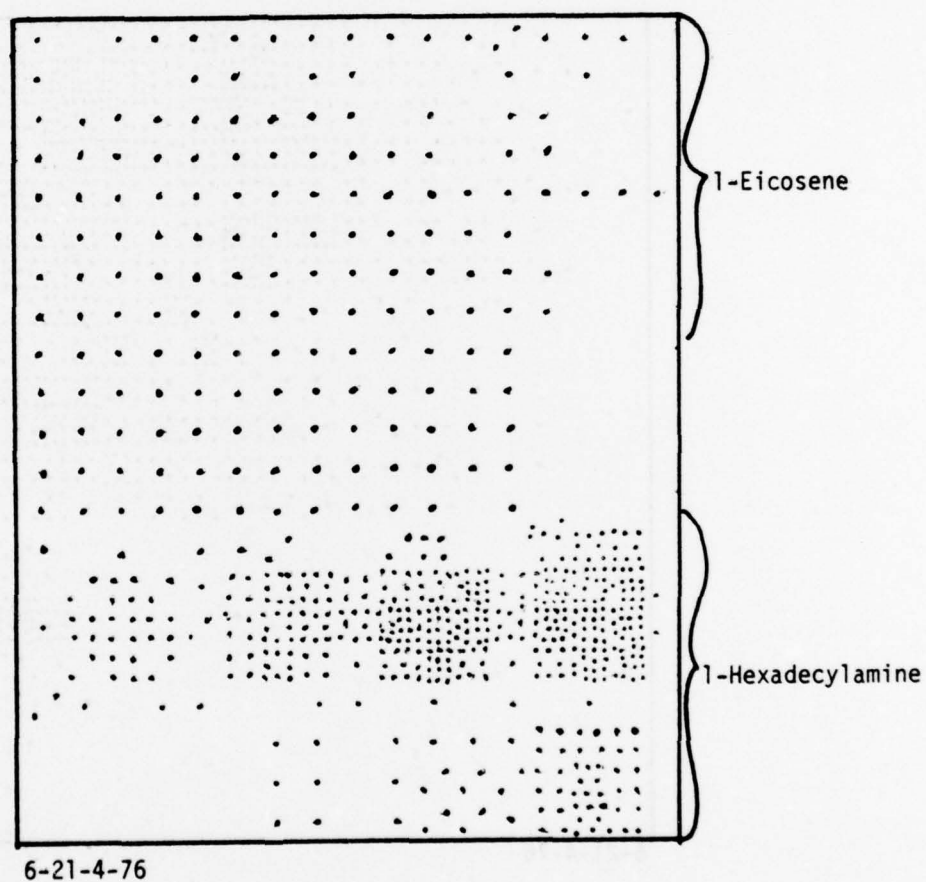


Figure A.32(c). An SPD replot, $.45 < \text{SPD} < .43$, same as for Figure A.19(c).

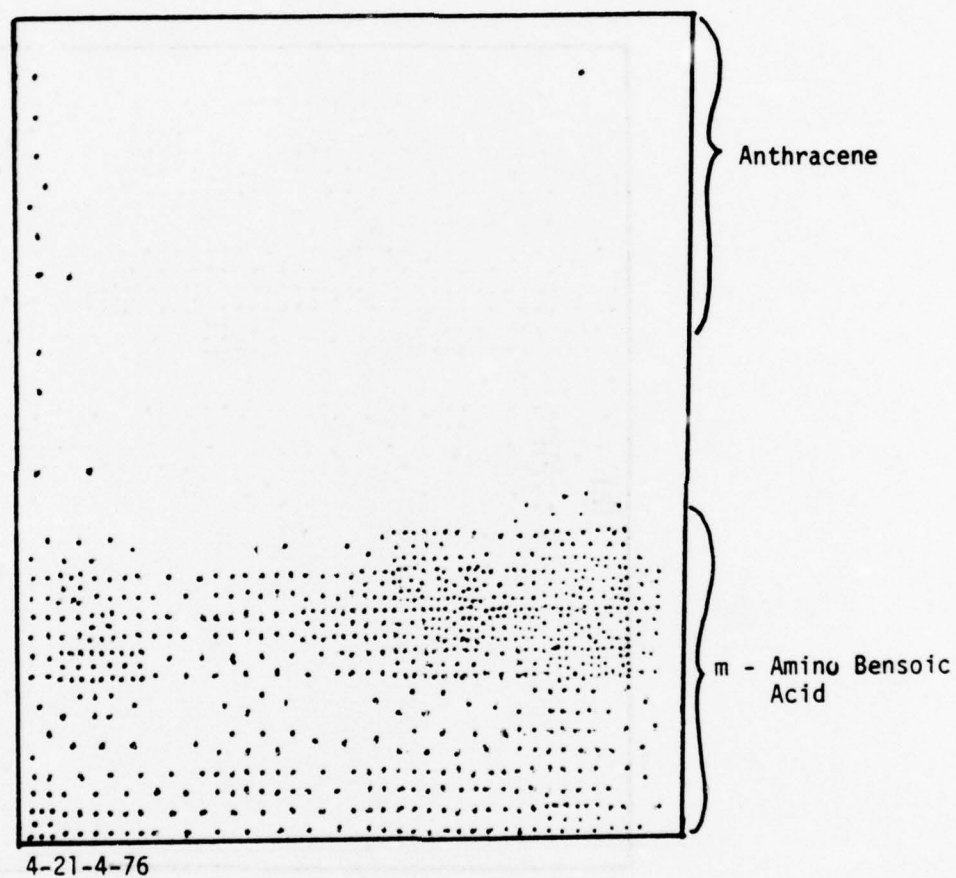
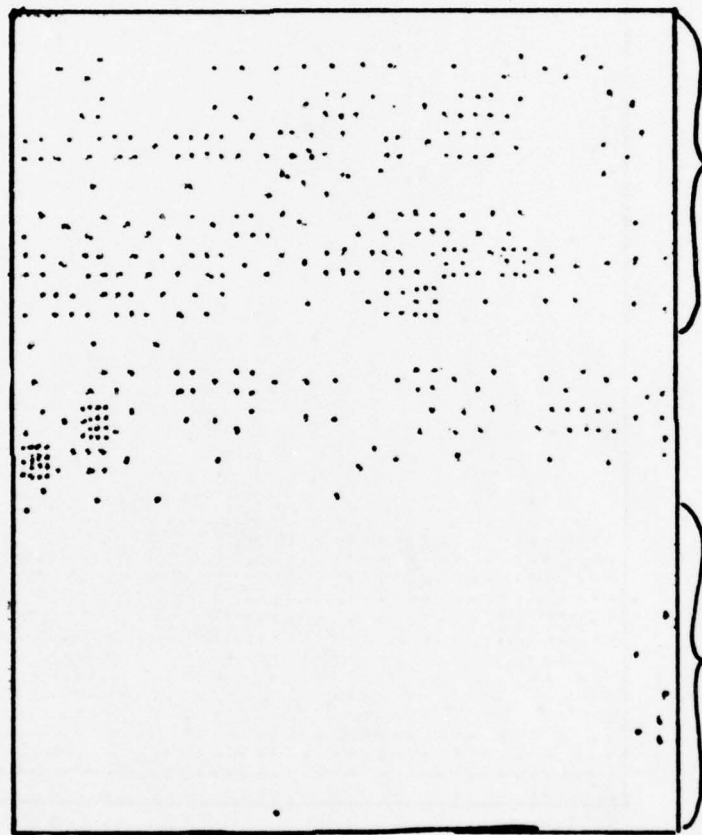


Figure A.33(a). A Δ replot, $162 < \Delta < 159.5$, same as Figure A.20(a) anthracene and m-amino benzoic acid.



4-21-4-76

Figure A.33(b). A ψ replot, $43.5 < \psi < 41.5$, same as Figure A.20(b).

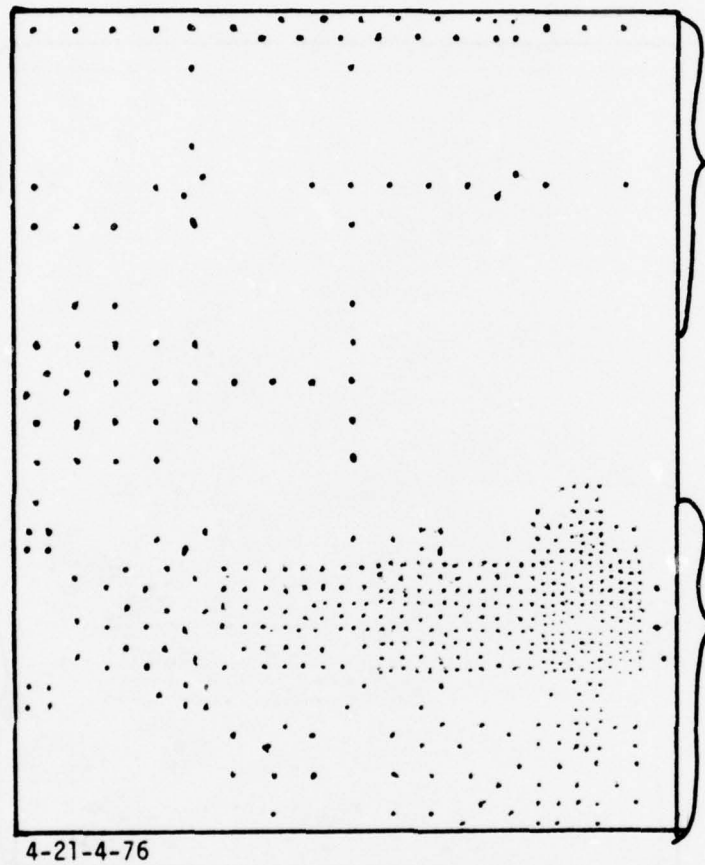


Figure A.33(c). An SPD replot, $.45 < \text{SPD} < .38$, same as Figure A.20(c).

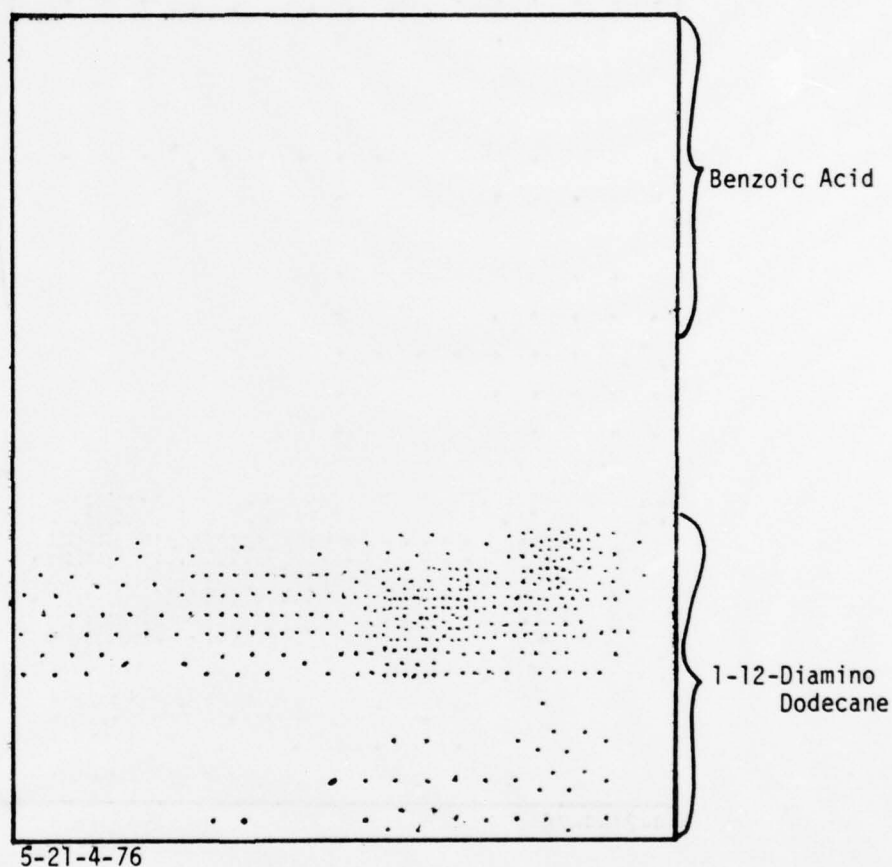


Figure A.34(a). A Δ replot, $162 < \Delta < 159.5$, same as for Figure A.21(a) benzoic acid and 1-12-diamino dodecane.

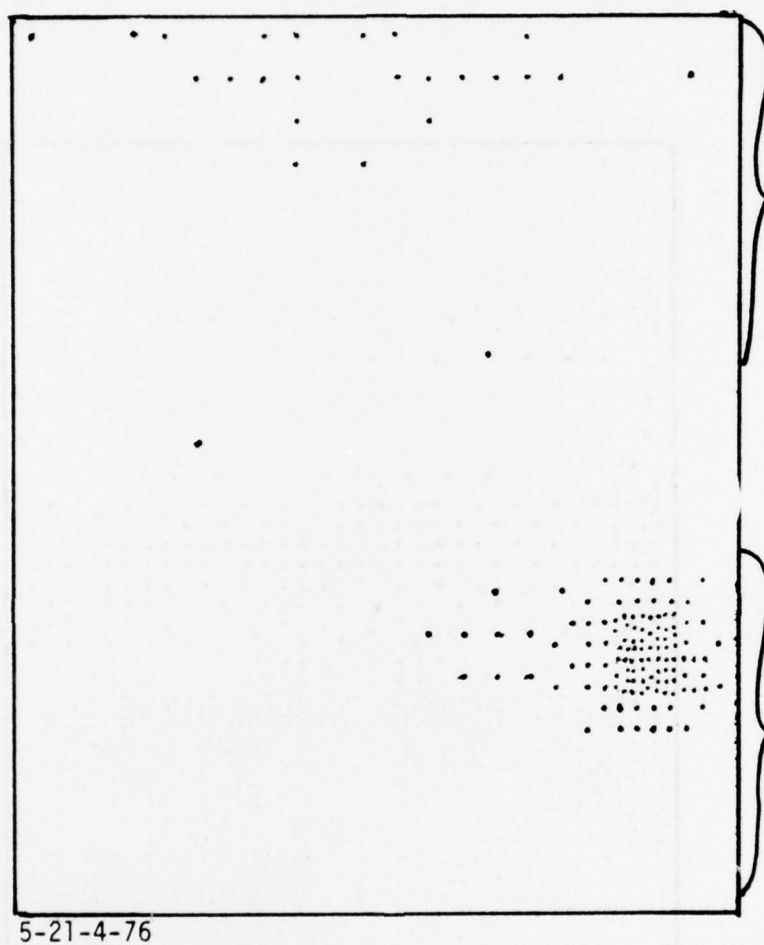


Figure A.34(b). A ψ replot, $43.5 < \psi < 41.5$, same as for Figure A.21(b).

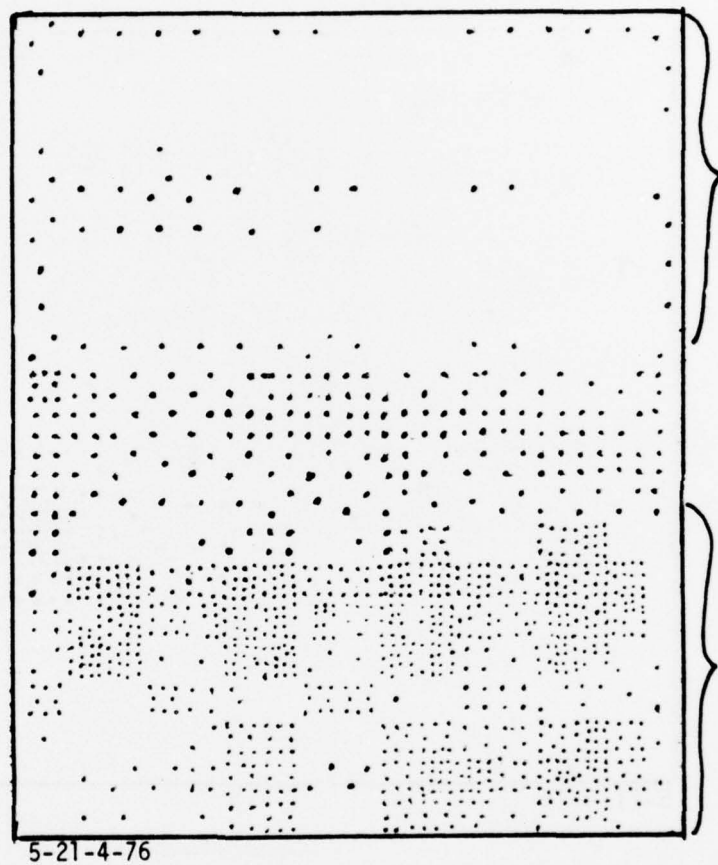
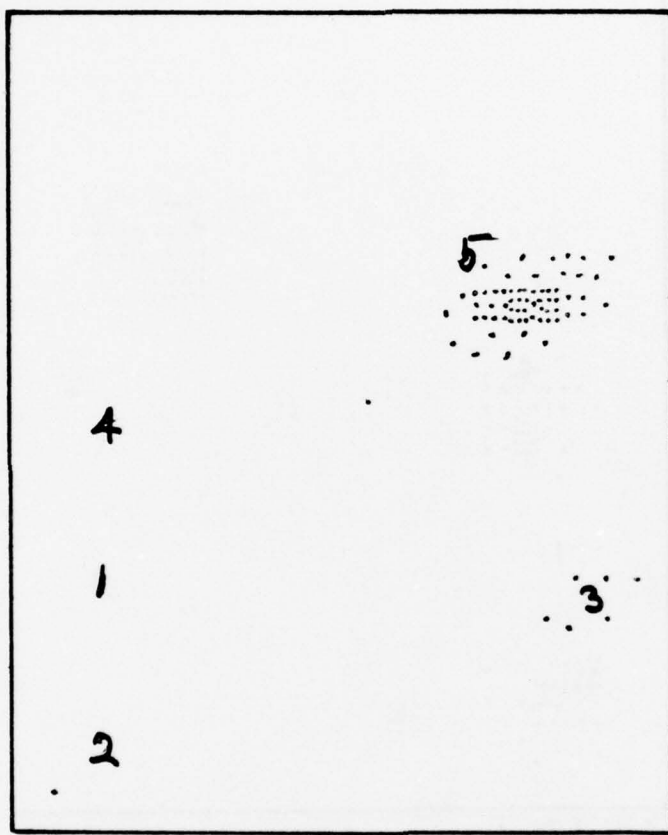


Figure A.34(c). An SPD replot, $.58 < \text{SPD} < .56$, same as for Figure A.21(c).



4-27-2-76

Figure A.35(a). $A \Delta$ replot, $164 < \Delta < 161$, same as for Figure A.23(a) stearic acid.

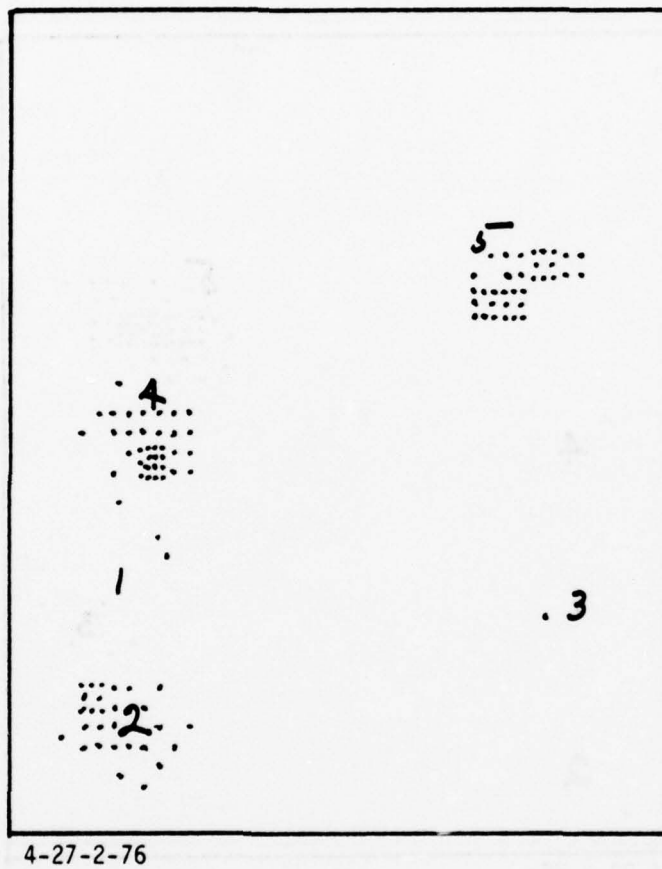
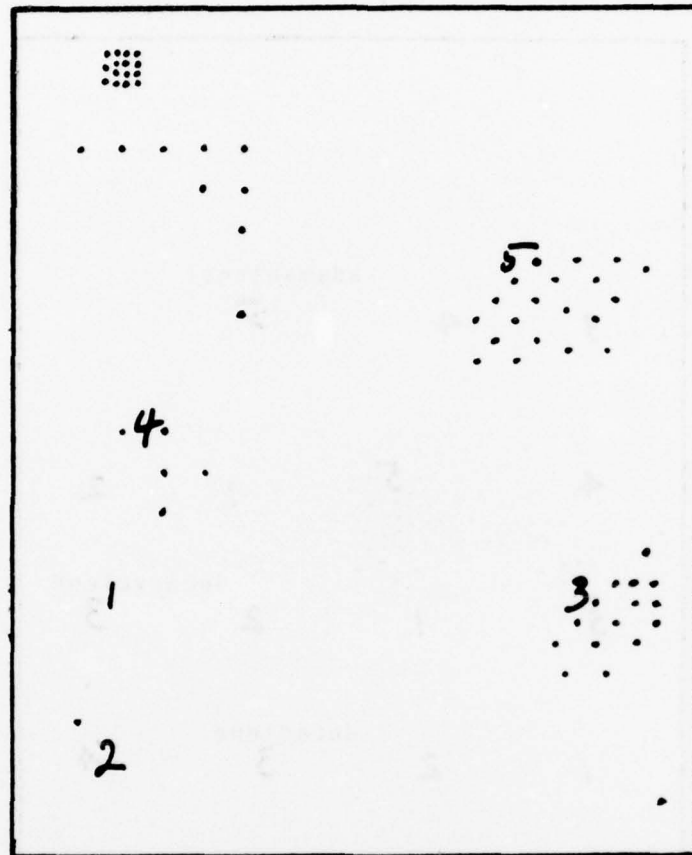


Figure A.35(b). A ψ replot, $43 < \psi < 41$, same as Figure A.23(a).



4-27-2-76

Figure A.35(c). An SPD replot, $43 < \text{SPD} < .35$, same as Figure A.23(a).

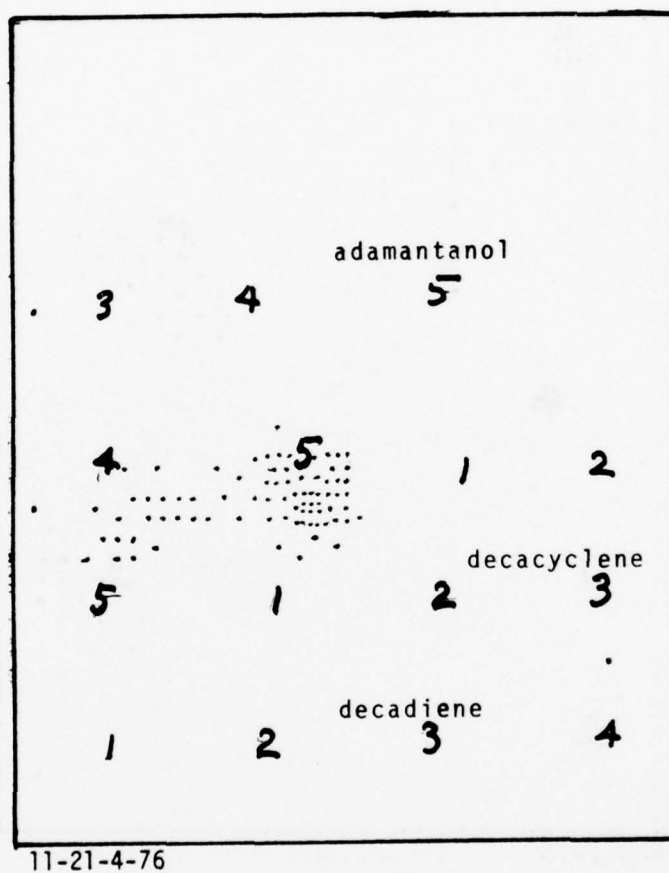
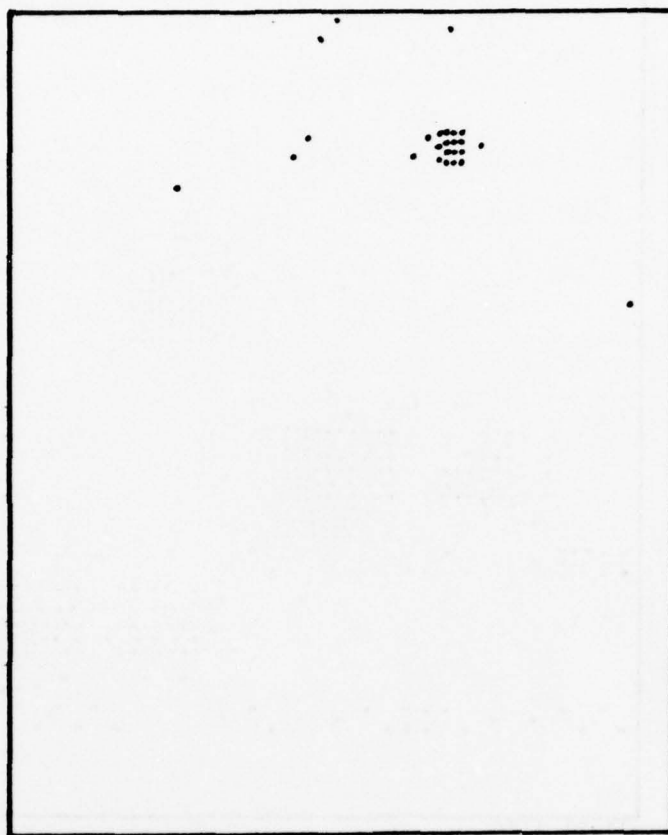


Figure A.36(a). A Δ replot, $164 < \Delta < 161$, same as for Figure A.24(a), May 1976, decadiene, decacyclene, and adamantanol.



11-21-4-76

Figure A.36(b). A ψ replot, $44 < \psi < 42$, same as for Figure A.24(b).

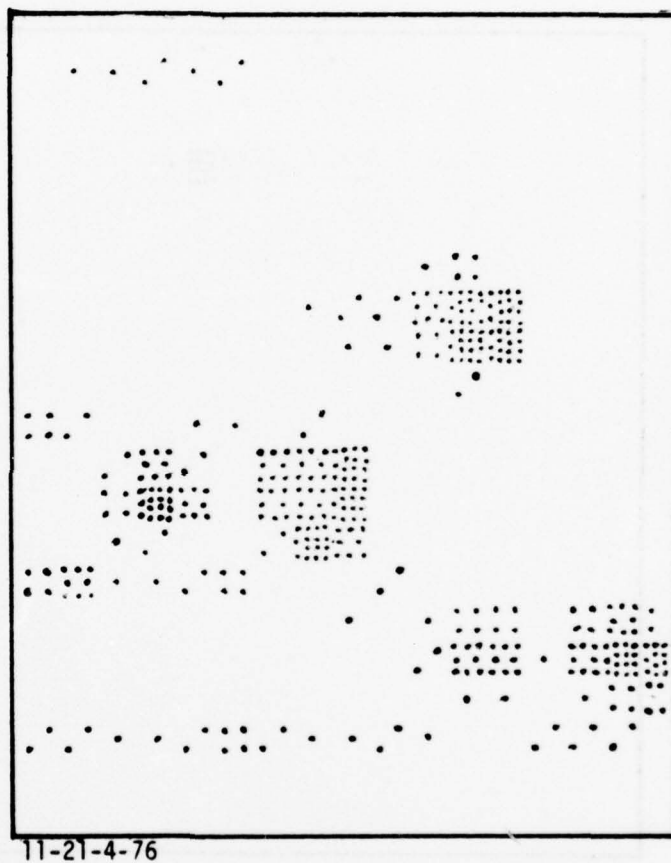


Figure A.36(c). An SPD replot, $.37 < \text{SPD} < .28$, same as for Figure A.24(c).

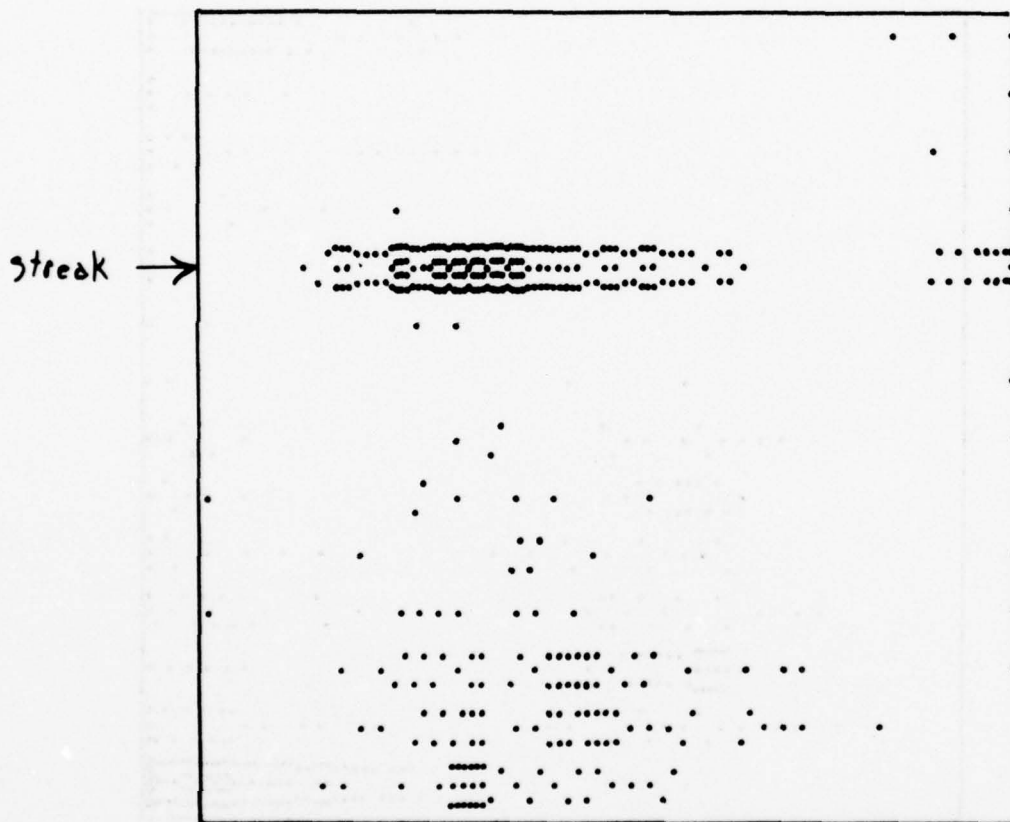


Figure A.37(a). Computer plot of $\Delta(144 < \Delta < 141)$ for 10" x 10" area of a production panel from McDonnell Douglas.

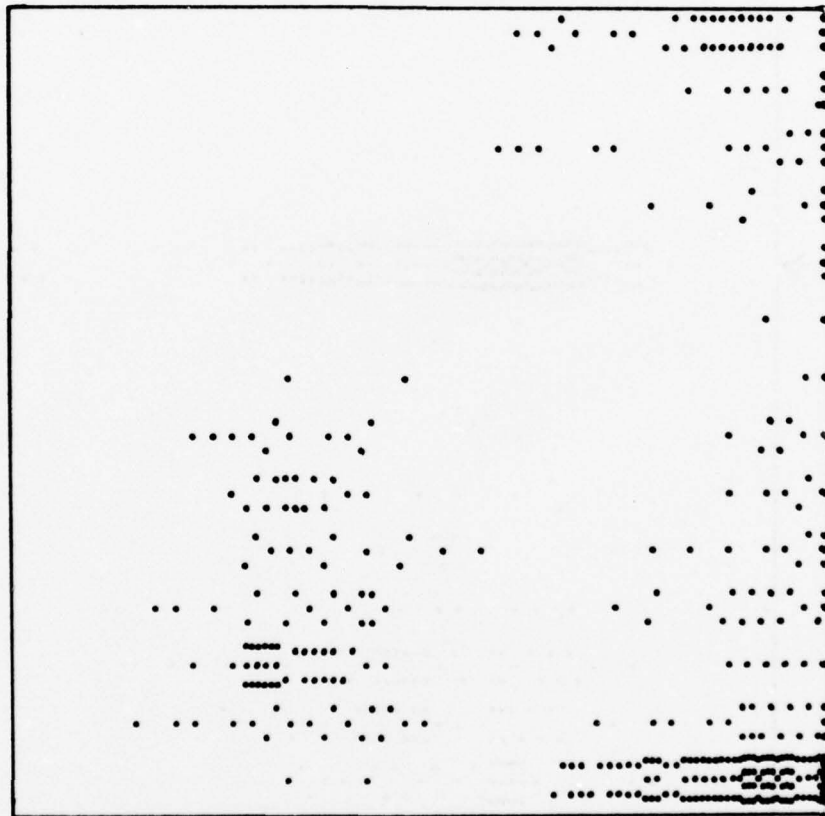


Figure A.37(b). Computer plot of ψ ($43 < \psi < 41$) for a production panel from McDonnell Douglas.

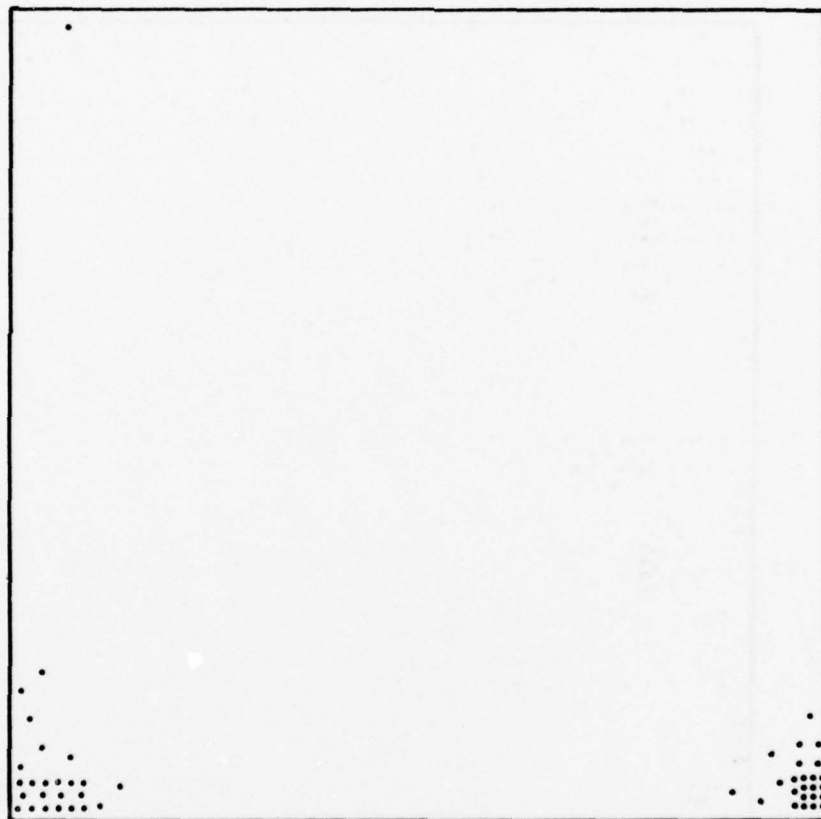


Figure A.37(c). Computer plot of SPD ($.55 < \text{SPD} < .35$) for a production panel from McDonnell Douglas

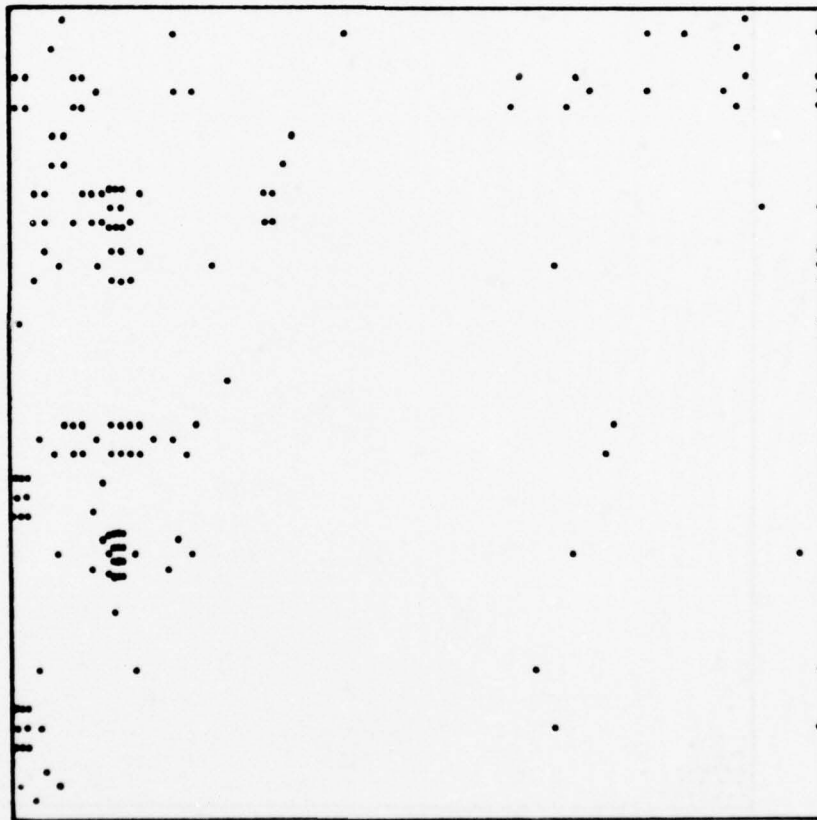


Figure A.38(a). Computer plot of Δ ($145 < \Delta < 142$) for another production panel from McDonnell Douglas

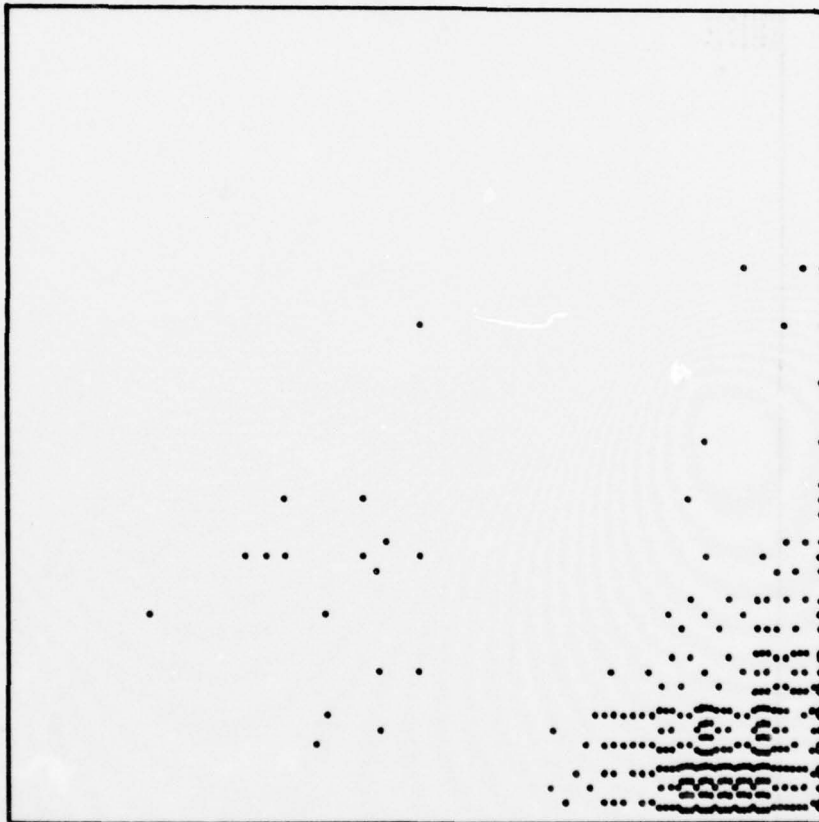


Figure A.38(b). Computer plot of ψ ($43 < \psi < 41$) for another production panel from McDonnell Douglas

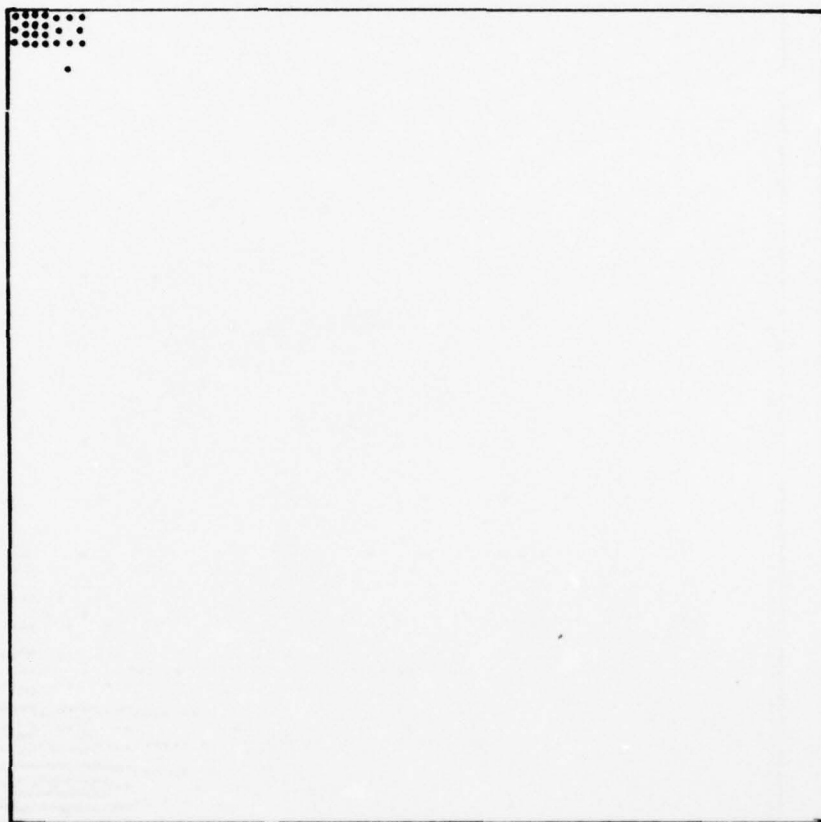


Figure A.38(c). Computer plot of SPD ($.42 < \text{SPD} < .22$) for another production panel from McDonnell Douglas

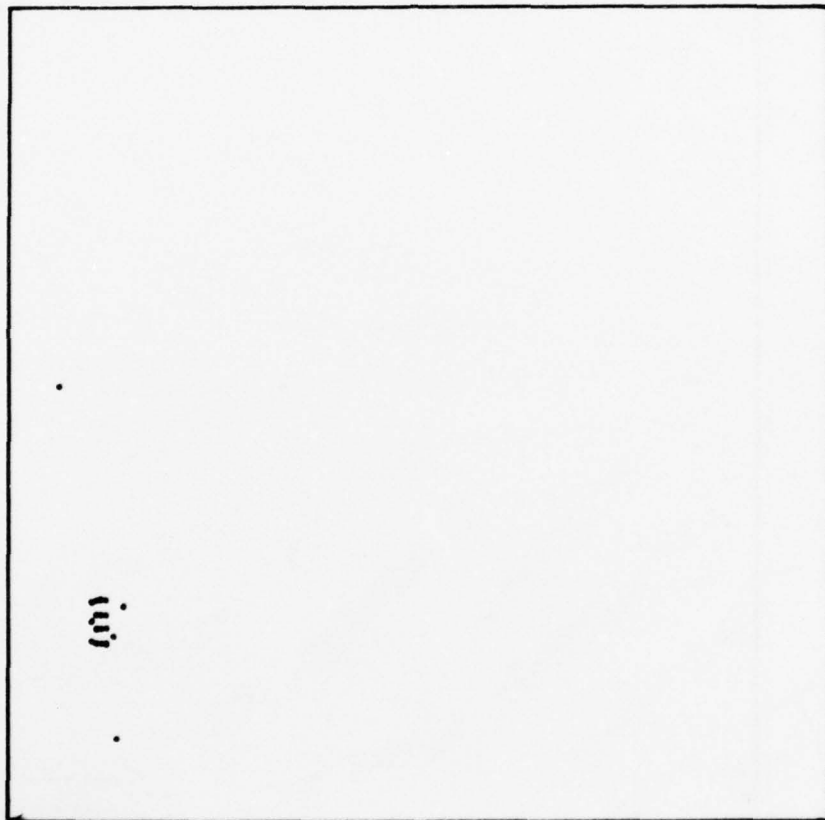


Figure A.39(a). Computer plot of Δ ($144 < \Delta < 141$) for another production panel from McDonnell Douglas

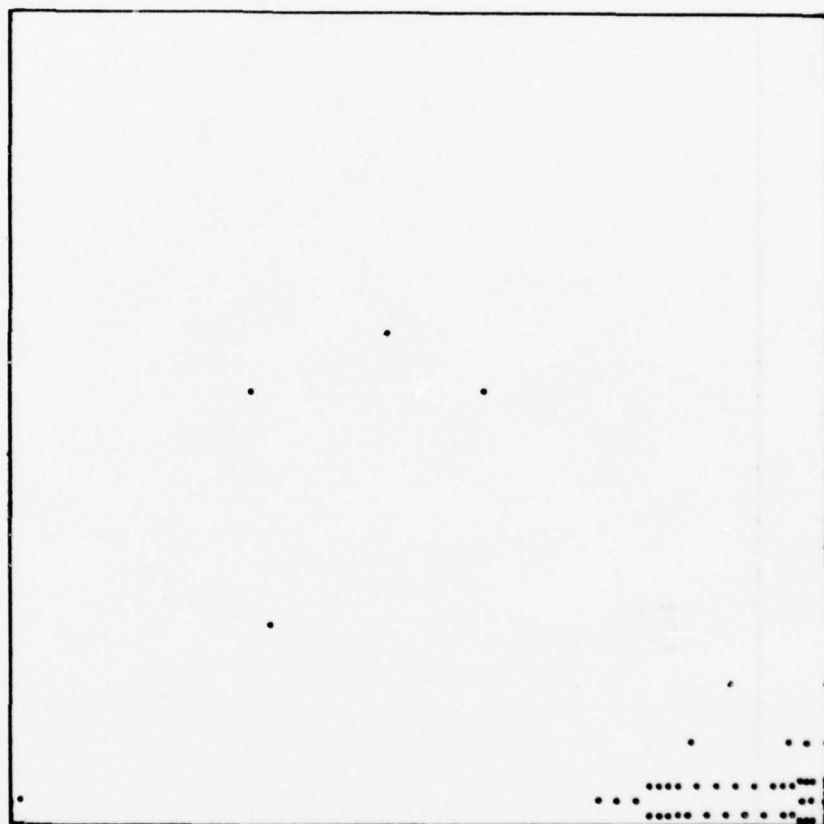


Figure A.39(b). Computer plot of ψ ($43 < \psi < 41$) for another production panel from McDonnell Douglas

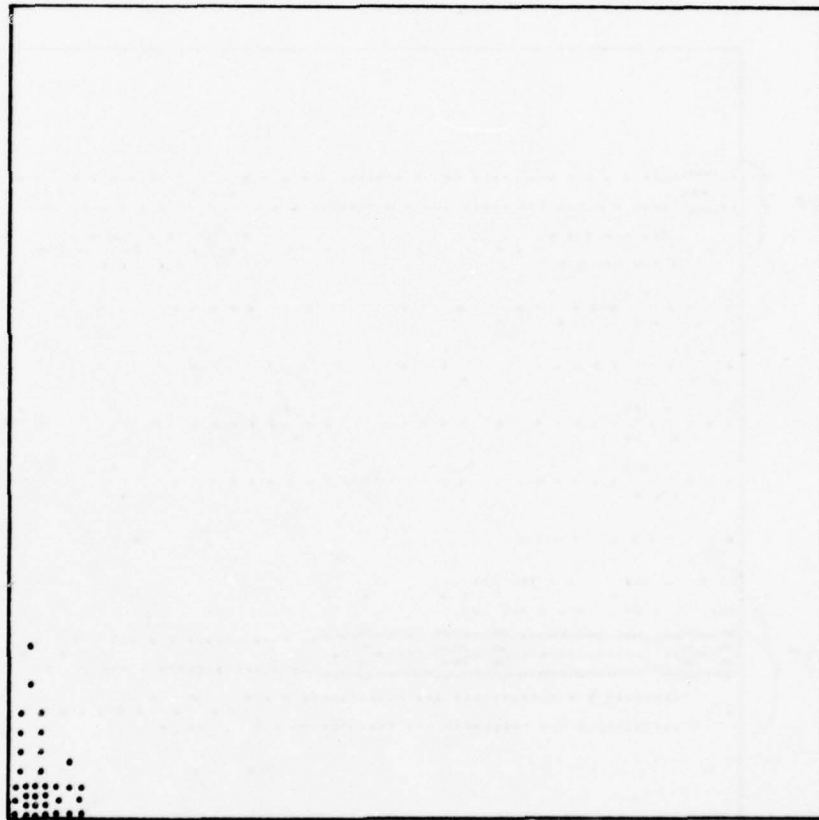


Figure A.39(c). Computer plot of SPD ($.43 < \text{SPD} < .23$) for another production panel from McDonnell Douglas

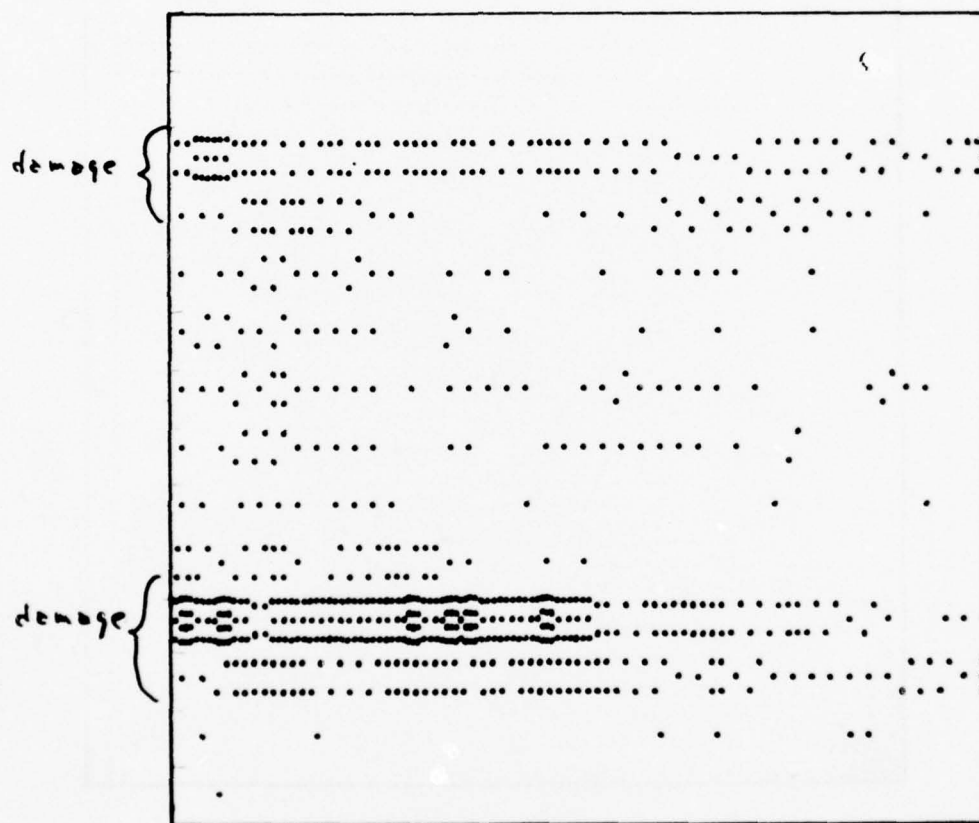


Figure A.40(a). Computer plot of Δ ($145 < \Delta < 142$) for another production panel from McDonnell Douglas

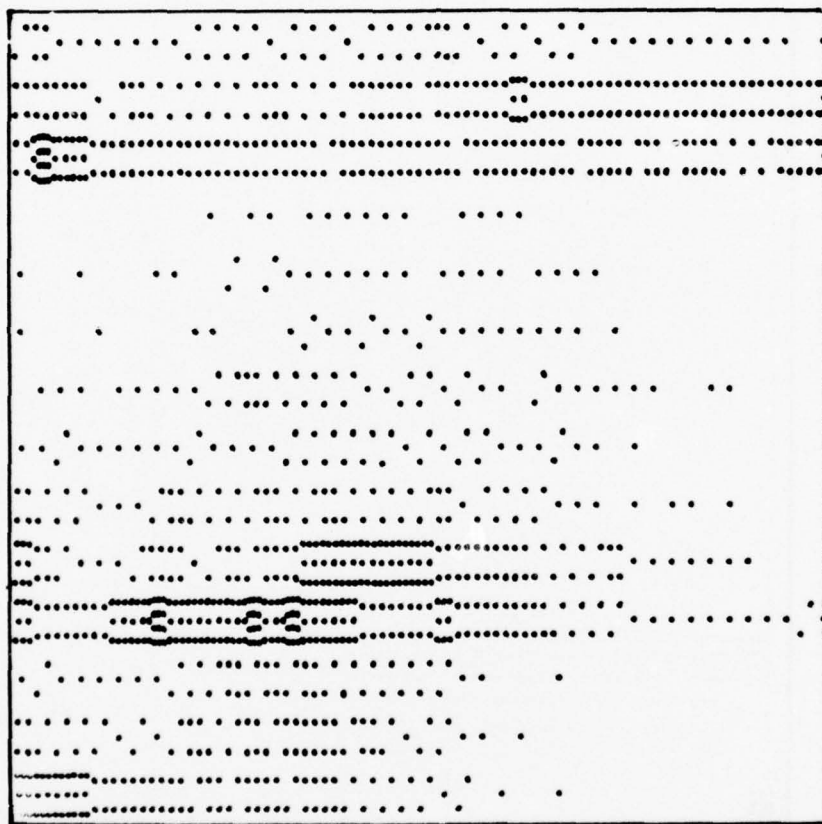


Figure A.40(b). Computer plot of ψ ($43 < \psi < 41$) for another production panel from McDonnell Douglas

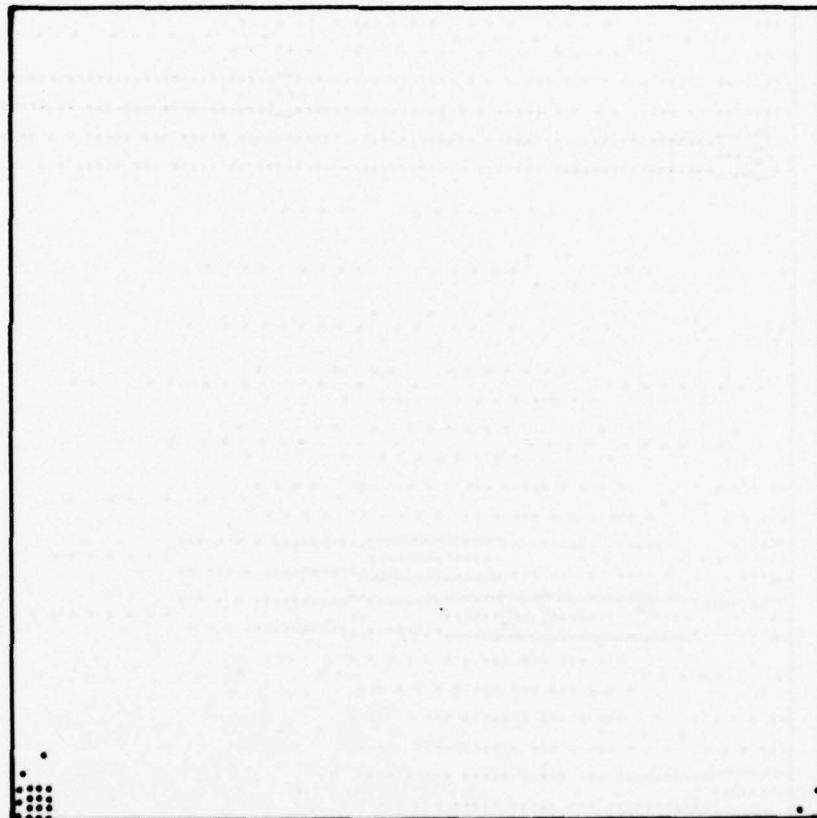


Figure A.40(c). Computer plot of SPD ($.45 < \text{SPD} < .25$) for another production panel from McDonnell Douglas

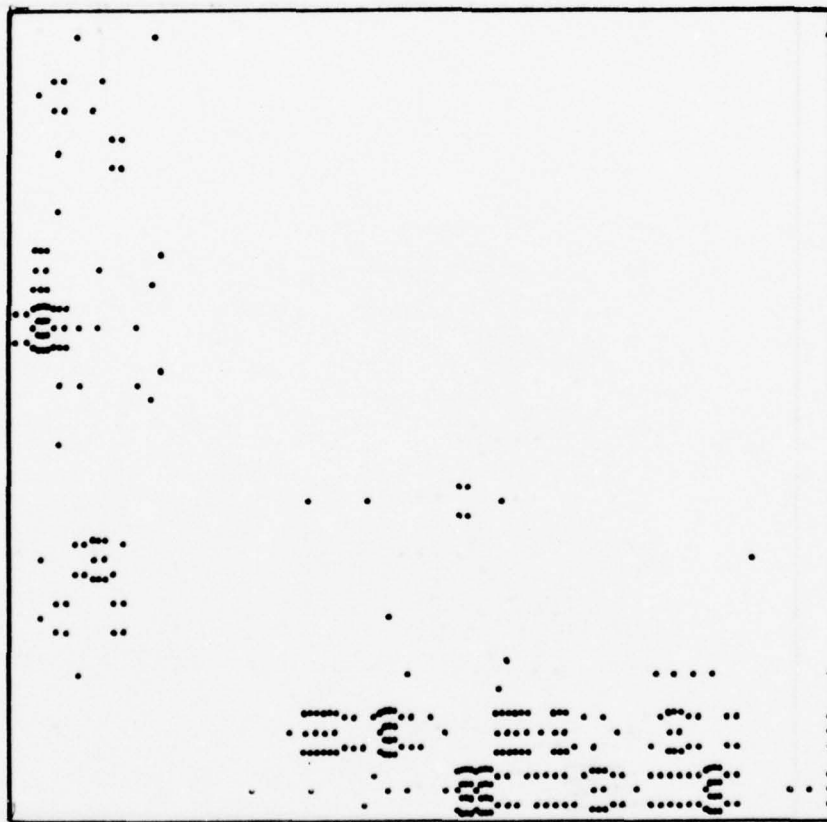


Figure A.41(a). Computer plot of Δ ($143 < \Delta < 140$) for another production panel from McDonnell Douglas

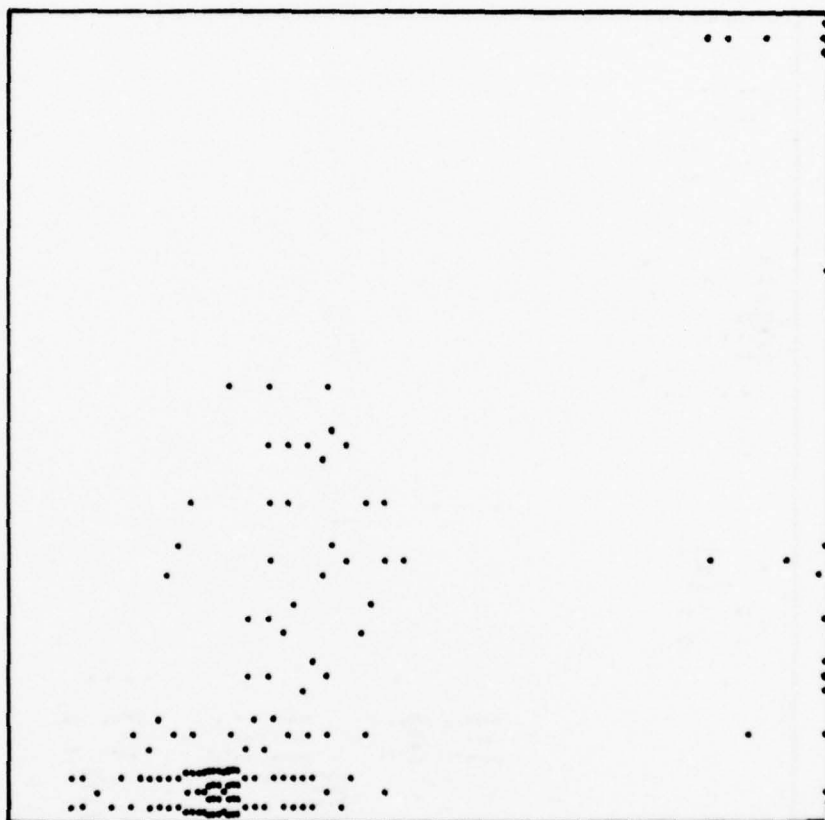


Figure A.41(b). Computer plot of ψ ($43 < \psi < 41$) for another production panel from McDonnell Douglas



Figure A.41(c). Computer plot of SPD ($.55 < \text{SPD} < .35$) for another production panel from McDonnell Douglas

Clean Cotton Glove Smudge		Soda Pop		Coffee
	3 in 1 oil		Fingerprints	
Ink		Lipstick		Hand Lotion
	Cigarette Smoke		Cough	
Stearic Acid		hexadecylamine		docosane

Figure A.42. Contamination pattern for panel 4 from McDonnell Douglas

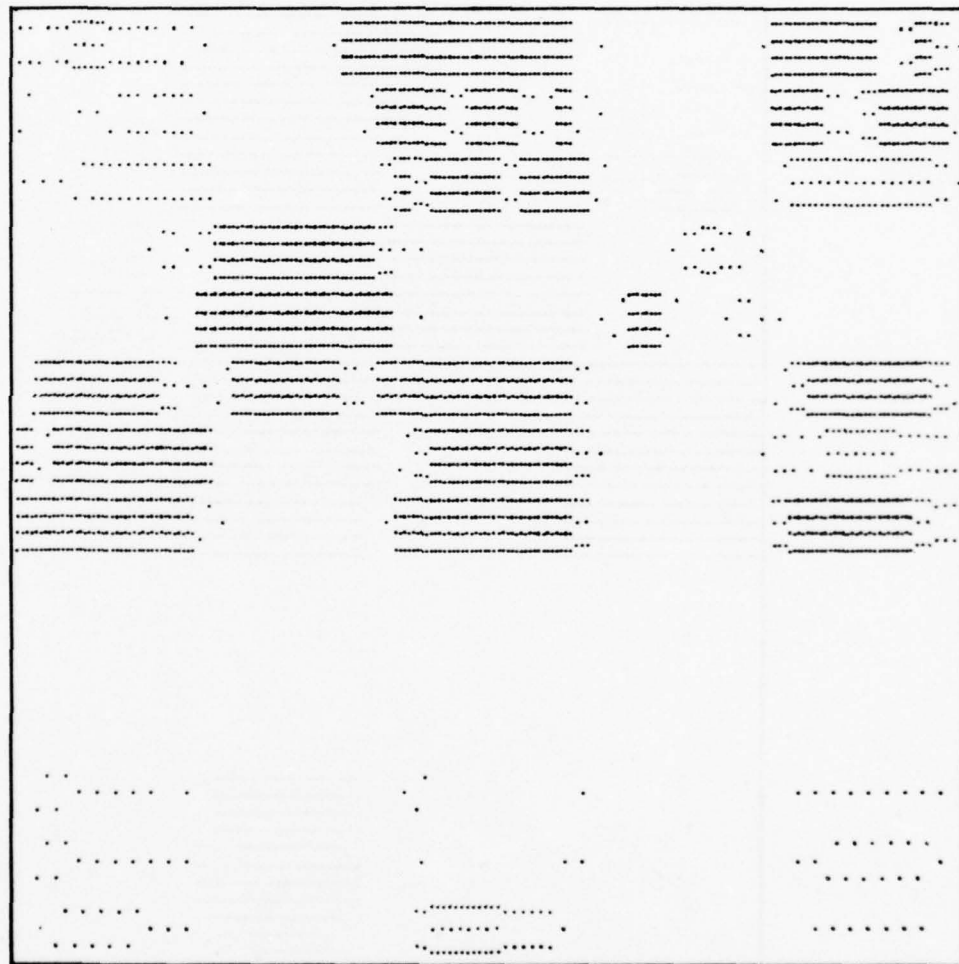


Figure A.42(a). Computer plot of Δ ($144 < \Delta < 141$) for contaminated panel 4 from McDonnell Douglas



Figure A.42(b). Computer plot of ψ ($43 < \psi < 41$) for contaminated panel 4 from McDonnell Douglas

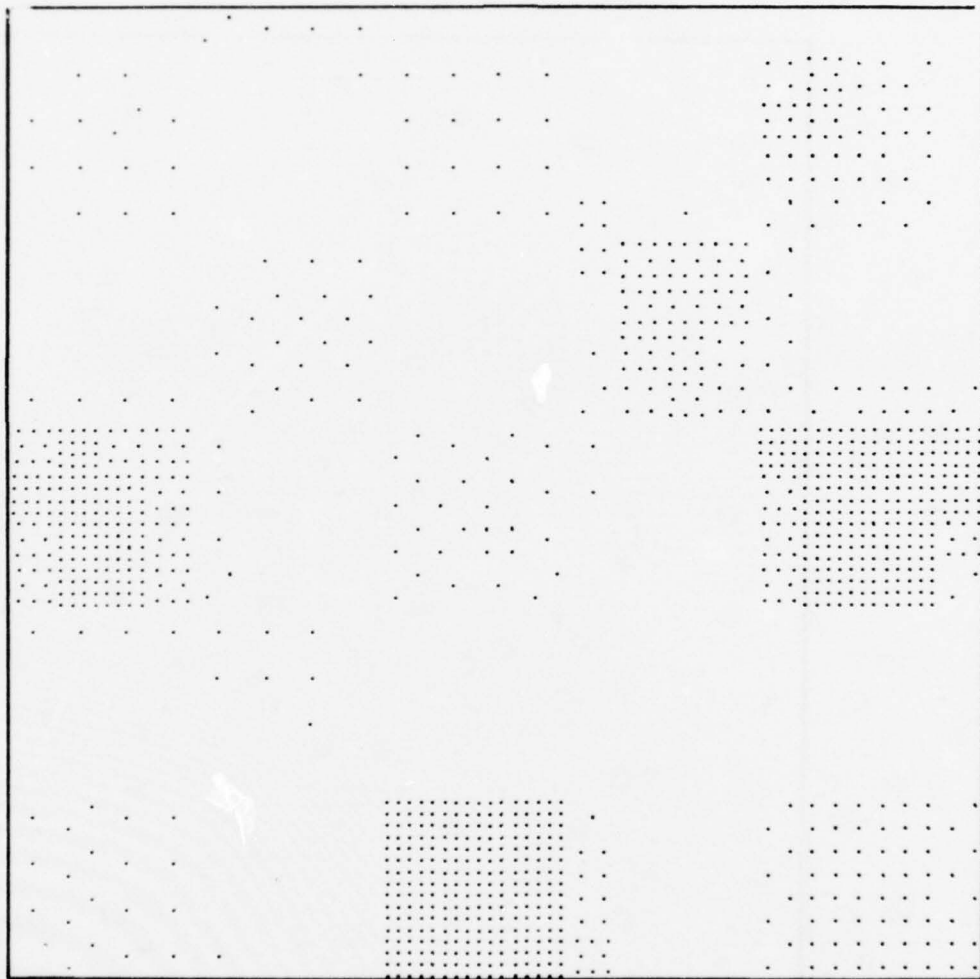


Figure A.42(c). Computer plot of SPD ($.28 < \text{SPD} < .28$) for contaminated panel 4 from McDonnell Douglas

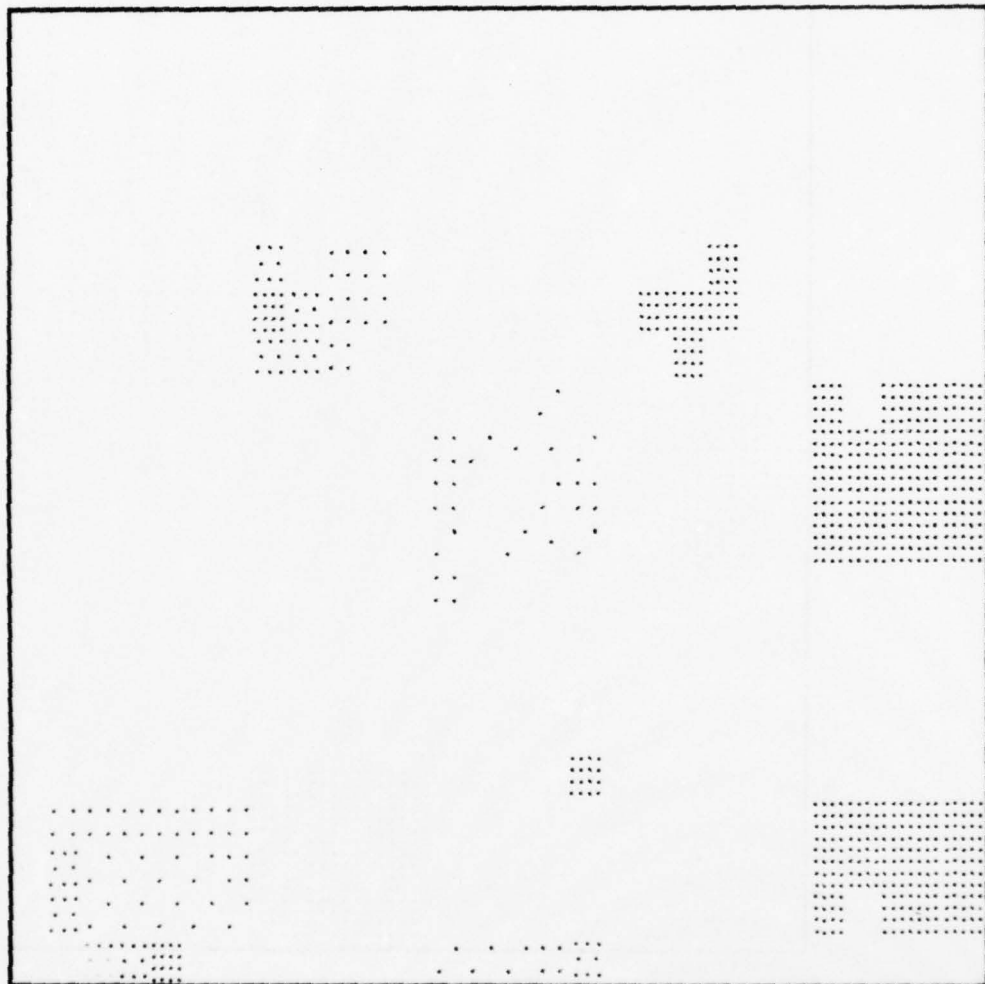


Figure A.42(d). Computer plot of wettability for contaminated panel 4 from McDonnell Douglas

APPENDIX B

Computer printouts of data for contamination on aluminum panels. The number on the tables relate to the appropriate figure in Appendix A.

Table B.1(a) (cont'd)

PUZZLE: 32276

2005 76.

[illegible]

Table B.1(a) (cont'd)

[illegible]

Table B.1(b)

PS: 32726
SAMPLE: 32726

3 AUG 76

[illegible]

Table B.1(b)(cont'd)

92 9111 76.

92.27% : 97.94% : 15d

[illegible]

52 JUL 76

[illegible]

Table B.1(c)

33 AUG 76

CDD SAMPLE: CHL. SAMPLE

474	353	200	287	267	336	456	603	594	603	655	637	663	672	637	672	999
465	448	362	370	422	474	588	629	655	680	732	732	698	663	698	698	613
613	482	439	422	456	508	474	517	534	560	620	637	613	603	735	853	686
620	508	508	439	422	448	508	568	603	637	715	706	706	637	663	603	566
990	766	551	577	431	508	525	577	680	680	715	680	663	672	663	586	508
741	620	525	534	588	560	613	637	629	629	689	775	803	784	725	680	566
594	646	603	560	577	629	646	603	672	637	637	706	723	741	698	655	543
560	646	637	603	613	637	646	698	749	741	732	775	758	715	741	655	543
551	560	586	663	663	663	663	680	784	741	749	766	749	775	741	646	508
534	508	551	629	603	629	723	870	313	741	663	698	758	766	775	706	577
508	508	525	620	620	646	655	698	784	827	784	775	732	775	784	672	551
534	508	508	525	637	586	646	706	741	775	706	706	741	792	766	637	508
491	491	534	517	560	577	663	766	723	706	646	637	715	775	732	637	508
465	560	508	456	491	525	637	663	655	637	637	663	663	766	741	672	543
413	543	534	491	482	534	603	577	534	568	613	629	655	741	775	706	566
431	482	517	482	491	508	543	568	551	508	560	568	663	715	749	646	525
474	508	560	525	508	525	525	560	637	525	508	620	698	732	732	680	629
456	508	508	508	508	543	543	568	655	637	525	508	613	689	698	646	613
456	508	508	491	543	586	613	689	663	655	603	560	577	672	646	663	603
422	525	613	560	560	603	613	603	613	637	620	568	594	646	672	637	620
301	508	560	534	465	482	508	164	508	672	629	577	534	613	655	680	686
0	250	319	258	207	164	155	189	258	276	258	301	362	431	474	603	646

Table B.1(c) (cont'd)

32 JUN 76

SPD SAMPLE: CARL SAMPLE

0	11	62	111	227	568	929	951	888	536	463	414	392	406	409	406	417
11	62	88	148	216	559	922	863	851	525	546	420	403	409	409	403	406
79	74	96	125	210	534	800	871	880	525	426	429	409	417	406	417	426
74	79	96	159	219	502	815	928	911	531	434	417	406	397	383	394	403
37	54	125	227	562	883	999	903	531	463	406	397	392	397	414	420	440
429	400	386	386	394	420	420	403	417	488	426	420	482	429	420	482	429
420	412	400	397	417	437	440	440	454	460	465	471	468	468	477	477	471
420	412	409	423	429	426	431	463	477	477	474	463	460	463	468	463	471
420	409	412	431	434	434	434	454	480	443	437	454	465	465	474	468	465
429	412	420	428	414	431	451	451	468	454	446	460	465	485	500	485	488
417	394	383	386	408	417	429	451	451	448	446	446	448	463	474	463	474
412	380	392	392	403	412	431	468	454	448	434	454	465	482	485	477	474
414	409	389	392	403	412	424	440	443	440	434	446	460	482	482	471	474
409	409	389	394	403	403	420	426	429	426	443	443	454	471	480	482	474
414	414	409	392	397	406	426	423	426	429	434	440	460	497	505	488	485
414	414	412	397	408	408	414	437	451	440	454	465	477	494	494	500	505
426	426	423	412	406	409	414	429	446	434	434	440	457	477	482	488	512
423	420	412	406	417	417	426	460	474	446	446	451	460	474	497	511	511
437	440	428	426	423	440	454	463	471	477	463	465	477	488	482	502	517
446	448	451	465	446	440	414	272	446	500	488	477	480	491	505	511	528
460	474	468	460	440	437	451	477	491	494	477	463	471	482	494	522	536

Table B.2(a) (cont'd)

DELTA	SAMPLE: 2-7-5-76										32 JUL 76
171	171	171	171	171	171	171	171	171	171	171	171
171	171	171	171	171	171	171	171	171	171	171	171
171	171	171	171	171	171	171	171	171	171	171	171
170	170	170	171	171	171	171	171	171	171	171	171
164	162	162	162	162	162	162	162	162	162	162	162
159	159	159	159	159	159	159	159	159	159	159	159
158	159	159	159	159	159	159	159	159	159	159	159
158	159	159	159	159	159	159	159	159	159	159	159
158	159	159	159	159	159	159	159	159	159	159	159
159	159	159	159	159	159	159	159	159	159	159	159
159	159	159	159	159	159	159	159	159	159	159	159
162	162	162	162	162	162	162	162	162	162	162	162
164	164	164	164	164	164	164	164	164	164	164	164
164	165	164	164	164	164	164	164	164	164	164	164
164	165	165	164	164	164	164	164	164	164	164	164
163	163	164	164	164	164	164	164	164	164	164	164
164	164	164	164	164	164	164	164	164	164	164	164
164	165	165	165	165	165	165	165	165	165	165	165
164	165	165	165	165	165	165	165	165	165	165	165
164	165	165	165	165	165	165	165	165	165	165	165

Table 8.2(b)

IS: 207-5-76

[illegible]

Table B.2(b)(cont'd)

[illegible]

Table B.2(c)

33 006 76

SPD SAMPLE: 2-2-5-76

735	703	753	797	809	946	960	999	925	877	940	907	863	877	907	883	880
663	732	845	783	809	892	901	960	980	842	860	818	806	832	877	812	765
394	519	525	531	694	714	735	789	637	646	640	694	688	713	756	680	563
187	267	190	248	311	335	448	494	335	480	486	240	202	194	252	557	572
24	44	148	83	98	80	74	30	53	157	172	130	276	187	110	90	95
581	545	474	542	561	421	433	454	480	489	393	376	344	291	313	267	264
646	655	786	788	670	628	548	572	676	664	557	614	611	566	575	623	590
379	213	412	519	551	504	564	513	498	448	427	513	489	320	296	388	264
68	184	210	33	3	98	127	255	178	210	184	122	119	356	385	320	234
729	611	537	581	498	557	534	522	474	424	474	457	314	225	308	391	
741	628	590	825	614	664	711	735	694	673	694	747	765	735	711	735	765
403	329	433	433	454	510	628	611	581	560	525	584	620	649	637	643	534
92	228	145	145	142	68	44	86	47	0	33	3	39	18	83	68	145
634	498	480	575	611	617	725	744	827	830	794	800	794	741	697	685	605
335	237	228	488	486	519	646	640	735	750	750	732	717	691	676	614	451
347	347	190	65	74	71	332	451	462	457	439	385	350	125	95	237	262
545	703	474	237	65	264	332	261	234	240	222	255	136	27	58	273	557
872	818	714	726	568	587	581	599	614	581	578	551	525	504	516	545	581
928	892	869	848	812	780	750	741	774	794	783	806	786	783	789	833	839
943	877	889	845	803	797	780	777	818	815	797	812	812	821	857	872	877
943	892	904	860	830	783	797	806	851	848	827	818	836	880	904	892	934
966	913	919	848	812	789	803	803	821	842	818	830	818	866	937	955	993

Table B.2(c)(cont'd)

12 JUL 76

SAMPLE: 2-7-5-76

SPD

834	507	297	925	938	962	0	928	944	999	895	840	864	885	731	742	797
662	742	633	797	821	821	944	748	742	748	835	722	784	815	613	392	411
313	153	153	319	461	582	613	423	552	496	337	294	398	447	558	392	264
43	319	276	313	172	25	147	172	190	153	368	607	472	270	288	392	80
104	80	55	43	61	104	31	55	0	135	294	386	343	380	435	454	25
729	668	650	613	650	625	631	717	711	637	644	594	509	521	607	588	668
306	594	594	658	613	631	674	607	509	545	558	503	380	349	496	221	699
297	374	208	147	165	270	368	331	386	313	92	135	637	662	558	570	619
178	116	159	116	6	25	49	74	141	184	202	294	588	686	656	668	276
729	693	637	631	669	766	784	784	784	784	803	815	729	699	705	760	754
441	472	435	349	380	521	570	533	503	515	619	686	674	637	613	594	515
398	190	288	282	135	43	135	55	12	74	37	67	6	153	74	215	43
153	257	325	362	331	239	178	200	239	104	110	92	74	43	98	74	233
67	190	454	472	484	681	613	693	650	650	631	668	644	650	631	509	423
80	129	55	43	208	405	460	498	478	466	454	472	294	141	12	123	331
619	368	37	545	797	772	539	552	509	582	637	392	368	374	12	116	245
545	454	380	37	92	31	110	104	49	49	61	55	12	129	319	545	61
827	876	827	748	699	662	650	680	711	729	711	674	680	637	699	705	784
809	889	827	766	705	674	674	729	717	723	729	723	717	723	735	766	858
827	938	864	784	711	711	729	766	760	760	729	754	784	797	827	938	
840	913	827	784	748	711	711	760	760	742	765	742	784	784	797	858	944

[illegible]

Table B.8(a)

[illegible]

Table B.8(a)(cont'd)

163	163	162	163	163	163	162	162	161	163	162	161	161	161	162	161	162
164	164	164	164	164	164	164	164	163	163	163	163	163	163	163	163	162
165	165	165	165	165	164	164	164	164	164	163	163	163	163	163	163	162
166	166	166	165	165	166	166	166	164	164	163	163	163	163	163	163	164
166	166	166	167	167	166	166	166	166	166	167	166	165	165	166	166	167
167	166	166	166	166	166	166	166	166	166	166	166	166	166	166	166	166
161	161	160	161	161	161	161	162	162	162	162	164	164	163	163	162	163
161	161	161	161	161	161	161	161	161	161	161	161	161	161	161	161	162
163	162	163	163	162	162	162	162	162	162	162	162	162	162	162	162	162
162	162	162	162	162	162	162	162	162	163	163	162	162	162	162	162	162
161	161	161	161	161	161	161	161	161	161	161	161	161	161	161	161	161
163	162	163	162	162	162	162	162	162	161	161	161	161	161	161	161	161
166	166	166	166	166	166	166	166	165	165	165	164	164	164	165	164	163
165	165	166	166	166	165	166	166	166	166	166	166	166	166	167	165	164
161	161	161	161	161	161	161	161	161	161	161	161	161	161	163	163	162
161	161	162	161	161	161	161	161	161	161	161	161	161	161	160	160	161
161	162	161	162	161	162	161	162	161	161	161	161	161	161	161	161	161
161	161	161	161	161	161	161	161	161	161	161	161	161	161	161	161	161
161	161	161	161	161	161	161	161	161	161	161	161	161	161	161	161	160
161	161	161	161	161	161	161	161	161	161	161	161	161	161	161	161	160
161	161	161	161	161	161	161	161	161	161	161	161	161	161	161	161	161

Table B.8(a) (cont'd)

[illegible]

Table B.8(b)

[illegible]

Table B.8(b) (cont'd)

[illegible]

Table B.9

860	706	639	647	737	680	696	704	622	467	360	475	475	229	328	409
770	811	762	843	794	819	942	917	762	737	459	467	377	254	368	368
745	876	868	942	942	983	999	917	712	655	590	491	418	450	418	516
540	745	581	917	974	950	909	770	737	753	764	590	467	491	459	483
598	450	802	958	983	983	901	843	819	786	745	696	647	590	557	516
459	663	901	835	835	898	647	655	680	696	737	663	590	557	614	557
221	328	262	434	426	426	467	516	581	483	467	573	557	614	647	467
262	351	254	442	489	197	303	418	418	319	401	385	491	426	442	360
426	483	573	540	841	532	467	458	565	590	516	467	491	418	483	458
319	442	425	524	581	467	418	590	622	483	483	483	459	450	500	483
123	180	229	205	197	115	213	254	197	139	229	287	262	262	295	221
172	401	424	360	237	311	442	458	221	123	262	319	254	221	303	270
197	409	540	549	442	475	459	516	328	360	328	434	426	450	516	393
237	336	319	385	549	557	532	557	393	393	401	442	418	500	459	352
295	229	246	0	246	319	319	303	213	256	303	319	262	246	311	287
287	262	270	180	205	295	352	328	352	303	336	336	295	164	246	295
418	532	352	254	197	295	270	295	319	336	270	270	221	197	123	139
491	285	508	377	180	270	319	303	360	295	270	221	123	246	197	180
377	336	385	336	205	295	328	319	262	229	221	287	254	246	360	418
164	131	237	254	186	278	221	246	205	262	319	352	360	319	311	401
221	49	188	246	270	262	311	360	328	352	442	418	418	459	483	508

Table B.19(a)

DATA		SAMPLE: 6-23-4-760										5 1000 76									
159	150	150	160	160	159	150	159	159	158	155	153	153	155	159	160	161	161	161	161	161	161
158	158	159	159	158	157	157	157	157	154	152	150	151	153	157	159	160	161	161	161	161	161
158	159	159	159	158	157	157	158	157	154	153	152	152	155	158	160	161	161	161	161	161	161
159	159	160	160	159	159	150	158	159	154	158	157	157	158	160	161	161	161	161	161	161	161
150	160	160	161	161	161	161	161	161	161	161	161	161	161	161	161	161	160	160	160	160	160
160	161	160	161	161	161	160	160	161	160	160	160	160	160	160	160	160	160	160	160	160	160
160	160	160	160	161	160	160	160	161	161	160	160	161	160	161	161	161	161	161	161	161	161
161	161	161	161	161	161	161	161	161	161	161	161	161	161	161	161	161	161	161	161	161	161
160	161	161	161	161	161	162	162	162	162	162	162	162	162	162	162	162	162	162	162	162	162
158	158	150	159	150	150	154	153	154	154	153	151	149	151	151	152	152	152	152	152	152	153
157	157	157	157	156	153	151	150	150	150	150	149	148	149	149	150	152	153	154	154	154	154
156	156	156	157	156	153	151	149	150	151	151	150	149	150	151	153	153	154	154	154	154	156
159	158	159	159	159	157	155	154	156	157	157	155	154	155	158	158	157	156	158	158	159	159
160	161	161	161	161	161	160	160	160	161	161	160	160	160	160	160	160	160	160	160	160	160
160	161	161	161	161	161	161	161	160	160	160	160	160	160	160	160	160	160	160	160	160	160
160	161	161	161	161	161	161	161	161	161	161	161	161	161	161	161	161	161	161	161	161	161

Table B.19(b)

PS1	SAMPLE: 6-24-4-76C															5 NOV 76	
41	41	42	42	42	42	42	42	42	42	42	42	42	42	42	42	42	42
41	41	41	42	42	41	41	41	42	42	42	42	42	42	42	42	42	42
41	41	41	41	42	42	42	42	42	41	42	42	42	42	42	42	42	42
41	41	42	42	42	42	42	42	42	42	42	42	42	42	42	42	42	42
41	41	41	42	42	42	42	42	42	42	42	42	42	42	42	42	42	42
41	41	41	42	42	42	42	42	42	42	42	42	42	42	42	42	42	42
41	41	41	41	41	42	42	42	42	42	42	42	42	42	42	42	42	42
41	41	41	41	41	41	42	42	42	42	42	42	42	42	42	42	42	42
41	41	41	41	42	42	42	42	42	42	42	42	42	42	42	42	42	42
41	41	41	41	42	42	42	42	42	42	42	42	42	42	42	42	42	42
40	41	40	41	41	41	41	41	41	41	41	41	41	41	41	41	41	41
40	40	40	40	40	41	41	41	41	41	41	41	41	41	41	41	41	41
40	40	40	40	40	41	41	41	41	41	41	41	41	41	41	41	41	41
40	40	40	40	40	41	41	41	41	41	41	41	41	41	41	41	41	41
40	40	40	40	40	40	40	40	40	40	40	40	40	40	40	40	40	40
40	40	40	40	40	40	40	40	40	40	40	40	40	40	40	40	40	40

Table B.19(c)

S 00N 76

SAMPLE: C-21-4-76C

SPD	100	109	103	103	72	122	132	119	76	197	160	129	95	123	119	134	162
144	123	123	107	82	117	119	125	92	193	122	136	99	115	119	132	160	
134	119	113	107	93	101	113	129	78	177	125	119	105	123	123	136	166	
129	115	107	99	45	95	107	113	72	154	167	86	27	76	95	97	117	
92	76	68	68	12	66	84	111	90	127	167	109	53	117	154	156	179	
123	103	113	123	58	84	99	125	68	123	163	167	37	103	129	134	169	
115	92	101	92	49	82	103	119	58	117	99	103	37	107	119	132	167	
117	99	99	84	31	78	117	109	43	161	90	88	34	86	101	109	132	
88	78	90	49	0	49	97	80	19	74	90	90	49	99	121	123	156	
111	99	90	84	37	82	109	99	31	90	163	97	49	101	115	125	156	
117	95	99	96	35	86	101	86	43	90	99	99	53	101	119	125	156	
115	84	84	86	60	86	103	92	41	88	99	101	66	109	201	187	165	
66	263	512	329	31	236	658	465	10	448	841	561	27	590	941	944	389	
192	668	765	750	337	835	915	913	613	933	966	978	621	968	983	993	952	
254	724	814	763	506	892	929	931	865	946	970	987	841	972	987	989	952	
144	643	816	773	144	787	941	962	255	882	976	993	308	855	999	989	378	
70	101	238	119	21	119	444	218	27	199	537	337	49	294	576	409	132	
749	380	417	372	167	403	543	565	234	485	889	880	302	728	833	835	497	
345	430	460	428	158	444	547	586	362	541	623	633	584	808	896	907	645	
345	483	512	413	113	430	543	594	234	510	650	672	282	765	911	919	368	
216	317	366	210	92	222	289	317	115	191	319	238	150	296	444	290	230	

REFERENCES

1. T. P. Remmel, "Characterization of Surfaces Prior to Adhesive Bonding" AFML Tech. Rep. NOR-75-145, Oct. 1975.
2. G. M. Hidy, "Characterization of Aerosols in California (A CHEX)" ARB Contract No. 358, April 1975.
3. T. Smith, "An Automated Scanning Ellipsometer", Surf. Sci. 56, 212 (1976).
4. P. P. Craig and V. Radeka, Rev. Sci. Inst. 41, 258 (1970).
5. T. Smith, "Mechanisms of Adhesion Failure between Polymers and Metallic Substrates", AFML-TR-74-73, June 1974.
6. T. Smith, "Auger Electron Spectroscopy and Ion Sputter Profiles of Oxides on Aluminum" Surf. Sci. 55, 601 (1976).
7. T. Smith, "Effect of Surface Roughness on Ellipsometry of Aluminum", Surf. Sci. 56, 252 (1976).
8. J. J. Bikerman, Proc. Roy. Soc. (London) A 170, 130 (1939).
9. M. W. White, "The Detection and Control of Organic Contamination on Surfaces" Marcel Dekker Inc. (1968) p. 361.
10. T. Smith, Materials Evaluation, May 1975, p. 101.
11. T. Smith, AFML-TR-74-73 Part II, Oct. 1975.